

THE SECRET LIFE OF SMALL ALCOHOLS:

the discovery and exploitation of fragmentation, adduct formation and auto-modification phenomena in differential ion mobility spectrometry leading to next-generation toxicity screening.

A thesis submitted to Loughborough University for the degree of Doctor of
Philosophy

Dorota Marta Ruszkiewicz

2016

Abstract

The research presented in this thesis started with the idea to study alcohols as modifiers and dopants in differential ion mobility spectrometry (d-IMS) to produce complicated chemical signatures to explore a concept of chemical labels for product security application. D-IMS is a gas phase atmospheric pressure separation and detection technique which distinguishes compounds based on differences in their ions mobility as their travel under a low and high electric field. The hypothesis was that alcohols will form typical d-IMS products such as protonated monomers and proton bound cluster ions. However, the very first experiments revealed unexpected phenomena which included changes in the mobility of ions over a narrow range of concentrations that could not be explained by existing theory. Another observation was the apparent regeneration of reactant ions. It became evident that the observed phenomena had not been described in the open literature and that addressing the research-questions that were being raised would be essential for the determination of alcohols by d-IMS and its use in medical applications for toxicity screening and monitoring of alcohols. The above discovery shifted the research objective towards a fundamental and comprehensive study on the behaviour of alcohols in d-IMS.

This thesis describes designed experiments and constructed systems allowing the efficient study of effect of concentration, electric field and temperature on the d-IMS responses of alcohols. The results of those studies are presented in Chapter 3, showing: extensive fragmentation of alcohols, including previously undescribed fragmentation patterns with regeneration of the hydrated proton; new phenomena of adduct ion formation within the d-IMS drift tube, observed in the case of methanol within a narrow range of concentration; and self-modification of the alpha function of alcohols. This knowledge was exploited by developing an non-invasive analytical method for recovery, separation and detection of toxins from human saliva (including alcohols, diols and GHB) using TD-GC-d-IMS (thermal desorption - gas chromatography - d-IMS) within a full range of toxicological concentration levels. The results of this study are demonstrated in Chapter 4. Finally, Chapter 5 describes extensive experimental design built for initial studies on dopants and modifiers and the very first results which led to rearrangement of the objectives of this thesis, giving a base for further studies on alcohols gas chemistry in mixed systems.

Two journal articles have been published for the work detailed in Chapters 3 and 4:

D.M. Ruszkiewicz, C.L.P. Thomas and G.A. Eiceman; *Fragmentation, auto-modification and post ionisation proton bound dimer ion formation: the differential mobility spectrometry of low molecular weight alcohols*; *The Analyst* (2016) **141**

D.M. Ruszkiewicz, L Criado-Garcia , G.A. Eiceman and C.L.P Thomas; *A rapid and non-invasive method to determine toxic levels of alcohols and γ -hydroxybutyric acid in saliva samples by gas chromatography-differential mobility spectrometry*; *Journal of Breath Research* (2016) **10**

“We cannot hope to build a better world without improving the individual. Toward this end, each of us must work for his own highest development, accepting at the same time his share of responsibility in the general life of humanity—our particular duty being to aid those to whom we think we can be most useful.”

“I am among those who think that science has great beauty. A scientist in his laboratory is not only a technician: he is also a child placed before natural phenomena which impress him like a fairy tale.”

— **Marie Curie**

‘The Future of Culture’ Debate (1933)

Acknowledgments

I would not have been able to write this thesis without help and support of those who were with me during this journey.

“Measure it, treasure it,
in units of love, which means you my friends,
you’re rich beyond your wildest dreams.“

Above & Beyond

I am mostly grateful to my supervisor, Paul Thomas, who has been able to manage my development as no one before. I want to thank you for your dedication, guidance, attention to details and for showing me the magic of "Eight Ps". I would like to thank you for your wisdom and all the stories which inspired me and gave me strength to keep going during dark moments of this journey. I would not start and finish this work without you. Thank you.

I want to acknowledge my deepest gratitude to Gary Eiceman, for sharing his knowledge and experience with me. I want to thank you for guiding me, when the science didn't make sense and for your insight and support, which continued from overseas even at six o'clock in the morning. It was a great scientific adventure. Thank you.

I want to give a big thank you to Matthew Turner who always found time to fix things and always was there for me. Thank you.

I greatly appreciate the financial and industrial support from John Hoggs Technical Solution, in particular Malcolm Tirrell, who made this work possible.

I would like to thank the research group: Victor, Lauren, Neil and Caitlyn, Helen, Cristina, Rob, Aadi, Liam, Shuo, Emily and Emma. We had great times together.

I want to thank my friends for giving me their love, support at every step on the way, for sharing tears and laughter and for legendary fun together.

I thank my "other half" Tomasz, for his patience, understanding and support but overall for his comfort and love.

Last but not least, I want to thank my parents and loving son. Mamo, Tato, nie udało by mi sie napisać tej pracy bez waszej miłości I wsparcia, dziękuję. Filipku, dziękuję za cierpliwość, miłość I przytulanki. Tą pracę dedykuję Wam.

Table of contents

Abstract	2
Acknowledgments	5
Table of contents	6
Glossary of terms	11
Chapter 1 Introduction	13
1.1 Aims, Objectives and Hypothesis	13
1.1.1 Primary hypothesis.....	13
1.1.2 Secondary hypothesis.....	13
1.1.3 Primary aim	13
1.1.4 Secondary aim	13
1.2 Introducing Differential Mobility Spectrometry	15
1.3 Alcohol Toxicity	20
1.3.1 Methanol.....	20
1.3.2 Ethanol.....	21
1.3.3 n-Propanol.....	23
1.3.4 Isopropanol	23
1.3.5 Ethylene Glycol.....	24
1.4 IMS and d-IMS Theory.....	27
1.4.1 History of IMS and d-IMS	27
1.4.2 Fundamentals of mobility of ions in gas-phase.....	29
1.4.3 Effect of electric field on mobility in d-IMS	32
1.4.4 Effect of temperature and pressure on d-IMS responses	36
1.5 Ion Processes.....	37
1.5.1 Proton and electron affinity	37

1.5.2	Proton transfer reaction.....	39
1.5.3	Atmospheric pressure chemical ionisation and ion formation.....	40
1.6	Moisture, Dopants and Gas Modifiers in d-IMS.....	45
1.6.1	Humidity effect on d-IMS	45
1.6.2	Gas modifiers.....	47
1.6.3	Dopants.....	50
1.7	Fragmentation.....	53
1.7.1	Fragmentation in IMS/d-IMS systems	53
1.7.2	Fragmentation of alcohols	57
1.8	Modelling.....	62
1.8.1	Reactant ion production in d-IMS	62
1.8.2	Product ion production in d-IMS	62
1.8.3	Formation of proton bound clusters –ion solvation equilibrium model	64
1.8.4	Ion-neutral collisions calculations	69
Chapter 2	Instrumentation and Experimental Approaches.....	71
2.1	Overview.....	71
2.2	Gases	71
2.2.1	Nitrogen and nitrogen generator	71
2.2.2	Helium.....	73
2.2.3	Gas purification and moisture control	73
2.3	Differential Ion Mobility Spectrometer	74
2.3.1	Software	75
2.3.2	Functionality of the SVAC d-IMS.....	76
2.4	Blanks and System Validation	77
2.5	Experimental Setups.....	84
2.5.1	Test Atmosphere Generator-d-IMS	84
2.5.2	Exponential dilution-d-IMS.....	85

2.5.3	D-IMS-MS	86
2.5.4	GC-d-IMS	87
2.5.5	TD-GC-d-IMS.....	88
2.5.6	Exponential dilution-PZX-d-IMS.....	91
2.6	Exponential Dilution Approach.....	97
2.6.1	Theory of exponential dilution.....	97
2.6.2	Exponential dilution studies approach	98
2.7	Permeation Vapour Sources	100
2.7.1	Theory of permeation process	100
2.7.2	Construction of permeation sources	100
2.7.3	Gravimetric method for permeation sources.....	100
2.7.4	Permeation sources studies approach and calculations	102
Chapter 3	Ion Chemistry of Alcohols in d-IMS.....	103
3.1	Study Overview and Objectives.....	103
3.2	Chemicals and Purity	104
3.3	Methods for Studying of n-Alcohols d-IMS Responses (experiments no 1.1 and 1.2)	105
3.3.1	Effect of concentration expt. no 1.1	105
3.3.2	Effect of ion temperature expt. no 1.2.1	109
3.3.3	d-IMS-MS studies expt. no 1.2.2	110
3.4	Results and Discussion.....	110
3.4.1	Preamble.....	110
3.4.2	Methanol.....	111
3.4.3	Ethanol.....	122
3.4.4	n-Propanol.....	129
3.4.5	n-Butanol.....	141
3.4.6	Summary of ion chemistry of alcohols.....	148

3.5	Conclusions.....	151
Chapter 4	Recovery and Detection of Alcohols and Toxic Substances from Human Saliva	153
4.1	Study Overview and Objectives.....	153
4.2	Experimental	153
4.2.1	Chemicals.....	153
4.2.2	PDMS sampler	154
4.2.3	Ethics, participant preparation and saliva sampling.	155
4.2.4	Methods	156
4.2.5	Data analysis.....	162
4.3	Results	164
4.3.1	Signal identification and calibration of the d-IMS responses.....	164
4.3.2	Characterisation of spiked saliva samples.....	173
4.4	Conclusions.....	180
Chapter 5	Alcohols Mixtures	182
5.1	Study Overview.....	182
5.2	Preliminary Experimental Design.....	182
5.3	Experimental	185
5.3.1	Chemicals	185
5.3.2	Methods.....	185
5.4	Results demonstration.....	189
Chapter 6	Thesis Summary.....	194
6.1	Overview of the Research Findings and Review of the Studies	194
6.1.1	Ion chemistry of alcohols	194
6.1.2	Recovery of toxic substances from human saliva	196
6.1.3	2-Butanol/Methanol mixed system experiment	196
6.1.4	Critical evaluation	197

6.2 Concluding Comments.....	197
References	199

Glossary of terms

K	$(\text{cm}^2 \cdot \text{V}^{-1} \cdot \text{s}^{-1})$	Mobility coefficient
K_0	$(\text{cm}^2 \cdot \text{V}^{-1} \cdot \text{s}^{-1})$	Mobility coefficient under electric field = 0
E	$(\text{V} \cdot \text{cm}^{-2})$	Electric field
E/N	(Td)	Reduced electric field
v_d	$(\text{cm} \cdot \text{s}^{-1})$	Ion drift velocity
μ	(kg)	Reduced mass
T_{eff}	(K)	Effective temperature
Ω	(cm^2)	Cross section area
k_B	$(1.380 \times 10^{-23} \text{ m}^2 \cdot \text{kg} \cdot \text{s}^{-2} \cdot \text{K}^{-1})$	Boltzmann's constant
α	(Td^{-2n})	Alpha parameter (relative variation of K_0 depending on E)
RF	(V)	Asymmetric radiofrequency voltage
V_d	(V)	Separation or dispersion voltage (RF)
V_c	(V)	Compensation voltage
E_d	(Td or $\text{V} \cdot \text{cm}^{-2}$)	Separation or dispersion field
E_c	(Td or $\text{V} \cdot \text{cm}^{-2}$)	Compensation field
t	(s)	Time
N	(m^{-3})	Gas density number
PA	$(\text{kJ} \cdot \text{mol}^{-1})$	Proton affinity
EA	$(\text{kJ} \cdot \text{mol}^{-1})$	Electron affinity
ΔH	$(\text{kJ} \cdot \text{mol}^{-1})$	Change in enthalpy
ΔS	$(\text{kJ} \cdot \text{K}^{-1} \cdot \text{mol}^{-1})$	Change in entropy
$\Delta_{base} G$	$(\text{kJ} \cdot \text{mol}^{-1})$	Change in gas phase basicity
ΔG	$(\text{kJ} \cdot \text{mol}^{-1})$	Change in Gibb's free energy

Q	(Coulomb C)	Electrical charge
F	(96485.333 C.mol ⁻¹)	Faraday constant
k	(cm ³ .molecule ⁻¹ .s ⁻¹)	Reaction equilibrium constant
R	(8.314 J.mol ⁻¹ .K ⁻¹)	Gas constant
PTR		Proton transfer reaction
APCI		Atmospheric pressure chemical ionisation
d-IMS		Differential ion mobility spectrometry
RIP		Reactant ion peak
PM		Protonated monomer
PBD		Proton bound dimer
PBCL		Proton bound cluster ion

Chapter 1 Introduction

1.1 Aims, Objectives and Hypothesis

The aim of this research was to characterise the gas phase ion chemistry of small aliphatic alcohols against changes in analyte concentration and ion effective temperature (combined effect of applied electric field and ion filter temperature) in differential ion mobility spectrometry (d-IMS) and to apply this technique to in-vivo monitoring and emergency medicine screening. Four aliphatic alcohols (methanol, ethanol, n-propanol and n-butanol) were chosen for study. Literature research revealed that these molecules had been observed to produce fragment ions in proton transfer reaction mass spectrometry (PTR-MS) and API-MS-MS. This led to the main hypothesis of this research. Also an ion-neutral equilibrium model was used to evaluate ion thermodynamics in a system with typical proton transfer chemistry, which assumes no fragmentation. These findings informed the construction and calibration of a new instrument and methodology to recover of alcohols from saliva, for non-invasive toxicological detection. This study was extended beyond alcohol compounds and also included ethandiol (ethylene glycol) and propandiol (propylene glycol) as well as gamma-hydroxybutyric acid (GHB).

1.1.1 *Primary hypothesis*

Alcohols generate fragment ions in d-IMS.

1.1.2 *Secondary hypothesis*

Alcohols modify their own responses

1.1.3 *Primary aim*

Describe C1 to C4 alcohol responses in d-IMS

1.1.4 *Secondary aim*

Apply these findings to develop a d-IMS methodology for alcohols in human saliva.

Table 1.1 summarises the experimental studies against research objectives.

Table 1. 1 Summary of experiments with objectives performed in this research studies together with used experimental approaches.

Exp't No.	Title	Objective	Hypothesis	Experimental Approach
1 Ion Chemistry of Alcohols				
1.1	Effect of concentration on alcohol responses	To characterise and evaluate effect of vapours concentration on d-IMS responses of alcohols: methanol, ethanol, n-propanol and n-butanol. To test an ion solvation model, to establish whether it can be used to predict clusters formation and ion kinetic of alcohols under changing concentration and effective temperature	Alpha parameter modification	1.1 Exponential dilution with d-IMS detection
1.2	Effect of ion temperature on alcohol responses	To characterise and evaluate effect of ion temperature, altered by d-IMS ion filter temperature and dispersion field	Fragmentation	1.2.1 Permeation sources with d-IMS detection 1.2.2 Exponential dilution with d-IMS/MS detection
2 Toxicity Studies				
2.1	Method development	To calibrate d-IMS responses for toxicological levels of methanol, ethanol, ethylene and propylene glycol	Sensitive resolution possible	2.1 Gas chromatography with d-IMS detection
2.3	Recovery and detection of alcohols from human saliva	Validate TD-GC-d-IMS system for recovery and detection of toxic substances from human saliva using a polydimethylsiloxane substrate.	Recovery and quantitation possible	2.2 Thermal desorption GC-d-IMS detection

1.2 Introducing Differential Mobility Spectrometry

Differential Ion Mobility Spectrometry (d-IMS) is a developing technique, working at atmospheric pressure, derived, in part, from linear ion mobility spectrometry (IMS). The technique is also called Field Asymmetric Waveform Ion Mobility (FAIMS). D-IMS is used to separate ions on the basis of non-linear relationships between an ion's velocity and the strength of the applied electric field that induces ion movement.

In this thesis, radioactive ^{63}Ni beta emitter was used as the ionisation source and nitrogen as a transport gas. Different types of ions and their clusters can be present within the system, depending on the concentration of available molecules (Section 1.5.3):

- Reactant ions (RI) are produced during the initial ionisation process of molecules present within the transport gas. In air or nitrogen the hydrated proton $(\text{H}_2\text{O})\text{H}^+$ is formed, which can be bound with other water molecules forming protonated hydrate clusters ions $(\text{H}_2\text{O})_n\text{H}^+$
- Next, as a result of proton transfer reaction or water exchange, between the RI and analyte molecules, M , product ions (PI) are formed, (MH^+) , called protonated monomers or their hydrated proton bound clusters $[(\text{H}_2\text{O})_{n-1}\text{MH}^+]$.
- Further, if the analyte concentration is high enough an analyte proton bound cluster can also be produced (M_nH^+) , often also called adducts, see Section 1.5.3.

Two fundamental d-IMS designs exist: planar [1] and cylindrical design 2. Both designs are used as standalone devices or for pre-separation in mass spectrometry (MS) [3,4,5,6]. Different commercial suppliers have adopted different nomenclatures with the result that the literature is not consistent in the terminology used. The cylindrical design is often referred to as FAIMS and the planar design d-IMS [7]; although μ -FAIMS has been adopted for a miniaturised multi-planar design. This study focuses on planar d-IMS, Figure 1.1.

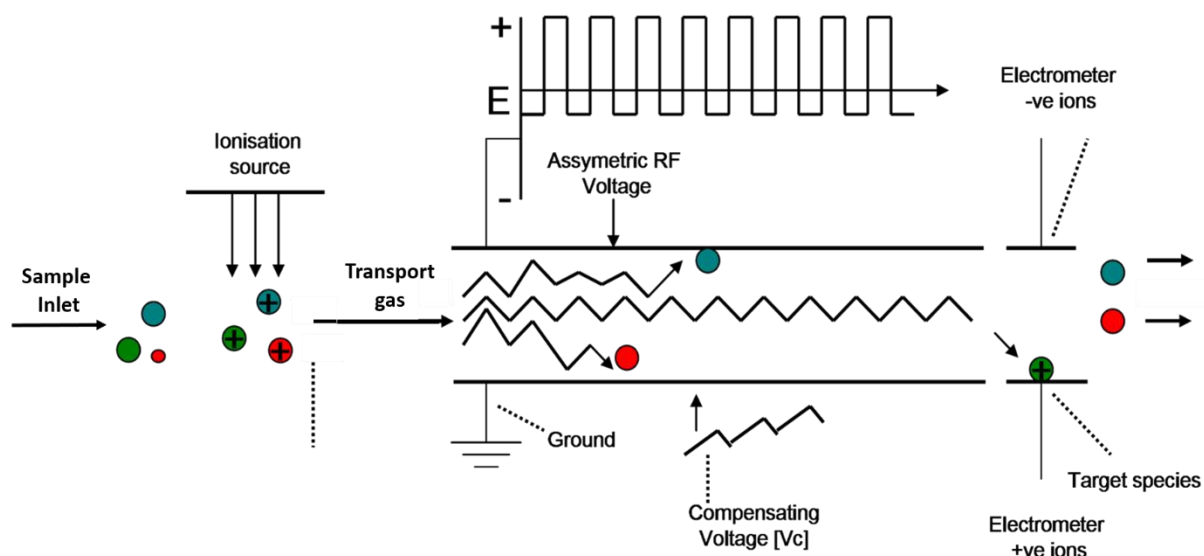


Figure 1. 1 Schematic of the functionality of a d-IMS. The application of asymmetric field (RF) allows separation of the species and a compensation voltage enables the transmission and detection of a specific ion swarm at a certain value for compensation voltage.

Sampled molecules are ionised by atmospheric pressure ionisation, and the product ions are continuously swept by a transport gas, such as air or nitrogen, between the two electrode plates of the drift-tube. During this transit the ions are subjected to a transverse oscillating asymmetric radio-frequency (RF) electric field, known as the dispersion or separation electric field (E_d). E_d is usually greater than 40 Td or 10000 V. cm^{-1} , and in planar d-IMS with a frequency between 1 MHz and 3 MHz [8]. The movement of the ions through the drift region is determined by the exact nature of the waveform of the separation field and the $\alpha(E/N)$ relationship of the ion cluster (See Equation 1.11). In general terms, the dispersion field causes the ions to be displaced perpendicularly to the transport gas flow in phase with the RF field, resulting in a specific zigzag motion. This is due to the switching polarity of the dispersion field. The mobility of the ions is different under the low and high electric field, as the ions go through constant clustering and de-clustering processes, (Section 1.4.3). A simple schematic of clustering/declustering process during the low and high part of the RF waveform is shown in Figure 1.2.

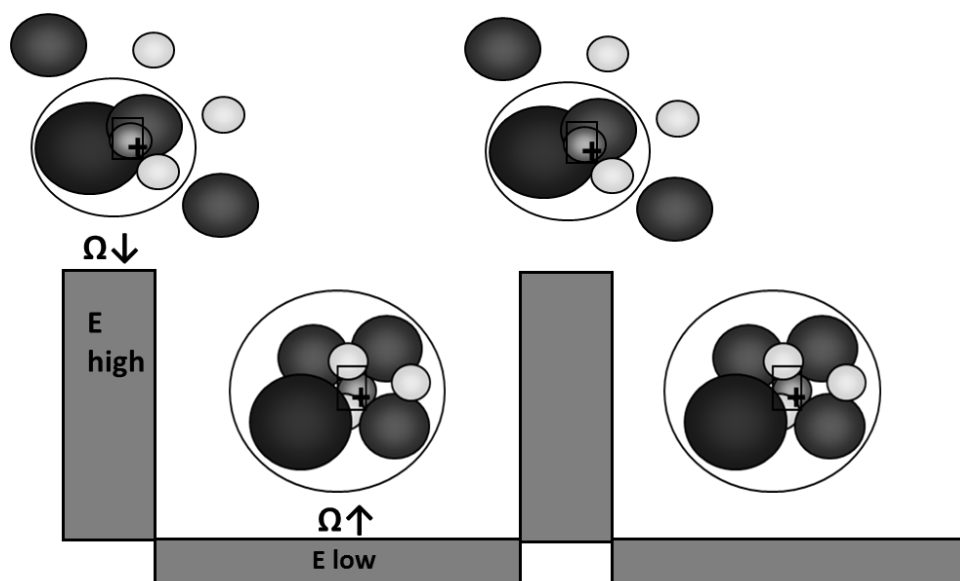


Figure 1. 2 Schematic of the clustering/declustering process under high and low part of the electric field waveform.

At low fields the ions cluster with neutral gas molecules via intramolecular forces (non-covalent interactions). The extent of this process depends on the experimental parameters temperature and pressure as well as the polarizability of the transport gas. For example helium does not form clusters at atmospheric pressure [9]. In air, hydrated proton (H_2O) H^+ will cluster with neutral water molecules present in the air mixture. The average number of clustered molecules drops from 2/3 at 87 °C to 0 at 245 °C [10]. As the temperature increases the thermal energy of the ion increases and it de-clusters reducing the energy of the ion's system. This process is repeated at the dispersion field waveform's frequency during the transit of the ion through the drift tube (on a ms scale). Clustering effects increase the difference in mobility of the ions at high and low fields and enables their separation. A graphical representation of the asymmetric waveform used in d-IMS is shown in Figure 1.3.

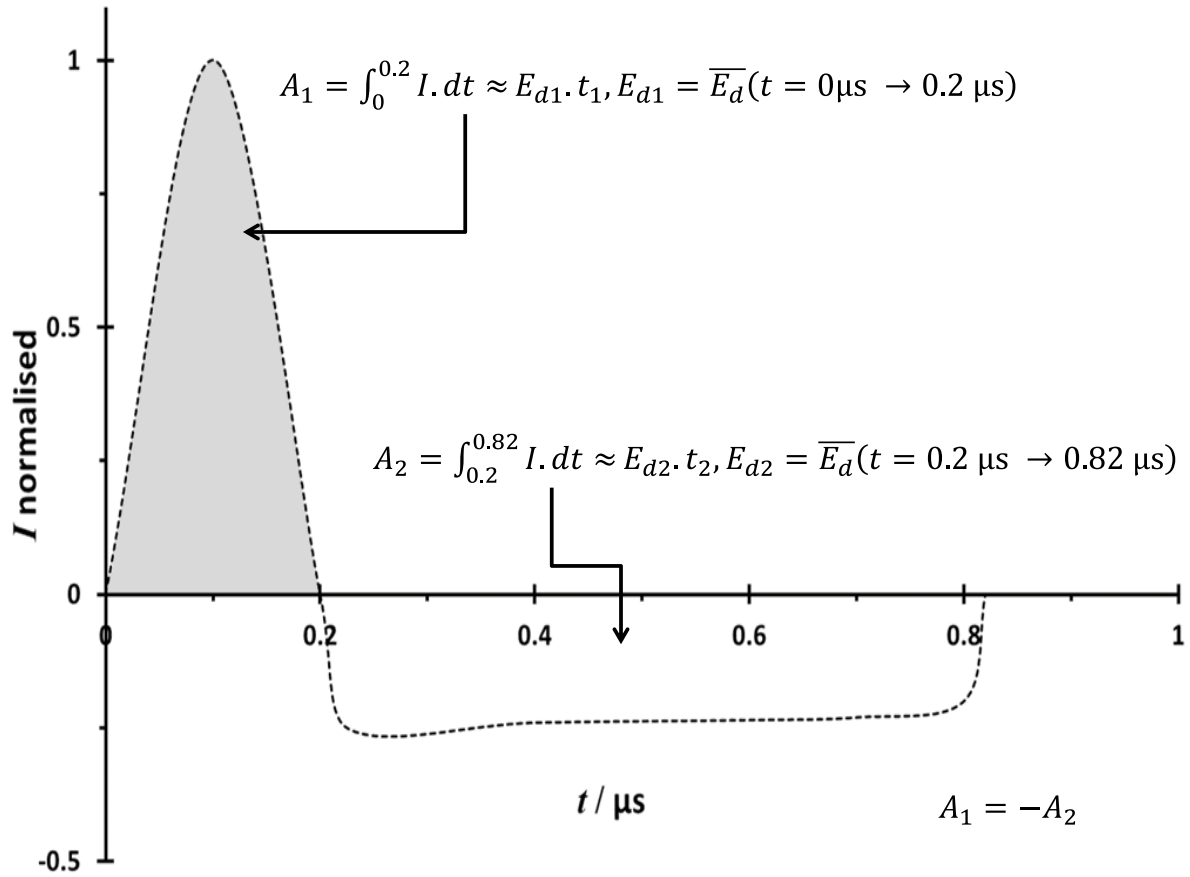


Figure 1.3 Asymmetric sinusoidal waveform of the SIONEX d-IMS SVAC operating under frequency of 1.18 MHz.

The applied asymmetric field is designed to satisfy the condition $E_{d1}t_1 = -E_{d2}t_2$, which during the complete cycle may be expressed by Equation 1.1 [11]. The waveform comprise short periods of positive E_{d1} and longer periods of E_{d2} of opposite polarity, where $E_{d2} < E_{d1}$. The velocity v_2 toward the electrode at the E_{d2} is defined in Equation 1.2, where K is mobility. From here the distance travelled (d_2) during the E_{d2} part of the waveform is shown in Equation 1.3, where t_2 is the duration of the low field. The effect of different waveforms has been studied since the creation of the technique in the 1980s and 1990s by Gorshkov, Krylov and Buryakov [12] followed by optimisation and more recent studies [13,14].

$$E_{d1}t_1 + E_{d2}t_2 = 0$$

Equation 1. 1

$$v_2 = K_2 E_{D2} \quad \text{Equation 1. 2}$$

$$d_2 = v_2 t_2 \quad \text{Equation 1. 3}$$

If an ion has a mobility which is independent of the field strength (i.e. $K(E_{d1}) = -K(E_{d2})$), the displacements during the high and low portions of the applied field will be equal, and there will be no displacement of the ion towards one of the electrodes.

$$K(E_{d1})E_{d1}t_1 + K(E_{d2}) E_{d2}t_2 = 0 \quad \text{Equation 1. 4}$$

If ion mobility significantly depends on electric field the displacement of ions during a period of the separation field will depend on the sign of mobility dependence ($\alpha(E)$, see Section 1.4.3). If $\alpha(E) > 0$, then positive ions will be displaced toward the top electrode at a distance $K(E_{d1})E_{d1}t_1 + K(E_{d2}) E_{d2}t_2 = \Delta K E_{d1} t_2$. Ions with $\alpha(E) < 0$, will be displaced in opposite direction. To stabilise the ions trajectory and allow the detection, a perpendicular secondary electric field, the compensation field (E_c), is applied. This field is imposed on the oscillating asymmetrical E_d field. The electric field conditions required to permit a particular ion to pass through the filter to reach the detector are specific to each ion species.

D-IMS can operate in two modes. When functioning as a programmable chemical filter, the E_c is fixed such that only one particular ion species is permitted to reach the detector, this increases sensitivity. Alternatively, when operating in a spectrometer mode, the E_c is scanned across a range of fields to allow various ions of interest to pass to the detectors. The time for ions to reach the detector is in magnitude of ms, depending on the length of the ion-filter and flow of the transport gas. The typical transport gas flow rate is between 300 and 500 ml.min⁻¹.

The central point in the operation of d-IMS involves the changes in the collision cross section of the ion clusters via the clustering/declustering mechanism, induced by frequently switching between low and high electric fields. The separation of ion clusters via clustering/declustering in d-IMS may be influenced by temperature, strength of the applied electric field, analyte concentration and the concentration of neutrals in the

surrounding atmosphere (known as the transport gas); this influences the alpha parameter within ion mobility equation (Section 1.4.3, Equation 1.11). The properties of the transport gas can be influenced by adding small polar molecules, called gas modifiers at elevated concentration levels (usually between 0.1% to 1.5%) which affects the clustering behaviour. Another way to manipulate responses in d-IMS is by the introduction of chemicals, called dopants, which alter the ionisation process and formation of product ions, by using differences in proton affinity between a dopant and an analyte.

1.3 Alcohol Toxicity

Alcohols analysis is of ongoing interest due to the high toxicity of those compounds. Improvement in speed and limit of detection for real life application in emergency medicine and monitoring exposure levels in surrounding environment is sought. Alcohol toxicity results in significant human morbidity and mortality with high economic and social costs. The abundance of alcohols and their easy availability as common solvents, as components of many household and commercial formulations, and in the case of ethanol as beverages, make them readily available with a high risk for exposure at dangerous levels. According to World Health Organisation (WHO) harmful use of alcohol causes approximately 3.3 million deaths, globally each year (5.9% of all deaths) and 5.1% of the global burden of disease is attributed to alcohol consumption [15]. 6,592 and 88,000 people died from alcohol toxicity in the UK and US, in 2013 and 2009 respectively [16,17] and 2.5% were due to acute poisoning.

1.3.1 Methanol

Methanol is associated with episodic poisoning outbreaks occurring worldwide [18,19,20]. Typical methanol intoxication is a result of oral ingestion of poorly purified or adulterated ethanol based beverages.

Ingested methanol reaches its maximum blood concentration 30 to 90 min after ingestion [21]. Methanol is primarily metabolized in the liver via alcohol dehydrogenase into formaldehyde. Formaldehyde is subsequently metabolized via enzyme aldehyde dehydrogenase into formic acid, which ultimately is metabolized to carbon dioxide, and water (Figure 1.4) [22]. It is the formic acid which is mostly responsible for the toxic effects of methanol poisoning.

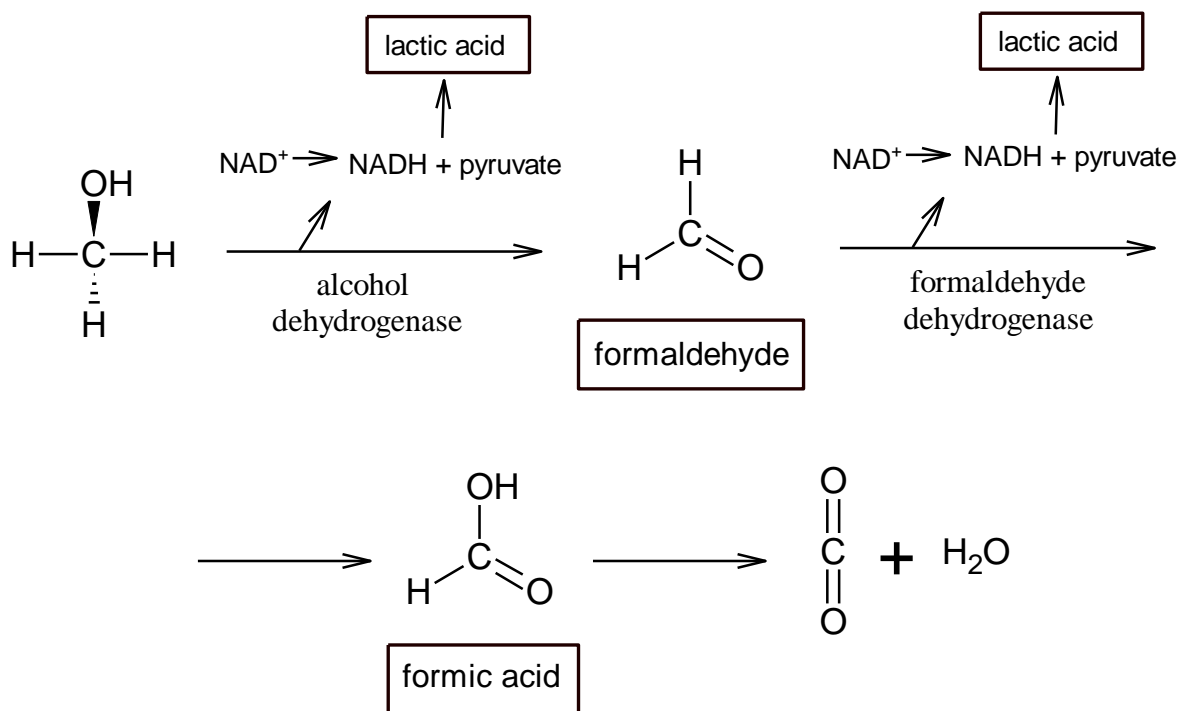


Figure 1.4 Scheme for the metabolism of methanol, where process of converting the toxic formic acid to carbon dioxide and water is slow in human, causing poisoning.

The acid causes metabolic acidosis due to: formic acid production; and, indirectly through acidic metabolites, such as lactic acid, produced from an increased NADH/NAD⁺ ratio from mitochondrial dysfunction. The acidosis from acidic metabolites exacerbates the formic acid toxicity due to the lower dissociation of formic acid and its resultant higher diffusion across cell membranes to produce more intracellular effects, causing the osmotic gap to fall and the anion gap rises. The toxicological effects from acidosis and neurosis include: blindness, coma and convulsions [23,24], in severe cases multi-organ failure and death [25, 21]. A small portion of methanol is excreted unchanged by the lungs without much of the toxicological effects. Although toxicity primarily occurs from oral ingestion, it can also occur from prolonged inhalation or skin absorption [26,27,28]. See Summary Table 1.2 for sources, toxicological levels and effects.

1.3.2 Ethanol

Ethanol is rapidly absorbed across digestive system, reaching a peak blood concentration 20-60 minutes after ingestion, 80% of ethanol passes through the liver to be detoxified. Toxic effects come directly from ethanol (by binding to brain and other receptors (especially GABA - neurotransmitter gamma-aminobutyric acid) and its metabolic product, toxic acetaldehyde (responsible for hangover symptoms) and

increased NADH/NAD⁺ coenzymes ratio [29]. Figure 1.5 illustrates a simple schematic of one of the roads for its metabolic process.

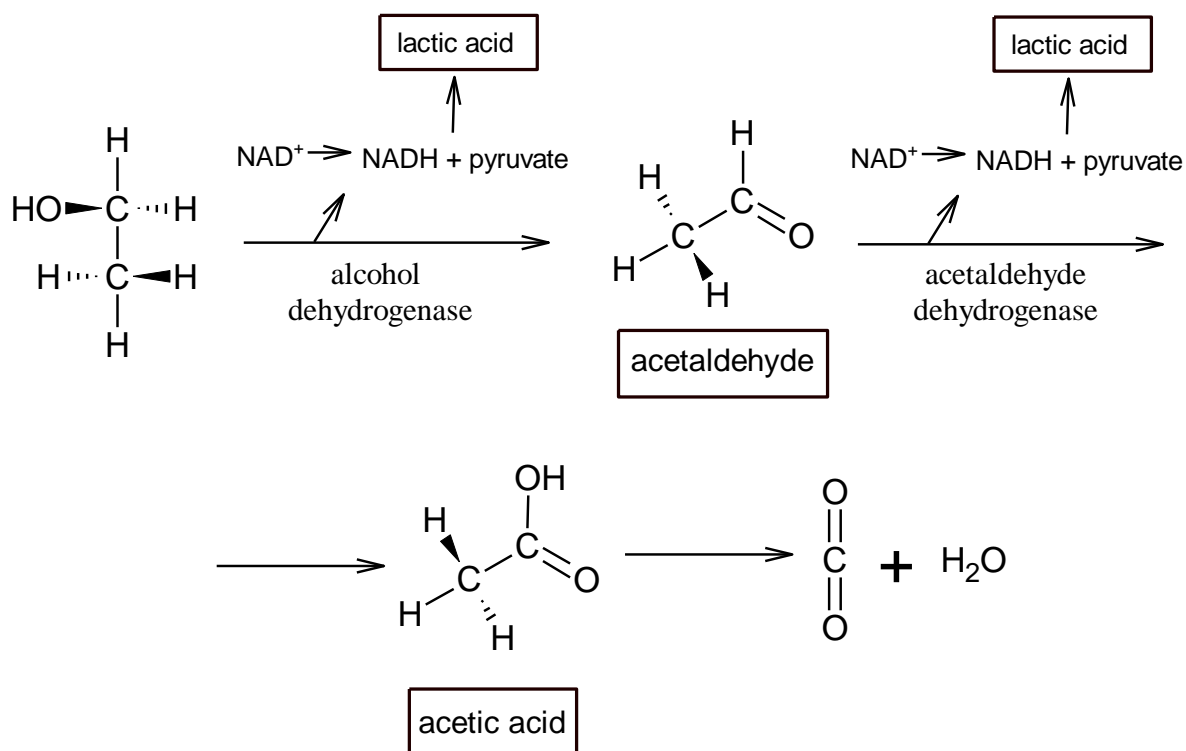


Figure 1.5 Scheme for the metabolism of ethanol in humans, with production of toxic metabolic products, mainly of acetaldehyde.

Ethanol debilitating effects in acute poisoning begin with degraded speech and motor skills [30] mild metabolic acidosis, vomiting, seizures, arrhythmia in severe cases cardiovascular collapse, permanent brain damage, coma and in some cases sudden death [31,32]. With chronic use it progresses to Alcoholic Liver Disease (ALD) (by prolonged expose to acetaldehyde) which is a spectrum of disease states that includes steatosis (fatty liver), steatohepatitis, and in severe cases, fibrosis and/or cirrhosis and death [33,34,35].

Number of deaths from accidental alcohol poisoning in England reached 157 in 2007 [36]. Estimated cost of ethanol misuse for the NHS in the UK amounts to £3.5 Billion yr⁻¹ (equivalent to £120 yr⁻¹ for every taxpayer) and £1 Billion yr⁻¹ is spent on providing accident and emergency services [38, 36]. Another impact of alcohol toxicity, with complex social implications, is a chronic alcoholism associate with ethanol-dependency. Debilitating progressive effects manifest themselves in employment and family care settings long before the individual experiences degraded motor skills, damaged liver function, and eventually death [37, 33, 34].

1.3.3 *n-Propanol*

1-Propanol is rapidly absorbed and distributed throughout the body following ingestion, reaching maximum concentration within 60 minutes. 1-Propanol is metabolized by alcohol dehydrogenase to propionic acid [38]. The relative affinity of ADH for 1-propanol is much higher than that of ethanol; therefore 1-propanol is rapidly eliminated from the organism. There is only one death reported related to acute poisoning from 1-propanol, which suggests low toxicity of the compound. In the case reported, it was recorded that a woman was found unconscious and died 4 - 5 h after ingestion [39]. Autopsy revealed a "swollen brain" and lung oedema. In a study group of 12 volunteers, erythema lasting for at least 60 min was observed in 9 individuals following a 5-min application of filter papers containing 0.025 ml of a 75% solution of 1-propanol in water on the forearms [40]. Reproductive and developmental toxicity studies found exposures of 7000 to 10,000 ppm 7 hours per day caused maternal toxicity and reduced mean body weights [41]. No other reports on human health effects following exposure to 1-propanol are available.

1.3.4 *Isopropanol*

Isopropanol is rapidly absorbed when ingested, and reaches a peak concentration approximately 30-120 minutes after ingestion. 20 to 40% of an absorbed dose is excreted unchanged to urine and saliva. Isopropanol is primarily metabolized via alcohol dehydrogenase to acetone, which is probably further metabolized to acetic acid and finally carbon dioxide and water [42,43]. The peak concentration of acetone is not present until approximately 4 hours after ingestion. Isopropanol position on the scale of toxicity lies between methanol and ethanol (due to toxicity of its metabolic product, acetone) the acetone produces CNS depressant effects and a fruity odour on the breath [44]. Other effects include: liver, kidney and cardiovascular depression, brain damage and in some cases death [45,46]. The Occupational Safety and Health Administration (OSHA) standards require that an employee's exposure to isopropyl alcohol not exceed an 8hrs TWA (time-weighted average) of 400 ppm in the working atmosphere in any 8 hours shift of a 40 hrs workweek [47]. Accidental ingestion of liquids containing high percentages of iso-propanol alcohol has been reported for children [48] and deliberate ingestion by adults, and young-adults in their teenage years, produces intoxication effects similar to ethanol [49,50].

Some concern has been expressed for the welfare of personnel in closed living quarters, such as spacecraft or submarines, from prolonged exposure to sub-clinical concentrations of iso-propanol with a risk of diminished performance in critical skills where sterile wipes for drawing blood samples are used frequently. Discussions at the conferences of the International Society of Ion Mobility Spectrometry revealed that the determination of alcohols on-board the International Space Station (ISS) by the Air Quality Monitor, a hyphenated and thoroughly integrated GC-d-IMS instrument [51] was problematic, and that further studies might be of benefit in this area.

As this research also sought to inform the development of acute-toxicity screening for simple diols (ethylene and propylene glycols) and γ -hydroxybutyric acid, within critical or emergency care medicine.

1.3.5 Ethylene Glycol

Ethylene glycol itself is nontoxic, but it is metabolized into toxic compounds. When ingested, is absorbed rapidly and peak concentrations are observed 1-4 hours after ingestion. Ethylene glycol is first oxidized into glycoaldehyde, which then undergoes metabolism changes to glycolic acid, glyoxalic acid, and oxalic acid (Figure 1.6) [52]. These four metabolites are responsible for the compound's major toxic effects which include tissue destruction, primarily from calcium oxalate tissue deposition and severe metabolic acidosis, primarily from the accumulation of glycolic acid. Lactic acid contributes to a lesser degree via the promotion of lactic acid formation due to reduced NAD/NADH ratios and hypocalcaemia [53,54], further affects the central nervous system, then the heart and the kidneys [55,56, 57].

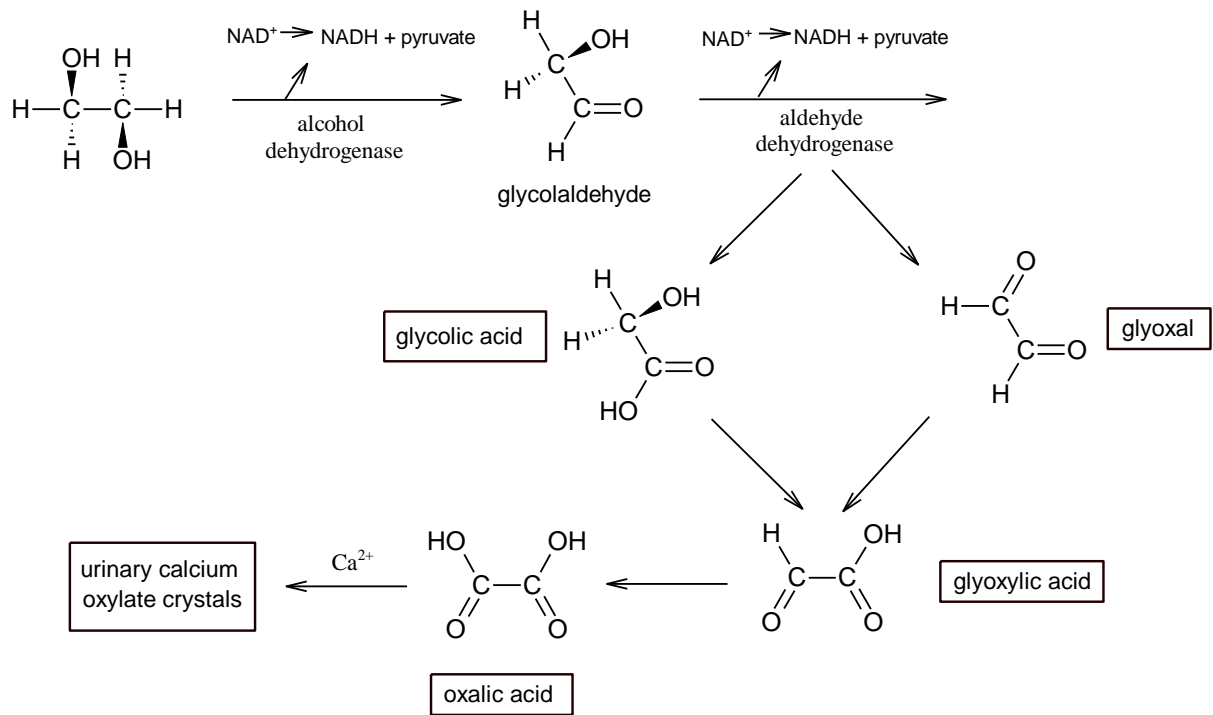


Figure 1. 6 Scheme for the metabolism of ethylene glycol, with production of toxic metabolites: glycolaldehyde, which then undergoes metabolism changes to glycolic acid, glyoxalic acid, and oxalic acid.

Table 1. 2 Summary of alcohols sources, their toxic metabolites, toxicological levels and effects [58].

Compound	Sources of exposure	Toxic effect on human	Toxic metabolite	[ROH _T] : [ROH _F]
Methanol	Common solvent and reactant in chemical reactions, antifreeze, canned heating fuel, printing inks, fuels as an octane boosting additive, fuel cells, paint removers, varnish, headlamps	Metabolic acidosis, blindness, and neurological impairments such as blindness, coma and convulsions [23,24], multi-organ failure and death [18,25]. Toxicity, primarily occurs from oral ingestion, it can also occur from prolonged inhalation or skin absorption [26,27,28].	Formic acid	200 / 890
Ethanol	Common solvent and reactant in chemical reactions, alcoholic beverages, mouthwash, hand sanitizers perfumes cough syrups	Degraded motor skills [30] (ethanol and acetaldehyde) progress to liver damage (NADH) [32] and in prolonged or acute poisonings (NADH, binded ethanol) to coma and death [31, 34].	Acetaldehyde	800 / 3500
Iso-propanol	Common solvent reactant in production of acetone and other chemicals, inks, coatings, cosmetics, as rubbing alcohol, foam inhibitor and deicing agent, antiseptic products	Central nervous system CNS depressant, drunk like effect of reduced motor skills, liver, kidney and cardiovascular depression, brain damage and in some cases death [45,46].	Acetone	400 / 1500
Ethylene glycol	lacquers and resins, coolants and heat transfer fluids, adhesives	Tissue destruction, severe metabolic acidosis, hypocalcemia [53,54], further affects the central nervous system, then the heart and the kidneys [55,56,57].	oxalic acid	1200 / 2000-4000

[ROH_T], blood alcohol concentration at which toxic effects are likely to be observed / mg.L⁻¹

[ROH_F], blood alcohol concentration at which fatal effect is likely to be observed / mg.L⁻¹

1.4 IMS and d-IMS Theory

Ion Mobility Spectrometry (IMS) is a technique, which separates ions based on the differences in their velocity in an electric field, in general at atmospheric pressure. Typically, ions are pulsed into a flight-tube (ion filter) under a homogeneous electric field and their flight-times are recorded. The time-of-flight is inversely related to the mobility of an ion. Ions are separated according to their mobility through the gas under low field conditions ($E < 1000 \text{ V.cm}^{-1}$). Differential ion mobility spectrometry (d-IMS), also known as field asymmetric ion mobility spectrometry (FAIMS) differs from IMS in the geometry of the ion filter and the ion separation mechanism. In d-IMS ions are separated through the non-linear dependence of their mobility in an oscillating radiofrequency electric field, also called dispersion or separation field (Section 1.2).

1.4.1 History of IMS and d-IMS

The fundamentals of IMS date from the late 19th century with Thomson's studies on ionised air via X-ray radiation. This discovery was followed by further explorations on ion behaviour in the gas phase and the development of apparatus that ultimately reached its modern form as an ion separation and characterisation technique in the 1970s, where the separation was based on differences in ions mobility under applied electrostatic field, at atmospheric pressure. The theory and technology of IMS has been described extensively in the literature [59] and its "sister" technique d-IMS, has been described as an evolved form of IMS [1,60].

After the discovery of X-rays in 1895 [61] and the conductivity of air due to the formation of ions from the exposure to X-rays led to Rutherford's and Thomson's studies of the mobility of ions in respect to the applied electric field at low field conditions in the early 1900s [62,63]. They described how the velocity of ions was proportional to the electric-field strength; the fundamental relationship of Ion Mobility Spectrometry Equation 1.5

$$V_d = KE \quad \text{Equation 1.5}$$

Note: V_d : ion drift velocity (cm.s^{-1}); K : mobility in ($\text{cm}^2.\text{V}^{-1}.\text{s}^{-1}$); E : electric field strength (V.cm^{-1}).

They obtained data for the velocity of ions in low electric field for vapours of air, chlorine, coal gas, hydrogen, sulphured nitrogen and mercury. Further experiments allowed the

measurements of the mass to charge ratio. The apparatus used in those experiments was a Crookes tube, or ray tube, which generated a stream of electrons. The basic features of the device are shown in the diagram below (Figure 1.7).

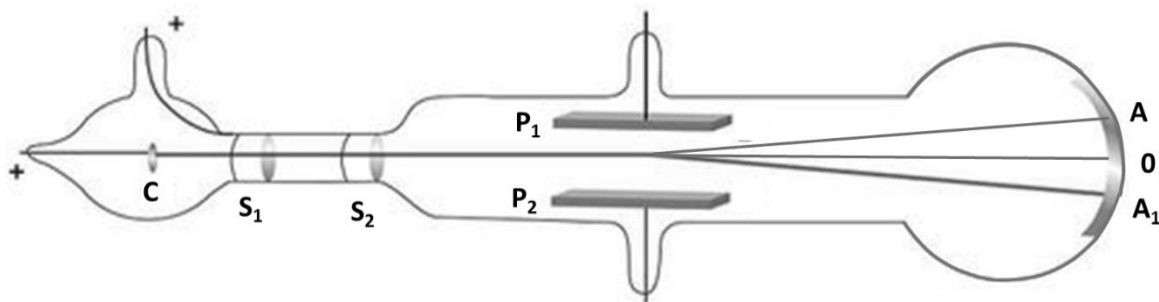


Figure 1. 7 Crookes tube used by Thomson, by which he observed the deflection of cathode rays by an electric field (and later measured their mass to charge ratio).

Electrons were emitted from the cathode (C) and accelerated toward the anodes (S_1 and S_2) by the electric field. Some of the electrons passed through slits in the anodes, forming a narrow beam. When the electrons reached the end of the tube (point O) they strike a fluorescent coating, causing it to glow. By applying a potential difference between a pair of parallel metal plates (P_1 and P_2) the rays were subject to deflection (path to point A). Instead of an electric field, a magnetic field was also used to deflect ions. In this case, the magnetic field was produced by two electromagnets (not shown on the diagram) and was oriented perpendicular to both the beam and the electric field, causing the beam to be deflected in the opposite direction (A_1). Thomson used electric and magnetic fields simultaneously, to exert force on and deflect the electron beam as it passed through the tube. By balancing the forces, he was able to calculate velocities, as well as a mass to charge ratio of the electron. In 1905 Langevin reported the individual velocities of ions in a weak electric field [64]. In doing so, an essential step in analytical IMS was demonstrated with the construction of a functional instrument, similar to the modern day drift-tube. Further, the collisional nature of mobility, and the role of attractive forces in effective collision cross-sections was noted with a preliminary description of ion-molecule interactions and its effect on mobility. IMS was developed in a systematic manner over the next 40 years resulting in 1938 in A.M.Tyndall's publication "The mobility of positive ions in gases" [65]. This noted the effect of pressure and temperature on ion mobility and the proportional relationship of ion velocity to electric field strength and pressure. The formation of ion clusters was becoming better

characterised especially the effect of cross-sectional area on ion mobility with Lattey's studies of ions in dried gases leading to the proposal that a layer of molecules surrounded the ions [66]. This was based on the finding that the velocity of negative ions were particularly dependent on moisture level at trace levels. One of the first practical uses of those discoveries was demonstrated by James Lovelock who studied ion detection in ambient conditions with a device that could be used to indicate trace levels of airborne vapour concentrations of organic vapours released by industry. The device was later distributed as the electron capture detector (ECD) used to make the first measurements of chlorofluorocarbons (CFC's) and their effect upon ozone which exists in the stratified regions of the Earth's atmosphere [67]. The association between IMS and ECD is that both techniques share common principles of gas composition and ionisation chemistry at atmospheric pressure.

In the 1960's Earl McDaniel and Edward Mason published an important book "The mobility and diffusion of ions in gases" [68] in which studies of interactions between small ions and molecules such as Ar or CO₂ using a drift-tube based on electrically isolated rings under low pressure were described. This work was undertaken mostly under a vacuum and resulted in models of interaction potential that became the basis for modern IMS drift-tubes development. In 1970 Karasek and Cohen demonstrated the first ion drift spectrometer under the name of "plasma chromatography" [69,70], which later was renamed an ion mobility spectrometer.

Development of the d-IMS technology started in Russia in the early 80's and the first studies were published in English by Buryakov in 1993 [1] showing the differential mobility spectra of a homologous series of tertiary amine ions in atmospheric air. The simplicity and size of this device was striking consisting of two parallel plates with dimensions of 0.5 cm x 1.5 cm, separated by a 0.5 mm gap; the first planar differential ion mobility spectrometer.

The demonstration of those two drift spectrometers initiated the era of exploration of ion and differential mobility spectrometry and the emergence of new analytical tools.

1.4.2 Fundamentals of mobility of ions in gas-phase

The motion of an ion through gas at ambient pressure is affected by multiple factors, and undoubtedly, the strongest factor is the electric field strength, Equation 1.5.

Other forces which influence the transport of ions through the drift-tube are the diffusive force, described by first Fick's Law (Equation 1.6), and electrostatic interactions between ions and transport gas molecule (ion-dipole interactions).

$$J = -D \frac{\delta C_{(x,t)}}{\delta x} \quad \text{Equation 1. 6}$$

Note: J : flux ($\text{g.cm}^{-2}.\text{s}^{-1}$); D : diffusion coefficient ($\text{cm}^2.\text{s}^{-1}$); $\frac{\delta C_{(x,t)}}{\delta x}$: concentration gradient (g.cm^{-2}).

The reason why ions have different mobilities is due to differences in their structures. A version of the Mason-Schamp equation (Equation 1.7) describes mobility in relation to the structural parameters of the species [71]

$$K = \frac{3ze}{16N} \times \sqrt{\frac{2\pi}{\mu k_B T_{eff}}} \times \frac{1}{\Omega} \quad \text{Equation 1. 7}$$

Note: z : ion charge; e : electronic charge; N : gas density number (mol.cm^{-3}); μ : reduced mass of ion (kg); Ω : cross sectional area of ion cluster (cm^2); T_{eff} : effective temperature (K); k_B : Boltzmann's constant ($1.380 \times 10^{-23} \text{ m}^2.\text{kg}.\text{s}^{-2}.\text{K}^{-1}$).

and

$$\mu = \frac{mM}{m+M}$$

where m is mass of the ion and M is a mass of drift gas molecules (kg).

The Mason-Schamp equation was recognized to only hold true for ion behaviour under the low field conditions, present in typical IMS (electric field E usually $< 1000 \text{ V.cm}^{-2}$, or reduced electric field (E/N) of $< 2 \text{ Td}$ [72]) treating K as a constant value.

It is important to note that in context of ion transport properties of gases, the electric field E is rarely used as such. Instead, reduced electric field (E/N) expression is used, the field normalized to the drift gas molecular density, N , since most transport properties scale in this quantity. The unit of (E/N) is Townsend Td (1 Td equals 10^{-17} V.cm^2).

The relationship, shown in Equation 1.7 does not describe fully the behaviour of ions in d-IMS where they are subjected to ion heating with electric field strengths as high as 200 Td and more [73].

T_{eff} , parameter in Equation 1.7, is a measure of the internal energy of ions moving through an electric field and can be simplistically understood as a sum of the temperature of the ions in the surrounding transport gas molecules (thermal temperature) and change in temperature gained from field heating, as shown in Equation 1.8.

$$T_{eff} = T + \Delta T_{field} \quad \text{Equation 1. 8}$$

The concept and theory of the T_{eff} has been developed for the drifting of monoatomic ions through gases under the influence of electric fields [68]. The effective temperature T_{eff} of a monatomic ion moving under the influence of a uniform electric field E through a monatomic gas is given by Equation 1.9 which defines T_{eff} for the use in calculations of mobility coefficient, K , in linear IMS (Equation 1.7)

$$\frac{3}{2} k_B T_{eff} = \frac{3}{2} k_B T + \frac{1}{2} M v_d^2 (1 + \beta) \quad \text{Equation 1. 9}$$

Note: T : drift gas temperature (K); M : mass of the drift gas molecule (g.mol⁻¹); v_d : drift velocity (cm.s⁻¹); β : small dimensionless correction factor, calculated from ion-neutral interaction potentials.

In linear IMS, the heat from the field is insignificant in comparison to thermal energy so by neglecting the small correction factor β , the second term of Equation 1.9 is reduced. In effect the T_{eff} is equal to the gas bath temperature (T).

In d-IMS where fields reach maximum amplitude as high as 200 Td and ions oscillate in the high and low fields for different durations [74,75,8], the second term describing the field heating, in Equation 1.9 becomes significant. Krylov and co-workers modified this Equation by introducing a factor ζ (≤ 1), a dimensionless factor which reduces the contribution of electric field to the effective temperature and acknowledges that not all the field energy is converted to the energy of ion motion through a bath gas [76]. From an examination of temperature effects on the differential mobility of a variety of ions, ζ

was found to be different for different ions and also to vary with transport gas temperature as shown in Equation 1.10.

$$\frac{3}{2}k_B T_{eff}^k = \frac{3}{2}k_B T + \frac{1}{2}\zeta M v_d^2 \quad \text{Equation 1. 10}$$

1.4.3 Effect of electric field on mobility in d-IMS

The value of the mobility coefficient, K , under high-field conditions is no longer constant. It becomes field dependent, and is a function of the reduced electric field strength. An ion's mobility under constant temperature and pressure, can be approximated by a sum of even powers of E/N and is described in Equation 1.11 [77,78].

$$K\left(\frac{E}{N}\right) = K_0 \left[1 + \alpha \left(\frac{E}{N}\right)\right] = K_0 \left[1 + \sum_{n=1}^{\infty} \alpha_{2n} \left(\frac{E}{N}\right)^{2n}\right] \quad \text{Equation 1. 11}$$

Note: K_0 : mobility coefficient under zero field conditions; α : alpha parameter, describing the dependence of ion mobility on E/N

Alphas are reported in units of Td^{-2n} and have no further physical meaning [79]. The alpha parameter is individual for each ion specie and describes a change in trajectory of the ions under specified d-IMS conditions, observed on the compensation field E_c scale. Its value can be positive, when ion coefficient mobility increases with increasing E/N or can be negative, when mobility decreases with increasing values of E/N .

Increasing E/N results in a difference between the high-field mobility (K) and K_0 and three types of ion behaviour are observed, Figure 1.8 [80]. Type A is caused by a positive alpha value ($\alpha > 0$) with mobility increasing with increasing E/N . Type C is caused by a negative alpha value ($\alpha < 0$) with mobility decreasing with E/N . Type B behaviour is more complex with an initial rise in the alpha value to a maximum followed by a decrease with E/N .

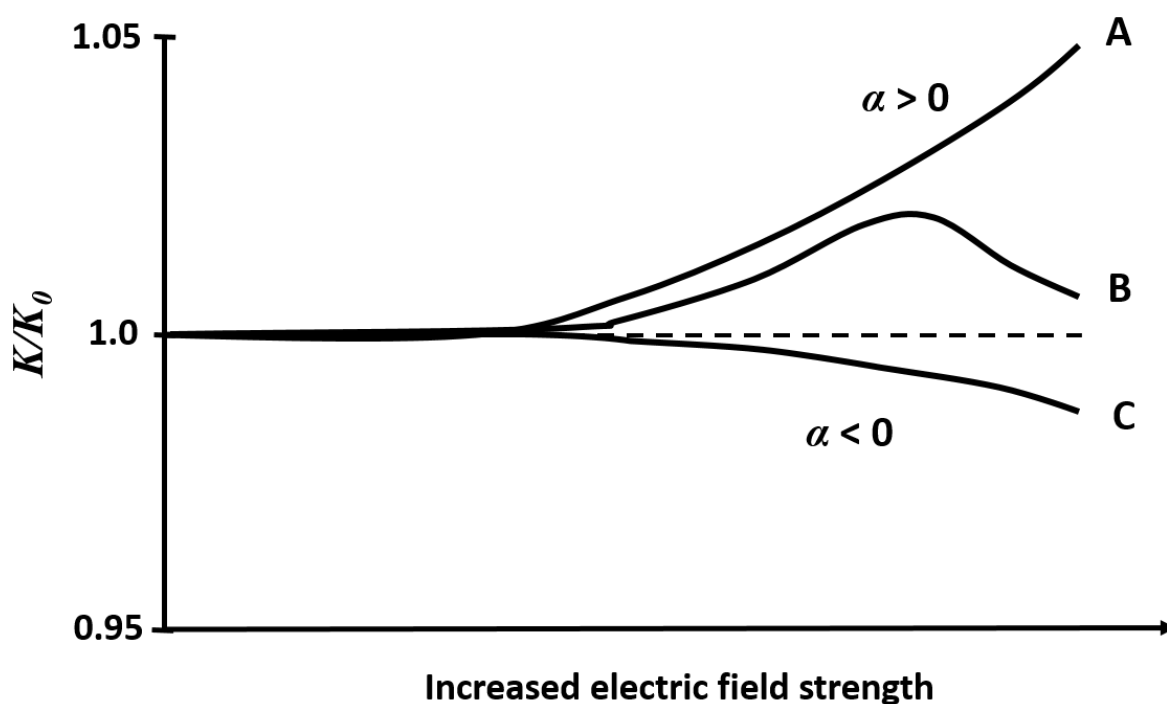


Figure 1.8 Three main profiles of ion-mobility dependence on the electric field [80].

The changes in the alpha function are physically observed in the d-IMS Spectra as changes in dispersion behaviour of ions and their position at the E_c scale. An investigation of the alpha-function for a homologous series of ketones, demonstrated that protonated monomer (PM) product ions exhibited positive alpha-function with mobility increasing with increased electric field. In contrast proton bound dimers mostly showed negative alpha and the opposite trend (Figure 1.9) [81].

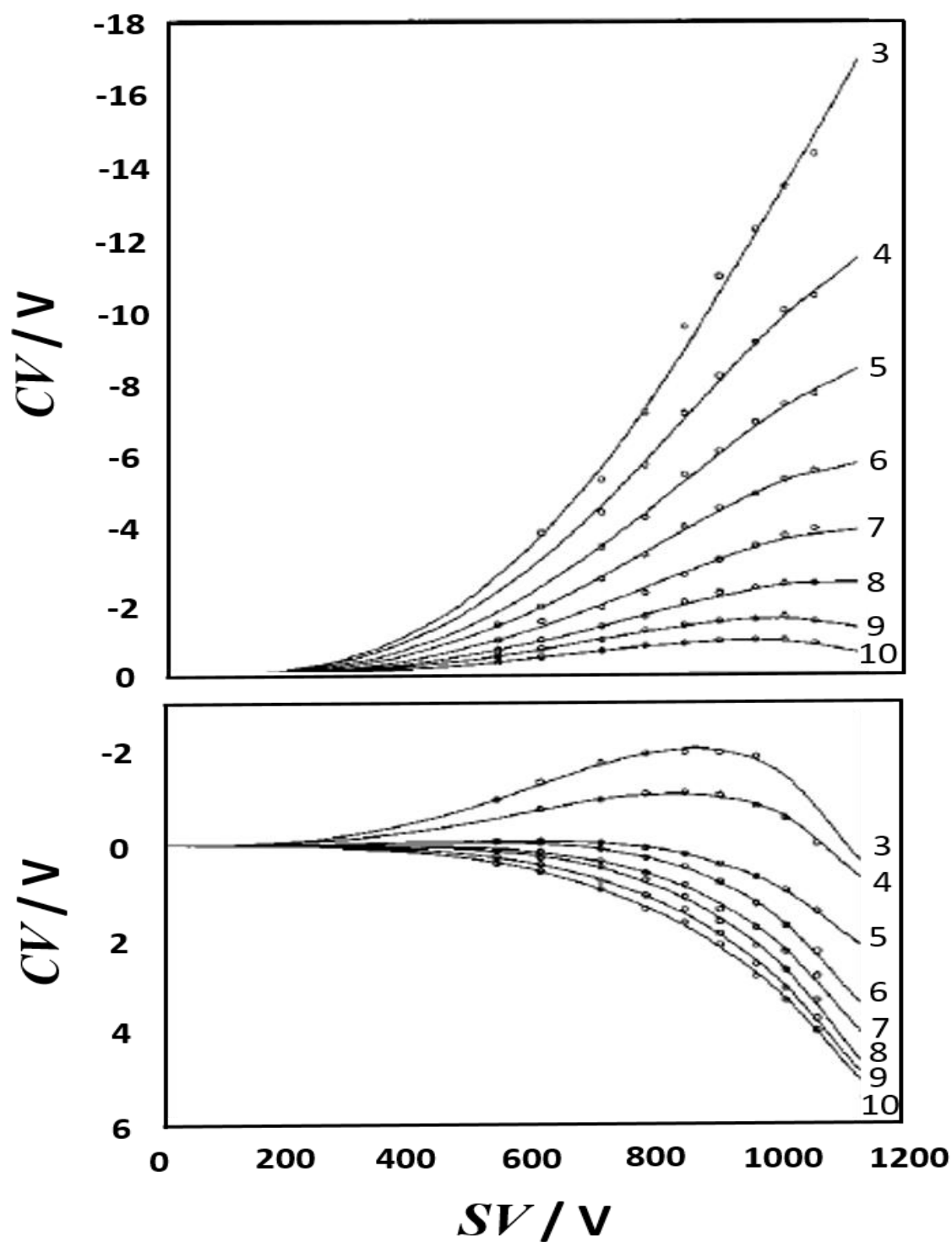


Figure 1. 9 Plots of compensation voltage (CV) versus amplitude of separation voltage (SV) for series of ketones ($R-CO-R'$) in air containing 0.1 ppm moisture as a supporting atmosphere top) for protonated monomers bottom) for proton bound dimers. Note: numbers from 3 to 10 on the right hand side of graphs relate to ketone carbon number [81]. Figure adapted with permission of the ACS.

Note: Authors often, use direct values of applied electric potential in V or electric field in $V.cm^{-2}$ and original units of reference material is presented, when graphics are used.

The ketone study demonstrated that a single type of ion may exhibit a wide range of mobility behaviours with a changing electrical field and such differences may be attributed to changes in the structure of the ion. Specifically, these phenomena may be explained by invoking clustering by an induced dipole moment in the molecules and rigid sphere theory.

The reduced electric field (E/N) affects the effective temperature (T_{eff}) of the ion and its extent of the clustering with neutrals. At low-fields the product ion, clusters with neutral molecules from the surrounding atmosphere (for example with water molecules, producing ion hydrates), through non-covalent interactions. Increasing the electrical field increases T_{eff} of the ion (parameter in 1 of mobility coefficient), causing energetic destabilisation of the ion cluster that results in dissociation (de-solvate). In effect the cross-section (CCS) of the clustered or de-clustered ions differs as well as its reduced mass (parameter Ω and μ in Equation 1.7, respectively) resulting in changes in mobility K , and a positive alpha trend, as seen in Figure 1.9 (top) for protonated monomers of ketones. The relative difference in Ω and μ will be more significant for the ions of smaller mass giving rise to a larger alpha-function [82]. The situation looks different in case of proton bound dimers of ketones (Figure 1.9 bottom), where with increased E/N mobility K decreases, showing negative alpha function. This is consistent with the rigid sphere model, explained by increase in collision frequency with neutrals as field or temperature increases. At high field strengths, the ions are accelerated more strongly by the field between collisions with drift gas molecules. This means that the resulting collisions are more energetic, and more energy is transferred to the drift gas molecules. This in turn increases the drift gas temperature, meaning the drift gas molecules are moving faster, and are therefore more likely to collide with ions, lowering the ions' mobility. This effect is more potent with increased mass of the ketone and the effect of increased mobility becomes less influential.

The clustering/declustering mechanism (Section 1.2, Figure 1.2) has been exploited to enhance the separation of ions in d-IMS and FAIMS by altering the surrounding gas atmosphere with additional neutral molecules (called gas modifiers), which increases the size of the formed clusters, in effect increases the difference in mobility of ion clusters at high and low electric fields.

Other aspects which influence changes in mobility of the ions under changes of electric fields are:

- Field-Induced structural changes: an example of that are proteins which tend to unfold under high field conditions [83]. In some cases, fragmentation of the ions may be possible [84] resulting in new ion species with increased or decreased collision cross-section, lowering or raising its mobility respectively.
- Orientation of ions with field: In low electric field conditions, the orientation of ions will be random, so their effective collision cross-section will be the average of their cross-sections in all possible orientations. In high fields, on the other hand, any ions with a permanent dipole will preferentially align along the direction of the field, and the cross-section in that orientation will determine their mobility [85].

1.4.4 Effect of temperature and pressure on d-IMS responses

Temperature is an important factor in the identification and quantification of reactant and product ions in mobility measurements, and at the same time is one of the most significant variable factors in IMS/d-IMS measurements. The effect of the temperature on ion behaviour has been introduced above (Sections 1.4.2 and 1.4.3) and in d-IMS the effects are more complicated.

Temperature affects the ion mobility in two ways. Temperature changes gas density, N , and hence the value of E/N and the field contribution to ion kinetic energy, which directly affects mobility of the ion (Equation 1.11) in a non-linear manner. In addition, gas temperature changes the ion and neutral kinetic energy distributions and hence changes the distribution of ion-neutral collision energies, what in effect may cause dissociation of the product ion and in extreme cases fragmentation.

Changes in pressure directly influence number of gas density in (E/N) parameter in mobility Equation 1.11, as it can be expressed as $N = P/kT$. Therefore, the mobility of ions can be influenced independently by electric field or gas pressure through the ratio of E/N . In practice, d-IMS operates under close to ambient pressure, meaning that pressure effects are not often a significant consideration.

In the study on d-IMS responses of methyl salicylate [76] a temperature and pressure were used as parameters to optimise a d-IMS response with respect to product ion resolution. Significant effect on the compensation field values were observed, with

changing temperature from 25 to 150 °C (Figure 1.10). The effect of pressure, within 0.42 to 1.1 Atm, showed small effect on the position of ions on the compensation field scale, but affected the width and intensity of the ion signal.

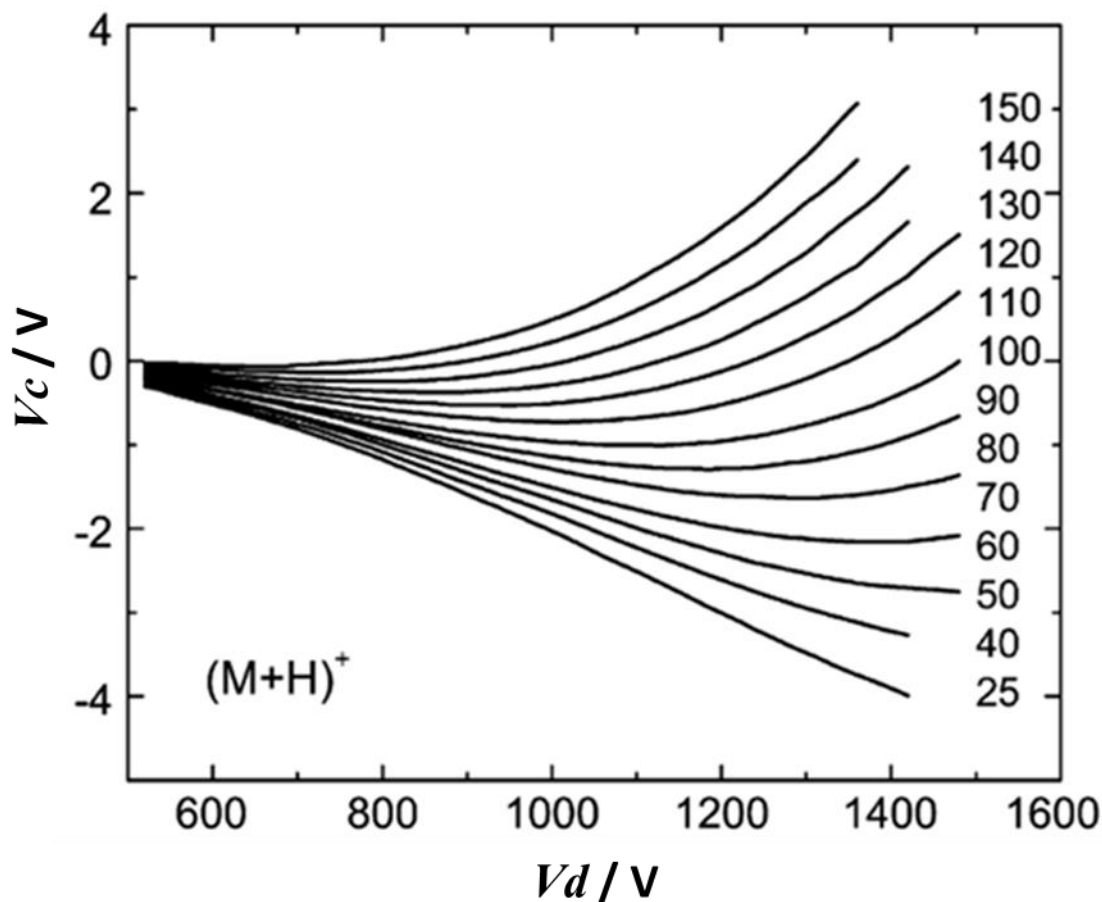


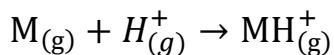
Figure 1. 10 Compensation voltage V_c vs. dispersion voltage V_d for methyl salicylate d-IMS responses for temperatures from 25 °C to 150 °C [76]. Figure adapted with permission of Elsevier.

Also, it was shown that the small differences in ion compensation field scale position, caused by pressure difference can be simplified by expressing both compensation and dispersion fields in Townsend units for (E/N) [76].

1.5 Ion Processes

1.5.1 Proton and electron affinity

The proton affinity (PA) is a measure of gas phase basicity and is defined as a change in enthalpy (ΔH) for reaction between a proton (hydrogen) and a molecule M , as shown in Equation 1.12.



Equation 1. 12

Because this reaction is hypothetically always exothermic, the ΔH has a negative value (Equation 1.13) and PA is reported as a negative of ΔH in kJ.mol^{-1}

$$PA = -\Delta H$$

Equation 1. 13

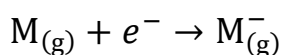
The higher the proton affinity, the stronger the base and the weaker the conjugate acid in the gas phase. Proton affinity is a deciding factor in proton transfer reactions, which is a basic mechanism in formation of positive product ions in ion mobility spectrometry.

PA relates to the gas phase basicity ($\Delta_{base}G$), and represent a willingness of the molecule to accept the proton and is a negative Gibbs free energy for the same reaction. The two are related via Equation 1.14, where T is a temperature in Kelvin and ΔS ($\text{kJ.K}^{-1}\text{.mol}^{-1}$) is a change in entropy in the reaction.

$$\Delta_{base}G = PA + T\Delta S$$

Equation 1. 14

The electron affinity (EA) is the energy released when a neutral molecule, M , in the gas phase gains an extra electron to form an anion, as in the reaction shown in Equation 1.15.



Equation 1. 15

The process has a negative change in the enthalpy and EA (kJ.mol^{-1}) is reported as opposite to that (Equation 1.16)

$$EA = -\Delta H$$

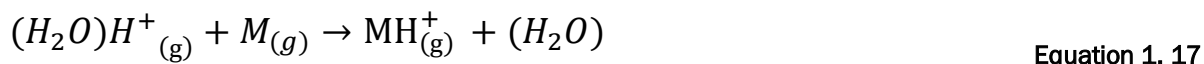
Equation 1. 16

The higher the electron affinity, the stronger the acid and the weaker the conjugate base in the gas phase.

Proton and electron affinities are defined for individual molecule at given temperature, usually 298 K.

1.5.2 Proton transfer reaction

Proton transfer to a molecule M is defined by reaction shown by Equation 1.12. In IMS and d-IMS most often the hydronium ion $(H_2O)H^+$ is used as reactant ion (RI) for the proton transfer reaction, which is a form of a Brønsted acid (AH^+) and a donor of the proton. Further reaction between the donor can occur with analyte molecule M as in Equation 1.17,



The change of the enthalpy for this reaction is shown in Equation 1.18.

$$\Delta H = PA_{(H_2O)} - PA_{(M)} \quad \text{Equation 1. 18}$$

In almost all practical cases, the proton transfer process represented in this reaction will be thermodynamically allowed (spontaneous) if the proton affinity of acceptor M is greater than that of proton donor $(H_2O)H^+$. By accepting protons, reactant M is acting as base. If the compound M has a basicity ($\Delta_{base}G$), above that of the donor then ΔG is negative, making reaction thermodynamically favoured, shifting equilibrium toward the product. The Gibbs energy change for reaction shown in Equation 1.18, can be expressed as in Equation 1.19

$$\Delta G_T^0 = \Delta G_{[O+H^+ \rightarrow (H_2O)H^+]} - \Delta G_{[M+H^+ \rightarrow MH^+]} \quad \text{Equation 1. 19}$$

where T refers to temperature in K and the 0 refers to the standard state.

Gas-phase basicities can be used to determine the spontaneity of a particular proton transfer reaction, but it is more common to make use of proton affinity instead. The relationship between the two has already been described above in Equation 1.14.

Studies of proton transfer reactions in the gas phase started in the second half of the twentieth century, with the development of spectrometric techniques such as infrared [86] nuclear magnetic resonance (NMR) [87], and mass spectrometry (MS) [88]. Studies initially covered kinetics and thermodynamics of the gas phase reactions [89,90], and

later has been applied to the monitoring and detection of various organic compounds in the gas phase, such as VOCs [91].

1.5.3 Atmospheric pressure chemical ionisation and ion formation





Atmospheric pressure ionisation (API) was originally applied to describe the process of chemical ionisation at atmospheric pressure and is now applied more broadly to describe any of several methods for generating ions at atmospheric pressure. This type of ionisation method is referred to as a soft ionisation method, in which molecular ions are formed. Such chemical ionization reactions near 1 atmosphere, occur with near-thermal electrons or low-energy solvated protons which usually result in negligible product ion fragmentation.

One of the earliest API methods was atmospheric pressure chemical ionisation (APCI) and was investigated by Evan Horning and co-workers who started with the consideration that “the yield of a gas-phase reaction does not depend only on the partial pressure of the two reactants, but also on the total pressure of the reaction environment” [92]. The assumption was that an increase in pressure would increase ion production rates and consequently increase the sensitivity of a detector.

During chemical ionisation (CI) the production of acidic or basic species in the gas-phase takes place, which react with gas-phase neutral analyte molecules (M) to yield either cations or anions. In APCI sources this happens under atmospheric pressure.

The generation of the ionised species requires an ionisation source and a variety of approaches have been described including: α and β emitters such as Americium (^{241}Am) [93], Tritium (^3T) [94] and Nickel (^{63}Ni) [95]; UV photo-ionisation [96]; pulsed and continuous corona discharge [97,98] electrospray ionisation [99] and distributed plasma ionisation [100]. Some of the basic features of ionisation sources are included in Table 1.3.

Table 1.3 Ionisation techniques used in IMS and d-IMS devices.

Source	Maintenance	Cost	Comments
Radioactive		£	Licensing required
Corona discharge		££	Maintenance required
Photoionisation		££	Low efficiency, gas is exposed to short wave UV irradiation
Electrospray		££	Long cleaning times

1.5.3.1 Formation of reactant ions with ^{63}Ni in nitrogen or air

In this thesis, radioactive ^{63}Ni beta emitter was used as the ionisation source, which is one of the most common sources used in IMS and d-IMS devices. The formation of reactant ions (RI) in ^{63}Ni source is discussed below.

An electron emitted from conventional Ni^{63} source has an average energy of 17keV, which in pure nitrogen or air (most common transport gases used in IMS, also used in this research), generates positively charged nitrogen cation radical as shown in Equation 1.20 [11]



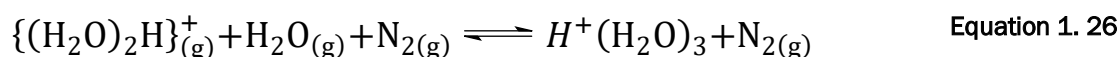
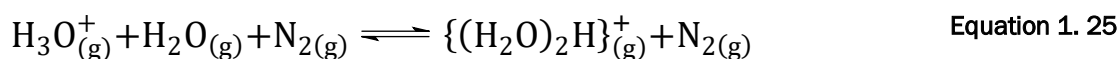
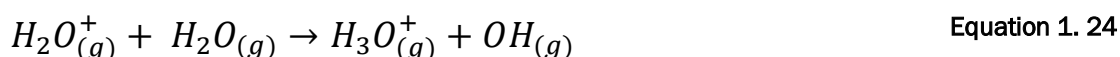
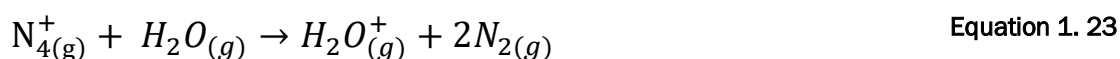
and through three body (Z) collisions [101] (which energetically stabilise the product) oxygen anion (O_2^{-}) can be formed as in Equation 1.21.



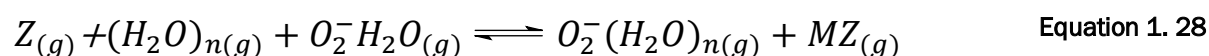
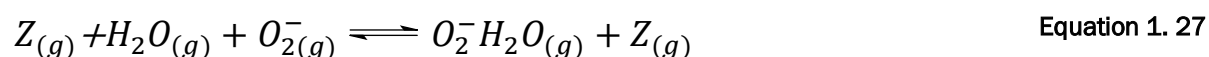
The secondary electrons (Equation 1.20) are energetic enough to ionise subsequent nitrogen molecules, and the ejected electrons will continue to yield ionisation products as long as their energy is higher than the ionisation potential of N_2 .

$\text{N}_{2(\text{g})}^{+}$ will undergo a sequence of ion-molecule reactions with other nitrogen molecules (Equation 1.22). The product of this reaction will finally react with water molecules resulting in the formation of hydrated protons (reactant-ions) through mechanism seen in Equation 1.23 and Equation 1.24. In gaseous atmospheric pressure conditions, the product ions are liable to form clusters due to large number of collisions, low ion energies and relatively high neutral vapour densities, so depending on the water concentration dimer and trimer ions can be formed (Equation 1.25 and Equation 1.26). For the hydrated bound clusters to be formed, they need to be stabilised by collision with a neutral molecule. The reaction is termed a three body reaction, and allows the ion to be 'cooled' from the excessive energy of the excited intermediate state via redistribution of that energy across the ion and neutral body.

It is important to explain that in clean air or nitrogen supporting atmosphere, hydrated protons, $H^+(H_2O)_n$, are the main ions present in ion source. This is how the positive ions are formed.



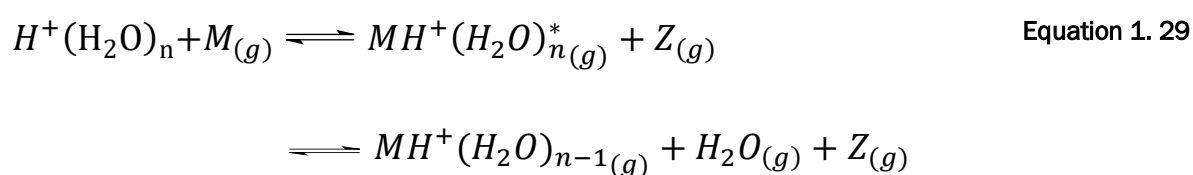
Negative ion formation from collision with electron depends on the energy of the electron and electronegativity of the analyte molecule. The thermalized electrons produced in the cascade of reactions with nitrogen, can be captured by oxygen as shown in Equation 1.21, and yielding negative reactant-ions as shown in Equation 1.27 and Equation 1.28,



where Z is a neutral: O_2 , H_2O , or other neutral molecule, which provides stabilisation in the electron capturing by collision process. "Only a few substances are known to capture (or attach) low energy electrons directly, to form negative ions, Even in these cases the attachment process is relatively inefficient" [102], due to instability of the intermediate product, which often have excess of energy in its excited form and by dissociation may cause recombination. The collision with a third body, works by distributing this energy and cooling the ion.

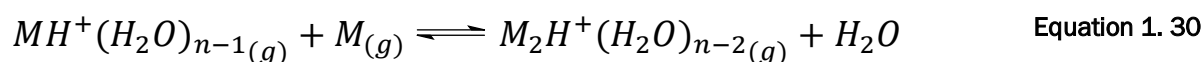
1.5.3.2 Positive-ion reactions

The most commonly used proton donor in proton transfer reaction, hence in positive polarity of IMS and d-IMS, is the hydrated proton, $H^+(H_2O)_n$ (as shown in Equation 1.26) which undergo collisions with analyte molecules (M) in the reaction region of an ion-mobility spectrometer. If a compound, M , is introduced into the reaction region with a residence time long enough for a collision with a reactant-ion to occur, then the proton transfer takes place between the ionised reagent gas and the M as per Equation 1.29. This can also be understood as a water-based displacement reaction [103].



Where, $MH^+(H_2O)_n^*$ is an electrically excited intermediate adduct ion, which may be stabilised by a third body, Z . The complex $(MH^+(H_2O)_n^*)^*$ contains all the energy of association between ion and molecule, some of which must be lost if a stable complex is to be formed. At atmospheric pressure this occurs by collision with neutral Z , to form stable product-ions capable of traversing the drift-tube.

This is a form of proton transfer reaction, in which, M with a higher proton affinity (PA) than the existing hydronium cluster $H^+(H_2O)_n$, acquires the ionic charge, with the displacement of a molecule of water. The rate of the product formation is determined by the concentration of reagent ions (RI), $H^+(H_2O)_n$ and analyte, M . If concentration of M is increased, the RI will be depleted due to increased charge-transfer toward the product. With further increase of M , then the product $MH^+(H_2O)_{n-1(g)}$ can cluster with another molecule M , forming a proton bound cluster complex as shown in Equation 1.30 [104].



Presence of proton bound dimer cluster (also called adduct) $M_2H^+(H_2O)_{n-2(g)}$ (where $n-2$ maybe equal to 0) further reduces the RI and protonated monomer peak intensities, and leads to the presence of a dimer peak in the spectrum [59,105]. As the concentration reach critical level, the rate of RI removal is greater than the rate of

formation and the product ion (PI) responses are no longer linear in relation to concentration. Beyond this level a logarithmic relationship is observed [59].

Proton affinity (*PA*) is used to predict the formation of product ions (PI) and due to relatively low *PA* of water molecule, many organic compounds can be ionised by APCI. The best available value for the proton affinity of water is $691 \pm 3 \text{ kJ.mol}^{-1}$, which is lower than those of most of organic compounds, with the exception of some of the aliphatic hydrocarbons and halo-alkanes. Below, a schematic of relationship between proton affinity and efficiency of the ionisation process is shown (Figure 1.11).

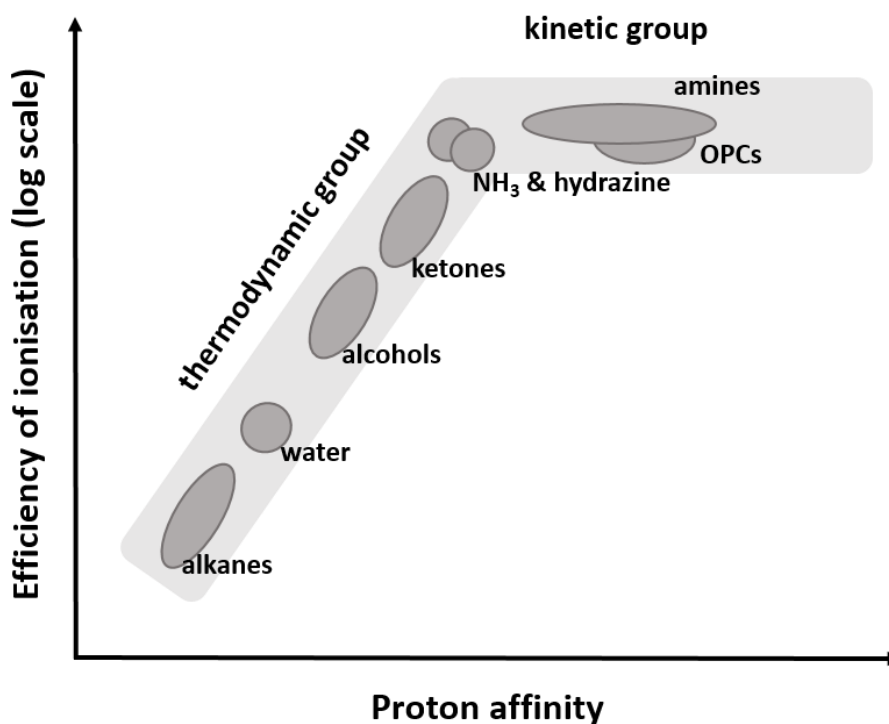
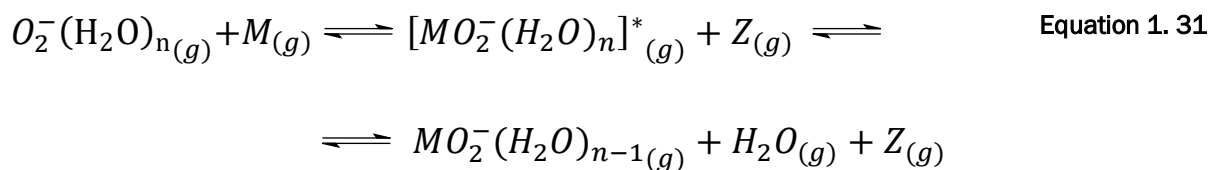


Figure 1. 11 General relationship between proton affinity and efficiency of ionisation process. Adapted from Puton et. al [106] with permission of Elsevier.

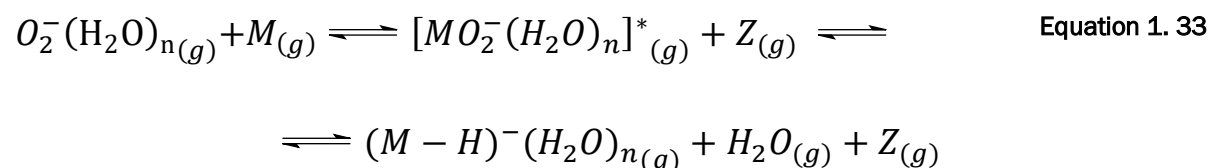
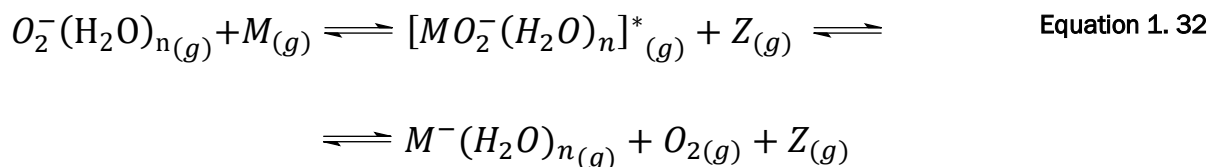
1.5.3.3 Negative-ion reaction

The hydrated adduct $O_2^-(H_2O)_n$ shown in Equation 1.28 is a main reactant ion (RI) in negative polarity, when clean air is used. The negative RI chemistry forms an intermediate adduct/cluster ion as the first step and with the further collision with the third body, *Z*, stable hydrated oxygen adduct/cluster ion can be formed (Equation 1.31) [107].



Other common reaction mechanism to generate negative-polarity IMS responses are:

- the charge transfer, with a molecule with a higher electron affinity (*EA*) than the hydrated oxygen cluster (Equation 1.32), and
- the release of protons from the existing hydrated cluster (Equation 1.33) also called proton abstraction.



1.6 Moisture, Dopants and Gas Modifiers in d-IMS

Mobility of ions can be influenced by different mechanisms, such as changing transport gas [108] moisture level [1,109] or gas composition. This section will focus on research done on altering d-IMS responses via clustering/declustering mechanism and altering ionisation process.

1.6.1 Humidity effect on d-IMS

Moisture in d-IMS increases the change in mobilities (ΔK) for an analyte between the high and low fields, by altering the degree of clustering and improving separation. This was first observed in early research of Buryakov [1] and then explored by Krylova and Eiceman in a study on organophosphorous compounds [109]. Increasing the humidity in the transport gas has been shown to change the alpha parameter of organophosphorous compounds at the level starting from around 50ppm (Figure 1.12). The study explained

the mechanism of this effect, based on clustering/declustering in d-IMS and the resulting alpha parameter in the mobility Equation 1.11. This is only valid if there is sufficient time under the low field condition for the ion to collide with a neutral solvent molecule. The level of 50ppm moisture is shown to be at the lower limit, with enough neutrals for the 1st successful collision during 0.6 μ s of low field period in air at ambient pressure. At elevated moisture levels the number of collisions will increase exponentially. The effect of mass of the analytes has also been shown to be consistent with the model, in which ions with the lower masses (e.g. trimethyl phosphate TMP) were affected to larger degree than those of the bigger ions (e.g. tri-n-butyl phosphate - TBP), supporting the clustering/declustering theory.

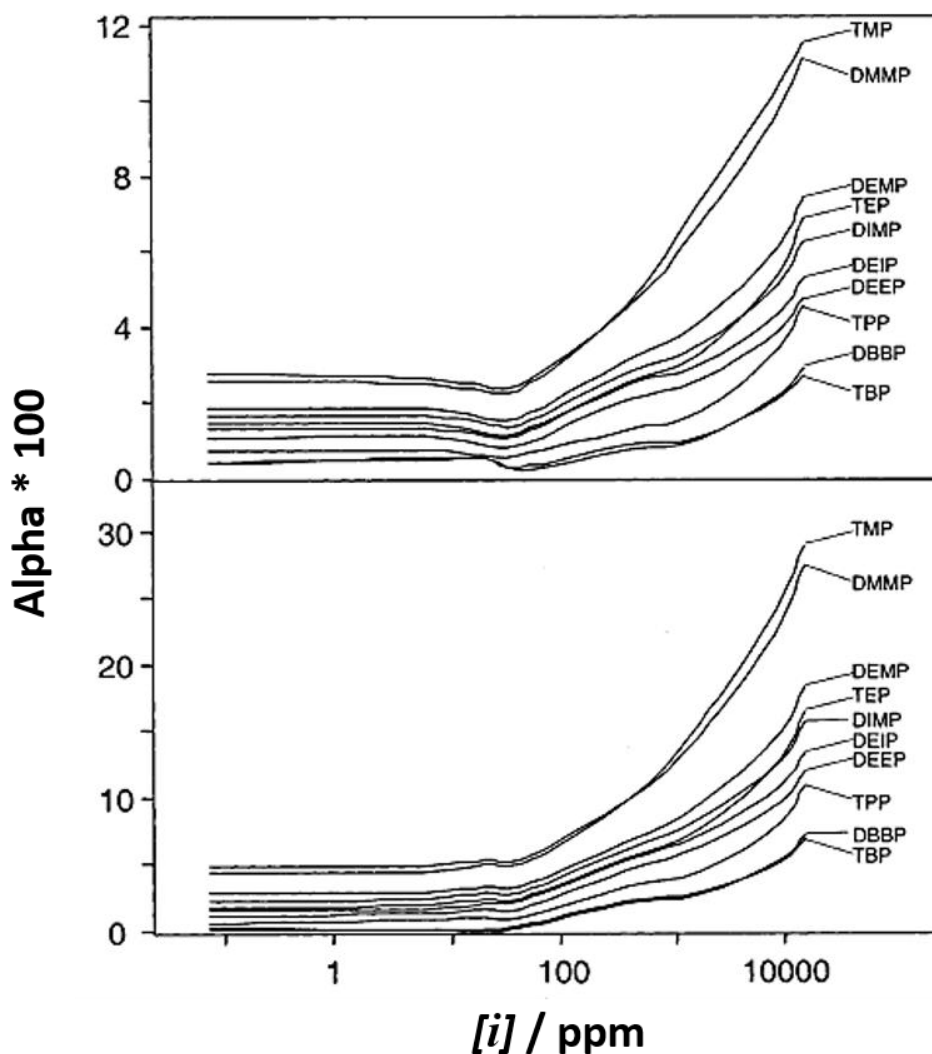


Figure 1. 12 Plot presenting effect of moisture on alpha parameter of organophosphorus compounds at field of 80 Td (top) and 140 Td (bottom) [109]. Graph adapted from Krylova et. al with permission of the ACS.

This effect is different to that observed in linear IMS applications, where increased humidity lowers the resolution in IMS spectra [110].

1.6.2 Gas modifiers

The addition of small neutral gas phase molecules to the transport gas of IMS and d-IMS has been observed to improve separation [111,71]. The mechanism is similar to the moisture effect (Section 1.6.1). The process happens by formation of ion-molecule clusters via non-covalent hydrogen bonding or Van der Waals interactions; a central element in ion separation in ion mobility in general and d-IMS in particular. This increases the CCS of the clustered ions under low field conditions and increases the difference between clustered and declustered ion. This was demonstrated initially, by Eiceman et. al. in the studies on the effect of moisture (described in the previous section [109]) in d-IMS and then extended to different additives. Vapours of water, acetone, methylene chloride, and propanol were used as modifiers in the drift gas in the studies on the field mobility dependence of the ions from twelve explosives in the negative mode of the d-IMS. Figure 1.13 represents example of the explosives responses without and with use of the methylene chloride in air, showing alternation of the responses observed of the compensation voltage scale.

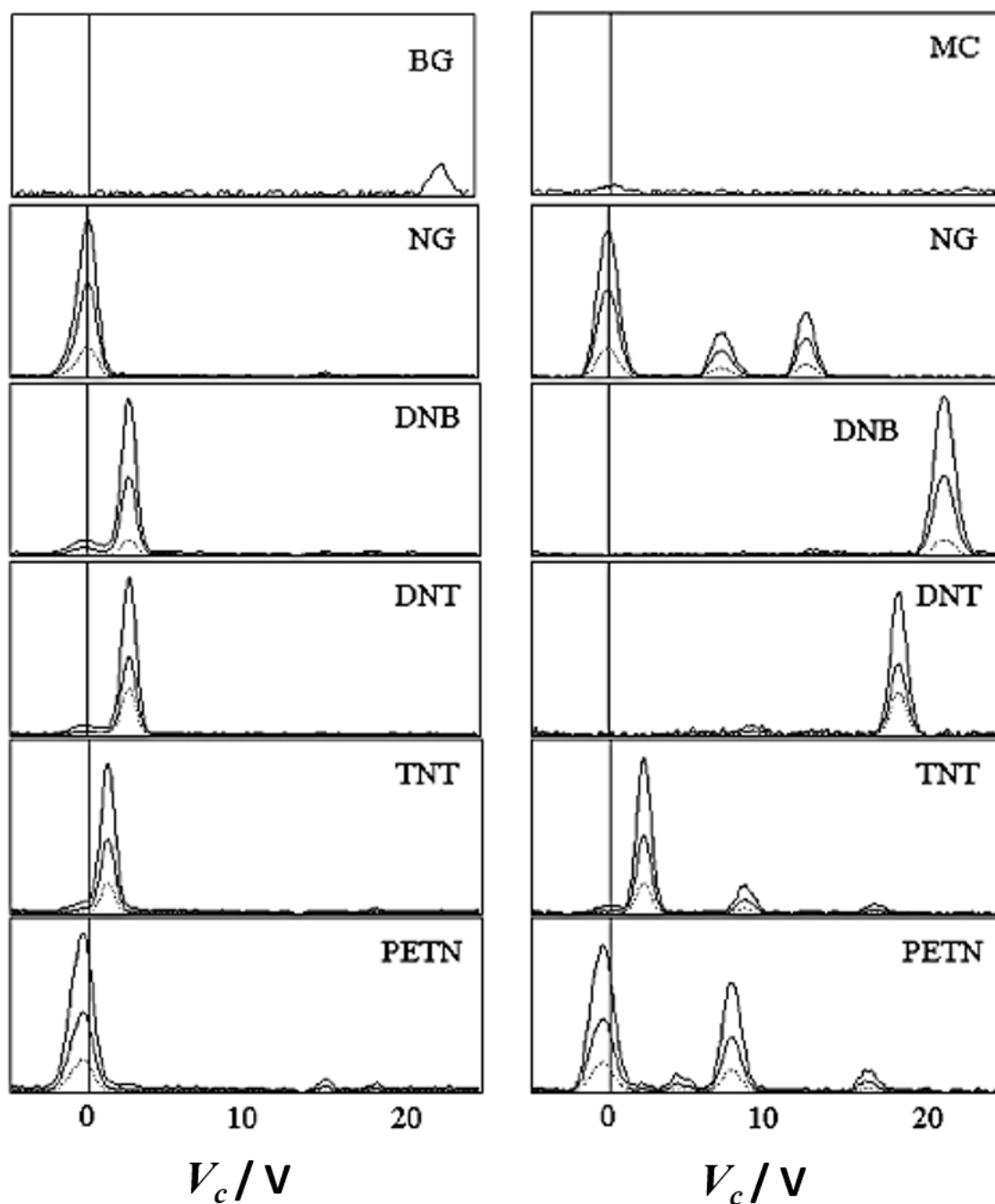


Figure 1. 13 Differential mobility spectra of the explosives in pure air (left) and 1000 ppm of methylene chloride in air (right). Explosives are from top: background spectrum; 1,2,3-propanetriol, trinitrate (NG); 1,3-dinitrobenzene (DNB); 2,6-dinitrotoluene (DNT); 2,4,6-trinitrotoluene (TNT); pentaerythritol, tetranitrate (PETN) [111]. Figure implemented from Eiceman et. al. with permission of the ACS Publications.

Impressive work was presented by Nazarov et. al [112] in a comprehensive study on gas modifiers and their effect on the large sample mixture of approximately 140 different chemicals with molecular mass selected to cover a large part of the chemical space. D-IMS separations were compared for a number of transport gas compositions including

pure nitrogen, nitrogen/helium mixtures and mixtures with added nonpolar and polar chemical modifiers. In the absence of modifiers, the bulk of ion species peaks were spread over a narrow region of V_c between 0 and 20 V. Dramatic improvement of ions separation was observed in case of using polar modifiers at the concentration level above 1000 ppm. All component peaks were shifted toward more negative V_c values. Example of the result is presented in Figure 1.14, when 1.5% isopropanol was used as a modifier. The Figure shows d-IMS responses for the mixture of 140 compounds with and without presence of the isopropanol in the transport gas. Conversely, there was little or no improvement when non-polar modifiers were used.

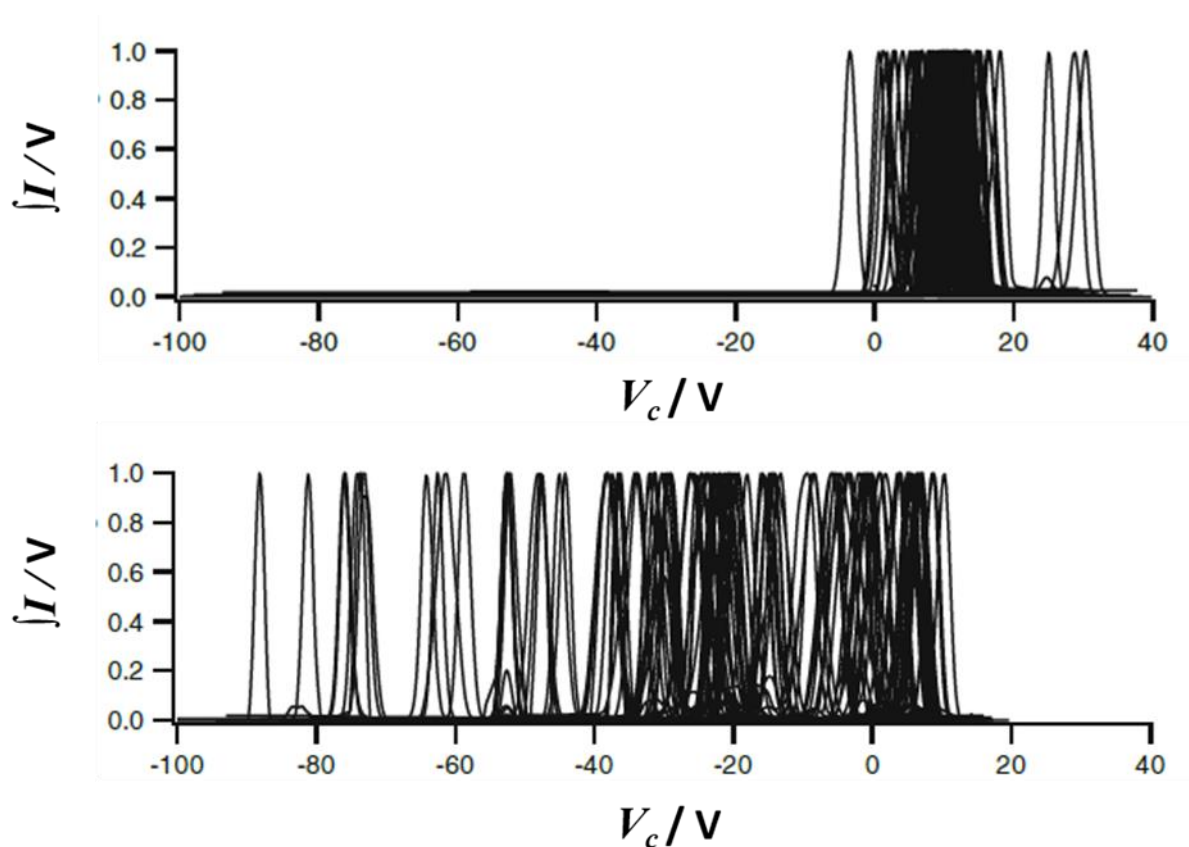


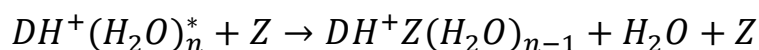
Figure 1. 14 Normalised d-IMS responses of complex, 140 compounds mixture, with pure nitrogen gas (top) and with addition of isopropanol at 1500 ppm level to the transport gas (bottom). Figure taken from Nazarov et. al. [112] with permission of the Springer Link.

The improved separations in the presence of chemical modifiers has been described for a number of applications such as separation of small molecules [113], peptides [114] and drug metabolites [115,116].

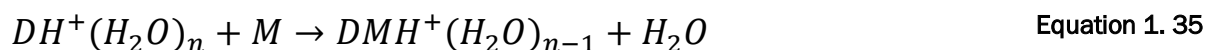
Clustered ion size depends on experimental conditions such as pressure, effective temperature [] and concentrations [117]. The effects observed in differential mobility in the presence of gas modifiers cannot be explained by ion-neutral molecule interactions alone: dimer/trimer formation; competitive clustering resulting and conformation changes also have effect on the process [113].

1.6.3 Dopants

Another way to manipulate d-IMS or IMS responses is to use chemical additives called dopants (*D*) which influence APCI, which preferentially ionizes the desired compound, while blocking potential interferences, increasing the detection selectivity and analytical space [118]. First work about dopant was done by Kim and co-workers, who added ammonia to the N₂ transport gas in IMS system to selectively ionise a series of amines [119]. Dopants alter the relative proton and electron affinities of the reactant ions, enabling charge-transfer reactions only to molecules that possess higher proton affinities than the dopant ions. When *D* with higher *PA* than reactant ion (RI) is introduced into the ionisation region, the hydrated protons (in positive polarity) are converted into alternate RI as in Equation 1.34 via collision with a third body *Z* [106].



When analyte *M* is introduced into the ionisation region it competes with alternated RI ($DH^+(H_2O)_n$) and only forms product ions, if its *PA* favours the proton transfer in to *M* as shown in Equation 1.35



The main reasons for using the alternative RI lies in the fact that they change chemistry of interactions between the analyte and interfering substances. Properly chosen dopant may bring the following advantages:

- It is possible that the alternated RI can interact with analyte but not with interfering substances. As a result the interfering peaks do not appear in the spectrum.

- Position of the ions observed in the presence of dopant are different to their E_c position in clean transport gas. This effect can be used for better resolution of overlapping peaks and peak shifting
- Ion products created with alternative ions can be more stable. The spectra may contain more analytically useful information.

1.6.3.1 *Examples of dopants*

One of the common dopants used in IMS/d-IMS studies is ammonia. Its high PA (853.6 $\text{kJ}\cdot\text{mol}^{-1}$ [120]) gives high efficiency of proton transfer from hydronium ions and by being greater than most of the organic compounds, it can effectively block their ionisation. This was used as an advantage in detection of narcotics [121,122]. Improvement of detection limits were shown for morphine, noscapine [121] and enhanced resolution of weak cocaine peak was achieved [122]. Detection of chemical warfare agents with ammonia also has been presented [123,124] and is often used in commercial instruments, such as in IMS portable devices from Smith Detection Ltd. [125]. Shift in the position of product ion of formaldehyde was observed when as little as 0.6 ppm of ammonia was used in addition to air transport gas. Without the dopant, the analyte signal, overlapped with intense peaks of hydrated protons (RI).

Acetone is another commonly used dopant in IMS/d-IMS detection, with PA of 832.6 $\text{kJ}\cdot\text{mol}^{-1}$, high enough for the elimination of interferences from organic compounds such as hydrocarbons, alcohols, esters and other which can often be found in the atmosphere. This property was used by Eiceman et.al. studies on detection of 19 organophosphorous (OPCs) compounds in presence of volatile organic compounds (VOCs) [118], showing increased sensitivity due to partial removal of interferences, after usage of acetone at the concentration levels between 100 and 2000 ppb. In studies on pesticides an enhanced selectivity for the analyte peaks was achieved due to discrimination of hydrated proton ions [126]. Acetone was also successfully applied in detection of chemical nerve agents such as dimethyl methylphosphonate, showing increased resolution between reactant ion peak (RIP) and product ion (PI) [127]. Example of spectra adopted from this work is shown in Figure 1.15.

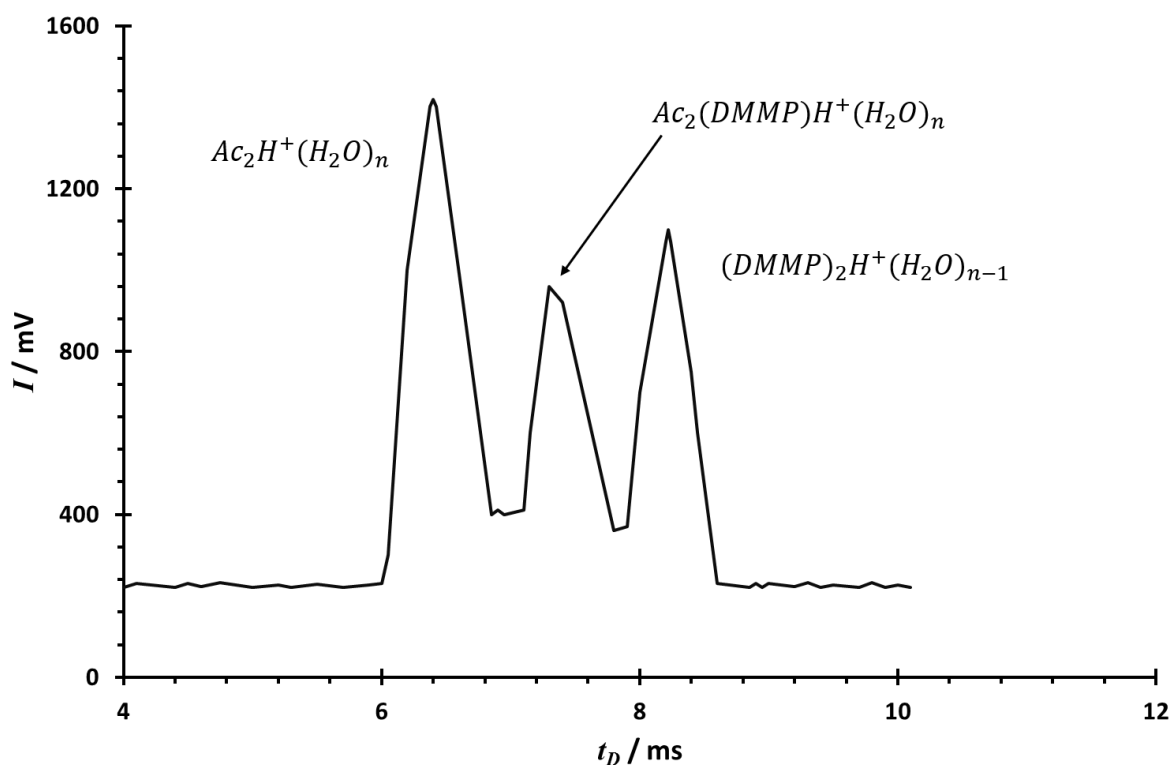


Figure 1. 15 Ion mobility spectrum of DMMP system doped with Acetone, which shifts monomer and dimer peaks to further drift times, resolving PI from RIP [127].

Negative mode dopants, with high EA such as chloromethane, methyl bromide or methylene chloride were successfully applied in various studies e.g. to enhance detection of explosives such as nitrotoluene and its derivatives [128, 129]. Another group of compounds which can be analysed in negative mode of IMS/d-IMS are acid and halogen gases. These compounds, despite their high EA are not always easy to detect due to their small size and mobility similar to the typical negative reactant ions present in air $O_2^-(H_2O)_{2(g)}$. This problem was overcome by doping the transport gas (air) with methyl salicylate at the concentration level between 3 to 10 ppm [130].

Other interesting achievement of using dopant was presented in work of H. Hill and co-workers, who achieved separation of amino acids enantiomers and other compounds, by doping a N_2 transport gas of the IMS with R or S 2-butanol, opening a new door for applied IMS [131].

1.7 Fragmentation

Fragmentation is a type of chemical dissociation of energetically unstable molecular ions. Fragmentation can occur in the ion source (in-source fragmentation) usually in “hard” ionisation techniques (such as electron impact, with typical electron collision energies of 70 eV [132]). To avoid extensive fragmentation, and complications of the spectra softer ionisation techniques are used. In methods using chemical ionization via protonation the most abundant ion is the quasi-molecular ion MH^+ . However, some fragmentation still occurs. If the fragmentation is caused by excess of internal energy obtained from the reaction, occurring during the initial ionisation, the reaction will be called dissociative proton transfer. If collisions between the product ions and the neutral molecules of the transport gas result in sufficient increased internal energy to cause fragmentation the reaction is termed collision induced dissociation (CID) and it is a type of post-ionisation fragmentation.

1.7.1 Fragmentation in IMS/d-IMS systems

A central idea of IMS and d-IMS is that product ions will not undergo any kind of chemical change following introduction into the drift region, [133] and only a few episodes of fragmentation have been reported, which are described below. For the first time the process was demonstrated in work of Eiceman and co-workers on fragmentation of butyl acetate isomers within a drift tube of linear IMS in 1988 [134]. They found dependence of fragmentation on the ion structure and the temperature, with the second being less pronounced. At elevated temperatures (150 °C), the major fragment ions, obtained from tert-butyl and iso-butyl acetates were $[C_4H_9]^+$ specie and protonated acetic acid from sec-butyl acetate. No fragmentation was observed for n-butyl acetate. Years later the same research group, studied n-alkyl carboxylic esters (including n-butyl acetate) in d-IMS drift tube [84]. The study showed fragmentation of esters (including n-butyl acetate) to protonated carboxylic acid. In the study the correlation between the separation field and mass was apparent, with increasing separation field requirement for the appearance of fragmentation of MH^+ with increasing mass, Figure 1.16. Also, the lower the gas temperature, the higher was the dispersion field needed to cause fragmentation. The rate of increase in T_{eff} established in the study, was estimated to be 1.5 °C per Townsend, and was the same for all the esters.

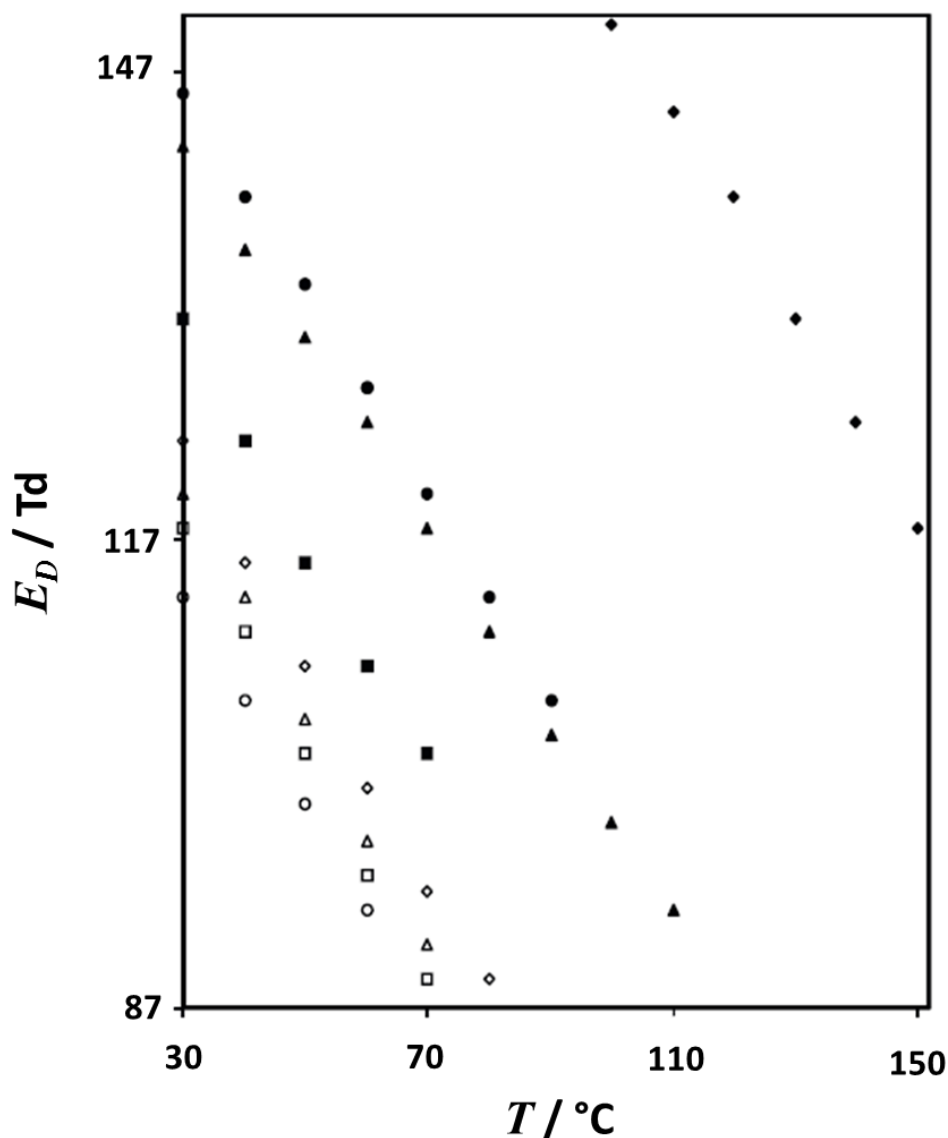


Figure 1. 16 Separation voltages for the first observation of a formation of protonated acid versus d-IMS temperature. Propyl acetate “○”, butyl acetate “□”, pentyl acetate “△”, hexyl acetate “◇”, propyl propionate “■”, propyl butyrate “▲”, ethyl propionate “●”, and ethyl hexanoate “◆”. Graph implemented from Eiceman et. al [84] with permission of Elsevier.

The explanation for the observed fragmentation in d-IMS provided by Eiceman lay in CID mechanism, where the activation energy required for fragmentation was achieved by temperature of the drift tube and applied electric dispersion field. As d-IMS, operates at atmospheric pressure and employ high asymmetric radio frequency field, an effective temperature T_{eff} of ion is higher than that of the surrounding gas temperature due to collisional heating [135]. As a result, with enough collisions it is possible for the CID to occur. If travel time for an ion through typical drift tube is in millisecond scale, as in case

of d-IMS and IMS, using basic calculation from kinetic theory of gases a mean free path and collision frequency can be calculated. It results in average of 1000 collision with N_2 neutrals, under standard conditions, that, in some cases, can give enough energy for fragmentation [134]. The energy and frequency of these collisions will be altered with changes to the reduced electric field. Additionally, thermal dissociation of dimer ions (M_2H^+) was observed to fragment ions without formation of the monomer at high electric fields (from 105 Td) as in case of propyl acetate showed in Figure 1.17. The mechanism is not fully understand but it is argued that the larger heat capacity of relative M_2H^+ to MH^+ would suggest that at given field and transport gas temperature the smaller ion attains a higher effective temperature to fragment.

Another study presented by Kendler and co-workers showed fragmentation of aromatic diaryl compounds in d-IMS [136], such as diphenyl methane (DPM) and bibenzyl (BB) by lost of benzene ring via suggested CID mechanism. Ionic fragmentation products, were examined and identified by mass spectrometry. In the study, a calculated energy barrier was used to predict an effect of temperature on dissociation of the benzene group. Low energy barrier for dissociation of DPM (calculated to be 4.1 kJ.mol^{-1}) results with weak dependence of ion fragmentation efficiency on the d-IMS temperature (signal intensity of a fragment was almost constant at dispersion field of 104 Td or $1300 V_d$ V between 40 and 120 °C) and field amplitude (fragment observed across entire experimental range 40 to 120 Td or 500 to 1500 V_d V). Higher energy barrier, calculated for BB (77.4 kJ mol^{-1}), was a good indicator of the dissociation/fragmentation process, with pronounce effect of field and temperature on the reaction efficiency. The fragmentation was not induced until 88 and 96 Td or 1100V and $1200 V_d$ V at 75 and 50 °C, respectively. Further decomposition of the fragment ions was observed at the highest electric field amplitudes.

Recently, the fragmentation occurring in d-IMS was reported by Maziejuk and co-workers, which was used for identification of sarin, mustard gas and methyl salicylate [137]. The compounds fragmentation was observed via discontinuities in dispersion plots and wasn't a subject for further energetic analysis.

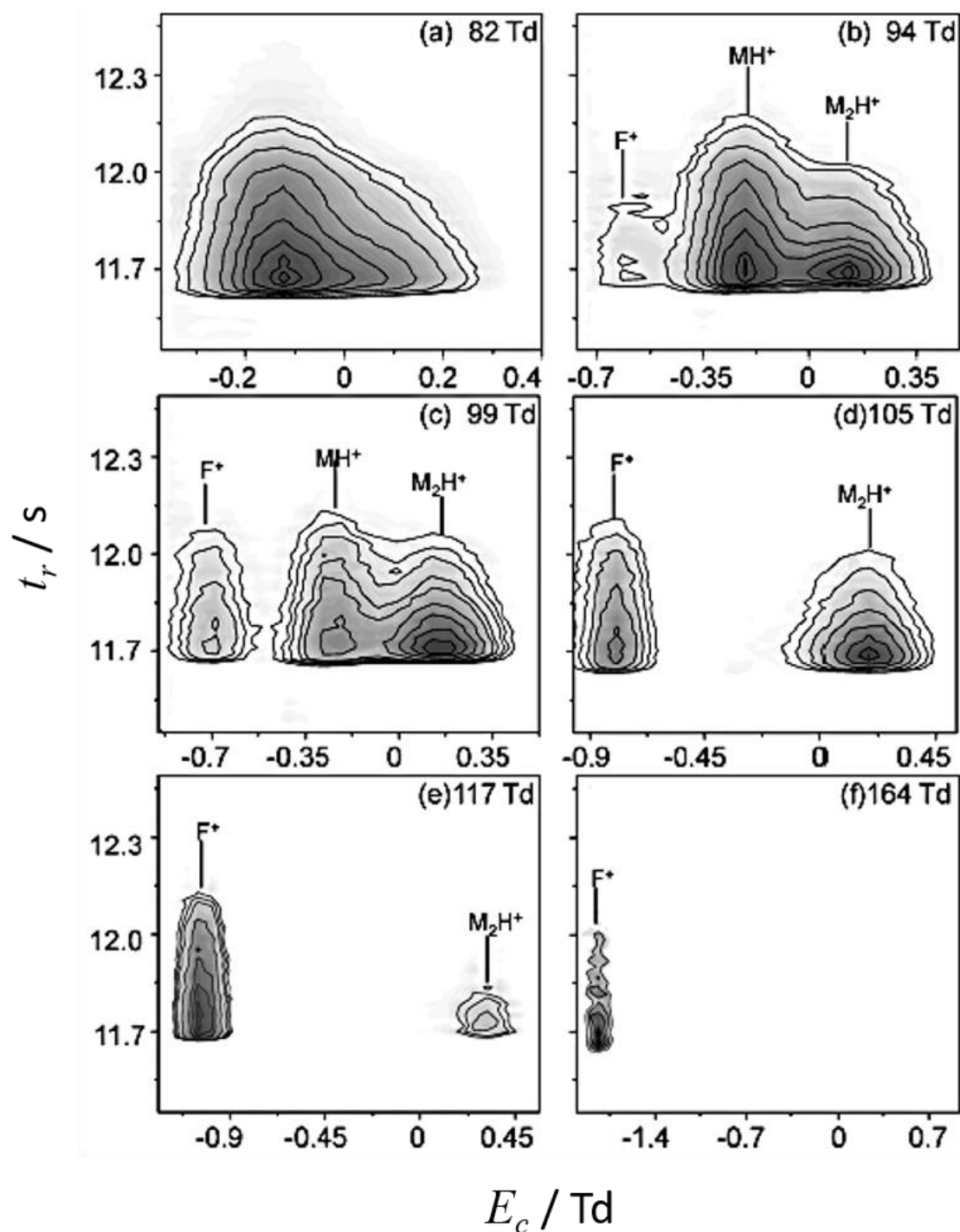


Figure 1. 17 GC-d-IMS topographic plots for propyl acetate, obtained under d-IMS analyser temperature of 100 °C and different separation fields from 82 Td (a) to 164 (f) . M_2H^+ represents propyl acetate dimer, MH^+ is propyl acetate monomer, F^+ is a fragment, t_r is retention time and E_c is compensation voltage . Graph implemented from X. An et. al. [84] with permission of Elsevier.

1.7.2 Fragmentation of alcohols

Elimination of water is one of the most important reactions of ionized alcohols (Figure 1.18 a). This behaviour was reported in several mass spectrometric and theoretical studies [138,139,140,141,142,143,144]. For example in electron impact mass spectrometry (EI-MS) dehydration as well as a loss of alkyl group by alpha cleavage of C-C bond [138] are the most common channels for alcohol fragmentation (Figure 1.18 b).

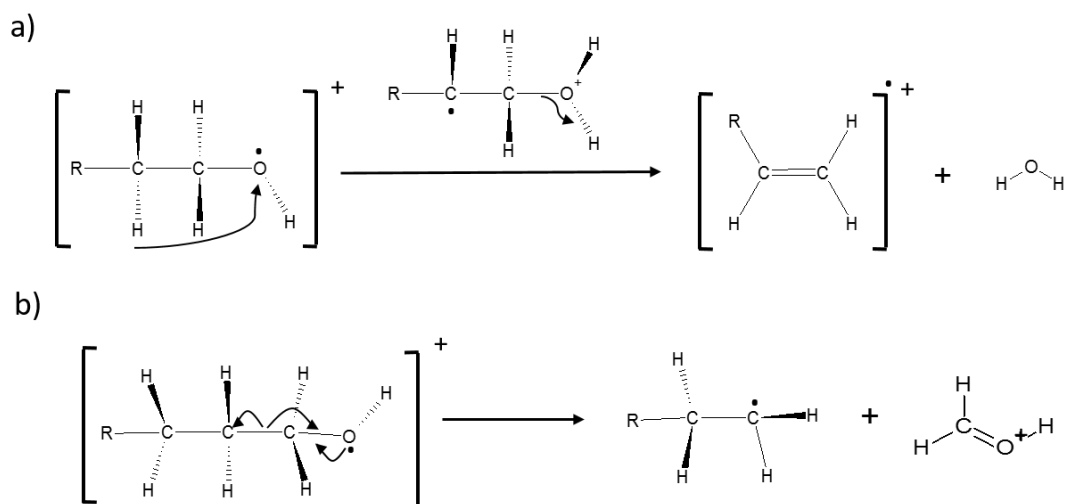


Figure 1.18 Mechanism of fragmentation of alcohols in EI-MS via loss of water (a) and alkyl group (b). The possible fragmentation channels increases with increased molecular mass of the compounds [145].

1.7.2.1 Fragmentation in chemical ionisation methods

In chemical ionization via protonation the most abundant ion is the quasi-molecular ion (MH^+). Still, fragmentation has frequently been reported as a result of dissociative proton transfer (DPT) or collision induced dissociation (CID).

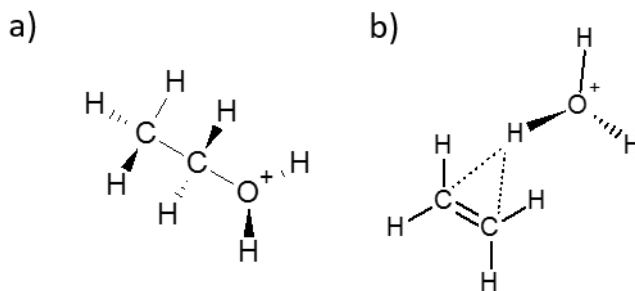
For example Karpas and co-workers studied alcohols from methanol to n-butanol in APCI-MS reporting fragmentation of protonated products via collisional induced dissociation (CID) [141]. The collisions were altered via gas collision thickness (GCT) and by electric potential on ion lenses, used to extract ions from corona discharge source. In those studies two channels for dehydration were shown for ethanol monomer ion, where proton (giving positive charge to the ion) was placed on either alkene $C_2H_5^+$ or on water (H_3O^+), Equation 1.36 and Equation 1.37



Both of those channels reactions are endothermic with 37.2 and 32.5 kcal mol⁻¹, Equation 1.36 and Equation 1.37, respectively. Under conditions used in the experiments, the reaction shown in Equation 1.36 was favoured by a ratio of 4:1 at “collisional gas thickness (CGT)” [sic] of 1.2 x 10¹⁴ cm⁻² and at CGT of 2.4 x 10¹⁴ cm⁻² the ratio dropped to 2:1. In an other study on CID of the protonated methanol ions, it was noted that “observed branching ratios did not always follow the thermochemistry, i.e. the least endothermic pathways were not always favoured” [146].

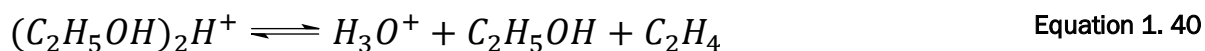
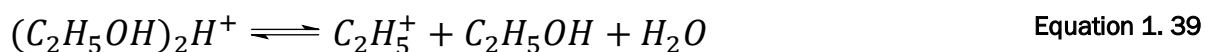
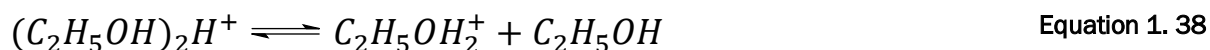
The result of the protonated monomer maybe considered from a point of view of its intermediate product. It was shown over 25 years ago that alkyl cations may exist as a “distinct moiety” in intermediate during decomposition of organic ions [147].

Ethanol may form two protonated low energy isomers, the covalent (structure a) and hydrogen bonded (structure b) where the proton from H₃O⁺ points toward the midpoint of the C=C bond.



The first structure is 67 kJ.mol⁻¹ lower in energy. Since, the barrier for isomerisation is lower than that for dissociation into either C₂H₅⁺ or H₃O⁺ both ionic dissociation from energetic ions of this structures can be formed [147].

The same study on alcohols by Karpas and Eiceman [141] showed three channels for dissociation of ethanol dimer ion in API-MS-MS, as in Equations 1.38, 1.39 and 1.40:



It was observed that varying the CGT affected the branching ratios of the product ions but it did not open new dissociation channels and only channels shown in reactions 1.38 and 1.39 were observed. However, increasing the ion collision energy can make additional dissociation channels accessible as in this case channel with production of hydrated proton (Equation 1.40).

Proton transfer reaction of ethanol caused some kind of confusion in proton transfer reaction mass spectrometry (PTR-MS). PTR-MS is similar to IMS at low pressure. The confusion was due to the fact that different branching ratios between molecular ion of $C_2H_5OH_2^+$ and fragment $C_2H_5^+$ were obtained in two studies by dissociative proton transfer. Warneke found a 50:50 branching ratio for those product ions [148] and in Blake's studies the same ion ratio was reported to be 93:7 [149]. This was explained in 2009 by Inomata and Tanimoto in deuterium labelling studies, showing that the dehydration with production of H_3O^+ ion was also an active channel for ethanol [150], causing differences with the results. The same results were later independently confirmed by Brown and co-workers also by deuterium labelling [144]. Brown in his work studied the effect of the reduced electric field (E/N) on product ions from reaction with H_3O^+ and 12 saturated alcohols in dry nitrogen. Alcohols react with H_3O^+ at collisional rate and methanol and ethanol show almost non-dissociative proton transfer at 300 K. It is helpful to note that in PTR-MS the reactions take place at conditions, which cannot be described as anywhere near 300 K, due to field heating, and the field effect determines the outcome of alcohol reactions. Brown showed in his comprehensive studies, that at 115 Td the dehydration channel for ethanol is already significant and at 138 Td its intensity is as strong as the molecular ion $C_2H_5OH_2^+$ (Table 1.4). Both product ions, protonated alkene and hydrated proton, were produced.

Results obtained for other alcohols also involved dehydrogenation and rearrangement between isomeric structures (explained as due to intermediate stages of carbocation's and their stability) and dissociation of alkyl group for higher alcohols (with carbon number ≥ 4). The rearrangement of the intermediate carbocation's was seen for example in case of 1-propanol which gave the same product ions as iso-propanol. The dominant reaction for both propyl alcohols observed was the loss of neutral water molecule from the protonated monomer resulting in formation of the $C_3H_7^+$ (m/z 43), occurring as a result of dissociative proton transfer. Both propyl alcohols exhibit loss of hydrogen molecules from the $C_3H_7^+$ product ion to form $C_3H_5^+$ and $C_3H_3^+$ product ions at m/z 41 and 39 respectively via loss of molecular hydrogen. The identical nature of the fragmentation suggests that the $C_2H_7^+$ carbocation of 1-propanol is quickly isomerising to the more stable secondary propyl carbocation.

Dissociation of alkyl group was a channel observed in an example of isomers of butyl and higher alcohols in Brown studies [151,143]. The initial loss of water from protonated monomer produces $C_4H_9^+$ ion (m/z 57). The carbocation fragmented further in identical manner for each butyl alcohol, again suggesting rearrangement from primary or secondary to the tertiary carbocation's isomer of $C_4H_9^+$. Further, the $C_2H_5^+$ (m/z 41) fragment was produced via loss of methane (CH_4) from $C_4H_9^+$, followed by dehydrogenation to form $C_3H_3^+$ ion (m/z 39). The only signal of protonated monomer MH^+ detected, was at the lowest E/N value used in the experiments of 91 Td and at very low signal intensity (1%). This, with support of other studies by SIFT data [151] is argued to be an indication that the initial loss of H_2O is caused by dissociative proton transfer. No fragmentation was observed in case of methanol, neither was reported elsewhere. Summary of reduced field (E/N) effect on product ions branching ratio for alcohols is summarised in Table 1.4 (adapted from Brown and co-workers).

No fragmentation was reported for alcohols in d-IMS in literature.

Table 1. 4 Product Branching ratio as a percentage for a series of saturated aliphatic alcohols, adapted from Brown and co-workers [144].

Compound (<i>PA</i> / kJ.mol ⁻¹)	<i>E/N</i> = 92 ± 1 Td		<i>E/N</i> = 115 ± 1 Td		<i>E/N</i> = 138 ± 1 Td	
	m/z (ratio %)	ion	m/z (ratio %)	ion	m/z (ratio %)	ion
MeOH (754.3)	51 (21) 33 (79)	<i>M</i> (<i>H</i> ₃ <i>O</i>) ⁺ <i>MH</i> ⁺	51 (2) 33 (98)	<i>M</i> (<i>H</i> ₃ <i>O</i>) ⁺ <i>MH</i> ⁺	33 (100)	<i>MH</i> ⁺
EtOH (776.4)	19 (?) 65 (20) 47 (75) 45 (4) 29 (1)	<i>H</i> ₃ <i>O</i> ⁺ <i>M</i> (<i>H</i> ₃ <i>O</i>) ⁺ <i>MH</i> ⁺ [<i>M</i> - <i>H</i> ₂] ⁺ [<i>M</i> - <i>H</i> ₂ <i>O</i>] <i>H</i> ⁺	19 (?) 65 (1) 47 (69) 45 (15) 29 (15)	<i>H</i> ₃ <i>O</i> ⁺ <i>M</i> (<i>H</i> ₃ <i>O</i>) ⁺ <i>MH</i> ⁺ [<i>M</i> - <i>H</i> ₂] ⁺ [<i>M</i> - <i>H</i> ₂ <i>O</i>] <i>H</i> ⁺	19 (?) 47 (43) 45 (17) 29 (40)	<i>H</i> ₃ <i>O</i> ⁺ <i>MH</i> ⁺ [<i>M</i> - <i>H</i> ₂] ⁺ [<i>M</i> - <i>H</i> ₂ <i>O</i>] ⁺
1-PrOH (786.5)	79 (4) 61 (3) 43 (93)	<i>M</i> (<i>H</i> ₃ <i>O</i>) ⁺ <i>MH</i> ⁺ [<i>M</i> - <i>H</i> ₂ <i>O</i>] <i>H</i> ⁺	41 (83) 43 (17)	[<i>M</i> - <i>H</i> ₂ <i>O</i>] <i>H</i> ⁺ [<i>M</i> - <i>H</i> ₂ - <i>H</i> ₂] <i>H</i> ⁺	43 (29) 41 (59) 39 (19)	[<i>M</i> - <i>H</i> ₂ <i>O</i>] <i>H</i> ⁺ [<i>M</i> - <i>H</i> ₂ <i>O</i> - <i>H</i> ₂] <i>H</i> ⁺ [<i>M</i> - <i>H</i> ₂ <i>O</i> - 2 <i>H</i> ₂] <i>H</i> ⁺
2-PrOH (793.0)	79 (3) 61 (5) 43 (1) 59 (91)	<i>M</i> (<i>H</i> ₃ <i>O</i>) ⁺ <i>MH</i> ⁺ [<i>M</i> - <i>H</i> ₂ <i>O</i>] <i>H</i> ⁺ [<i>M</i> - <i>H</i> ₂] <i>H</i> ⁺	43 (85) 59 (1) 41 (14)	[<i>M</i> - <i>H</i> ₂ <i>O</i>] <i>H</i> ⁺ [<i>M</i> - <i>H</i> ₂] <i>H</i> ⁺ [<i>M</i> - <i>H</i> ₂ <i>O</i> - <i>H</i> ₂] <i>H</i> ⁺	43 (31) 59 (1) 41 (52) 39 (16)	[<i>M</i> - <i>H</i> ₂ <i>O</i>] <i>H</i> ⁺ [<i>M</i> - <i>H</i> ₂] <i>H</i> ⁺ [<i>M</i> - <i>H</i> ₂ <i>O</i> - <i>H</i> ₂] <i>H</i> ⁺ [<i>M</i> - <i>H</i> ₂ <i>O</i> - 2 <i>H</i> ₂] <i>H</i> ⁺
1-BuOH (789.2)	93 (3) 75 (1) 73 (5) 57 (91)	<i>M</i> (<i>H</i> ₃ <i>O</i>) ⁺ <i>MH</i> ⁺ [<i>M</i> - <i>H</i> ₂] <i>H</i> ⁺ [<i>M</i> - <i>H</i> ₂ <i>O</i>] <i>H</i> ⁺	73 (2) 57 (91) 41 (3)	[<i>M</i> - <i>H</i> ₂] <i>H</i> ⁺ [<i>M</i> - <i>H</i> ₂ <i>O</i>] <i>H</i> ⁺ [<i>M</i> - <i>H</i> ₂ <i>O</i> - <i>H</i> ₂] <i>H</i> ⁺	57 (55) 55 (7) 41 (26) 39 (12)	[<i>M</i> - <i>H</i> ₂ <i>O</i>] <i>H</i> ⁺ [<i>M</i> - <i>H</i> ₂ <i>O</i> - <i>H</i> ₂] <i>H</i> ⁺ [<i>M</i> - <i>H</i> ₂ <i>O</i> - <i>CH</i> ₄] <i>H</i> ⁺ [<i>M</i> - <i>H</i> ₂ <i>O</i> - <i>CH</i> ₄ - <i>H</i> ₂] <i>H</i> ⁺

1.8 Modelling

1.8.1 Reactant ion production in d-IMS

The initial number of reactant ions produced in the 5mCi ^{63}Ni source of the d-IMS was obtained by calculating electrical charge (Q) in Coulomb units (where, 1 Coulomb is roughly 6.241×10^{18} times the elementary charge) of the reactant ion. This was done by converting measured voltage of the signal heating the detector plate, to Amperes. Next, the Faraday constant F ($\approx 96485.333 \text{ C mol}^{-1}$ [152]) was used to calculate the number of moles of electrons. From here, Avogadro constant ($\approx 6.022 \times 10^{23} \text{ mol}^{-1}$) was used to calculate the number of produced RI. The obtained averaged value for the reactant ion peak (RIP) concentration was $\approx 3.3 \times 10^8 \text{ cm}^{-3}$, which is in agreement with values suggested by Siegel in his work on Atmospheric Pressure Ionisation [153].

1.8.2 Product ion production in d-IMS

Assuming proton transfer always leads to the production of protonated monomer, i.e. no fragmentation, the increase in concentration of protonated monomer $\Delta[MH^+]$ produced in a time period, Δt , can be expressed as in Equation 1.41.

$$\Delta[MH^+] = [M][H_3O^+]k\Delta t \quad \text{Equation 1. 41}$$

Note: $[H_3O^+]$: number density of reagent ion available for proton transfer reaction ($3.3 \times 10^8 \text{ cm}^{-3}$);
 $[M]$: number density of analyte; k : reaction rate constant

The value of k used, is well known, typical Langevin rate constant for ion-molecule reactions ($k = 10^{-9} \text{ cm}^3 \text{ molecule}^{-1} \text{ s}^{-1}$) [154,64].

The reaction is second order. Assuming, that one of the reactants is in excess (as in this case, neutral molecules of the analyte M), the reaction can be expressed as a pseudo-first order where new rate constant, k' , can be expressed as in Equation 1.42.

$$k' = k[M] \quad \text{Equation 1. 42}$$

Now, production of the product ion is dependent on single reactant concentration $R \rightarrow P$, (assumed proportional to concentration) and the rate can be expressed as a decrease in reactant ion concentration as in Equation 1.43.

$$-\frac{d[H_3O^+]}{dt} = -k'[H_3O^+] \quad \text{Equation 1. 43}$$

Note: Whether the product-ions go on to form some dimer is not of consequence in the sum of the charges on product(s), which is given by the loss of charge by the reactant-ion.

Rearrangement of this equation produces the corresponding integrated rate as shown in Equation 1.44.

$$\frac{d[H_3O^+]}{[H_3O^+]} = -k' dt \quad \text{Equation 1. 44}$$

Now as in d-IMS experiments, where the ion dwell time in the reaction region is governed by the gas flow in d-IMS, t is constant (typical 1 ms residence time in d-IMS), the integrated form of Equation 1.43 is represented by Equation 1.45.

$$[H_3O^+] = [H_3O^+]_0 \exp^{-k't} \quad \text{Equation 1. 45}$$

Assuming all lost reactant-ions $[H_3O^+]_0$ turn up as product-ions MH^+ then the sum of these gives total product ion as seen in the following expression (Equation 1.46)

$$[MH^+] = [H_3O^+]_0 - [H_3O^+]_0 e^{-k't} = [H_3O^+]_0 (1 - e^{-k't}) \quad \text{Equation 1. 46}$$

A plot of $[MH^+]$ versus $[M]$ or $\ln[MH^+]$ versus number of density N is not linear although the plot of the log of the reactant-ion concentration is.

Figure 1.19 shows d-IMS product-ion (PI) formation and reactant ion (RI) depletion, calculated for methanol in relation to number of density N of the analyte neutrals (x axes, bottom) also expressed in corresponding concentration (x axes, top). 50% of the RIP ions is expected to be depleted at the concentration of methanol $\approx 0.035 \text{ mg m}^{-3}$ to be completely lost at around 0.1 mg m^{-3} , where only PI should be observed.

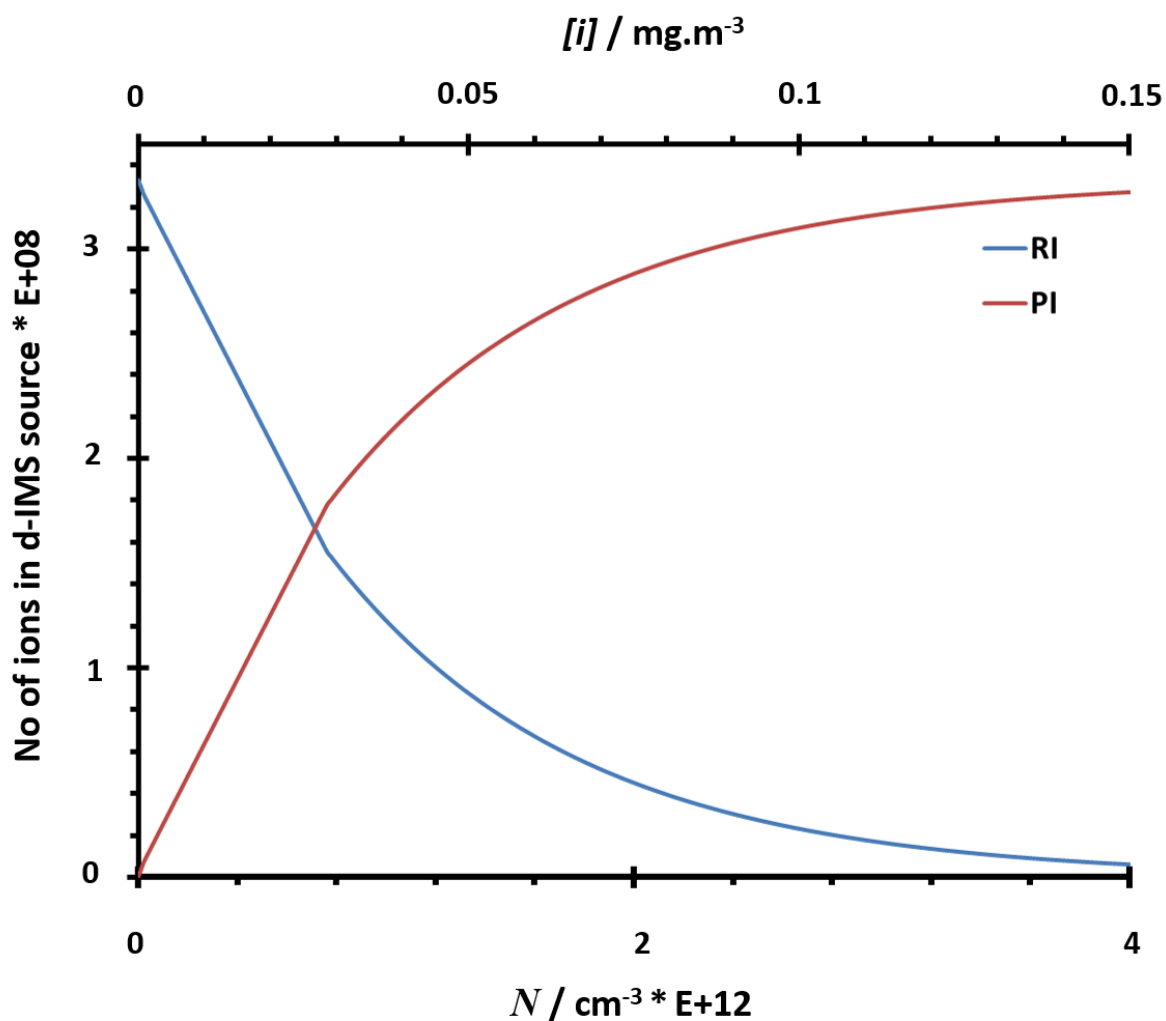


Figure 1. 19 Formation of product-ion and depletion of reactant-ion as a function of concentration $[N]$.

1.8.3 Formation of proton bound clusters –ion solvation equilibrium model

Model on ion-molecule equilibrium was used, to establish whether the model can be used to predict the responses for n-alcohols in d-IMS. Calculation of equilibrium constant and fractional ion abundance vs concentration were proposed for reactions in which between 1 to 7 solvent molecules are attached to a equilibrated protonated central ion of $(ROH)H^+$. The theoretical thermodynamic parameter values were obtained from the Paul's Kabarle's work on ion- equilibrium.

A discovery of ion-molecule equilibrium under thermal conditions by Paul Kabarle in the mid 1960s [155] led to an understanding of the importance of ion solvation for the energetics and reactivities of solvated ions. Very early in this work, the hydrated

hydronium ion clusters arising from his laboratory air were recognised and characterised by his team using high pressure mass spectroscopy, leading to discovery of clustering equilibrium. This work was followed, by series of papers by Kebarle and his co-workers, describing obtained fundamental thermochemical data, such as proton affinities, hydride ion affinities, and electron affinities on series of molecules. It can be assumed, that steady-state equilibria exist [59] in the reactant region of the instrument because of the duration of time the analyte spends in this ion rich region (ms scale). Protonated monomer molecules are produced via initial proton transfer reaction. These reactions are followed by the third body dependent clustering reactions (Equation 1.29). The bonding between the ion and 'solvent' or other neutral molecule in the system is relatively weak compared to a 'normal' chemical bond, typically in the order of 200 kJ.mol⁻¹ or less. A protonated molecule MH^+ can be clustered quite strongly by the same molecule (M) as in Equation 1.47. Example of protonated water and methanol clusters structures are shown in the Figure 1.20.

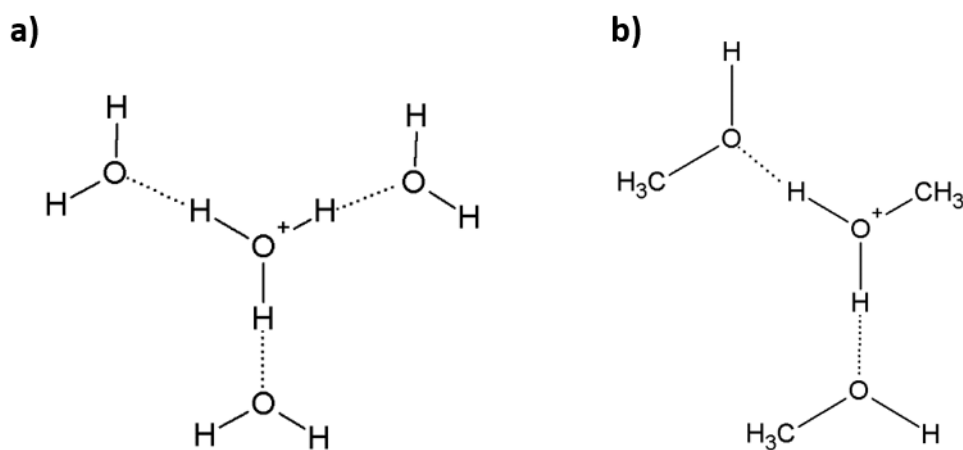


Figure 1. 20 Structure of protonated cluster of water (a) and methanol (b).

For the clustering reaction represented by Equation 1.47 leading to a stabilized complex, the equilibrium constant, for first ligand (molecule M) attachment, (K_1), can be represented in the form of presented in Equation 1.48.



$$K_1 = \frac{[M_2H^+]}{[MH^+][M]} \quad \text{Equation 1. 48}$$

Known thermodynamic parameters, for each of the association chemical processes, allows (K_n) to be calculated via Equation 1.49.

$$K_n = \exp\left(\frac{-\Delta G_n}{RT}\right) \quad \text{Equation 1. 49}$$

Note: ΔG : Change in Gibbs free energy (kJ.mol^{-1}); R : Gas constant ($8.314 \text{ J.mol}^{-1}\text{K}^{-1}$); T : temperature (K)

Gibbs free energies for the processes can be calculated using thermochemical parameters in a way shown in Equation 1.50.

$$\Delta G = \Delta H - T\Delta S \quad \text{Equation 1. 50}$$

Note: ΔH : Change in enthalpy (kJ.mol^{-1}); ΔS : change in entropy ($\text{J.K}^{-1}\text{mol}^{-1}$)

Knowing K value for temperature T and assuming that concentration of M is in much excess by rearranging the Equation , the thermodynamic model can be derived and the relative and fractional ion abundance for each of the association processes at any temperature for a fixed ambient concentration of M , can be calculated.

Data used in this thesis to build a basic theoretical model of alcohol cluster formation in the Ni^{63} source was taken from one of Kabarle's studies on methanol protonated clusters [156] and provided values for change in enthalpy and change in entropy (Table 1.5), with an error stated by the author, to be around 10%. Those values were taken as a representative for all alcohols used in this study.

Table 1.5 Thermochemical data from protonated clusters in equilibrium for Methanol vapours, where n is a number of associated molecules to the central ion, $-\Delta H$ is negative change in enthalpy and $-\Delta S$ is negative change in entropy [156].

n	1	2	3	4	5	6	7
$-\Delta H$	138.5	89.2	67.4	69.1	52.3	49.8	50.2
$-\Delta S$	127.7	118.1	121	120.2	130.2	137.8	149.5

Equilibrium distribution of fractional methanol clusters vs temperature at 650 mg.m^{-3} concentration level, in relation to changing temperature is presented in Figure 1.21. In presented example it is seen that only clusters from dimer to hexamer are expected to be formed, with significant intensities over the temperature range from 298 to 550 K. At 298 K, the methanol product-ions will consist mainly of $(\text{MeOH})_5\text{H}^+$ while at 550 K the $(\text{MeOH})_2\text{H}^+$ will be the major ion thermodynamically favoured to be formed.

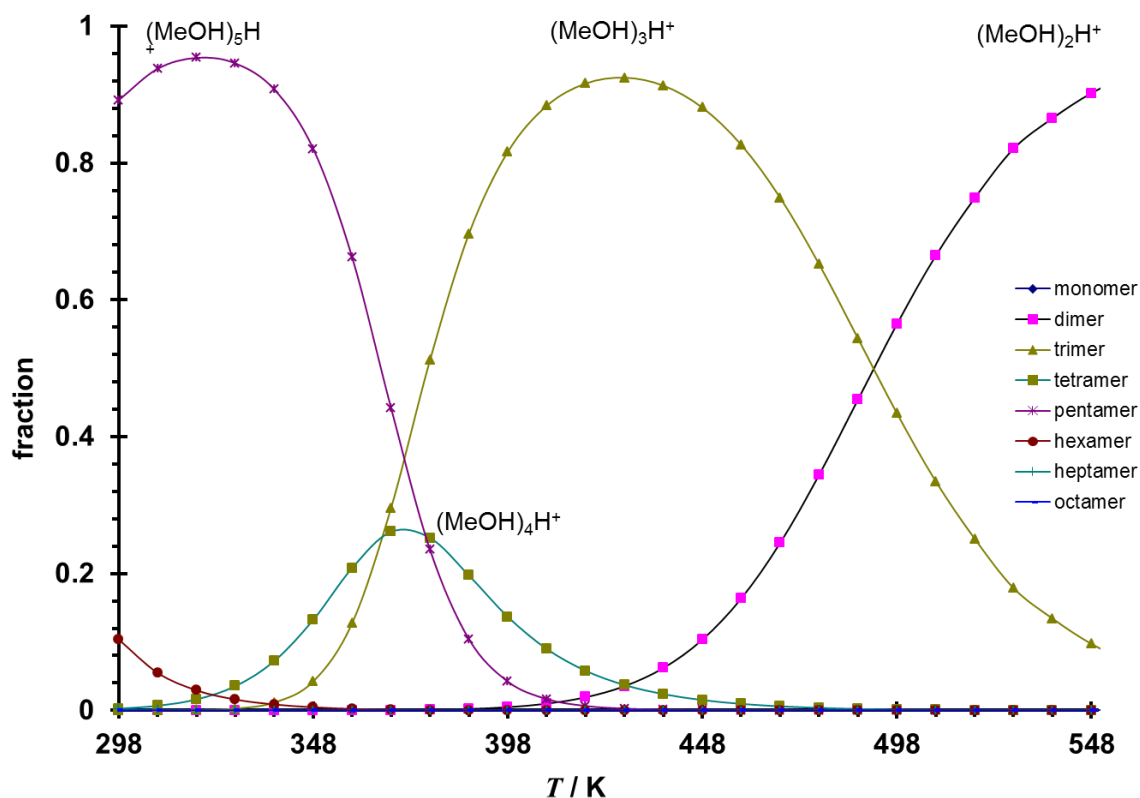


Figure 1.21 Equilibrium distribution of fractional methanol clusters vs temperature at 650 mg.m^{-3} concentration level.

Using the same set of data, ion cluster distribution for changing concentration can be estimated for a fixed temperature. Figure 1.22 presents equilibrium distribution of fractional methanol clusters against concentration at constant 540° K temperature. A change in methanol concentration from to 500 to 100 mg.m^{-3} does not change the

nature of the important ions, where the higher methanol clusters are slightly more favoured (dimer and trimer). The monomer ion is expected to be formed from around 80 mg.m⁻³, rising with reducing concentration to reach 50:50 monomer/dimer ratio at around 0.15 mg.m⁻³.

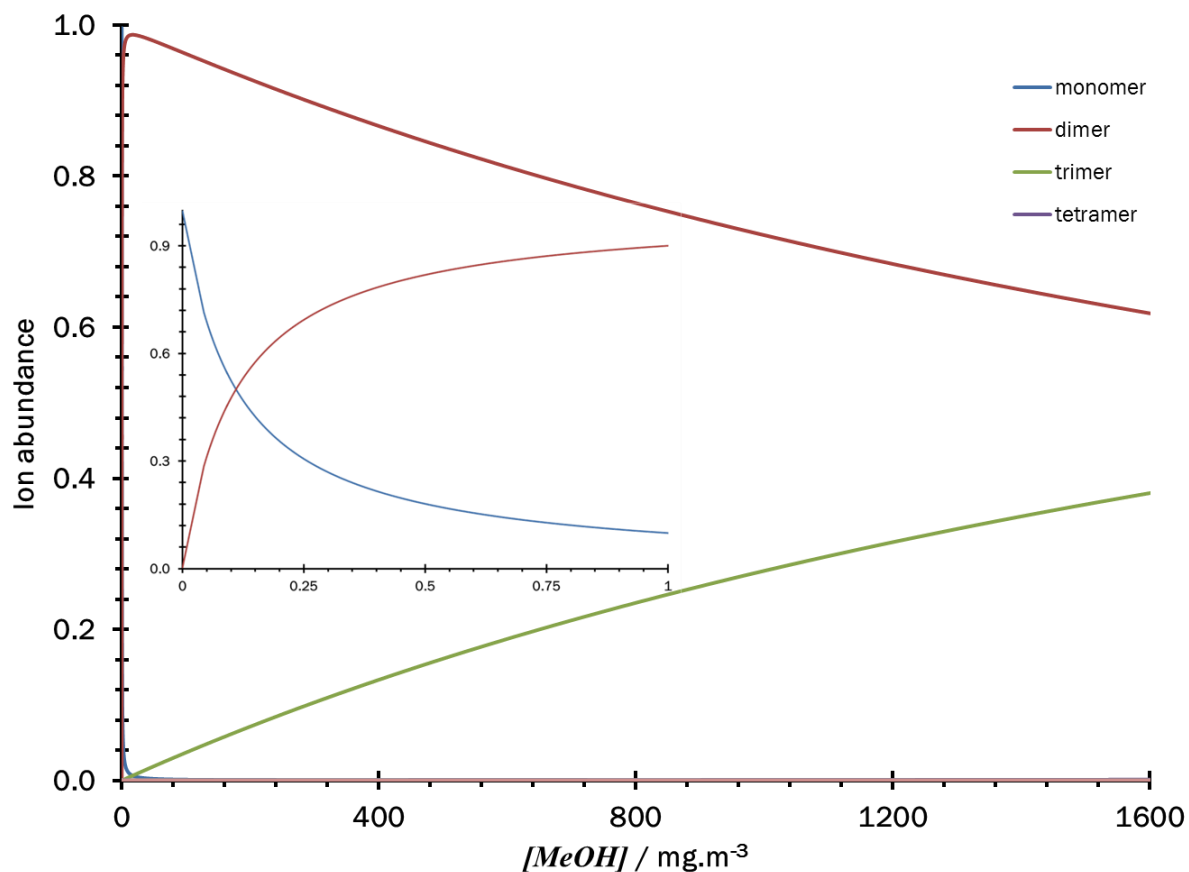


Figure 1.22 Equilibrium distribution of fractional methanol clusters vs concentration at 540° K temperature, estimated for methanol clusters for n = 1 to 4.

Summary of the fractional clusters for each of the alcohols at the calculated effective temperatures (thermal + field heating) used in the series experiments investigating alcohol d-IMS responses in relation to concentration is presented in Table 1.6.

Table 1. 6 Theoretical calculations of fractional ROH cluster ions formation in d-IMS at T_{eff} between 481 and 523 K, where $[i]$ is the concentration in mg.m^{-3} of the alcohols at which specific ions and their ratios are formed (PM – protonated monomer, PBD and PBT– proton bound dimer and trimer, respectively).

Compound	T_{eff}	$[i]$ PBT \geq 95 %	$[i]$ 1:1 PBT:PBD	$[i]$ PBD \geq 95 %	$[i]$ 1:1 PM:PBD	$[i]$ PM \geq 95 %
MeOH	523	Out of range	2605	121	0.15	0.008
EtOH	481	Out of range	569	39.7	0.0005	Out of range
n-PrOH	505	Out of range	2143	111	0.06	0.003
n-BuOH	505	Out of range	2564	137	0.076	0.004

1.8.4 Ion-neutral collisions calculations

In d-IMS ions travelling through the drift-tube are constantly going through a clustering/declustering process, where at the low part of the field form clusters via non-covalent interactions. A model of this behaviour was described in the previous sections and literature [109]. If a typical collision rate constant ($k = 10^{-9} \text{ cm}^3 \text{ molecule}^{-1} \text{ s}^{-1}$) is again taken for ion-neutral encounter and assuming that the concentration of neutrals is in much excess than that of the ions, the kinetics of the process will be a pseudo first order and the time for ion-neutral collision can be expressed in the form of $1/k[N]$. Knowing a low part of the dispersion field period of the device being around $0.58\mu\text{s}$, we can calculate collision frequency at any level of atmospheric concentration. If level of neutrals is sufficiently high, a collision will take place. It will result in change in a cross section area of the ion, its trajectory and finally its position on the compensation field, E_c , scale. The calculations for each of the four alcohols and the neutral gas density level (N) for the first ion-molecule collision, was calculated to be around $1.75 \times 10^{+15}$ molecules per cm^{-3} , which is around 50 ppm concentration level. This is in agreement with existing theory [109]. Figure 1.23 shows calculated level of alcohol's concentration $[i]$ for first ion-neutral collision against molar mass M for methanol, ethanol, n-propanol and n-butanol.

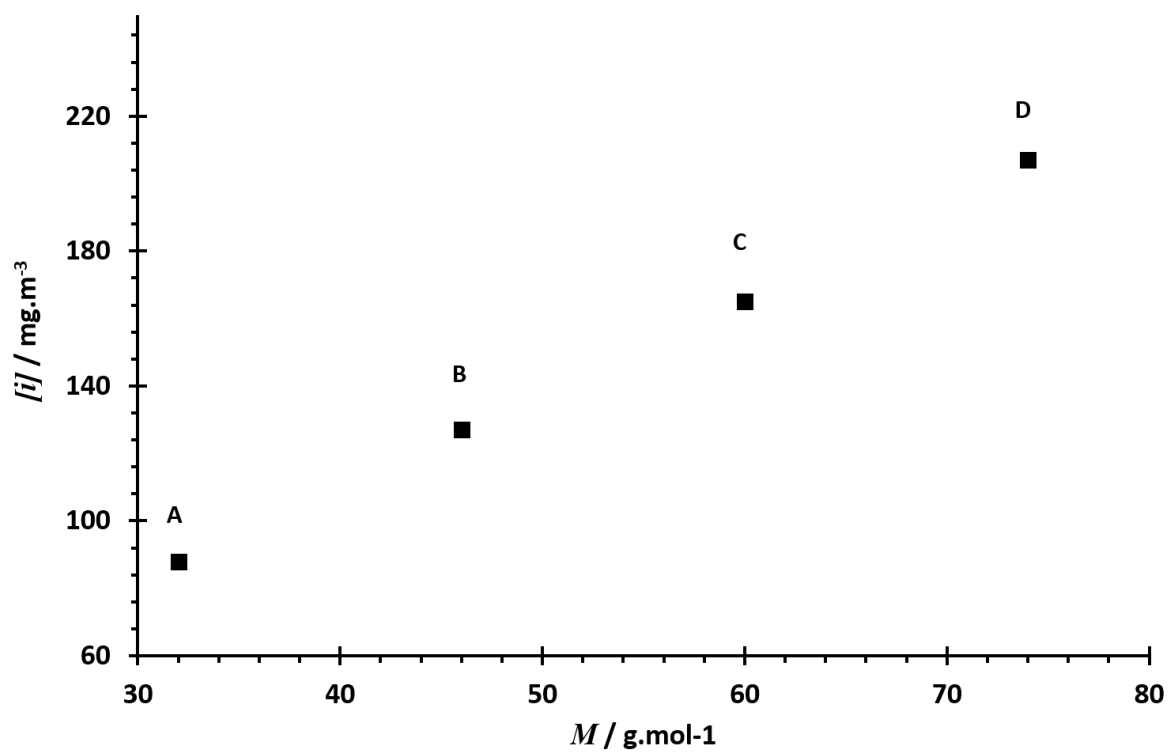


Figure 1. 23 Level of concentration of neutral alcohol molecules $[M]$ mg.m⁻³ for first ion-neutral collision against molar mass M in g.mol⁻¹ calculated for first four saturated aliphatic alcohols: 88 mg.m⁻³ (A - methanol), 127 mg.m⁻³ (B - ethanol), 165 mg.m⁻³ (C - n-propanol) and 207 mg.m⁻³ (D - n-butanol).

Chapter 2 Instrumentation and Experimental Approaches

2.1 Overview

In this chapter, instrumentation, design of the experimental systems as well as experimental approaches used in this thesis, are described. The experiments listed in the Introduction Table 1.1 were undertaken using different instrumentation arrangements.

2.2 Gases

2.2.1 Nitrogen and nitrogen generator

Nitrogen and compressed air are gases of choice for d-IMS systems. A constant flow of nitrogen was obtained from a high purity nitrogen gas generator, manufactured by Pick Scientific, UK (model NP-10L-HP). The generator provided a nitrogen output flow of up to 10 litres per minute, distributed around devices in the laboratory.

2.2.1.1 Functionality

The High Purity Nitrogen Generator utilizes a 'Pressure Swing Adsorption' (PSA) method to extract pure nitrogen from air. This is where un-wanted gases can be selectively adsorbed from compressed air into a porous carbon molecular sieve material (CMS). The Peak Scientific Instruments Ltd. generator utilizes a double column system where one column is pressurised, then equalised with the 2nd column, prior to venting taking place for the first column. The schematic of the functionality is shown in Figure 2.1 with part description in Table 2.1 and technical specifications included in Table 2.2.

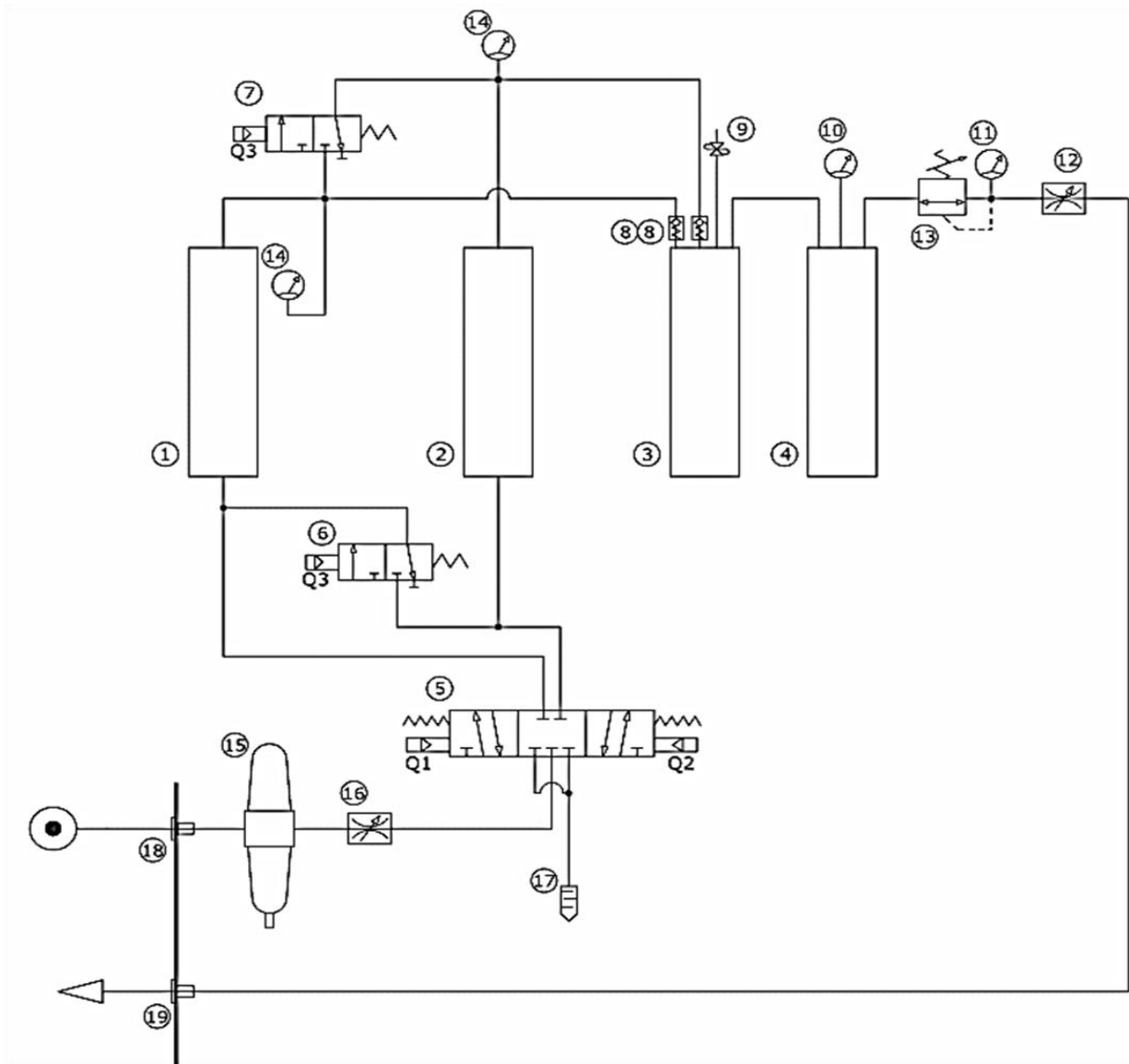


Figure 2. 1 Schematic of high purity nitrogen gas generator Pick Scientific, Model NG 10L-HP. Compressed Air passes through the inlet double breathing air filter (15) and then flow is controlled (16) depending on the cycle the PLC set Output Q1 'ON' with Outputs Q2 and Q3 set to 'OFF', allowing column 1 (1) to pressurise and column 2 (2) to vent to atmosphere. After the set time of 2 minutes, the PLC will pulse Outputs Q1 & Q2 to 'OFF' and setting Output Q3 to 'ON' for 1 second allowing the pressure in both columns to equalise. The PLC will then set Output Q2 'ON', with Outputs Q1 and Q3 set to 'OFF', allowing Column 2 to pressurise while permitting Column 1 to vent to atmosphere. Again after 2 minutes the PLC will pulse Outputs Q1 & Q2 to 'OFF' and setting Output Q3 to 'ON' for 1 second allowing the pressure in both columns to equalise. This cycle will continue even if there is no demand of the gas. Delivery pressure is controlled using regulator (13) and the flow regulated using flow controller (12). Figure adopted from manual [157].

Table 2. 1 Numeration with parts description used in Figure 2.1.

#	Part	#	Part
1	CMS column 1	11	Front panel output pressure gauge
2	CMS column 2	12	Output flow regulator
3	Nitrogen storage tank, intermediate	13	Output pressure regulator
4	Nitrogen storage tank final	14	CMS column pressure gauge, internal
5	Pneumatic process control valve	15	Filter, double breathing air
6	Bottom press. Equalising solenoid valve	16	Inlet flow regulator
7	Top press. Equalising solenoid valve	17	Silencer
8	Non-Return Valve	18	Air inlet bulkhead connection
9	Safety pressure return valve	19	N2 gas outlet bulkhead connection
10	Tank pressure gauge		

Table 2. 2 Nitrogen Generator technical specifications.

Parameter	Specification	
Minimum Operating Ambient Temperature	5	°C
Maximum Operating Ambient Temperature	35	°C
Minimum Air Pressure	120 / 8.2	Psig / Bars
Maximum Air Pressure	130 / 8.96	Psig / Bars
Nominal Outlet Pressure	80 / 5.5	Psig / Bars
Max Output	10	L.min ⁻¹
Current Load	2.0 / 230	A / V

2.2.2 Helium

High purity helium (BOC, UK) cylinders were used to provide carrier gas for Thermal desorption (TD) and Gas Chromatography (GC) systems. The gas was purified (as described in section 2.2.3) before reaching instrumentation.

2.2.3 Gas purification and moisture control

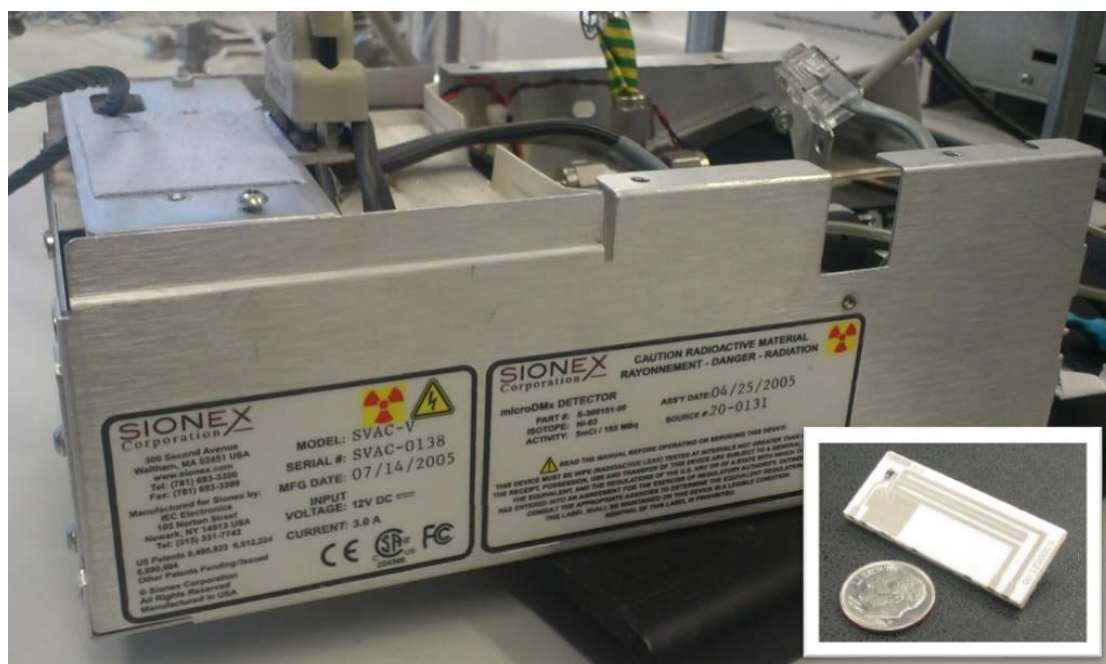
Final polishing of the gases was achieved with gas filters placed upstream of the instrumental systems to further remove traces of water and other contaminations. For this purpose charcoal and moisture filters were used. Charcoal filter (Varian, UK, Part # 10172), was packed with high capacity activated carbon and used to remove hydrocarbons, at room temperature. Moisture filter was also supplied by Varian, removed moisture, oils and other contaminations.

The level of water in d-IMS analysis, plays a crucial role in cluster formation. The level of water was routinely checked using moisture monitor (Series 35 from Panametrics, UK). For all of the experiments, where d-IMS was used as a detector, water level was set to be around 25 mg.m⁻³ ± 5 mg.m⁻³. The monitor was connected to the transport gas, just

before the d-IMS inlet (after, previous d-IMS disconnection) and left for 24 hours equilibration, before the reading was taken.

2.3 Differential Ion Mobility Spectrometer

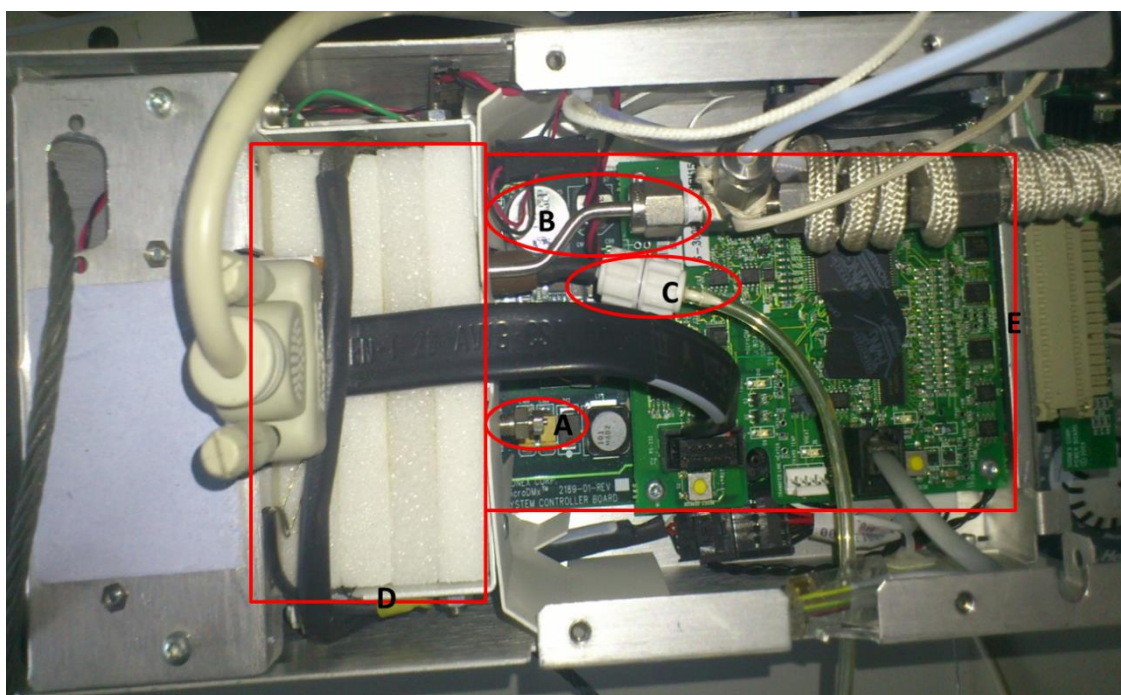
d-IMS separates and detects analytes based on a chemical species' ion mobility in low and high electric fields and its operation schematic can be found in Section 1.2. The d-IMS used for this study was a Sionex® micro-DMX stand-alone device, model number SVAC-V, obtained from Sionex Corporation, Massachusetts, USA.. Approximately 300 cm³.min⁻¹ purified nitrogen was used as the transport gas. The sample inlet port to the d-IMS was sealed off during the experimental process and analyte vapours were mixed with a transport gas before entering the d-IMS. Pictures 2.1 and 2.2 shows side and top view of d-IMS device used in these studies, highlighting basic parts of the instrument.



Picture 2.1 Side view of the d-IMS SVAC-V (Sionex, US) with radioactive ⁶³Ni ionisation source. Picture in the bottom right corner shows a d-IMS sensor.

The device uses a ⁶³Ni β -emitter as the ionisation source, with an activity of 5 mCi. After ionisation the vapours are flowed continuously via a transport gas, such as air or nitrogen, into the detector area with its parallel plates spaced 0.5 mm apart, with total sensor length of 2cm (picture 2.1 down, right corner). Once in the detector area, the ions experience a uniform oscillating asymmetric radio frequency electric field (RF) or separation field (E_d) which in planar devices operates under 1 to 3 MHz frequency and ranges from 40 to 120 Td (or 500–1500 V_d V). Each ion species will exhibit discrete

mobility characteristics. To make the d-IMS sensor tunable, a perpendicular tuning field E_c known as the compensation field E_c is applied. This field is superimposed on the oscillating asymmetric E_d field and keeps the ions of interest centred between the parallel plates and is detectable simultaneously by both negative and positive electrometers. The electric field conditions required to permit a particular ion to pass through the filter to the detector are specific to each ion species.



Picture 2.2 Top view of the d-IMS SVAC-V (Sionex, US) highlighting: blocked sample inlet (A), transport gas inlet (B) and outlet (C) placed above of the control electronics (E) and isolation of the d-IMS chip (D).

2.3.1 Software

Spectrometric parameters were controlled and monitored using the accompanying SionexmicroDMx™ Expert software, version 2.01, relayed to a central processing computer via a 9-pin COM to 9-pin serial COM cable. The software was run in this study from a HP Compaq nx6110 lap top, operating on Windows XP system. Spectrometer methods are controlled using the software, including setting the RF (or V_d) voltage and the scanning compensation voltage (V_c / V) range.

2.3.2 Functionality of the SVAC d-IMS

During analysis, V_c can either be scanned against a fixed value of dispersion voltage (V_d), or dispersion profiles can be run to scan V_c (between -43 to 15 V) against pre-defined stepped increases in V_d . Both approaches were used in this work and are discussed in Sections 2.6.2 and 2.7.4 below. Example data from a blank dispersion plot with a spectrum collected at fixed V_d are shown in Figure 2.2 and 2.3. Depending on the requirement of the experiment, a time of the scan across the V_c scan times could be set over the range 3 to 1000 ms and the number of V_c steps could be varied to optimise either resolution or intensity (sensitivity) of the responses.

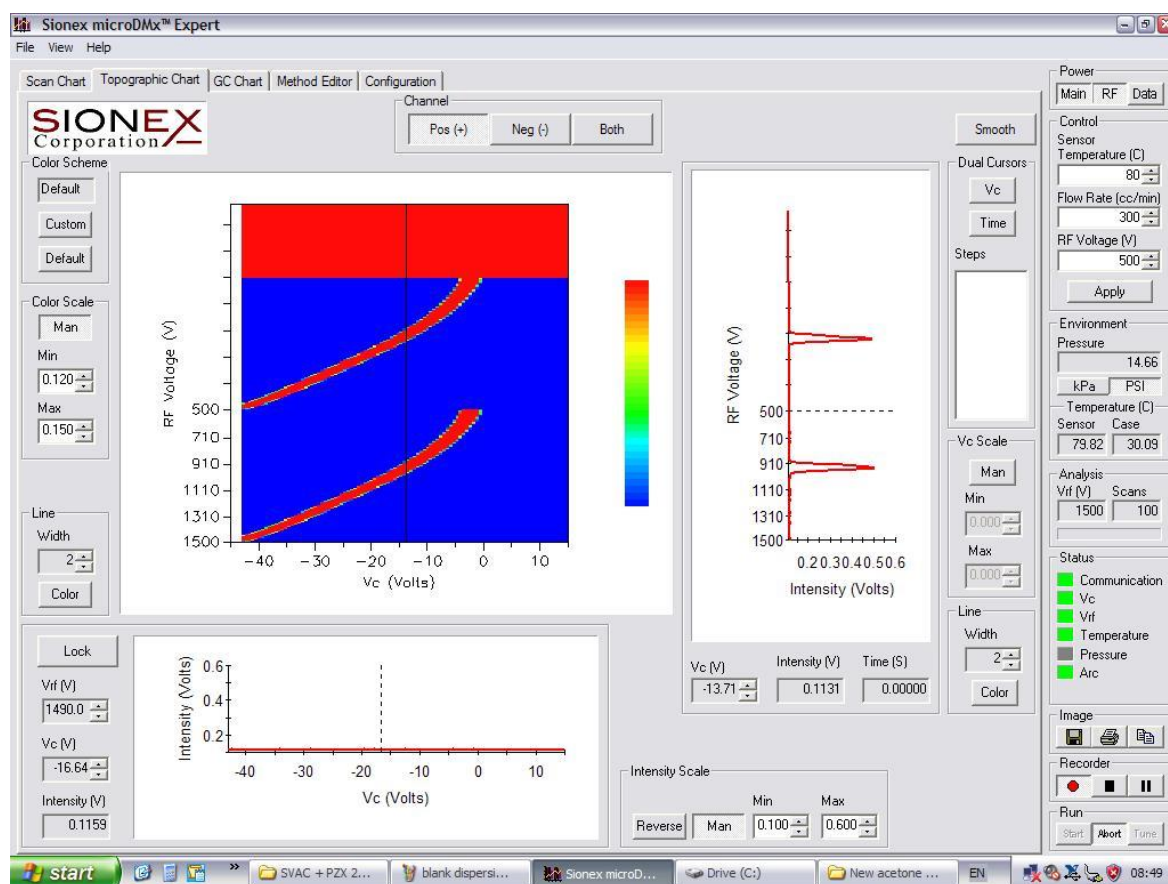


Figure 2.2 A Screenshot of a d-IMS SVAC (Sionex) dispersion profile, showing a blank dispersion plot of reactant ions only. The dispersion voltage (V_d) was ramped from 500 V to 1500 V (or 40 to 120 Td) using a V_d (RF) step size of 10 V. The V_c scan at each V_d step was between -43 V and +15 V. The d-IMS filter temperature and V_d are controlled from the right panel on the screen. The response intensity is displayed in colour coordinates.

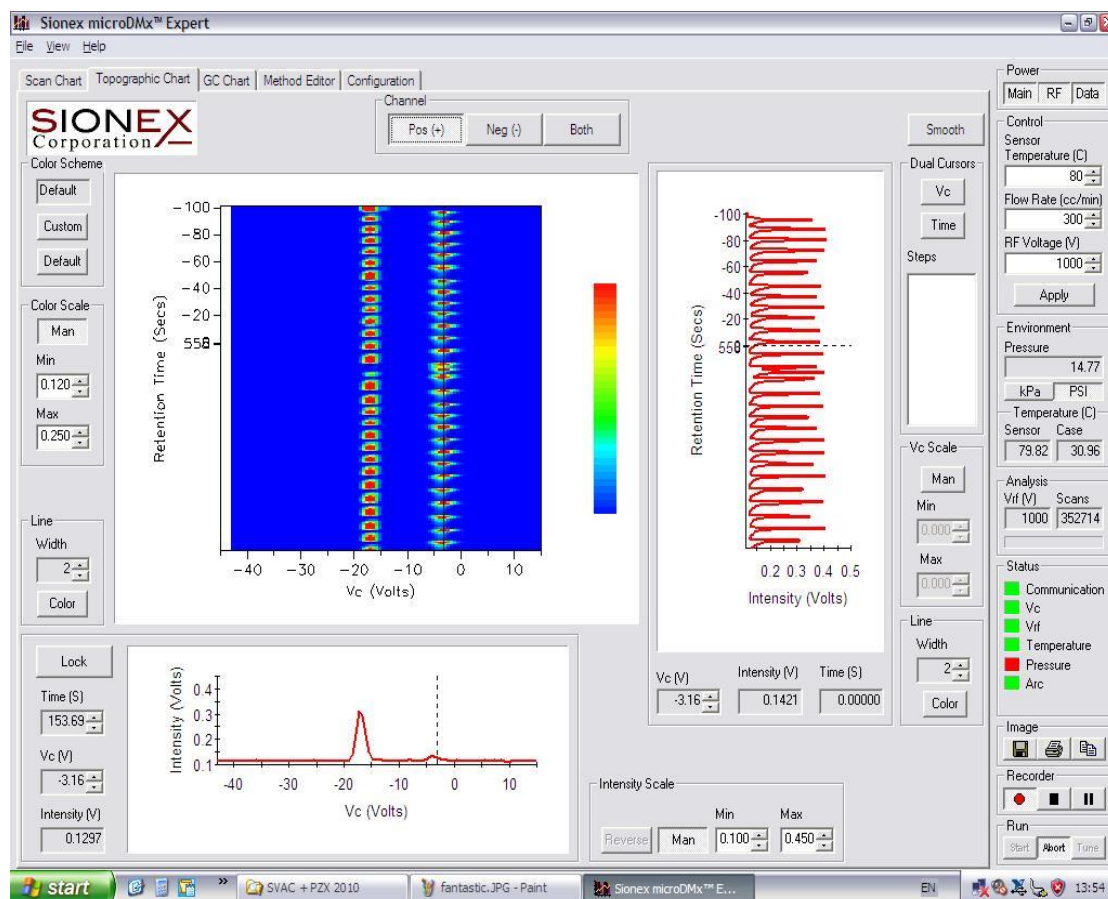


Figure 2.3 Screenshot of the detector and conductivity responses from the d-IMS SVAC (Sionex). The d-IMS filter temperature and V_d voltage are controlled from the right panel on the screen. Retention time is used as the x-axis variable, as the d-IMS can be interfaced to a gas chromatograph. The screenshot shows example of responses in the positive ion mode generated from 2-butanol injections with a piezoelectric actuator (Section 2.5.6.3), where the reactant ion peak (RIP) is shown at a compensation voltage of -17.46 V, and the 2-butanol dimer ion at -4.16 V, when applying a fixed V_d of 1000 V (or 80 Td).

2.4 Blanks and System Validation

The d-IMS was verified free from contamination before, during and after the experiments performed by evaluating programmed dispersion field responses (Section 2.3.2). This included instrument and system blanks. The instrument blank was determined from spectra collected with the d-IMS connected to the purified nitrogen stream only for the d-IMS transport gas. The system blank was determined for a full instrumental set-up allowing pure nitrogen to pass through all of the components of the experimental system before introduction to the d-IMS detector.

The blank dispersion plots were recorded as an Excel Matrix of signal current intensity, I , vs time, t (which corresponds to change in dispersion voltage V_d) vs compensation voltage V_c (Figure 2.4 orange, purple and green, respectively).

	A	B	C	D	E	F	G	H	I
1									
2	Vc	-43	-42.41	-41.83	-41.24	-40.66	-40.07	-39.48	-38.9
3	ret time								
4	0	0.1098	0.1127	0.1118	0.1127	0.1119	0.1131	0.1116	0.1114
5	1.016	0.1124	0.1121	0.1102	0.1117	0.1121	0.1132	0.1128	0.1136
6	2.016	0.1109	0.1129	0.1127	0.1117	0.112	0.1128	0.1112	0.1109
7	3.031	0.1125	0.112	0.1121	0.1117	0.1139	0.1126	0.1114	0.1106
8	4.047	0.1125	0.111	0.1121	0.1136	0.112	0.1125	0.1135	0.1122
9	5.063	0.1128	0.1118	0.1093	0.1112	0.1128	0.1117	0.1124	0.112
10	6.063	0.1101	0.1133	0.1131	0.1124	0.1087	0.112	0.1096	0.1124

Figure 2.4 Example of the fragment of the Excel data matrix, obtained from collecting d-IMS dispersion plots.

A visual basic macro was specially produced by the author to process the data, where time and compensation voltages were scaled and converted to dispersion voltages and electric fields (respectively) axes, before background subtraction of the raw data (r) to produce a contour and surface plot and extracted spectra at specific dispersion voltages or fields. This allowed detailed inspection of the profiles to determine that only ions corresponding to the reactant ion from $(H_3O)^+$ chemistry were present. The diagram for processing dispersion plots is shown in Figure 2.5. Post-macro processing was done for individual figures, which included surfaces rotation or colour pallet change.

In some cases traces of ammonia were detected, with signals observed at E_c values lower than those for the reactant ions $(H_3O)^+$. The ammonia signals were accepted when present at level below the limit of quantification ($LOQ < 8 * \text{signal}/\text{noise}$) as the signal did not interact with the reactant and product ions (RIP and PI, respectively) and there was sufficient charge associated with the RIP $(H_3O)^+$ to ensure that the experimental results could be relied upon.

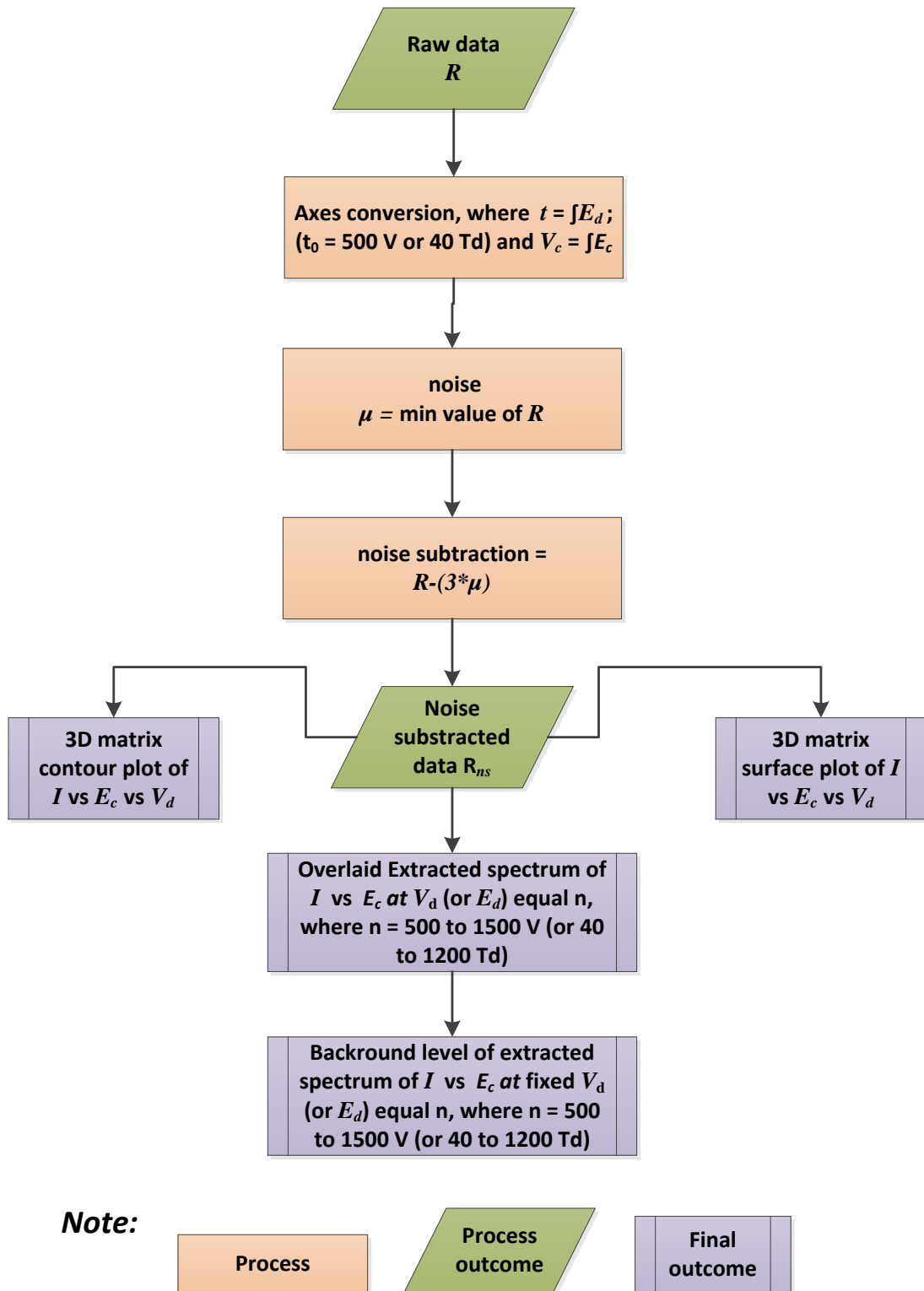


Figure 2.5 Workflow for processing collected dispersion plots during d-IMS experiments. Steps include: axes conversion, background subtraction, production of contour and surface plots, graphs of extracted Spectra and their background zoomed levels.

Example of the Figures produced using the macros are shown in Figures 2.6, 2.7 and 2.8.

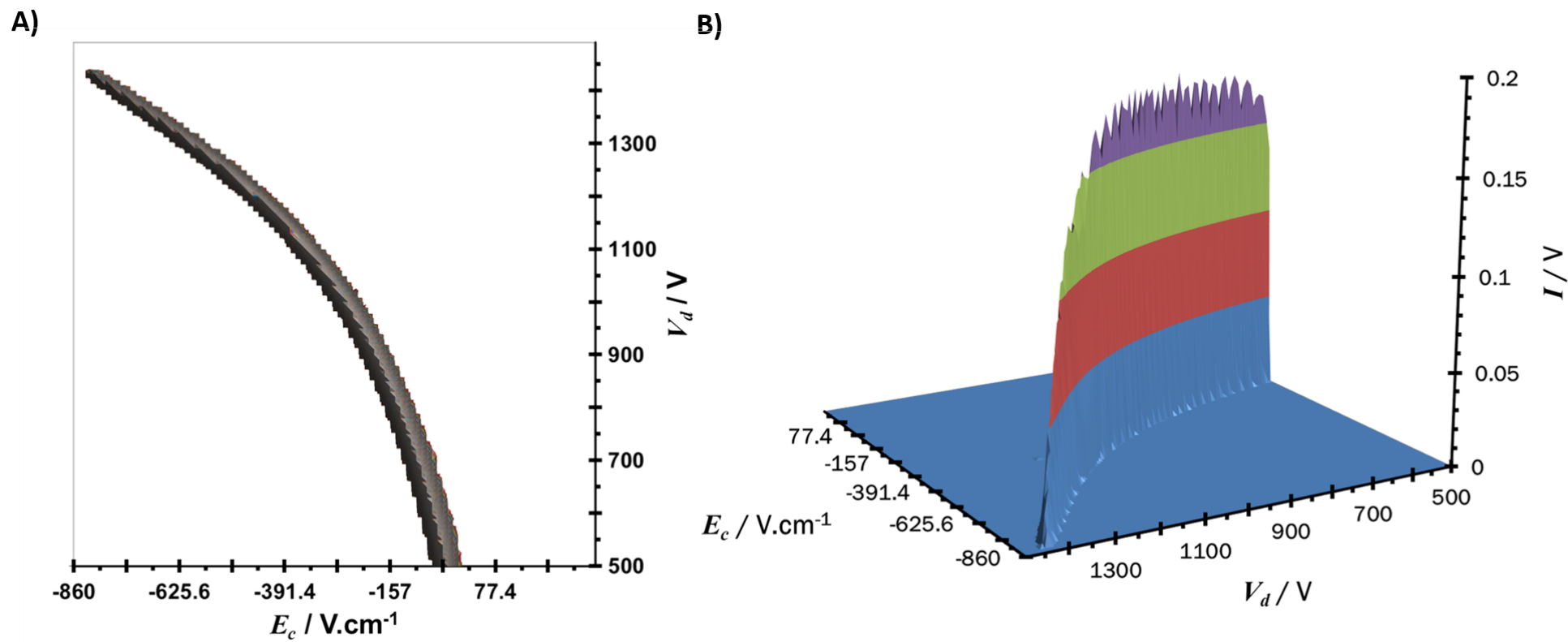


Figure 2. 6 Example of full system blank dispersion plot collected at 100 °C d-IMS temperature, with the dispersion field voltage amplitude (V_d) programmed from 500 V to 1500 V. A) Shows a topographic graph of the RIP, where V_d / V is plotted against the compensation field ($E_c / V.cm^{-1}$) and B) Shows a 3D surface graph showing the relationship of the RIP signal to V_d . Figures A and B, were produced using specially pre-recorded macro.

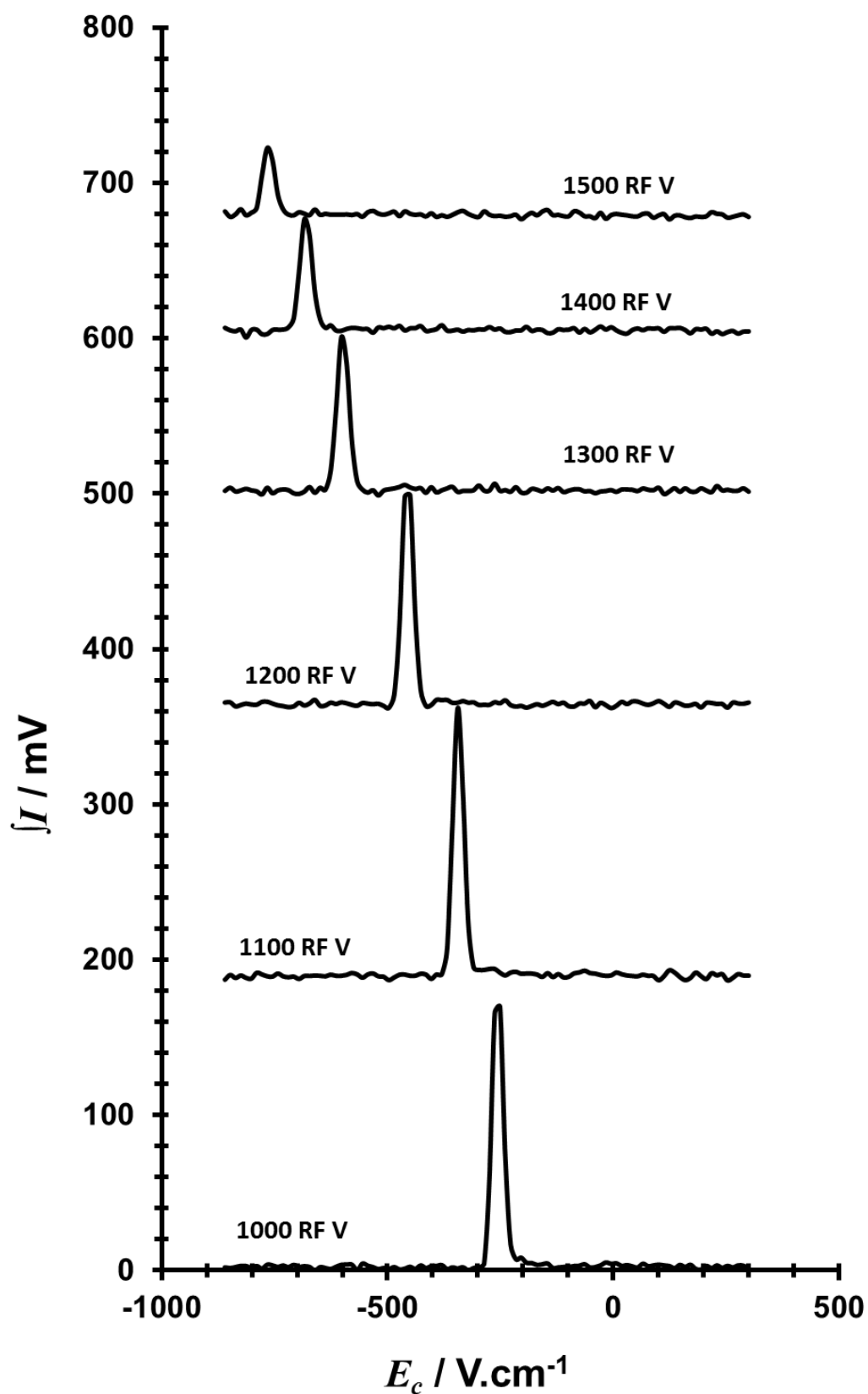


Figure 2. 7 Overlapped extracted spectra of system blank at 100 °C, showing relationship between RIP peak position on the compensation field scale (E_c in $\text{V}\cdot\text{cm}^{-1}$) and dispersion voltages. The figure was produced using pre-recorded macro.

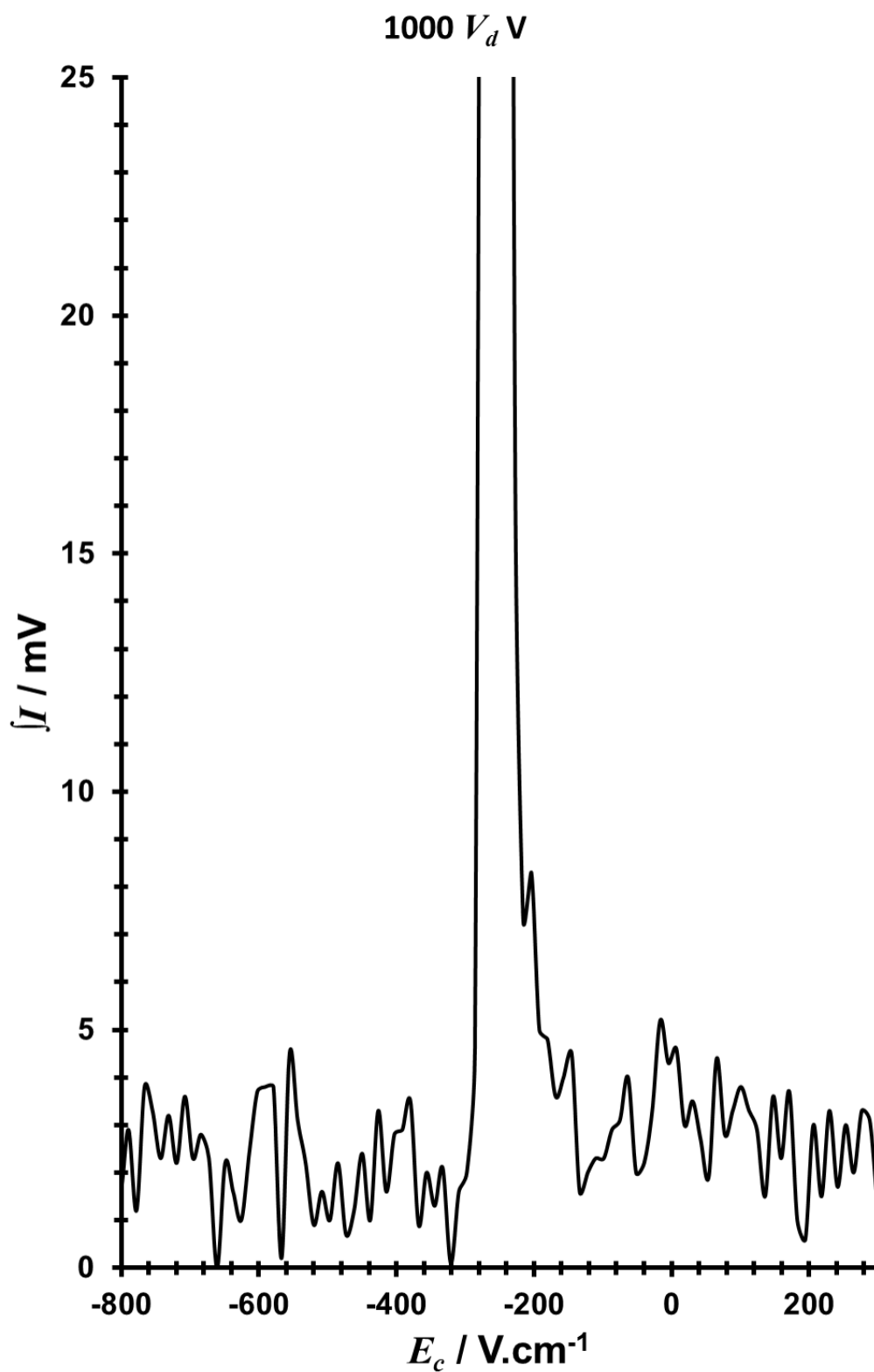


Figure 2.8 Extracted spectrum of system blank collected at 100 °C at 1000 V of dispersion voltage V_d , showing close look at the background noise. The figure was produced using pre-recorded macro.

Validation of the instrument included set of twenty blank dispersion plots under conditions given in Table 2.3, run for period of two separate days to determine the reproducibility of the following data parameters:

- The position of the reactant ion peak, in the positive mode of the d-IMS, at the compensation field V_c scale, (H_3O^+)
- The RIP intensity in the positive mode of the d-IMS / mV.

Table 2. 3 D-IMS operational parameters used for the study of instrument performance.

Parameter	Level
Ionization source	^{63}Ni
Scan frequency	1 Hz
D-IMS filter temperature	80° C
Inlet gas	Nitrogen, 300 cm ³ min ⁻¹
Relative Humidity	30ppm

Statistical data analysis was used to calculate the reproducibility of the results. This included a mean value and the relative standard deviation RSD % of intensity of the reactant ion peak at different V_d V (between 600 and 1300 V) with an interval of 100. Average intensity, relative standard deviation and 95% confidence limit were calculated and summary of the analysis is shown in Table 2.4.

Table 2. 4 Statistical data for intensity I of reactant ion peak at different V_d voltages for positive mode used to determine reproducibility of the instrument performance and acceptance limits.

V_d / V	\bar{I} / mV	RSD %	+/- 95 % / mV
600	268.1	3.39	±3.98
700	270.3	3.00	±3.55
800	259.2	2.73	±3.1
900	240.6	2.53	±2.67
1000	232.9	2.38	±2.43
1100	216.5	2.30	±2.18
1200	180.8	3.84	±3.04
1300	152.1	3.66	±2.44

Position of the reactant ion was another parameter studied to set the limits on instrument performance, which characterised a trajectory of the RIP. This was done by tracking position of the RIP on the V_c scale at the highest intensities of the d-IMS spectra at chosen V_d . The range of V_d chosen for a statistical analysis was between 600 V to

1300 V for +ve mode with the interval of 100. The mean value, relative standard deviation and 95% confidence limit were calculated and are given in Table 2.5.

Table 2.5 V_d vs. V_c , to describe reproducibility of the RIP position on the V_c scale and establish acceptance limits of the instrument performance.

V_d / V	\bar{V}_c / V	RSD %	+/- 95 % / V
600	-3.75	0	± 0
700	-5.95	0.3	± 0.01
800	-8.74	0.6	± 0.02
900	-12.23	2.3	± 0.15
1000	-16.61	3.3	± 0.24
1100	-21.37	3.2	± 0.24
1200	-26.41	5.8	± 0.67
1300	-33.62	8.9	± 1.31

2.5 Experimental Setups

2.5.1 Test Atmosphere Generator-d-IMS

Figure 2.9 shows the experimental arrangement for optimisation of the d-IMS responses and experiment no 1.2.1 (Table 1.1 of Chapter 1).

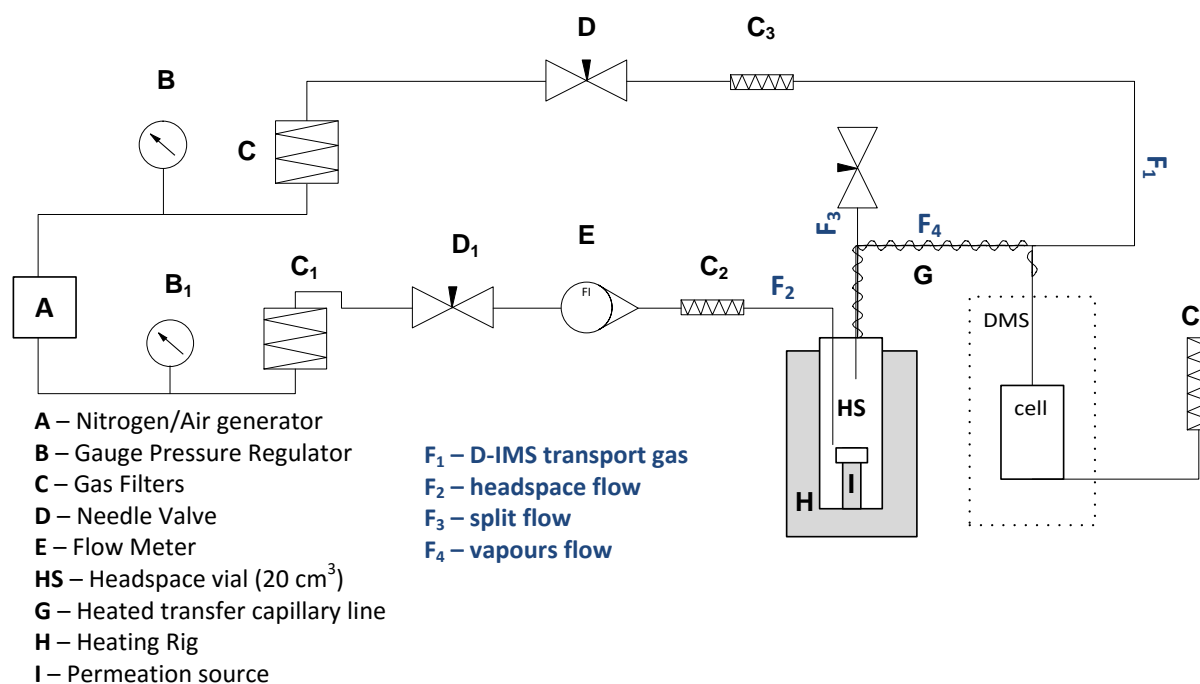


Figure 2.9 Schematic of the experimental setup used for introducing alcohols vapours to the d-IMS ion filter in experiment no 1.2.1, as well as optimisation studies on alcohols responses. The main part of the system contains test atmosphere generator (TAG) with permeation sources and d-IMS analyser.

The system was constructed to generate low concentrations (ppb level) of vapours and inject them into the d-IMS filter. Nitrogen transport gas was supplied by the nitrogen generator and dried (C and C_1) and purified (C_2 and C_3) through filters. Flow was controlled with stainless steel needle valves D_n (Swagelok, UK). The test atmosphere generator (TAG) was a thermostatically controlled stainless steel rig (H) which housed a 20 cm³ glass gas chromatographic headspace vial (HS). Pre-calibrated permeation sources (I) were placed into the vial. The vial was capped with a silicone septum, and crimp-sealed with an aluminium lid. The septum of the HS vial was pierced with a 1/16" steel tube and small flow (F_2) of filtered nitrogen gas passed through the steel tube into the headspace of the vial, sweeping vapour and exiting through a 0.53 mm i.d. deactivated capillary silica tubing (Restek, UK) inserted into a depth of 1 cm into the septum of the sealed vial and connected to 1/8" stainless-steel steel tubing maintained at elevated temperature with a temperature controller, type k thermocouple (RS, UK) and heating cord (Omega, UK); to suppress condensation of the VOC within the pipework. The flow from the headspace vial was split through a tee union and a 1/8" stainless steel needle valve (D2) (Swagelok, UK) to give two flows F_3 and F_4 . F_4 was mixed with the transport gas (F_1) using a sheath flow approach [158] and connected to the d-IMS filter; see Section 2.7.4 for details of concentration calculations.

2.5.2 Exponential dilution-d-IMS

Figure 2.10 shows experimental set up used in experiments number 1.1, displayed in Table 1.1 Chapter 1. The general set up was similar to that shown with Figure 3.9. However, the TAG system was exchanged with a 500 cm³ exponential dilution rounded bottom flask, (F) (custom made), placed in a heating mantle (Heidolph, MRHei-Standard), controlled with a digital temperature controller (Heidolph). The flask was insulated to ensure constant temperature across the entire surface. In this setup the split was removed and all the vapours were transferred via a heated 20 cm long 0.53 I.D silica capillary tubing, into the d-IMS transport gas, using a sheath flow interface. More details about the exponential dilution elements are in Section 2.6.

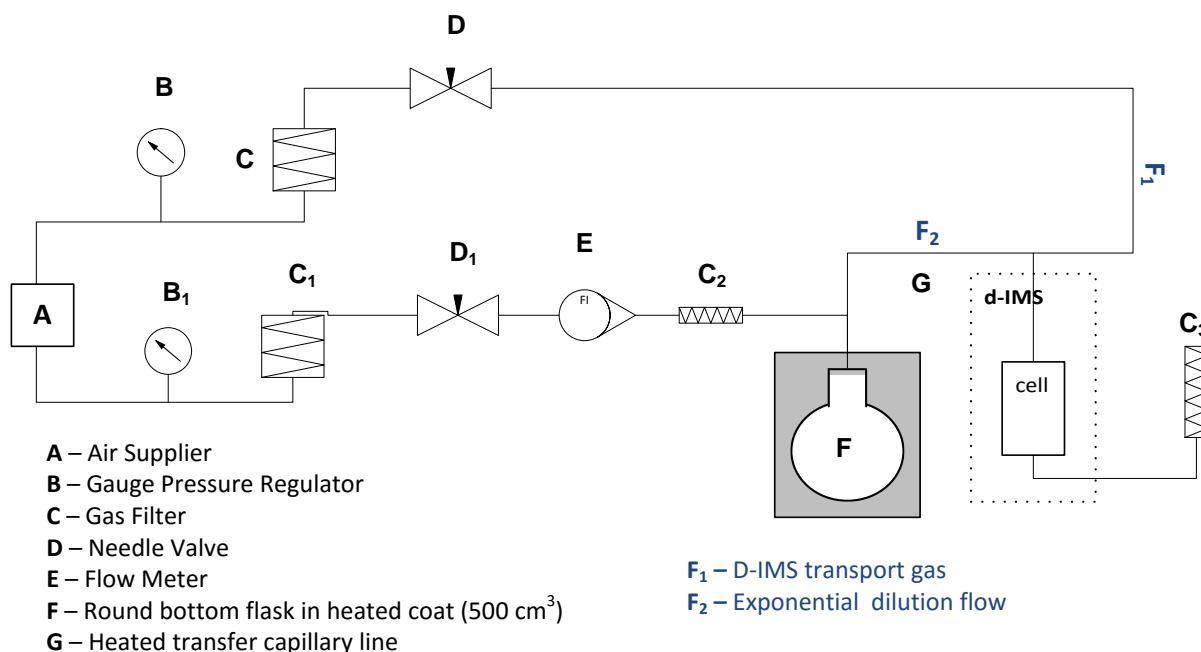


Figure 2. 10 Schematic of the experimental setup used in experiment 1.1.2 and 2.1. The heart of the system use an exponential dilution approach.

2.5.3 D-IMS-MS¹

Figure 3.11 shows the set-up used in Experiment no 1.2.2 (Table 1.1, Chapter 1). Test-atmospheres of alcohols were delivered to the d-IMS/MS from a 3 dm³ exponential dilution flask via heated transfer line. A Shimadzu model 2020 mass spectrometer (Columbia, MD) was modified to incorporate a d-IMS ion filter built with dimensions, electronic controls, and ionisation source similar to the Sionex SVAC (Section 2.3). The device uses a sinusoidal voltage waveform to generate an electric field to heat ions instead of an asymmetric waveform to generate a dispersion field for ion filtering. The d-IMS assembly included two ceramic plates with thickness of 1 mm, length of 30 mm, and width of 25 mm separated by a Teflon gasket (0.5 mm x 30 mm x 25 mm) with a 3 mm wide centre channel for gas and ion flow. These are held between two Teflon plates (4 mm x 30 mm x 25 mm) and secured under compression by two aluminium plates (5 mm x 30 mm x 25 mm) with six screws. At each end of this assembly are aluminium end caps (20.5 mm x 5 mm x 25 mm) attached to the aluminium plates with four screws. An 1/8"

¹ This experimental work was performed by Prof. G.A Eiceman team, New Mexico State University (NMSU) and analysed in Loughborough by the author.

stainless steel union (Swagelok Corp., El Paso Valve and Fitting, El Paso, TX) was threaded into one cap, as an inlet. A 111 MBq ^{63}Ni foil was fitted into the interior volume of this fitting. The other cap connected to the mass spectrometer with a stainless 1/8" to 1/16" reducing union (Swagelok) fitted with a capillary line to the mass spectrometer held by compression in the 1/16" end of the union. This assembly was insulated using glass fibre insulating sheeting and the temperature was controlled by conduction from the transfer line, heated using resistive wire.

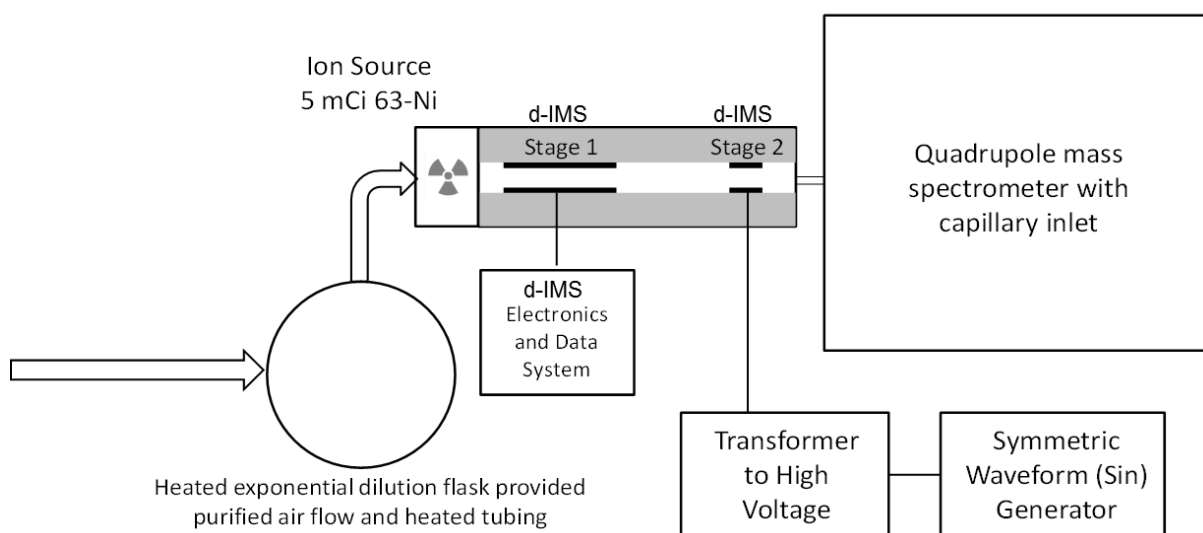


Figure 2.11 Schematic of the experimental setup used in d-IMS-MS studies on alcohols, with exponential dilution flask, two stage tandem d-IMS with 5mCi Ni63 radioactive source and 0.5 mm gap between the electrodes and quadruple mass spectrometer.

2.5.4 GC-d-IMS

Figure 2.12 represents schematic of the system used in experiments number 2.1 (Table 1.1 in Chapter 1). This setup was used in cases of quantitative calibration of d-IMS responses of analytes studied in the thesis. This allowed a fast and efficient calibration of compounds at pre-optimised conditions (Fixed V_d V).

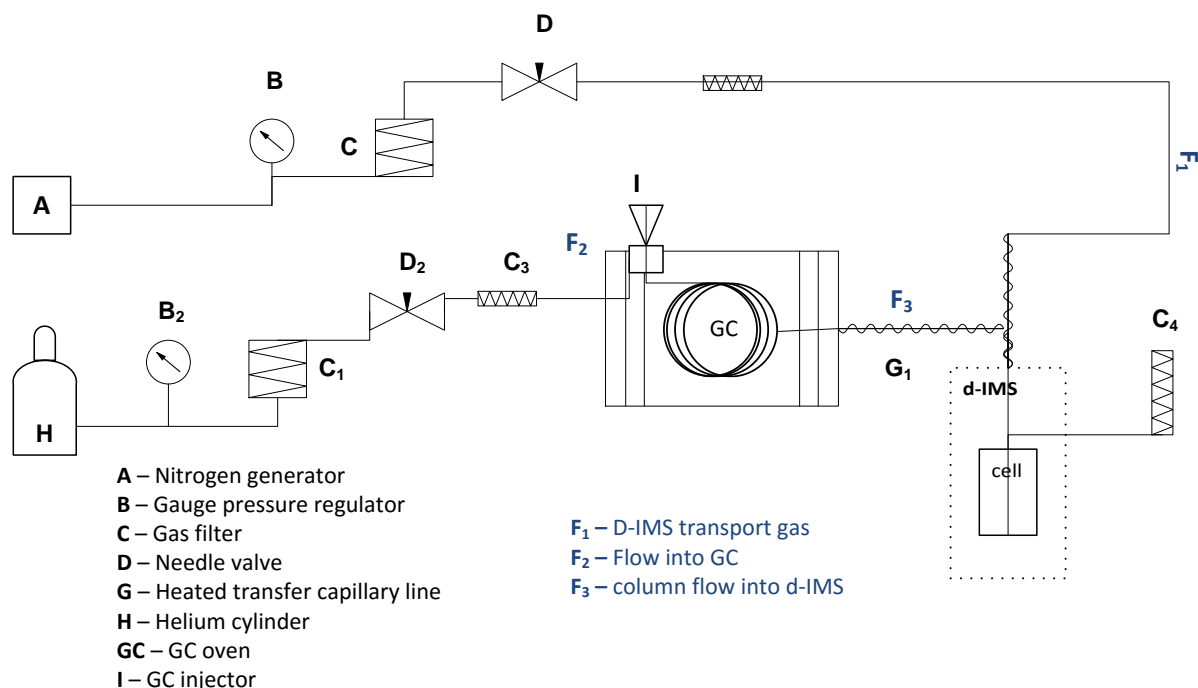


Figure 2. 12 Schematic of the experimental setup used in experiment 2.1 with GC column connected into the d-IMS transport gas using sheath flow.

The Helium carrier gas was purified and dried (C₁ and C₃ respectively), controlled via stainless-steel needle valve (D₂) and connected to the GC injector port (I). A 30 m long wall-coated open-tubular capillary GC column with an internal diameter of 0.32 mm and a 0.5 µm thick trifluoropropylmethylpolysiloxane stationary phase (Rtx-200MS, Restek, UK) was connected directly into the injection port fitted with a deactivated sky liner (Restek, UK). The column was connected to the d-IMS transport gas using a sheath flow [159] interface and heated transfer line (G₁). 20 cm long 1/4" stainless-steel tubing, with 20 cm of the end GC column was inserted inside of the tube, and heated with heating cord (Omega, UK) to 100 °C and wrapped with insulation. A thermocouple type k (RS, UK) inserted between the heating rope and the stainless tube connected to a temperature controller (RS, UK) was used to regulate the temperature of the transfer-line.

2.5.5 TD-GC-d-IMS

In experiment number 2.2 (Table 1.1) a thermal desorption-GC-d-IMS system (Figure 2.13) was used with a two-stage thermal desorption unit (Markes International Unity 2) fitted with a Tenax TA/ Carbograph 1TD cold trap for refocusing/pre-concentration purposes. A heated transfer line (G) with deactivated 1.5m long 0.23 mm I.D. capillary

line was connected to a 30m long by 0.32 mm I.D. GC column with a 0.5 μm thick trifluoropropylmethylpolysiloxane stationary phase (Rtx-200MS, Restek, UK). The further part of the system construction was as described in Figure 3.12.

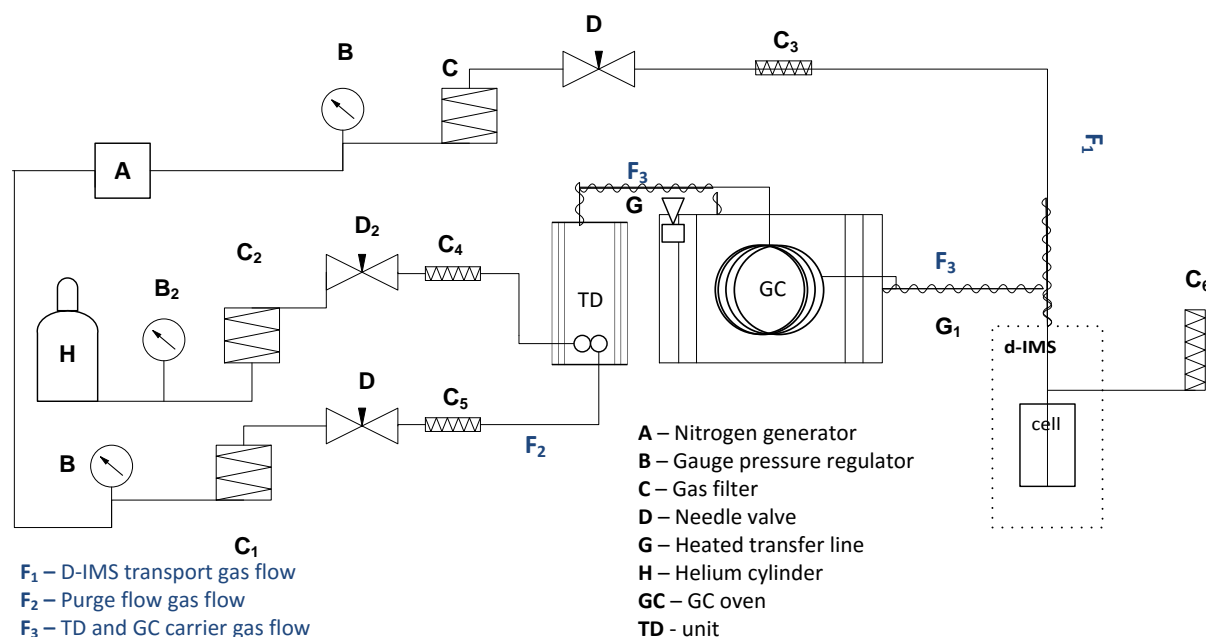


Figure 2. 13 Schematic of the experimental setup used in experiment 2.2 (Table 1.1, Chapter 1) with Thermal desorption (TD) and gas chromatogram (GC) mixed with d-IMS transport gas using sheath flow approach.

2.5.5.1 Unity thermal desorption system

The Unity thermal desorption unit consists of a sample tube (Tenax and Carbograph), a cold trap (Tenax), split tube (Charcoal), various solenoid valves and two needle valves (NV), see Figure 2.14. The Unity has three adsorbent traps. The sampling trap, a cold trap and a split trap, with the flow of helium across this network controlled by a combination of multi-port valves, needle valves and solenoid shut-off valves.

Valve 3 controls the desorption flow, and the split flow is controlled by Valve 2. (These flows can be varied to optimise a method with the manually adjusted needle Valves NV1 and NV2, with flows measured using an Alltech DFC digital flow meter (Alltech part # 4700)).

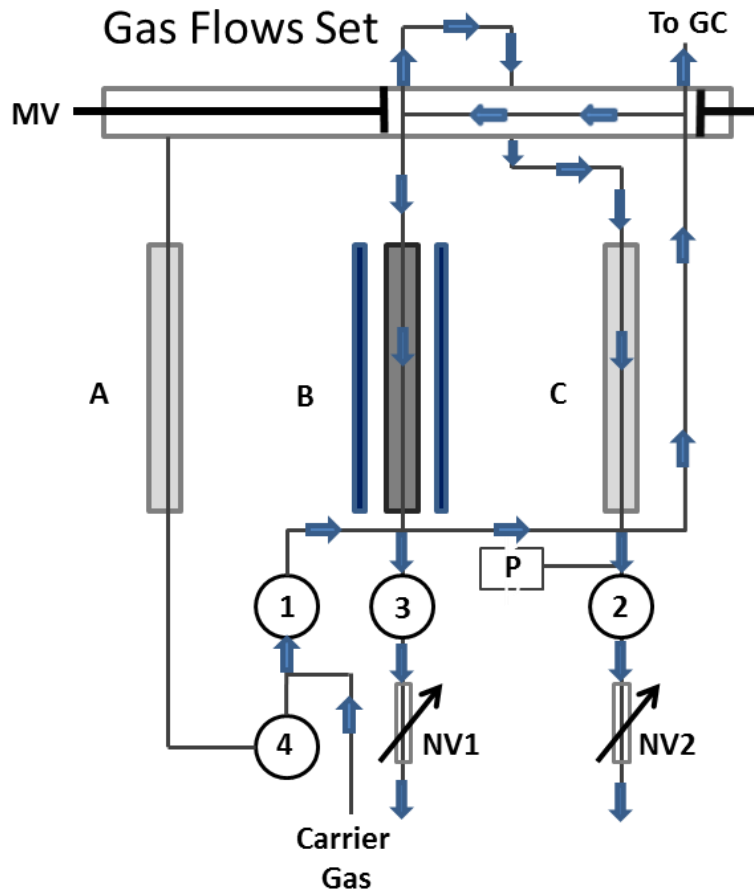


Figure 2. 14 Unity Schematics showing A) sample tube B) cold trap C) split tube, P) is the pressure transducer and MV) is the multi-port valve. Solenoid valves are labelled 1 to 4 and needle valves (NV) 1 and 2.

A typical 2-stage thermal desorption method is outlined below:

- Pressure test: A leak test ensures that no sample losses occur during thermal desorption. The system is pressurised and then valves 2, 3 and 4 are shut off and the multi-port valve isolates the column from the thermal desorption circuit. The pressure in the thermal desorption circuit is monitored by the pressure transducer, Figure 2.15 A.
- Prepurge stage: Valves 1, 2 and 4 are opened, Valve 3 is shut and the multi-port valve isolates the column from the thermal desorption circuit. This purges residue air from the adsorbent sample tube and associated tubing and fills them with helium carrier gas. If necessary any displaced volatiles may be retained in the split trap, or Valve 3 opened to direct them to the cold trap, Figure 2.15 B.
- Primary thermal desorption: The cold trap is cooled to -10°C . Valves 1, 3 and 4 are opened and Valve 2 is closed, the multi-port valve isolates the column from the

thermal desorption circuit. Note that the flow into the cold trap can be split to optimise the loading of analytes on the column; this would involve opening Valve 2 and carefully adjusting Needle Valve 2. The adsorbent sample trap is then thermally desorbed at the set temperature and for the appropriate time, Figure 2.15 C.

- Secondary thermal desorption. Once the thermal desorption process is complete, Valves 1, 2 and 4 are opened and Valve 3 is shut. The multi-port valve is switched to the inject position resulting in the cold trap being back-flushed while it heats up at max. $40^{\circ}\text{C s}^{-1}$ to a set temperature for a predetermined time. As soon as the cold trap starts to heat a signal is sent to the GC to start the run and the recovered analytes are carried on to the column via a heated transfer line Valves 2 and Needle (deactivated fused silica, Restek). At this stage a final split may be used controlled by Valve 2 before the flow reaches the transfer line and column another split is encountered, Figure 2.15 D.

2.5.6 Exponential dilution-PZX-d-IMS

Two independent analyte delivery systems were used for introduction of vapours of modifiers and dopants (in this case can be understood as analytes) into a d-IMS filter to study d-IMS responses of mixed alcohol system. Digitally controlled injections of dopant from a piezoelectric actuator were performed during an exponential washout of modifier vapours across four orders of magnitude concentration levels. Figure 2.16 shows schematic of the constructed system.

The setup was an extension of the exponential system presented in Figure 2.10. Exponentially diluted vapours were transferred continuously via flow (F_9) into the d-IMS transport gas (F_8). A separate interface (H) for the piezoelectric injector was connected to the transport gas line allowing ng-range injections of a second compound (analyte/dopant) to be vaporised and mixed with d-IMS transport gas. This was done by employing venturi pump (G), to draw vapour from the evaporation zone below the piezoelectric injector (F_4) into a dilution flow (F_5) to finally reach a d-IMS transport gas (F_8). The concentration of vapours from the piezoelectric injections was controlled digitally by changing frequency of the injections. The interface and a backpressure system controlling piezoelectric injector itself was designed and built in house by previous researchers [160, 161]. In this thesis the design was fully reconstructed.

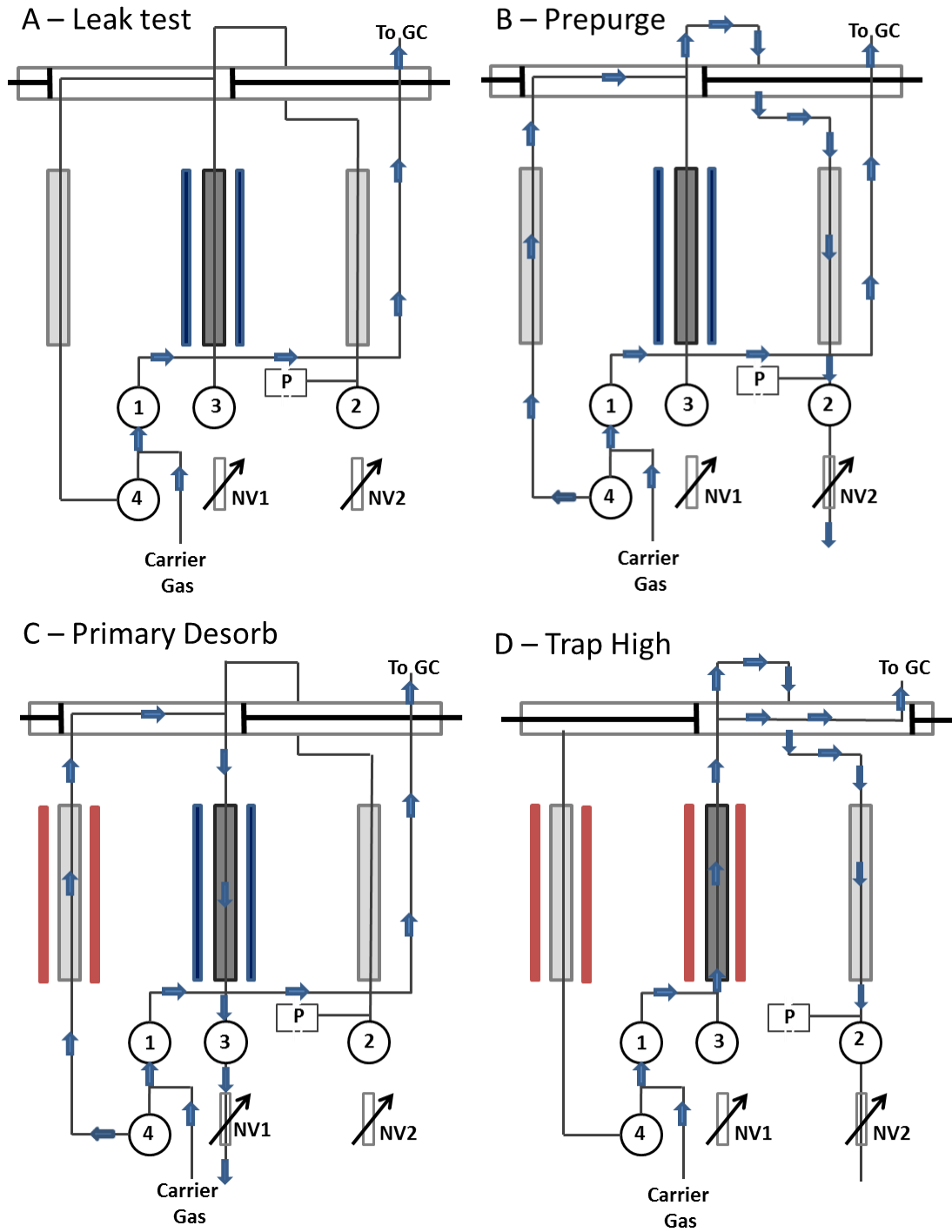


Figure 2. 15 Schematics of unity during a thermal desorption run. A - leak test, B - prepurge stage, C - primary desorb stage and D - cold trap high

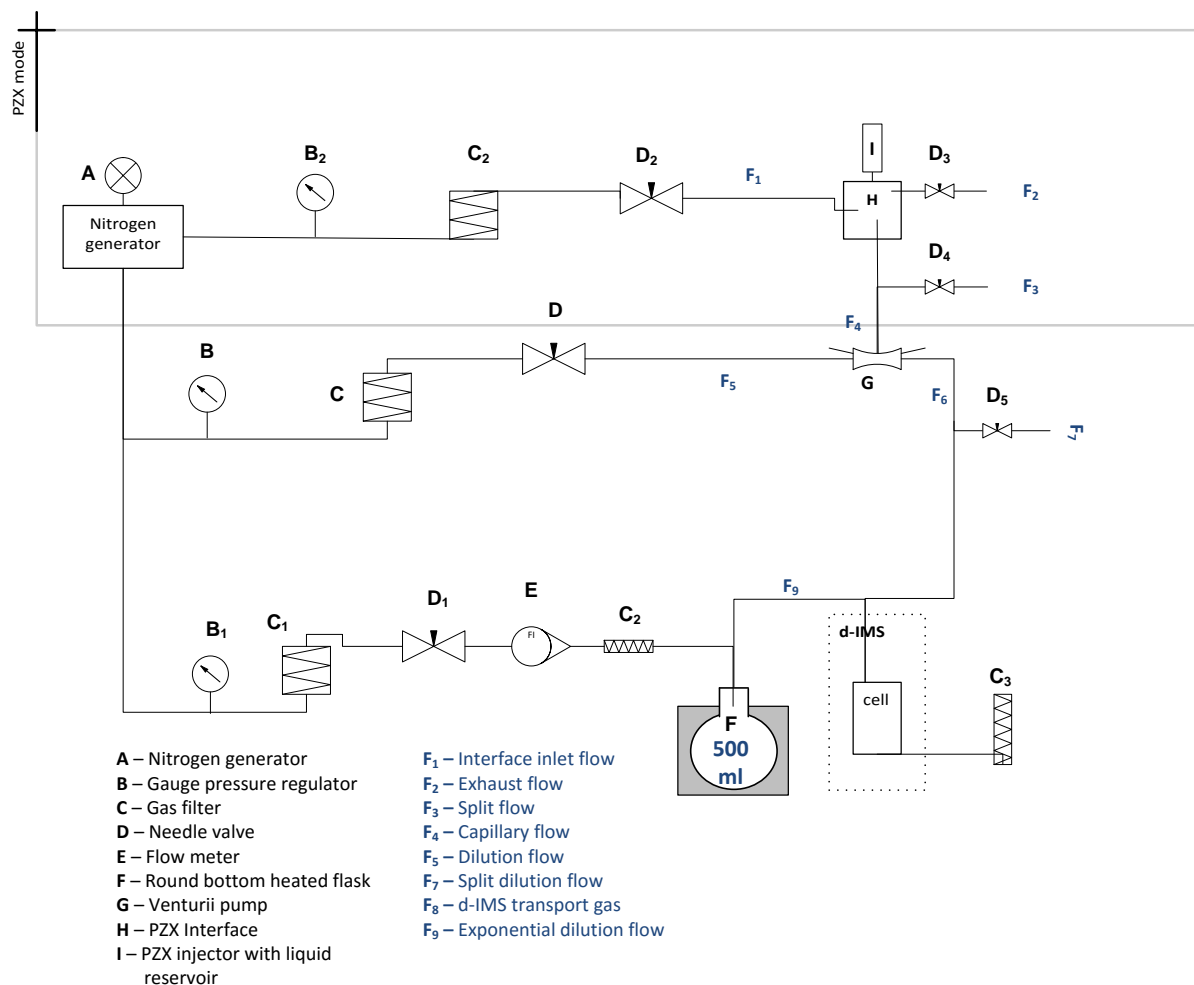


Figure 2.16 Schematic of the experimental setup used in experiment used to study mixture of potential dopant and modifier. The heart of the system use an exponential dilution approach and interface for the piezoelectric injector.

2.5.6.1 Functionality of the interface, backpressure system and piezoelectric actuator

Figure 2.17 shows the interface (H – Figure 2.16) for the piezoelectric injector (PZX) in more detail. Liquid was jetted from the liquid reservoir with a piezoelectric actuator (Microfab Technologies, TX, USA) - **A** through a 2 mm I.D. × 92 mm glass injection liner (Fluka, Gillingham, UK) - **B** packed with about 10µg of deactivated glass wool to promote efficient vaporisation. The injector and liner were aligned with a PTFE interface block - **C**, which held **A** and **B** 1 mm apart.

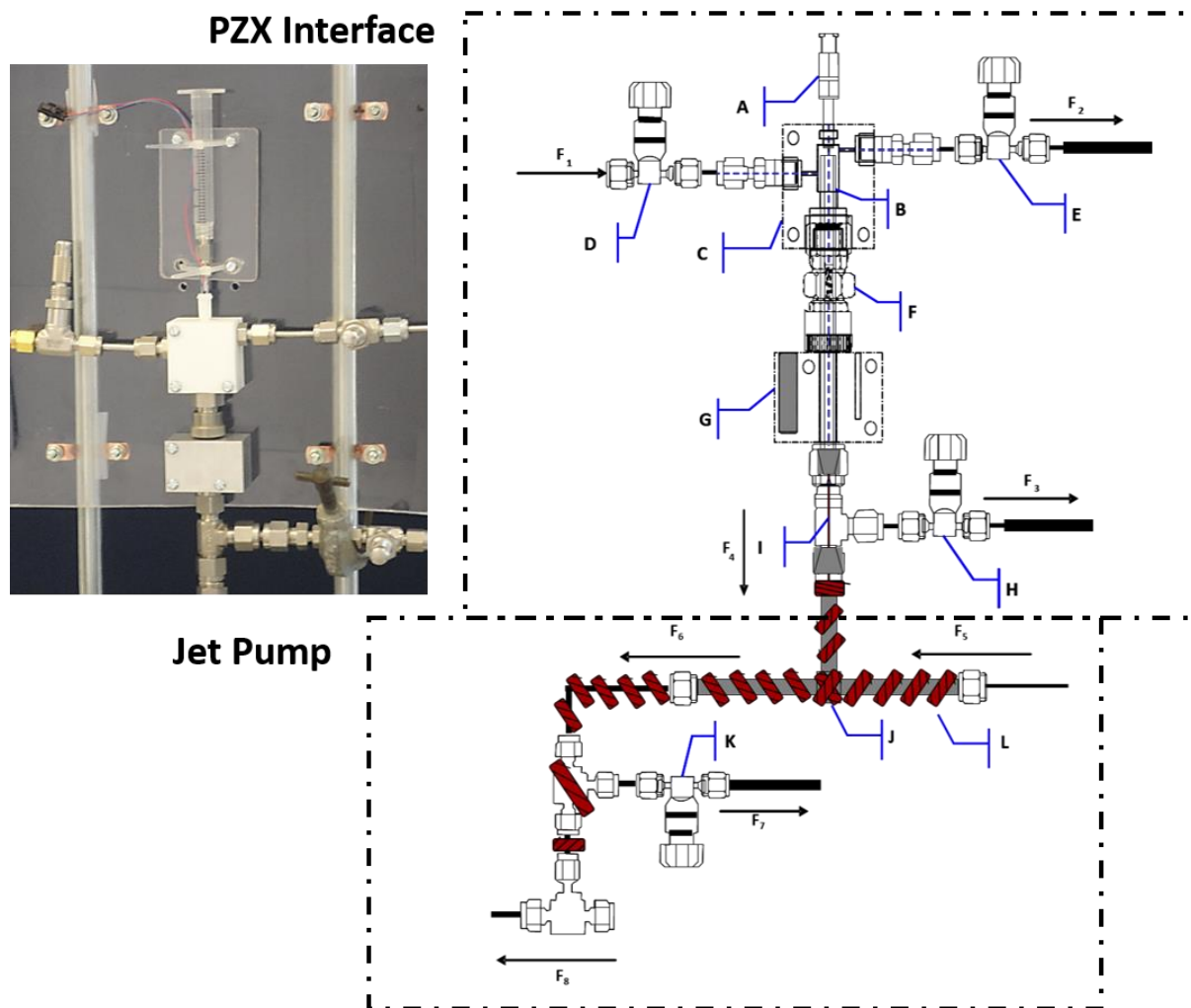


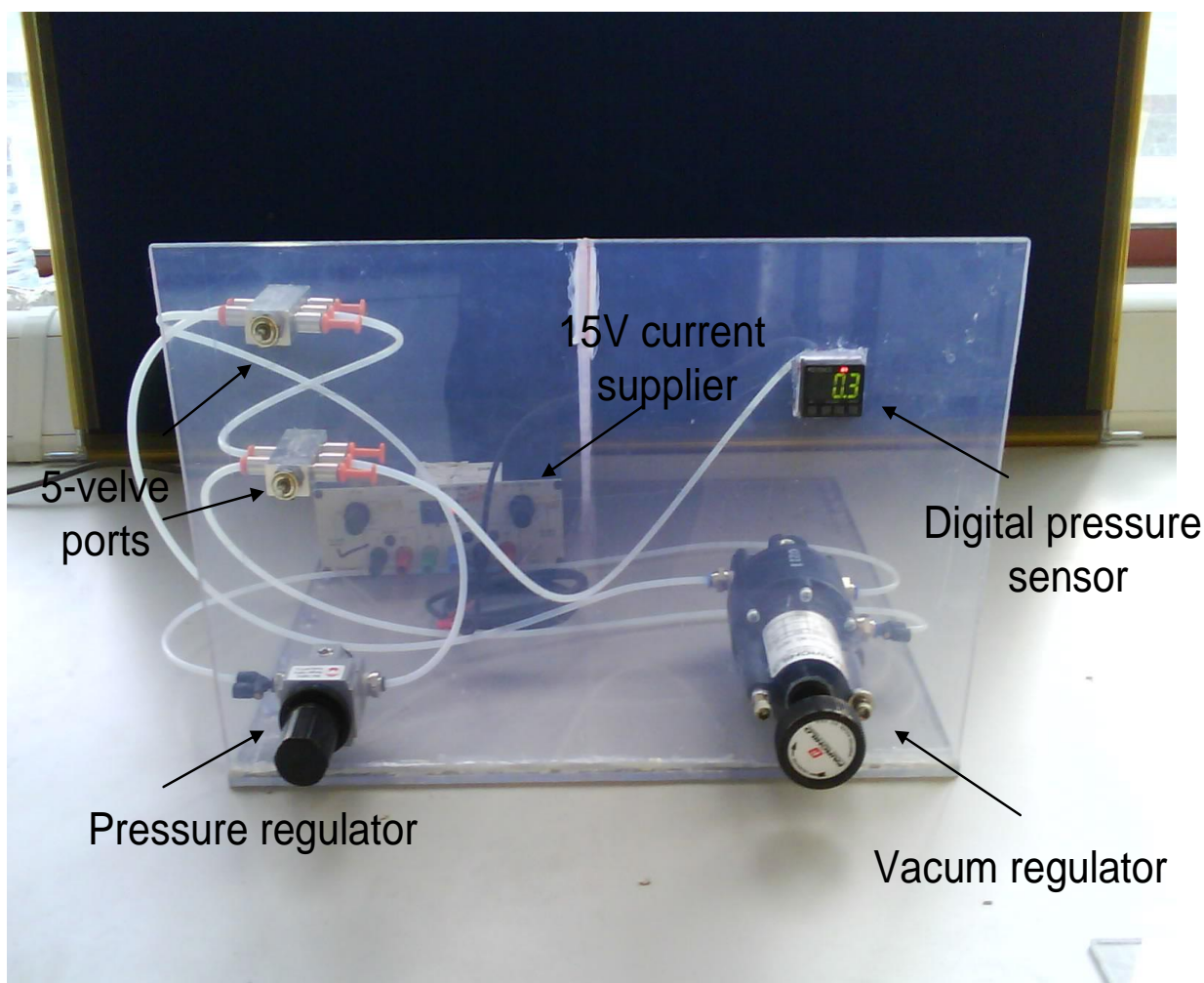
Figure 2.17 Schematic of PZX interface functionality, connecting piezoelectric injector with d-IMS transport gas via Jet pump. Left top: picture of constructed interface.

The actuator was fitted into a 4 mm diameter orifice at the top of the PTFE block. $250 \text{ cm}^3 \text{ min}^{-1}$ (F_1) of compressed nitrogen, controlled with a $1/8$ " stainless-steel needle valve type S (D) was directed around the outside of the liner (A) into the interface between the actuator (A) and injection liner. Volatile impurities arising from the injector were removed through an exhaust line (F_2), controlled via a $1/8$ " stainless-steel needle valve type S (E). To provide a gastight seal around the liner, the interface was attached to an ultra-torr $1/4$ " stainless steel NPT union (Swagelok, Manchester, UK). The bottom of the liner was fitted into a stainless steel heating block (G) (Albrook Engineering, Loughborough, UK) with a heating cartridge (RS, Herts. UK) controlled via a k-type thermocouple and temperature controller (RS, Nottingham, UK) and maintained between $70 \text{ }^\circ\text{C}$ and $120 \text{ }^\circ\text{C}$. The base of the liner (B) was held in the heating block by a $1/4$ "

stainless steel nut (Swagelok, Manchester, UK) with a 1/4" PTFE ferrule and a viton™ o-ring seal attached to a 1/4" stainless steel tee-union where the vapours were split (Swagelok, Manchester, UK) (F). The split ratio was controlled with a 1/8" stainless-steel needle valve type S (H). 0.32 mm I.D. × 16 cm (I) deactivated silica capillary tubing (Alltech Associates, IL, USA) was inserted through a reducing ferrule through the tee-union (F) into the base of the liner, the split point. The capillary tubing carried the injected vapours (F_4) into the dilution gas (F_5) of the jet pump (J), which was attached into the interface, allowing effective vapour transfer into the d-IMS device. (The jet pump worked on the Venturi effect, creating a vacuum and suction through the capillary.) A 1/4" stainless-steel (Swagelok, Manchester) tee union introduced an additional split (F_7), controlled by another 1/8" stainless steel needle valve (K). The jet pump was heated with a heating cord (L), to prevent condensation of the vapours and suppress hysteresis effects. The manifold was attached to the d-IMS transport gas (F_8) via 1/8" stainless steel tee union. Constructed interface is shown on the picture in Figure 2.17.

2.5.6.2 *Backpressure system for piezoelectric actuator*

Pressure within the piezoelectric injector reservoir was controlled via a backpressure system. The function of back pressure system was to supply the purge gas to the actuator and control the operating pressure in the liquid reservoir of the dispenser during actuation. This was controlled by a pressure regulator (Norgren, Staffordshire, UK) fitted with 1/4" stainless steel NPT connections. The purge gas was balanced in the gas manifold with a vacuum generated by pressure rotary vane vacuum pump. The vacuum regulator in the manifold provides the pressure for the actuation between - 0.1 kPa and - 0.3 kPa; measured by a digital backpressure sensor. A positive purge pressure of 1.2 kPa was applied to the reservoir to blow through potential blockages. Switching between control and purge modes was controlled with 2-way 5-port valves, see Picture 2.3.



Picture 2. 3 Backpressure system built to control pressure of liquids in PZX reservoir.

2.5.6.3 Piezoelectric actuator and bipolar waveform

The piezoelectric injector used in this study was a Microfab dispensing device with 60 μm crystal orifice (Microfab Technologies, TX, USA; part no B11-57-02). In order to generate a drop, a voltage pulse was sent to the crystal head with a bipolar waveform using an external driver (JetDrive™ 4, Microfab Technologies, TX, USA). The shape of the waveform used is shown in Figure 2.18 The bipolar waveform started at an isoelectric point (0 V), a positive-polarity wave was applied to the crystal for a specified time period, before a negative-polarity wave, termed an echo wave, was applied.

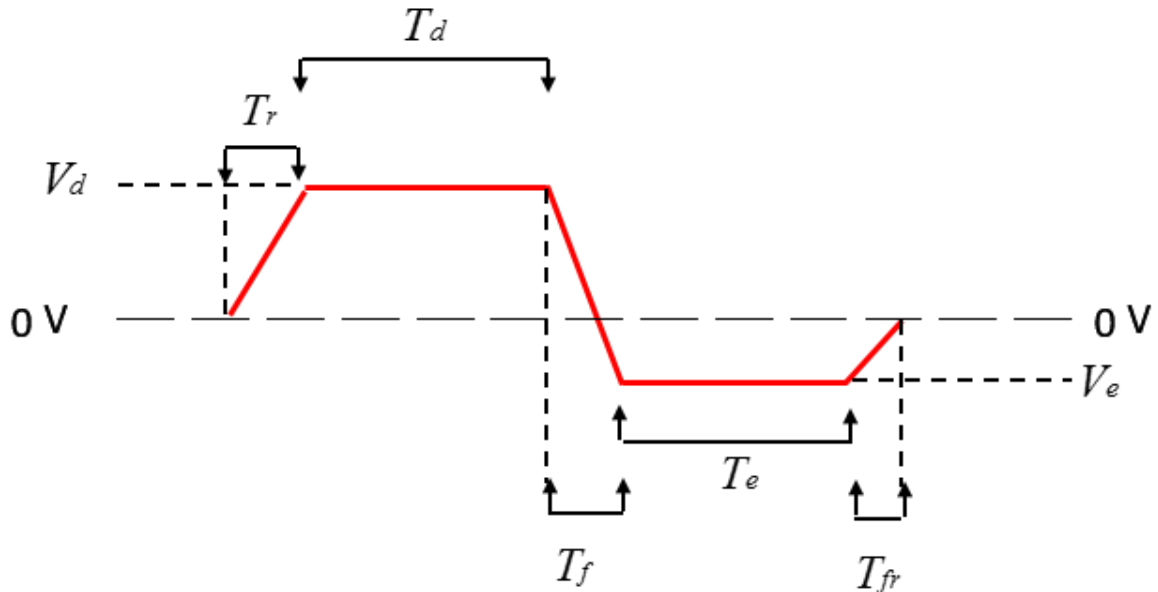


Figure 2. 18 Features of a bipolar waveform. T_r is the rise time from the isoelectric point to the V_d , T_f is the fall time from the V_d to the V_e and T_{fr} is the final rise time from V_e to the isoelectric point.

The voltages applied to the crystal (dwell voltage, V_d and echo voltage, V_e) and the time these voltages were held (dwell time, T_d , and echo time, T_e) control the jetting properties and the piezoelectric crystal injector was controlled with compatible JetServer™ software.

2.6 Exponential Dilution Approach

2.6.1 Theory of exponential dilution

The exponential dilution method allows for efficient study of concentration relationships and is widely used [162,163]. Concentrations as low as 0.1 ppb may be produced [164].

The method involves mixing analyte vapour with a clean gas, within a defined volume. There are two approaches:

- Exponential concentration involves a dilution volume containing pure diluent gas into which an analyte stream is mixed at a constant rate. The concentration of the analyte flowing out of the dilution volume increases, exponentially, with time.
- Exponential dilution starts with a mixing volume filled with a known concentration of analyte followed by pure diluent gas constantly flowing into the mixing volume

causing the concentration of the analyte flowing out of the flask to reduce exponentially.

The concentrations of the analyte over time is controlled by gas flow and mixing volume, see Equation 2.1.

$$[i_t] = [i_0] \exp\left(-\frac{tF_2}{V}\right) \quad \text{Equation 2. 1}$$

Note: $[i_t]$: concentration of analyte at time t ($\text{mg}\cdot\text{m}^{-3}$); $[i_0]$: initial concentration of the analyte ($\text{mg}\cdot\text{m}^{-3}$); F_2 : flow rate of the gas through exponential dilution flask in ($\text{cm}^3\cdot\text{min}^{-1}$); V : volume of the exponential dilution flask (cm^3); t : time (min)

Figure 2.19 shows the relationship between $[i_t]$ and t presenting how concentrations may be generated, simply by monitoring time.

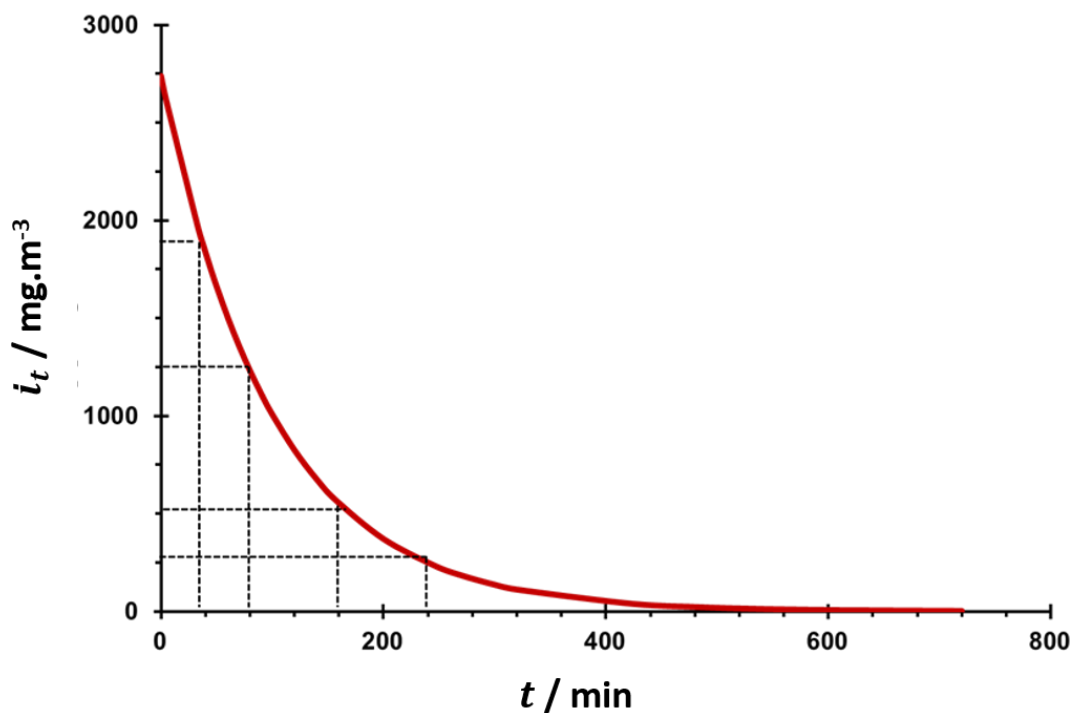


Figure 2. 19 Figure displaying the means by which concentration can be monitored according to time measure.

2.6.2 Exponential dilution studies approach

In these experiments a specified amount of purified liquid was injected with a 250 μl volume glass syringe through a septum into heated 500 cm^3 volume exponential flask and allowed to vaporise and mix for 60 s. Figure 2.20 shows a close up of the

exponential dilution system. Next a diluent flow of purified nitrogen was mixed into the flask resulting in exponentially decreasing concentration analyte vapour to be mixed into the d-IMS transport gas flow. The gas inlet and outlet in the flask were constructed in-house to promote mixing, by diffusion, by placing the inlet at the centre of the flask and the outlet at the top of it. The concentration of analyte in the d-IMS transport gas (Figure 2.10) was calculated using Equation 2.2. Fixed dispersion fields scans were applied to collect d-IMS data.

$$[i_{d-IMS}] = \left(\frac{F_1 + F_2}{F_2} \right) [i_t] \quad \text{Equation 2. 2}$$

Note: $[i_t]$: concentration of analyte at time t ($\text{mg}\cdot\text{m}^{-3}$); $[i_{d-IMS}]$: concentration entering d-IMS ($\text{mg}\cdot\text{m}^{-3}$); F_2 : flow rate of the gas through exponential dilution flask in ($\text{cm}^3\cdot\text{min}^{-1}$); F_1 : flow rate of the transport gas ($\text{cm}^3\cdot\text{min}^{-1}$)

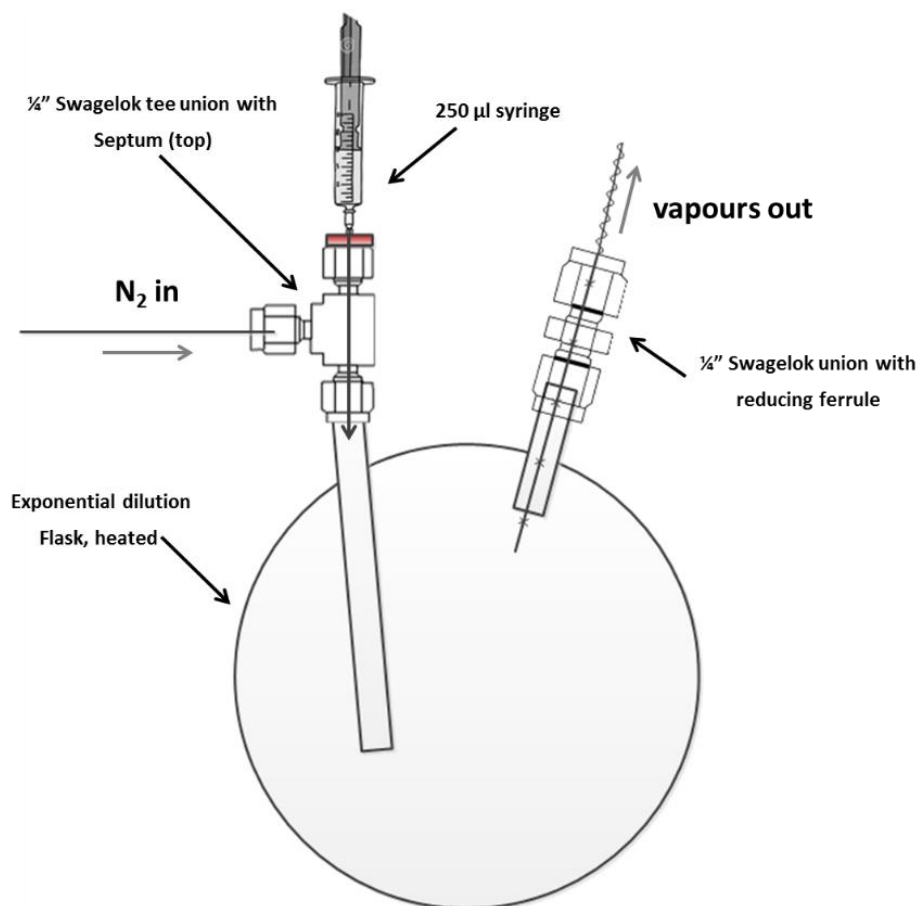


Figure 2. 20 Illustration of the exponential dilution injection system, showing heated flask, tee union injection port with septum and inlet and outlet N₂ flow, as performed in experiment number 1.1 (Table 1.1).

2.7 Permeation Vapour Sources

2.7.1 Theory of permeation process

Permeation is one of the oldest known phenomena for achieving low level of concentration (ppm and ppb) of gas vapours [164]. They involve storage of liquid or solid standards within an inert container fitted with a permeable membrane, through which the standard permeates. The permeation rate is constant at constant temperature, allowing generation of stable concentrations. The permeation of gas through the membrane is a diffusion process and is driven by concentration gradients between the inner and outer surfaces of the membrane wall.

2.7.2 Construction of permeation sources

The sources were built from 2 cm³ clear glass chromatographic vials (Chromacol, Dorset, UK), capped with an assembly composed of an 8 mm diameter Al cap and a PTFE membrane. Example of constructed permeation sources is shown in Picture 2.4. The membranes used had a wall thickness of 0.5 and 0.1 mm, and was sealed into position using a PTFE washer with 0.2 mm thickness (Alltech, Stamford, UK). The sources were conditioned at 40 °C in a conditioning oven for a period of minimum 6 weeks (until the equilibrium was established).



Picture 2.4 Side and top view of the permeation sources, showing vial, PDMS membrane and cap.

2.7.3 Gravimetric method for permeation sources

Once equilibrated the sources were calibrated gravimetrically using an electronic balance (Ohaus Discovery, Thetford, UK) model DV-215CD with 0.01 mg resolution. Each vial was weighed in triplicate at randomised time intervals over a period of two to four weeks. The

linear mass loss observed with time is the flux of the analyte which can be used to calculate concentration of vapours in a diluent gas stream. Figure 2.21 shows an example of mass loss from an equilibrated methanol permeation source over 20 days.

The release rate of the analyte through the permeation source is calculated via Equation 2.3

$$Q = \frac{dm}{dt} = \frac{\Delta m}{\Delta t} \quad \text{Equation 2.3}$$

Note: Q : release rate at time t (ng.min⁻¹); $\frac{dm}{dt}$: flux or analyte release (ng.min⁻¹) Δm : change in mass (ng); Δt : change in time (min)

Alcohol vapour sources were calibrated gravimetrically and summary of the results are shown in Table 2.6.

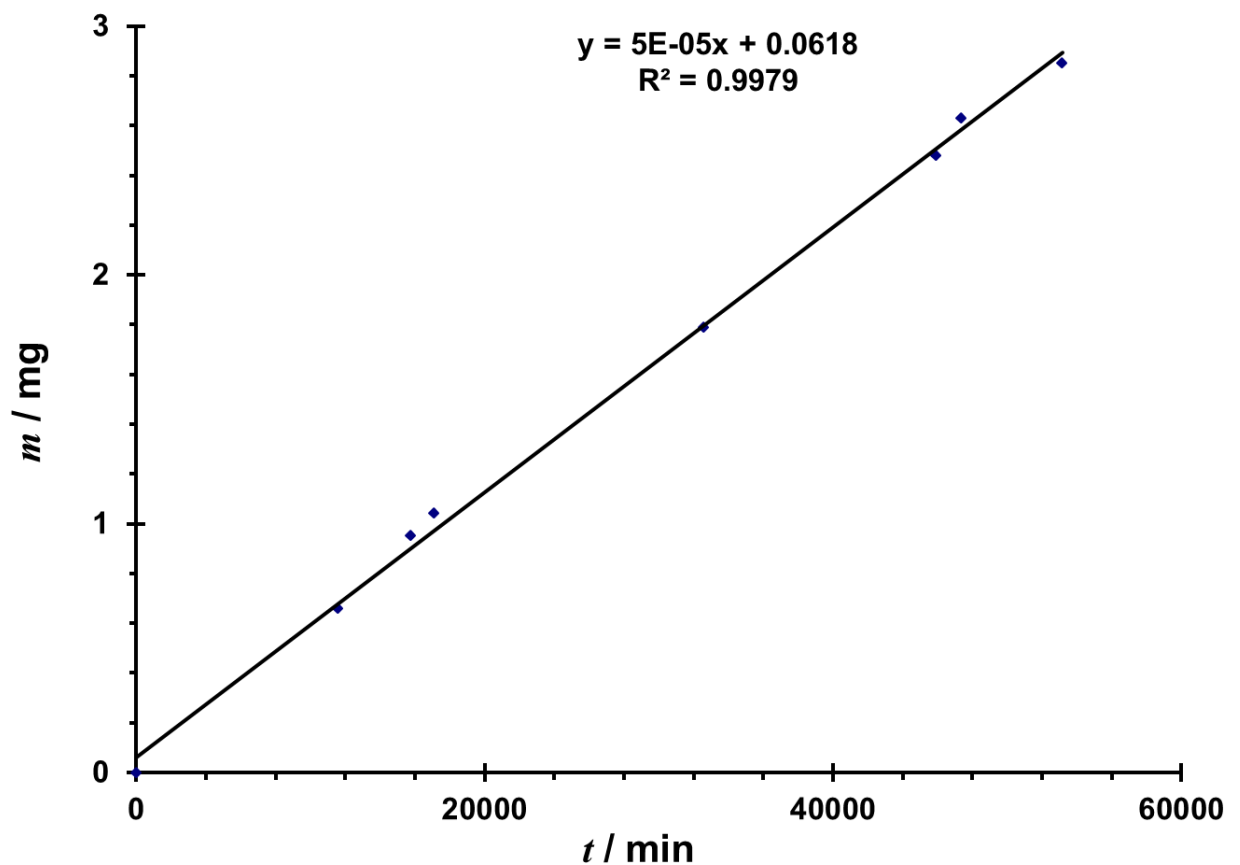


Figure 2.21 Example of methanol permeation source calibration using gravimetric method where m is mass loss over time t .

Table 2. 6 Details of permeation source vials used for optimisation of d-IMS responses of alcohols and in Experiment number 1.2.1, where d_{memb} is a membrane thickness, t_{cal} is a calibration time, m_{in} and m_{fin} are initial and final masses of permeation sources, Q is mean calculated rate of diffusion.

Compound	d_{memb} / mm	t_{cal} / min	m_{in} / g	m_{fin} / g	Q / ng.min ⁻¹
MeOH	0.5	53155	2.67243	2.66958	65.2
EtOH	0.5	90250	2.84192	2.83294	99.5
n-PrOH	0.1	90265	2.83331	2.82049	142.03
n-BuOH	0.1	56202	2.48272	2.47757	63.96

2.7.4 Permeation sources studies approach and calculations

Stable concentrations of the analytes vapours, generated from calibrated permeation sources were introduced into the d-IMS transport gas using calibrated permeation sources (System schematic is shown in section 2.5.1) and data was recorded in the form of dispersion plots (Section 2.3.2) with compensation-field scans run against a programmed increase in the dispersion field-strength.

The concentration of analyte vapours exiting the headspace vial $[i]$ (Figure 2.9) can be calculated via Equation 2.4 and concentration in the d-IMS filter, $[i_{d-IMS}]$, can be calculated via Equation 2.5.

$$[i] = \frac{Q}{F_2} \quad \text{Equation 2. 4}$$

Note: $[i]$: concentration of analyte exiting headspace vial (mg.m⁻³); Q : analyte release rate (mg.min⁻¹) F_2 : flow rate entering headspace vial (cm³.min⁻¹);

$$[i_{d-IMS}] = \frac{[i]}{\left(\frac{F_4 + F_1}{F_4}\right)} \quad \text{Equation 2. 5}$$

Note: $[i_{d-IMS}]$: concentration of analyte entering d-IMS (mg.m⁻³); $[i]$: analyte concentration exiting headspace vial (mg.min⁻¹); F_4 : gas flow after split, directed toward d-IMS; F_1 : d-IMS transport gas (cm³.min⁻¹)

Chapter 3 Ion Chemistry of Alcohols in d-IMS

3.1 Study Overview and Objectives

Interest in rapid alcohol detection is an ongoing challenge for medical toxicological applications. D-IMS provides a potential for fast detection and monitoring at sub-ppb_(v/v) concentrations for those compounds, in a clinical or portable detector. Success in this activity requires an understanding of alcohol ion-chemistry in d-IMS. The study described in this chapter was performed with methanol, ethanol, n-propanol and n-butanol (Table 3.1) and the combined effects of temperature and electric field strength and concentration were investigated. Concentration influences ion-molecule interactions and changes the alpha function for analyte ions. Temperature and electric field strength combine to give an effective temperature (T_{eff}) that affects the kinetic and thermodynamic factors of ion formation, and ultimately ion fragmentation reactions.

It is helpful to note that in this Chapter, compensation voltages will be converted (and presented) to the values for the compensation field in $V.cm^{-1}$ to better express small changes in the position of ions additionally the values will be presented in the values of reduced electric field in Td. Values of dispersion voltages will be presented as are (in V) and additionally, converted and expressed in units of Td of reduced electric fields. For the simplicity of the Figures presentation a E° symbol will be used for reduced electric field (E/N). Further in d-IMS product ions such as monomer or dimers can exist as hydrated or non-hydrated clusters depending on the temperature and moisture level. For simplicity, the ions in this thesis will be described as monomer or dimers clusters and hydrated formula will be used only when d-IMS-MS data exists.

There were three main research objectives for this study:

- Investigation of the effect of concentration on d-IMS responses to n-alcohols, using an exponential dilution approach to produce wide range of concentrations at fixed dispersion field scans.
- Investigation of the effect of T_{eff} on d-IMS responses of n-alcohols, using permeation sources to introduce ppb levels of vapour concentration followed with collection of dispersion plots.

- Analysis and evaluation of the results using existing ion solvation models (Section 1.8.3).

3.2 Chemicals and Purity

Methanol, ethanol, n- propanol and n-butanol (Table 3.1) were obtained from Fisher Chemicals, Loughborough, UK; GC and HPLC purity $\geq 99.5\%$. The alcohols were purified further by purging 10 ml of the liquids with small flow (around 1 to 2 ml.cm⁻³) of high-purity nitrogen (Figure 2.1) 200 ppm (v/v) solutions of each alcohol in dichloromethane DCM were prepared and analysed by GC-MS (Table 3.2). The resultant data indicated purity $\geq 99.98\%$. In all of the collected chromatograms, presence of chloroform peak was observed. Chloroform was used as injection syringe washer. Figure 3.1 shows example of GC-MS TIC chromatogram collected for n-propanol solution.

Table 3. 1 Properties of the alcohols: *M* - molecular mass, *PA* - proton affinity, *Bp* - boiling point, *d* - density, CAS number. Note: ^a ChemSpider and ^b NIST

Compound	<i>M</i> ^b / g mol ⁻¹	<i>PA</i> ^b / kJ mol ⁻¹	<i>Bp</i> ^b / °C	<i>d</i> ^a / g cm ⁻³	CAS
		1			
Methanol	32	754.3	64.7	0.79	67-56-1
Ethanol	46.1	776	72.6	0.79	64-17-5
n-Propanol	60.1	786.5	95.8	0.80	71-23-8
n-Butanol	74.1	789.2	117	0.81	71-36-3

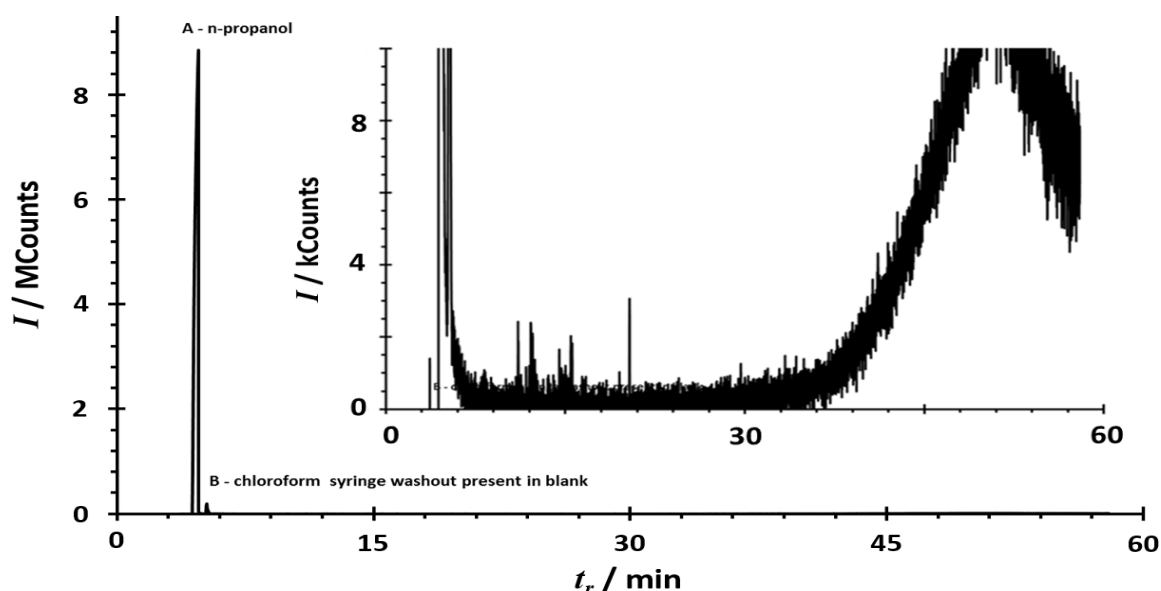


Figure 3. 1 TIC Chromatogram of n-propanol collected by GC-MS, obtained from injecting 1 μ l of 200 ppm (v/v) solution in DCM. Insert: Zoom of the background level chromatogram.

Table 3. 2 Parameters and Settings used when run purity tests on n-alcohols using GCMS.

HP 6890 gas chromatograph conditions	
Column	DB5 (Restek, UK)
Column length	60 m
Column diameter	0.32 mm
Stationary phase film thickness	0.5 μm
Column flow: constant pressure	25 psi
Carrier gas flow	Helium 2 ml min ⁻¹
Split mode	Split 1:10
Total run time	58 min
Temperature program	
1st starting temperature	30 °C (5 min)
Temperature ramp rate	6 °C min ⁻¹
1st end temperature	300 °C (8 min)
Agilent 5973 Mass Spectrometer conditions	
Scan type	SIM and Scan
Mass range	30 to 455 m/z
Tune type	Auto
Ionization type	EI
Solvent delay	3.5 min
Scan time	0.29 Secs
MS source temperature	230 °C
MS Quad temperature	150 °C
Emission current	34.59 mA

3.3 Methods for Studying of n-Alcohols d-IMS Responses (experiments no 1.1 and 1.2)

3.3.1 Effect of concentration expt. no 1.1

Exponential dilution approach (Section 2.6) with fixed d-IMS dispersion voltages (V_d) was used in a series of experiments to characterise the effect of analyte concentration on d-IMS responses to: methanol, ethanol, n-propanol and n-butanol. The value for V_d was determined in preliminary studies that recorded dispersion plots (Section 2.3.2) for each alcohol at concentrations between 0.04 mg.m⁻³ and 0.01 mg.m⁻³ and with d-IMS filter temperature of 100 °C. The optimisation criteria were the lowest dispersion field required to fully resolve the alcohol product ions from the reactant ions. This ensured that ion losses due to a reduced acceptance aperture into the d-IMS ion filter were minimised and product ion intensities were maximised. In the collected dispersion plots (Figure 3.2) presence of reactant ion (RIP) and product ions (PI) was evident and the

dashed line indicates the chosen dispersion field for further studies, also shown in Table 3.3.

Table 3.3 Conditions chosen for studying effect of concentration on d-IMS responses of alcohols under fixed V_d V during exponential washout experiments.

Compound	V_d V optimised
Methanol	1300
Ethanol	900
n-Propanol	1100
n-Butanol	1100

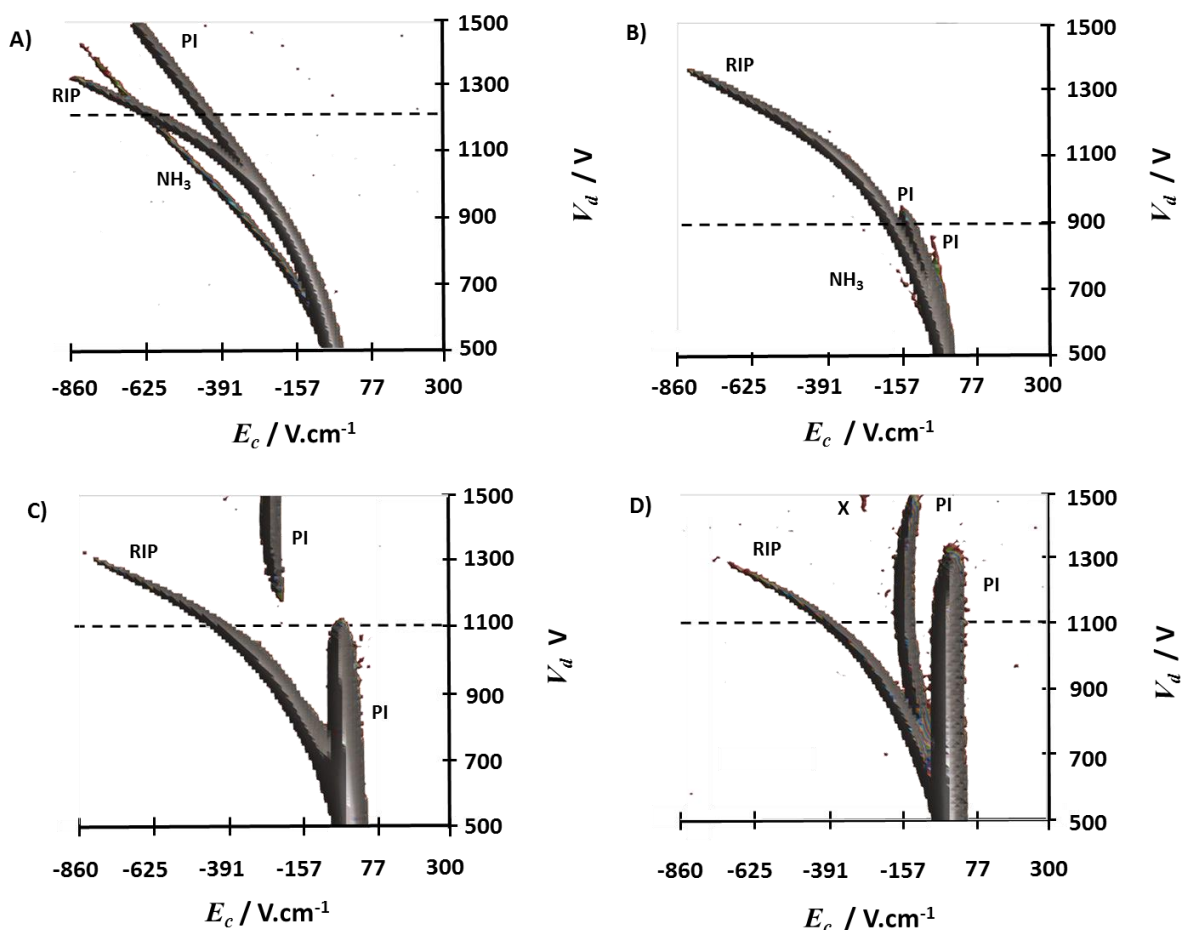


Figure 3.2 Dispersion plots of four alcohols: methanol (A), ethanol (B), n-propanol (C) and n-butanol (D) collected during optimisation experiment at the d-IMS temperature of 100 °C and concentration level between 0.04 and 0.01 mg.m⁻³ vapours concentration level. Dashed line shows chosen dispersion voltage (V_d) for performing exponential dilution experiment to study effect of concentration on d-IMS responses of alcohols.

Alcohol test-atmospheres were generated for the d-IMS over seven orders of magnitude concentration range by injecting 75 μ l to 200 μ l of a pure alcohol standard into a heated

exponential dilution flask (Section 2.6). The liquid was then allowed to diffuse and mix for 60 s before a flow of between $6 \text{ cm}^3\cdot\text{min}^{-1}$ to $19 \text{ cm}^3\cdot\text{min}^{-1}$ (Section 2.5.2, Figure 2.10 (F_2)) of purified nitrogen was passed through the exponential dilution flask and subsequently mixed into the transport gas of the d-IMS analyser. Differential mobility spectra were continuously recorded by scanning the compensation field for between 12 hr to 15 hr, generating up to 54,000 spectra per experiment. The transport-gas ($300 \text{ cm}^3\cdot\text{min}^{-1}$ to $320 \text{ cm}^3\cdot\text{min}^{-1}$) was purified nitrogen with a water concentration maintained between $20 \text{ mg}\cdot\text{m}^{-3}$ and $30 \text{ mg}\cdot\text{m}^{-3}$ (25 ppm (v/v) to 42 ppm (v/v)). D-IMS analyser temperatures were maintained initially at $100 \text{ }^\circ\text{C}$ and later extended to the range of temperatures between 45°C and 130°C depending on the compound and experiment. Summary of individual experiments and parameters for the operation of the d-IMS analyser are shown in Table 3.4.

Table 3. 4 List of individual experiments with instrumental parameters used in studies on concentration effect of alcohols d-IMS responses, using exponential dilution approach. D-IMS transport gas flow F_1 (Figure 2.10) was set between 300 to 320 $\text{cm}^3.\text{min}^{-1}$, moisture level in the transport gas was between 25 and 30 $\text{mg}.\text{m}^{-3}$ and number of compensation field E_c steps were set to 100 in all experiments. Note; T_{exp} : temperature of the exponential dilution flask; T_{d-IMS} : temperature of the d-IMS ion filter; T_{eff} : calculated temperature of ion, effective temperature; E_d : dispersion field; E_d/N : reduced dispersion field; E_c : compensación field range; E_c/N : reduced compensation field range; V_{inj} : injected volume of alcohol liquid into the exponential dilution flask; t_{scan} : scan time; F_2 : exponential dilution flow, mixing with transport gas flow.

Alcohol exp no	$T_{exp}/\text{ }^\circ\text{C}$	$T_{d-IMS}/\text{ }^\circ\text{C}$	$T_{eff}/\text{ }^\circ\text{K}$	$E_d/\text{ kV}.\text{cm}^{-1}$	$E_d/N/\text{ Td}$	$E_c/\text{ V cm}^{-1}$	$E_d/N/\text{ Td}$	$V_{inj}/\text{ }\mu\text{l}$	$t_{scan}/\text{ ms}$	$F_2/\text{ ml}.\text{min}^{-1}$
Methanol										
1	120	90	513,	25	100	-860 to 100	-3.44 to 1.2	100	200	10.5
2		100	523,	25	100	-860 to 60	-3.44 to 0.24	100	200	8.0
3		115	528,	25	100	-860 to 100	-3.44 to 0.4	100	200	8.8
4		130	533	25	100	-860 to 40	-3.44 to 0.16	135	200	8.0
5		60	509	29.4	117	-860 to -100	-3.44 to -0.4	160	200	19.5
Ethanol										
1	120	90	471	18	72	-520 to 100	-2.08 to 0.4	100	200	10.5
2		100	481	18	72	-540 to 60	-2.16 to 0.24	200	100	7.8
3		108	489	18	72	-540 to 60	-2.16 to 0.24	100	200	9.7
4		115	496	18	72	-540 to 60	-2.16 to 0.24	100	200	9.7
5		35	416	18	72	-520 to 100	-2.08 to 0.4	75	200	16.5
1-Propanol										
1	150	80	485	22	88	-660 to 100	-2.64 to 0.4	30	200	9.0
2		100	505	22	88	-860 to 100	-3.44 to 0.4	75	200	21
3		115	520	22	88	-660 to 100	-2.64 to 0.4	75	200	15
4		60	441	18	72	-500 to 200	-2.00 to 0.8	30	200	13
1-Butanol										
1	160	100	505	22	88	-660 to 100	-2.64 to 0.4	200	10	8.0
2		70	475	22	88	-660 to 100	-2.64 to 0.4	90	200	10.2

3.3.2 Effect of ion temperature expt. no 1.2.1

Stable concentrations of the analytes vapours, ranging from 0.025 mg.m⁻³ to 0.001 mg.m⁻³ were introduced into the d-IMS transport gas using calibrated permeation sources (Section 2.7.3, Table 2.6). Schematic of the setup is shown in Section 2.5.1, Figure 2.9. Data were recorded in the form of dispersion plots (Section 2.3.2) with compensation-field scans run against a programmed increase in the dispersion field-strength across the range of E_d/N 40 Td to 120 Td at ion-filter temperatures across the range 45°C to 130 °C. Experimental parameters used to capture the dispersion plots are summarised in Tables 3.5 and 3.6.

Table 3. 5 Instrumental parameters used in capturing dispersion plots, during studies on effect of ion temperature on alcohol d-IMS responses.

Symbol.	Parameter	Value
F_1	d-IMS transport gas flow	300 to 320cm ³ .min ⁻¹
F_2	Headspace flow into the d-IMS transport gas	1 to 5 cm ³ .min ⁻¹
F_2 split	Headspace flow split	1:10
T_{HS}	headspace vial temperature	40 °C
T_{d-IMS}	d-IMS temperature	45 to 130 °C
T_H	Transfer line temperature	100 °C
Hd	d-IMS humidity	20 to 30 mg.m ⁻³ or 25 to 41 ppv
E_d/N and E_d	Reduced dispersion field or dispersion voltage	40 to 120 Td or 500 to 1500 V_d V
E_c/N and E_c	Reduced compensation field or compensation field scan range	-3.44 to 1.2 Td or -860 to 300 V.cm ⁻¹
N_s	Number of E_c steps	100
	Step duration	10 ms

Table 3. 6 D-IMS ion filter temperatures used in capturing dispersion plots, during studies on effect of ion temperature.

Alcohol	d-IMS temperature / °C
Methanol	80, 100 and 120
Ethanol	80, 100 and 120
n-Propanol	70, 80, 100, 108, 115 and 130
n-Butanol	40, 50, 55, 70 and 100

3.3.3 d-IMS-MS studies expt. no 1.2.2²

The identity of product ions produced by dispersion field heating was studied by a d-IMS/MS. Exponential dilution approach was used, and vapours were delivered to the d-IMS/MS from a 3 dm³ exponential dilution flask at a flow rate of 1 dm³.min⁻¹ following the injection and mixing of 0.4 µl of a pure alcohol standard into the exponential dilution flask. The temperature of the ion filter was set to 80 °C. The mass spectrometer was scanned continuously from m/z 20 to m/z 400 at 0.5 Hz over the analytes' concentration ranges of 0.02 mg.m⁻³ to 100 mg.m⁻³. The full schematic of the set-up can be found in Section 2.5.3.

3.4 Results and Discussion

3.4.1 Preamble

In a ⁶³Ni source protonation to form a product ion $MH^+(H_2O)_{n-1}$ is formed by water displacement from the reactant ion $(H_2O)_nH^+$ and then, subsequently, proton bound clusters M_nH^+ may be formed by association of MH^+ with M at sufficiently elevated vapour concentrations (Section 1.5.3). Models of ion production in d-IMS and ion solvation can be used to produce a distribution profile of ions expected to be formed in the ionisation process, see Sections 1.8.2 and 1.8.3. The effect of concentration of the alcohols on ion formation may be discerned from the topographic plots of d-IMS responses (present on E_c scale) for methanol (Figure 3.3) ethanol (Figure 3.10) n-propanol (Figure 3.14) and n-butanol (Figure 3.22). At elevated concentration levels, high enough to result in one or more ion neutral collisions during the 600 ns duration of the low field portion of the dispersion waveform a single signal from mixed proton bound clusters $(ROH)_nH^+$ (where n=2 to 4) was observed for each alcohol with changing dispersion behaviour with concentration, see clustering/declustering and the sections on modification effects 1.6.1 and 1.6.2. The lower limit for alpha modification for each alcohol was estimated to be 90 mg.m⁻³, 132 mg.m⁻³, 165 mg.m⁻³ and 210 mg.m⁻³ for methanol, ethanol, n-propanol and n-butanol, respectively (Section 1.8.4); highlighted by a vertical black line in the Figures 3.3, 3.10, 3.14, and 3.22. This behaviour was consistent for all alcohols and the experimental results confirmed the calculated

² This experimental work was performed by Prof. G.A Eiceman team, New Mexico State University (NMSU).

predictions. Below the alpha modification threshold concentration, unexpected anomalies in the spectra were observed, including fragmentation and association. It was these observations that led to further experiments on effect of ion temperatures manipulated by combining d-IMS ion filter temperature and applied dispersion field.

3.4.2 Methanol

3.4.2.1 Concentration relationships

A topographic plot of Methanol d-IMS responses across concentration levels from 3850 mg.m⁻³ to 0.001 mg.m⁻³ is shown in Figure 3.3. The main trends in the d-IMS methanol responses in respect to changing concentration can be categorised within three zones:

- Zone 1: Modification, highest concentration (down to 90 mg.m⁻³), dominated by proton bound cluster $(MeOH)_nH^+$ (n= 2 to 4),
- Zone 2: Dominated by proton bound dimer $(MeOH)_2H^+$ and adduct formation (80 to 10 mg.m⁻³),
- Zone 3: Dominated by protonated monomer $(MeOH)H^+$ (10 to 0.001 mg.m⁻³).

3.4.2.2 Zone 1

Changing dispersion behaviour with concentration, observed in zone 1 is a result of alternation of clustering/declustering behaviour through collisions with neutral alcohol molecules under low part of applied dispersion field, which in effect changes the alpha function in the mobility coefficient (Equation 2.11). The neutral molecules within the gas stream, work simply as modifier for methanol cluster ions $(MeOH)_nH^+$ (Section 1.6.1 and 1.6.2) which is in agreement with the predicted results for ion collisions (Section 1.8.4) and model of modification of the alpha function which threshold was calculated to be at 88 mg.m⁻³ concentration level.

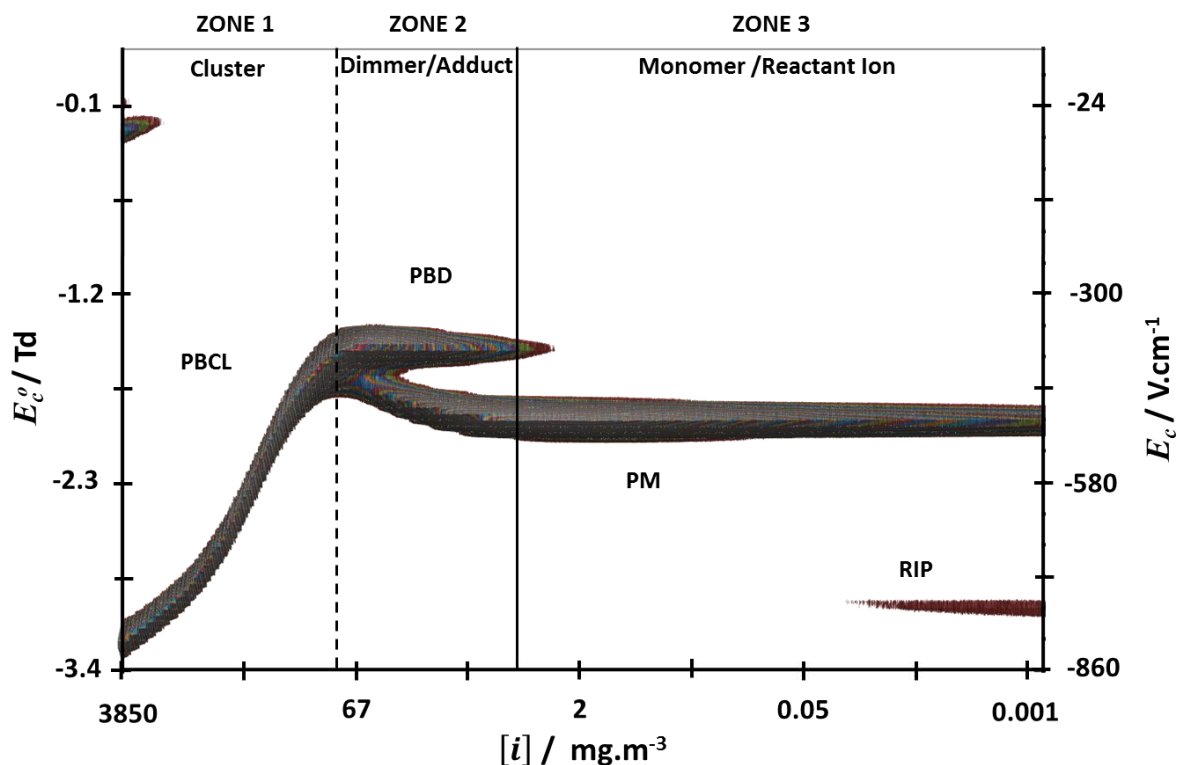


Figure 3.3 Topographic plot of the MeOH d-IMS responses across 6 orders of magnitude concentration range (3850 to 0.001 mg.m^{-3}) collected at 100 °C and dispersion field of 100 Td or 1250 V_d V. Three distinct behaviours are classified into zones 1, 2 and 3: proton bound cluster (PBCL) $(\text{MeOH})_n\text{H}^+$ is observed within the Zone 1, finishing at 90 mg.m^{-3} concentration level (black dashed vertical line indicates calculated level for the first ion-neutral collision); domination of proton bound dimer (PBD) and adduct formation (Zone 2), domination of protonated monomer (PM) and reactant ion peak (RIP) formed with reducing concentration. Ions position on the E_c scale of -386, -482 and RIP -748.4 V cm^{-1} or E_c/N of -1.54, - 1.93 and -2.99 Td (PBD, PM and RIP respectively).

3.4.2.3 Zone 2

An anomaly in the ion behaviour was observed over a concentration range of 80 to 10 mg m^{-3} . As ions separate from the proton bound cluster ion two features are observed:

- First feature, at the E_c position of -386 V.cm^{-1} (or -1.54 Td), was identified as a proton bound dimer $(\text{MeOH})_2\text{H}^+$. The formation of the dimer ion is thermodynamically favoured within the above concentration range and temperature (Section 1.8.3).
- Second feature emerged from the clustered ion signal shifting towards lower E_c with decreasing concentrations to finally stabilize at the E_c position of -482 V.cm^{-1} (or -1.93 Td) is assigned to the protonated monomer $(\text{MeOH})\text{H}^+$.

This behaviour is most likely associated with an adduct formation and will be further discussed in the next Section.

3.4.2.4 Zone 3

As the concentration exponentially reduced from 10 to 0.001 mg.m⁻³, three features were present:

- Proton bound dimer $(MeOH)_2H^+$
- Protonated monomer $(MeOH)H^+$
- Reactant ion peak $(H_2O)H^+$

The observed kinetics were typical for product ion formation in d-IMS. However, the quantitative distribution of ions was not in agreement with theoretical calculations (Section 1.8.3) that predicted that at a concentration of 10 mg.m⁻³ the proton bound dimer is expected to be a dominant ion feature (95% abundance). The reason for the difference in ion distribution may lay in the hydration of the product ions, which this model does not take into the account.

Extracted d-IMS spectra collected at 10 and 0.02 mg m⁻³ are shown in Figure 3.4 with proton bound dimer, protonated monomer and RIP signals indicated at E_c of -386 V.cm⁻¹, -482 V.cm⁻¹ and -748.4 V.cm⁻¹ or -1.54 Td, - 1.93 Td and -2.99 Td.

3.4.2.5 Methanol anomaly - model

The behaviour of the methanol ions in d-IMS over the range 80 to 10 mg.m⁻³ was unexpected, and has not been documented before. Figure 3.5 shows a close up of the concentration of interest from Figure 3.3. Thermodynamic calculations for methanol, indicate that at T_{eff} 523° K, and over this concentration range, most of the ions are predicted to be proton bound dimer $(MeOH)_2H^+$ (\approx 98% of ion abundance at 85 mg m⁻³). However, another feature may be seen to merge with the $(MeOH)_2H^+$, which has an unstable E_c value with reduced concentration level. At concentrations below 80 mg.m⁻³ the monomer $(MeOH)H^+$ is expected to start formation; with dimer:monomer ratio of 500:1 at 80 mg.m⁻³ and increasing to 150:1 at 20 mg.m⁻³. Instability of the feature within this concentration range, cannot be explained by simple modification of the alpha function under low part of the electric field (as in case seen for elevated concentration

levels) and is more understood as a chemical reaction taking place inside the ion filter during ≈ 2 ms transit time of the ions in d-IMS filter.

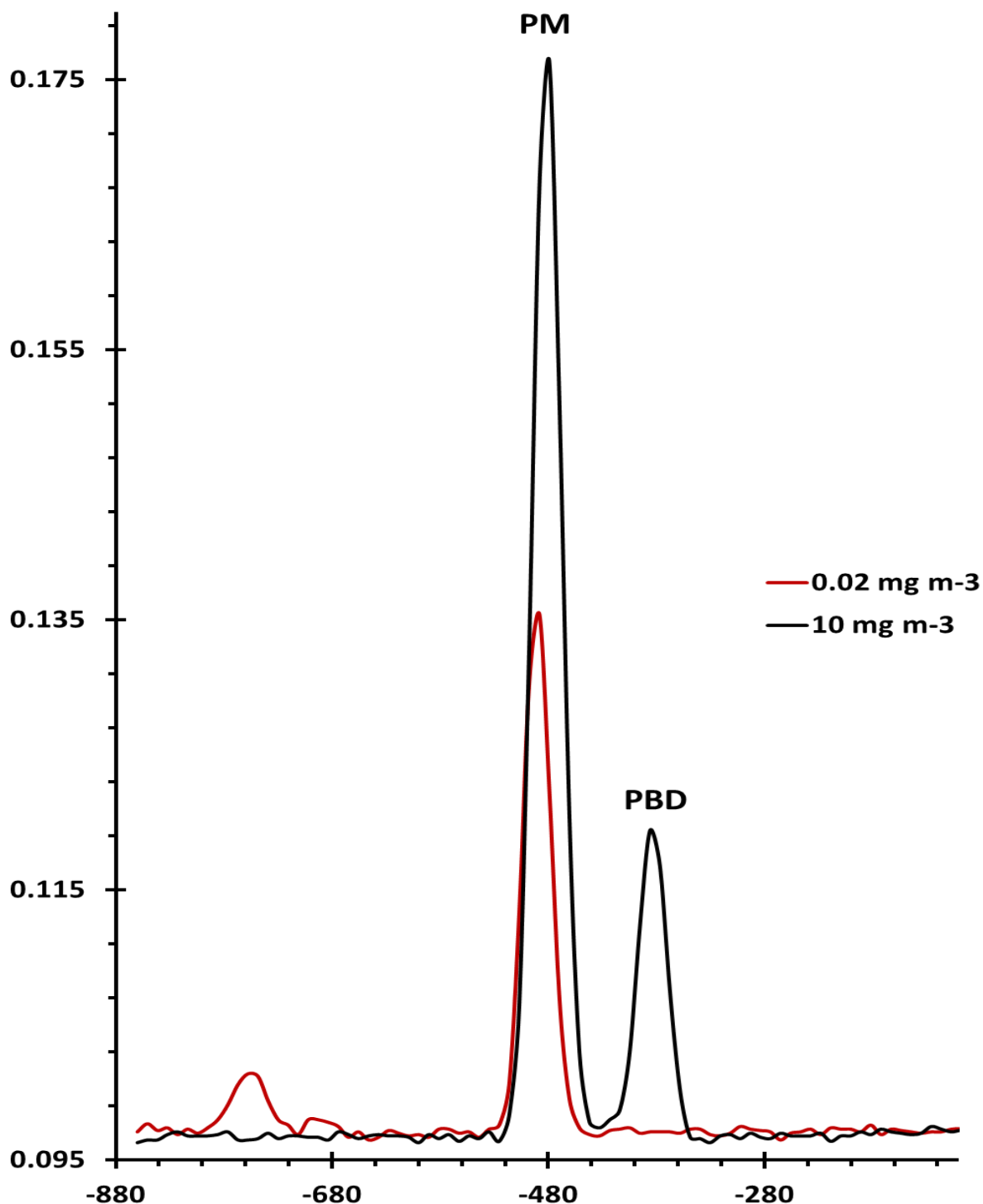


Figure 3. 4 D-IMS extracted spectrum of methanol at 10 and 0.02 $\text{mg}\cdot\text{m}^{-3}$ concentration level, collected during exponential dilution experiment at d-IMS temperature of 100 $^{\circ}\text{C}$ and 1250 V_d V or 100 Td. PBD - proton bound dimer, PM - protonated monomer and RIP - reactant ion peak RIP are present, positioned at the E_c scale at -386, -482 and -748.4 $\text{V}\cdot\text{cm}^{-1}$ (or -1.54, -1.93 and -2.99 Td), respectively.

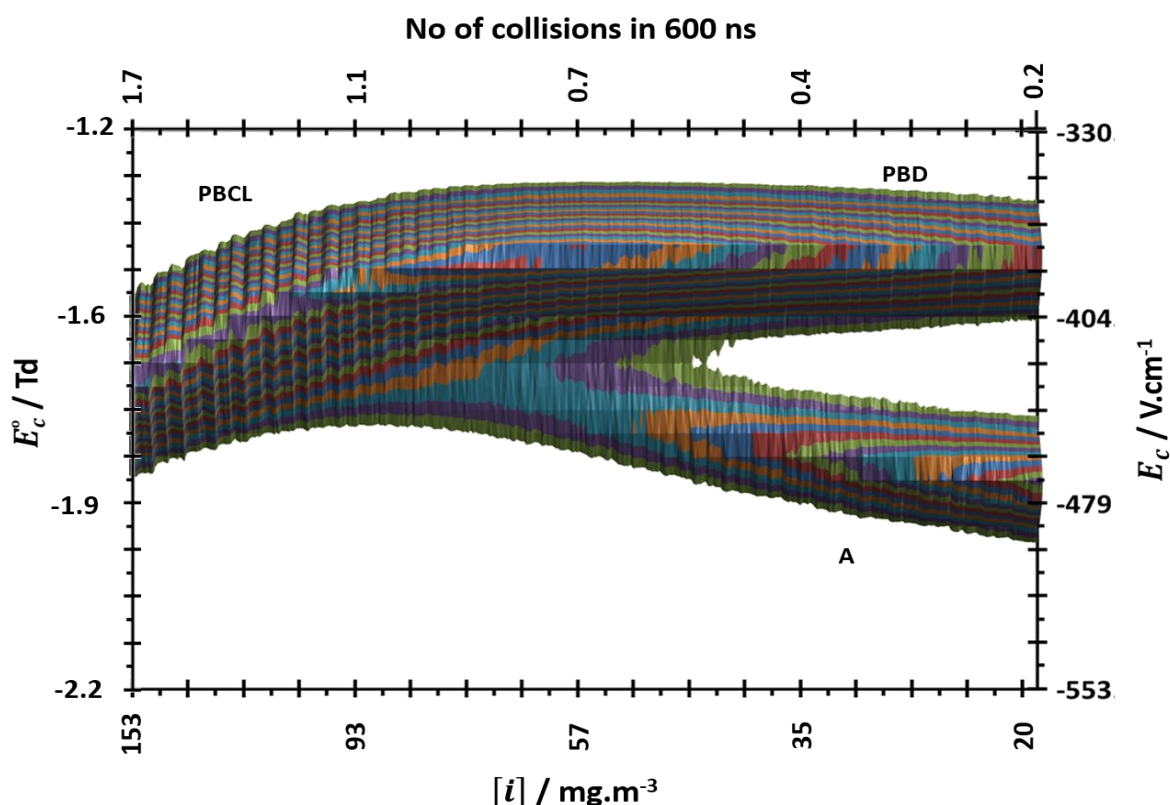
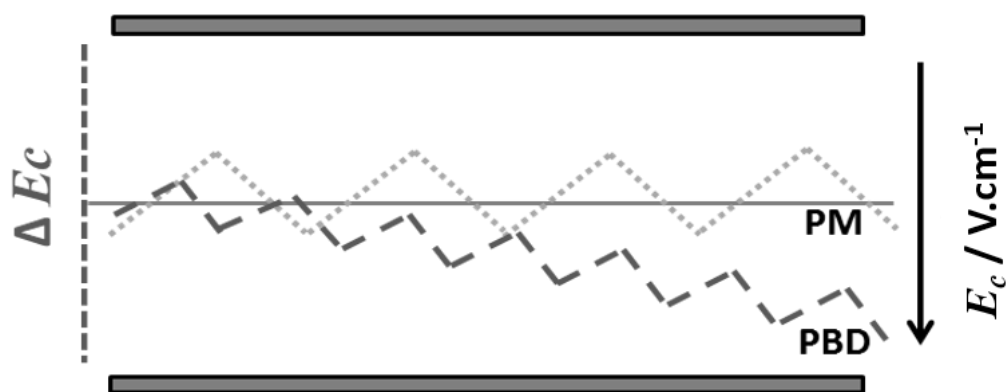


Figure 3.5 Topographic plot of methanol d-IMS responses resulted from exponential washout experiment at d-IMS filter temperature of 100 °C and 100 Td or 1250 V_d V, zooming on concentration range from zone 2 (Figure 3.3). Where: PBCL is Proton bound cluster; PBD is Proton bound dimer (PBD) and A is the adduct ion. Calculated number of collisions with neutrals during low portion of the dispersion field is shown at the top of the graph.

Figure 3.6 shows a schematic of this hypothesis. The ion may be envisaged as entering the drift tube as a $(MeOH)H^+$ (dotted line). The residence time of 2 ms in the d-IMS ion filter gives enough time for the ion to collide with a neutral alcohol molecule (ROH) yielding a $(MeOH)_2H^+$. The number of collisions on a 2 ms time scale was calculated to be 3037 at 80 $mg.m^{-3}$ concentration level and 377 at 10 $mg.m^{-3}$ concentration level. The newly created proton bound dimer ion (via collision in the drift region) has a different trajectory (dashed line) compared to that of the protonated monomer and proton bound dimer formed in the reaction region. The result is a shift in the ion's position on the E_c scale such that it falls between the monomer and proton bound dimer positions on the E_c scale. This is concentration dependant, the higher the concentration, the earlier the collision takes place, and the closer to the typical proton bound dimer the signal will be observed.

Expected behaviour



Observed behaviour

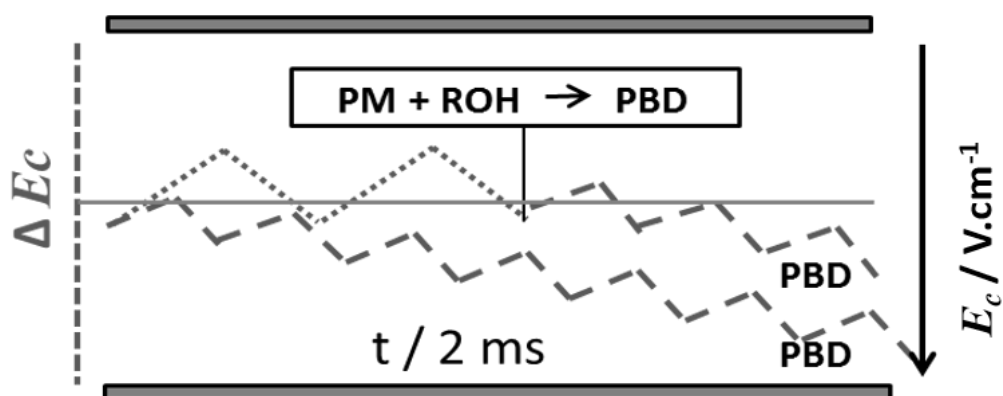


Figure 3.6 Schematic of the mechanism explaining the d-IMS ion behaviour, observed for the methanol within the concentration zone 2 (80 to 10 mg.m⁻³). ΔE_c is a change of the position on the E_c scale, t is a travel time of an ion through the d-IMS ion filter.

Indirect support for this hypothesis was obtained from exponential dilution experiments of the methanol alcohol, using increased d-IMS filter temperatures up to 130 °C. Figure 3.7 shows topographic plots of methanol at 104, 115 and 130 °C (A, B and C respectively). The experiments revealed that the higher temperature reduce this effect, which becomes unobservable at the temperature of 130° C. Since ions are heated by the field, a possible arguments of delicate ion composition (cauterisation) would not fit as ion undergoes dissociation with increased temperature.

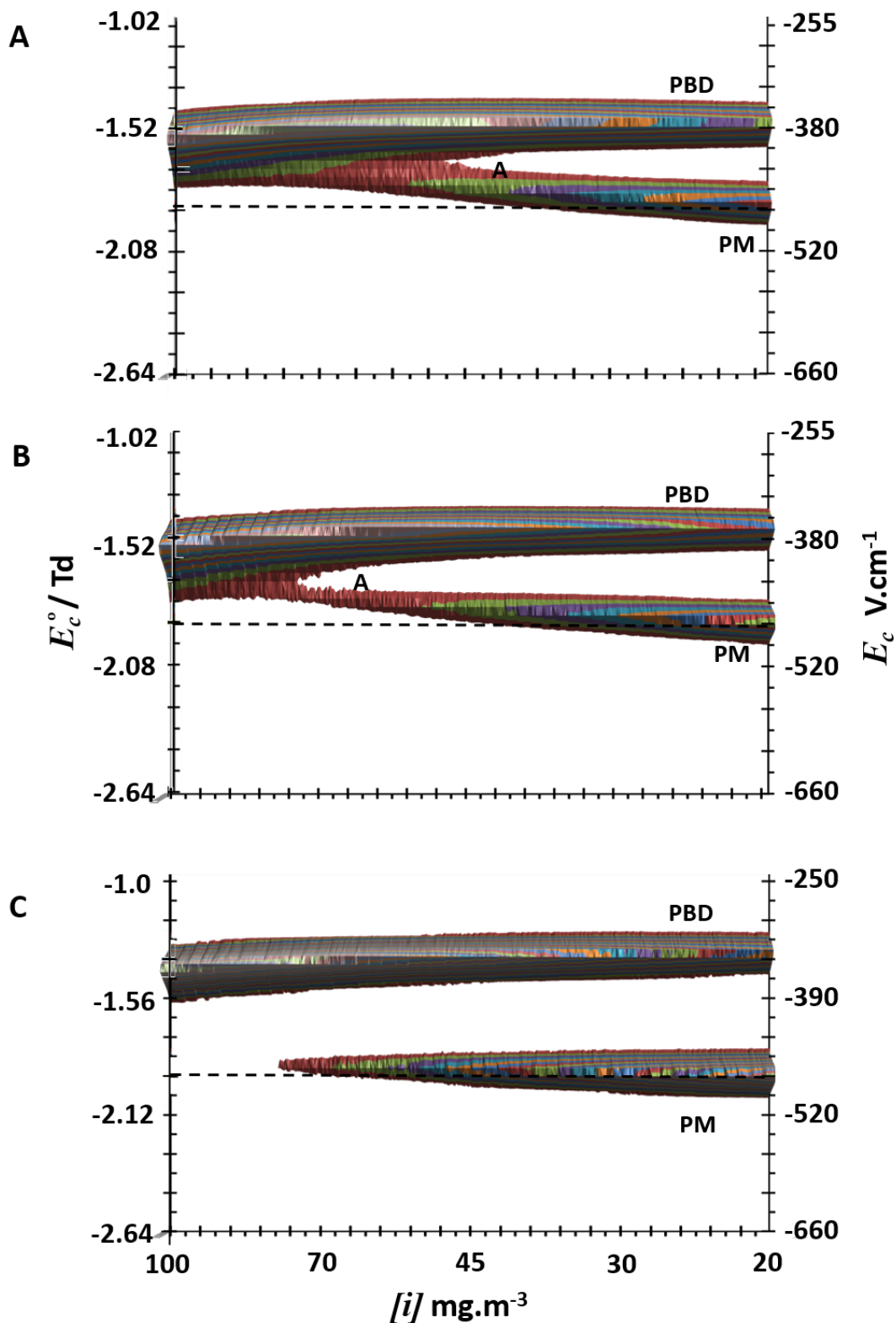


Figure 3. 7 Topographic plots of the d-IMS methanol responses, within 100 and 20 $\text{mg}\cdot\text{m}^{-3}$ concentration range, obtained during exponential dilution experiments at d-IMS temperatures of 104, 115 and 130 °C (A, B and C respectively). Dashed line indicates typically expected position of the protonated monomer (PM) on the E_c scale. Proton bound dimer is indicated as PBD.

Another explanation of the phenomena maybe that proton bound dimer and protonated monomer are exchanging during transit through the drift tube. Collision numbers at this concentration and residence time are 20 to 50. This may be expected to cause band broadening. Previously, Preston and Rajax [165] showed that exchange of neutral adducts on an ion core can be located over a range of drift times without band broadening or resolution of the two ion clusters providing the exchange is rapid in comparison to residence time in the drift tube.

The two mechanisms cannot be fully unpacked from the experiments in this thesis, nevertheless this highlights the possible influence of neutrals in the drift tube; something that should be considered in the design of future instruments.

3.4.2.6 Methanol vs ion temperature

These studies focused on the way the effective temperature of ions, generated by the interaction of dispersion field and d-IMS filter temperature, affected responses. Studies were performed at a constant methanol concentration of $10 \mu\text{g}\cdot\text{m}^{-3}$, generated from a permeation source (Table 3.6). Figure 3.8 presents dispersion plots of methanol vapours at 80, 100 and 120 °C (top) and a control blank (bottom)

Two features were observed in methanol dispersion plots identified as the reactant ion (RIP) $(\text{H}_2\text{O})_n\text{H}^+$ and protonated monomer ion $(\text{MeOH})\text{H}^+$.

The combined effect of ion filter temperature and ion heating with increased dispersion field resulted in increased curvature in the reactant ion dispersion plot consistent with an increase in the low field mobility of the RIP. This can be seen in the E_c values for the RIP at the maximum levels for E_d in Figure 3.8 and Figure 3.9. The position of the reactant ion peak at electric field of 96 Td ($1200 \text{ V } V_d$) changed from -1.8 Td ($-449 \text{ V}\cdot\text{cm}^{-1}$) at 80 °C to -2.56 Td ($-649 \text{ V}\cdot\text{cm}^{-1}$) at 120 °C . At 80 °C the highest E_d value at which an RIP was observed was 110 Td ($1380 \text{ V } V_d$) and the E_c value for the reactant ion was -3.44 Td ($-860 \text{ V}\cdot\text{cm}^{-1}$). Increasing the ion-filter temperature to 120 °C caused the highest E_d value at which an RIP was observed to decrease to 105 Td with an E_c value for the RIP of -3.44 Td. This effect of ion-filter temperature may be attributed to the transport gas water concentration of $25 \text{ mg}\cdot\text{m}^{-3}$, at which level the RIP would be mostly $(\text{H}_2\text{O})_3\text{H}^+$ at the lower fields. However at high dispersion field value the effect of dissociation can be already noticeable.

The dispersion behaviour for the protonated methanol product ion was even less affected by temperature than that observed for the reactant ion. This was expected as over the range 80 °C to 120 °C thermodynamic calculations predict the protonated methanol monomer $(MeOH)_nH^+$ ($n=1$) the calculated fractional values for $n = 2$ were 0.14 at 80 °C, 0.05 at 100 °C, and 0.01 at 120 °C. The observed changes in the dispersion behaviour are shown in extracted spectrum of methanol responses at 96 Td (or 1200 V V_d) as presented in Figure 3.9, where the position on the E_c scale for the methanol monomer ion changed from -1.65 Td (414 V cm^{-1}) at the temperature of 80 °C to -1.7 Td (-426 V. cm^{-1}) at the temperature of 120 °C. The minimum value for E_d required to isolate the protonated monomer from the reactant ion was decreasing with increasing temperature: 98 Td (1225 V V_d) at 80 °C, 89 Td (1110 V V_d) at 100 °C and 78 Td (975 V V_d) at 120 °C.

A minor presence of an ammonium ion (below 10 times signal to noise ratio) was observed in these dispersion plots while neither proton bound dimer nor fragment ions were observed throughout this range of ion-filter temperatures and E_d values.

The results obtained from the experiment on methanol responses vs ion temperature may be regarded as a reference experiment where the effect of increasing the filter temperature on differential mobility may be discerned and the alpha-function for the protonated methanol monomer was little affected by filter temperature.

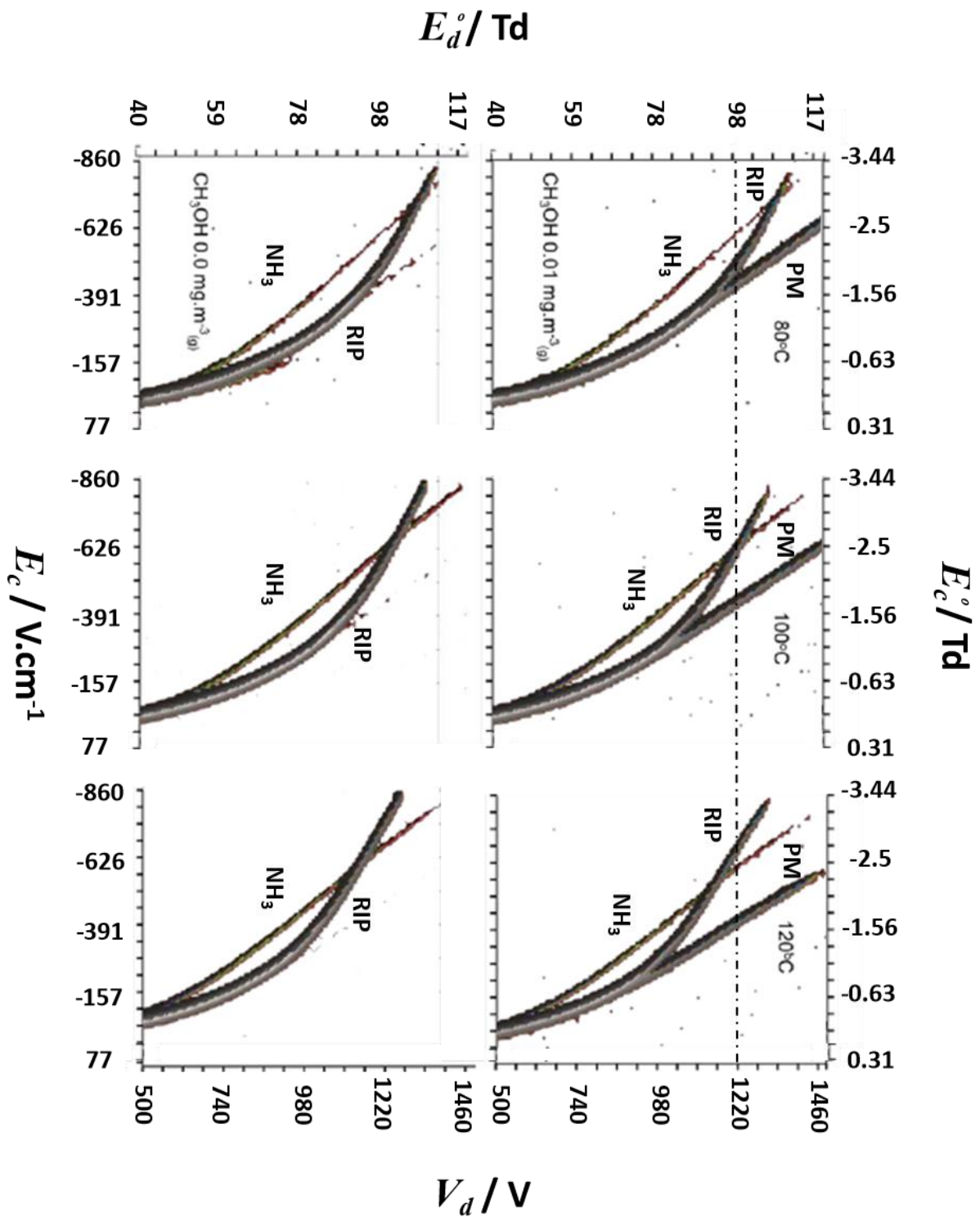


Figure 3. 8 Dispersion plots of methanol at 10 $\mu\text{g.m}^{-3}$ concentration level at 80°C, 100°C and 120°C ion-filter temperature, together with control blank recorded at 100°C. Signal against dispersion fields E_d (Y axes) and compensation fields E_c are plotted (X axes).

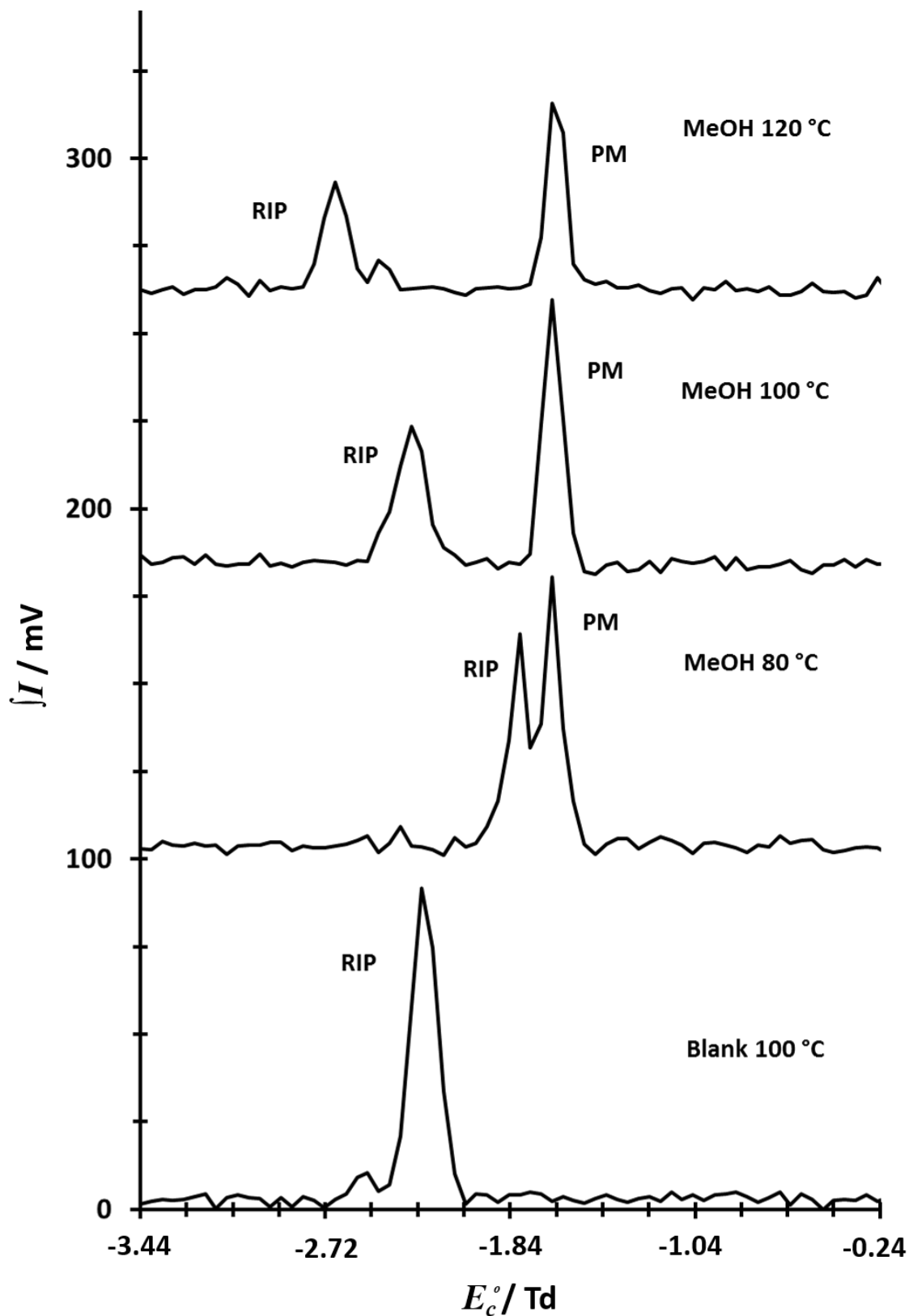


Figure 3.9 Extracted spectrum of methanol d-IMS responses at E_d^0 of 96 Td (1200 V V_d) for methanol at the concentration level of $10 \mu\text{g}\cdot\text{m}^{-3}$ at ion filter temperature of 80, 100, 120 °C and blank spectrum at 100 °C. The RIP is a reactant ion peak and PM is methanol protonated monomer.

3.4.3 Ethanol

3.4.3.1 Concentration relationships

A topographic plot of ethanol d-IMS responses across concentrations from 3600 mg.m⁻³ to 0.0005 mg.m⁻³ is shown in Figure 3.10. The changes in d-IMS ethanol responses with respect to changing concentration may be categorised within four zones:

- Zone 1: Modification, highest concentration (3600 to 130 mg.m⁻³), dominated by proton bound cluster ($EtOH)_nH^+$ (n= 2 to 4),
- Zone 2: transition from proton bound trimer ($EtOH)_3H^+$ to proton bound dimer ($EtOH)_2H^+$ (n= 2 and 3) (130 to 5 mg.m⁻³),
- Zone 3: Dominated by proton bound dimer ($EtOH)_2H^+$ (5 to 0.3 mg.m⁻³),
- Zone 4: Production of low intensity protonated monomer ($EtOH)H^+$ and domination of reactant ion ($H_2O)_nH^+$.

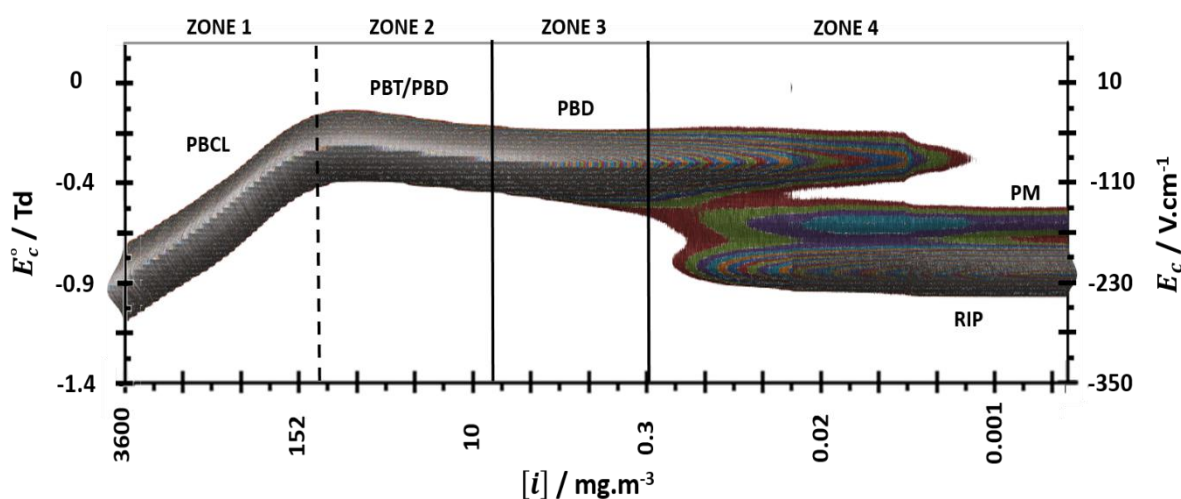


Figure 3. 10 Topographic plot of ethanol d-IMS responses resulting from an exponential washout experiment over the concentration range 3600 mg.m⁻³ to 0.0001 mg.m⁻³ at the d-IMS filter temperature of 100 °C and 72 Td or 900 V_d V. Zones 1 to 4 shows different ions and dispersion behaviour, related to the concentration levels. Note: PBCL - proton bound cluster ($EtOH)_nH^+$ where n= 2 to 4; PBT - proton bound trimer ; PBD - Proton bound dimer; PM - protonated monomer; RIP - reactant ion peak. Black dashed line shows calculated level for the first ion-neutral collision.

3.4.3.2 Zone 1

The changes in the dispersion behaviour of the proton bound cluster ion ($EtOH)_nH^+$ (n= 2 to 4) within the zone 1, was influenced by the collisions with neutrals at concentrations of 3560 mg.m⁻³ to approximately 130 mg.m⁻³ (zone 1) and agreed with theoretical

calculations (Section 1.8.4). The calculated limit for first successful ion/neutral collision is 133 mg.m^{-3} ; indicated by a dashed line in Figure 3.10.

3.4.3.3 Zone 2

Below 130 mg.m^{-3} , a single peak was observed, down to 5 mg.m^{-3} (Zone 2) with a noticeable shift in its position on the E_c scale, from -0.29 Td to -0.37 Td (-73.4 to -91.6 V cm^{-1}) between 120 mg.m^{-3} and 5 mg.m^{-3} (Figure 3.10). The ions produced in the source, within the Zone 2, were modelled to be proton bound trimer $(EtOH)_3H^+$ and proton bound dimer $(EtOH)_2H^+$, with the distribution between them of 14:86 and 1:99 at 120 and 5 mg.m^{-3} , respectively. The signals of the trimer and dimer are unresolved and since ions and unreacted sample vapour flow together through drift tube, the slide in E_c values can be attributed to the same phenomena proposed for the anomaly observed with methanol (Section 3.4.2.5); by formation of proton bound trimer adduct ion or exchange, between trimer and dimer during transit [165].

3.4.3.4 Zone 3

From 5 mg.m^{-3} to 0.3 mg.m^{-3} (Zone 3) a single stable signal was observed at the compensation field of -0.37 Td or -91.6 V.cm^{-1} , assigned as a proton bound dimer.

3.4.3.5 Zone 4

From 0.3 mg.m^{-3} to 0.001 mg.m^{-3} (Zone 4) two additional signals were observed, detected at the position of the compensation fields of -0.63 and -0.85 Td (-152 and -212 V.cm^{-3}). The signals are assigned as a protonated ethanol monomer $(EtOH)H^+$ and a reactant ion $(H_2O)H^+$ (respectively). The position of the protonated monomer on the compensation field scale also shifted slightly at the initial part of the ion formation, this may be attributed to a transition between monomer and dimer.

3.4.3.6 Extracted spectra

Extracted spectra showing the compensation field position of unresolved proton bound trimer and dimer peak at the concentration level of 100 mg.m^{-3} , proton bound dimer at 5 mg.m^{-3} , protonated monomer and reactant ion at 0.1 mg.m^{-3} are shown in Figure 3.11.

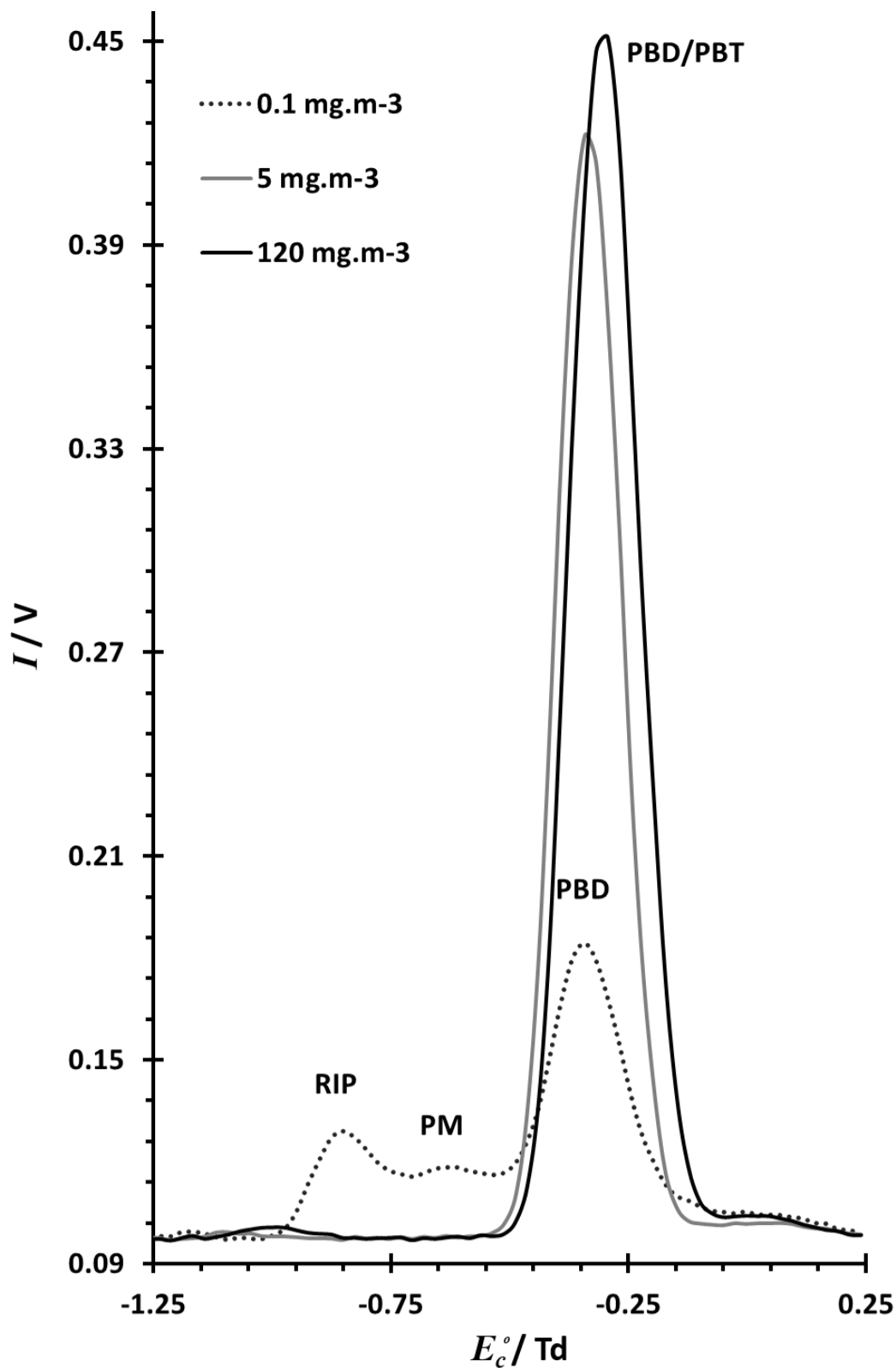
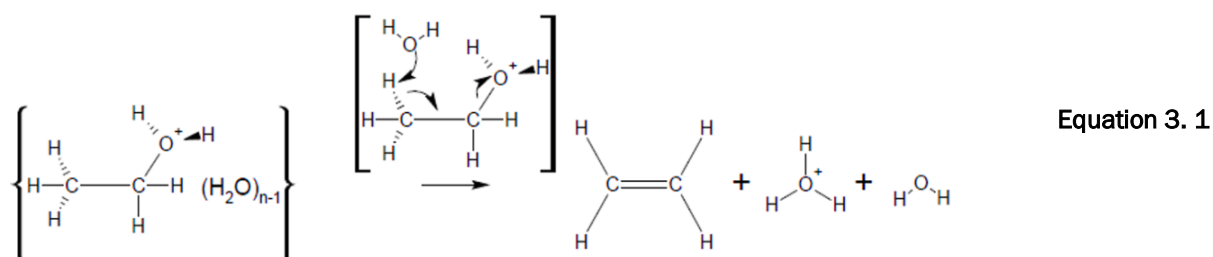


Figure 3. 11 D-IMS spectrum of extracted ions obtained for ethanol from exponential dilution experiment at 100 mg.m⁻³, 5 mg.m⁻³ and 0.1 mg.m⁻³ and a d-IMS filter temperature of 100 °C and 72 Td or 900 V_d V. A Mixture of Proton bound dimer and trimer (PBD/PBD), Proton bound dimer (PBD), protonated monomer (PM) and reactant ion peak (RIP) are observed, with ions position on the E_c^0 scale of -0.29 Td, -0.366 Td, -0.63 Td and -0.848 Td (-73.4 V.cm⁻¹, -91.6 V.cm⁻¹, -158.2 V.cm⁻¹ and -212.8 V.cm⁻¹), respectively.

3.4.3.7 Ethanol anomaly

An anomaly in ion kinetics was observed at lower concentrations (Figure 3.10, Zone 4), where the protonated monomer signal appeared to be suppressed. Instead the RIP remained the dominant ion within the zone. The ion formation kinetics for APCI sources (Section 1.8.4) predicts the formation of the protonated monomer to be thermodynamically favoured via a proton transfer reaction at these concentrations. Importantly, the presence of a hydrated proton was not predicted above ethanol concentrations of $0.05 \text{ mg}\cdot\text{m}^{-3}$; an order of magnitude lower than the results obtained in this experiment.

This anomaly can be explained by fragmentation/dissociation of the ethanol monomer ion (Section 1.7.2). Studies of Inomata [150] and Brown [144] support the proposition that the protonated ethanol monomer undergoes a dehydration reaction with increasing electric field strength to produce a protonated alkene as well as fragments to produce H_3O^+ and neutral ethane. In this case we propose the following mechanism of the latest reaction (Equation 3.1, schematic reproduced with permission of Royal Society of Chemistry [166]).



The fragmentation hypothesis was further explored with additional studies on the effect of ion temperature on ethanol d-IMS behaviour. In the first instance the exponential dilution experiment was repeated at d-IMS temperatures between $35 \text{ }^\circ\text{C}$ to $115 \text{ }^\circ\text{C}$ and fixed dispersion field of 72 Td or 900 V_d (Section 3.4.3.8) followed by the collection of dispersion plots and studying dispersion field-temperature interactions (Section 3.4.3.9).

3.4.3.8 Preliminary investigations into the ion temperature effects

Figure 3.12 presents topographic plots of the ethanol responses across 4640 mg.m^{-3} to 0.005 mg.m^{-3} . At 4640 mg.m^{-3} to around 130 mg.m^{-3} the dispersion behaviour of proton bound cluster $(EtOH)_nH^+$ (where $n = 2$ to 4) may be viewed as being modified from collisions with neutrals with a single feature shifting on the compensation field scale. The difference in ion kinetics is seen between the two temperatures at concentrations below 1 mg.m^{-3} . At $35 \text{ }^\circ\text{C}$ (Figure 3.12 bottom) a dimer/monomer/RIP transition typical of a stable and equilibrated system was observed, with the yield and behaviour of product ions in satisfactory agreement with theoretical predictions. At $115 \text{ }^\circ\text{C}$ (Figure 3.12 top) dimer formation has been suppressed with an enhanced hydrated proton presence and no protonated monomer formation observed. A temperature of $35 \text{ }^\circ\text{C}$ was not high enough to cause fragmentation/dissociation, which was observed at $100 \text{ }^\circ\text{C}$ (Figure 3.10) where traces of the monomer and hydrated proton H_3O^+ formation were discernible. Increase in temperature to $115 \text{ }^\circ\text{C}$ caused increase in the fragmentation/dissociation yield through dehydration (Equation 3.1) and complete loss of the monomer ion. Over a concentration range of 130 mg.m^{-3} to 3 mg.m^{-3} a single signal, slightly shifting on the compensation scale (towards lower values with decreasing concentration) was observed. Again, this phenomenon may be attributed to the possible formation of proton bound trimer in the ion-filter or exchange between trimer and dimer during transit through the filter, as in mechanism described in Section 3.4.2.5.

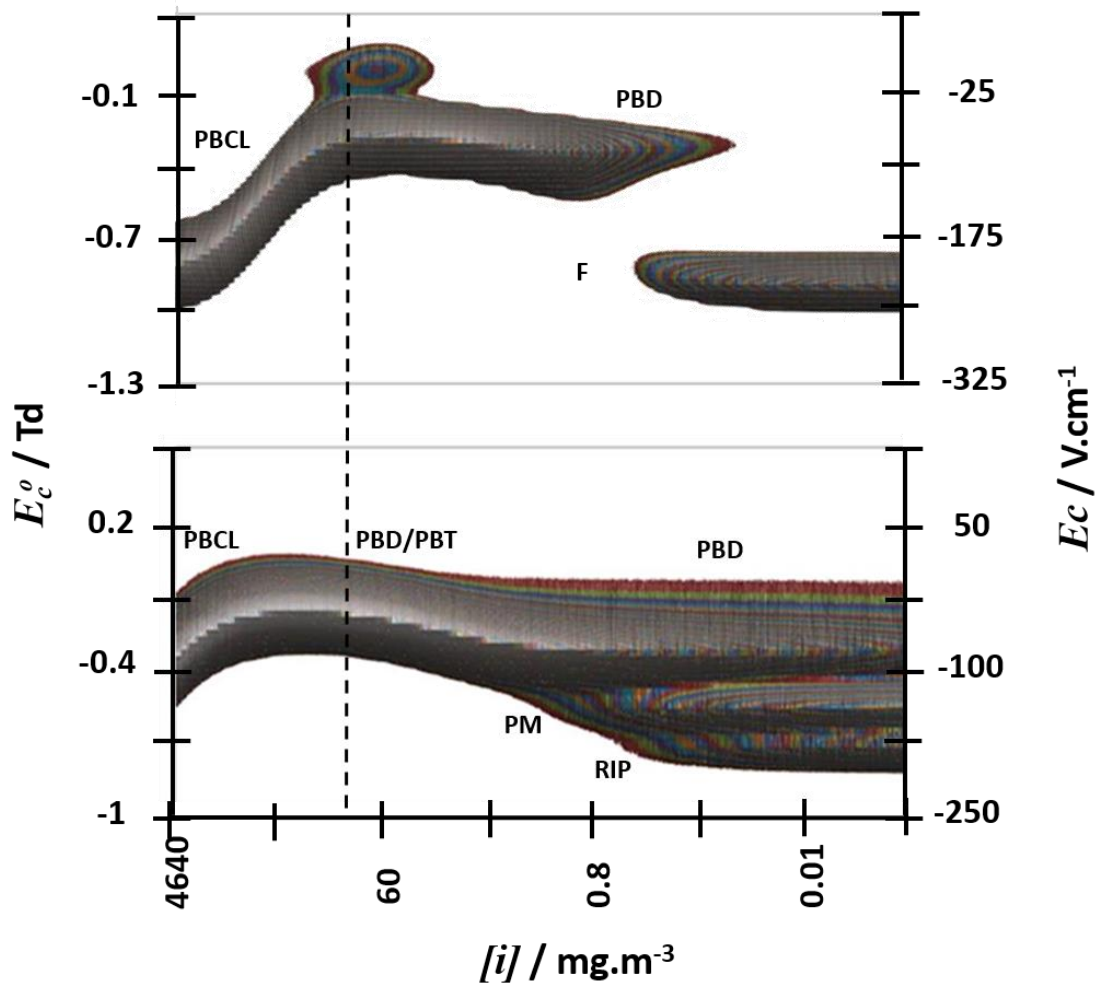


Figure 3.12 D-IMS responses of ethanol at d-IMS filter temperatures of 115 °C (top) and 35 °C (bottom) and fixed 900 V_d V or 72 Td E_d , within 4640 and 0.005 mg.m^{-3} concentration range. Note: PBCL - proton bound cluster ($\text{EtOH})_n\text{H}^+$ where $n= 2$ to 4; PBT - proton bound trimer; PBD - Proton bound dimer; PM - protonated monomer; RIP - reactant ion peak; F - fragment.

3.4.3.9 Dispersion field interactions

In the second set of experiments the effect of field and temperature was studied by recording dispersion plots generated from permeation sources (Section 2.7) at different concentration levels and temperatures (80, 100 and 120 °C). Examples of the results are shown in Figure 3.13 collected at an ion filter temperature of 80 °C and two different concentration levels. At a concentration of 1.9 mg.m^{-3} (Figure 3.13, top) a proton bound dimer, may be seen to decompose with increasing dispersion field and at the E_d^0 values above 80 Td (or E_d 1050 V_d V) is completely depleted. However, no protonated monomer ion is being formed as a dissociation product (as could be expected in d-IMS), instead, a signal of only hydrated proton H_3O^+ is observed, which at this concentration level cannot

be associated with typical reactant ion formation, what suggests fragmentation. The H_3O^+ ion intensity increases with increasing dispersion field reaching a maximum at a dispersion field of 89.6 Td or 1120 V_d V.

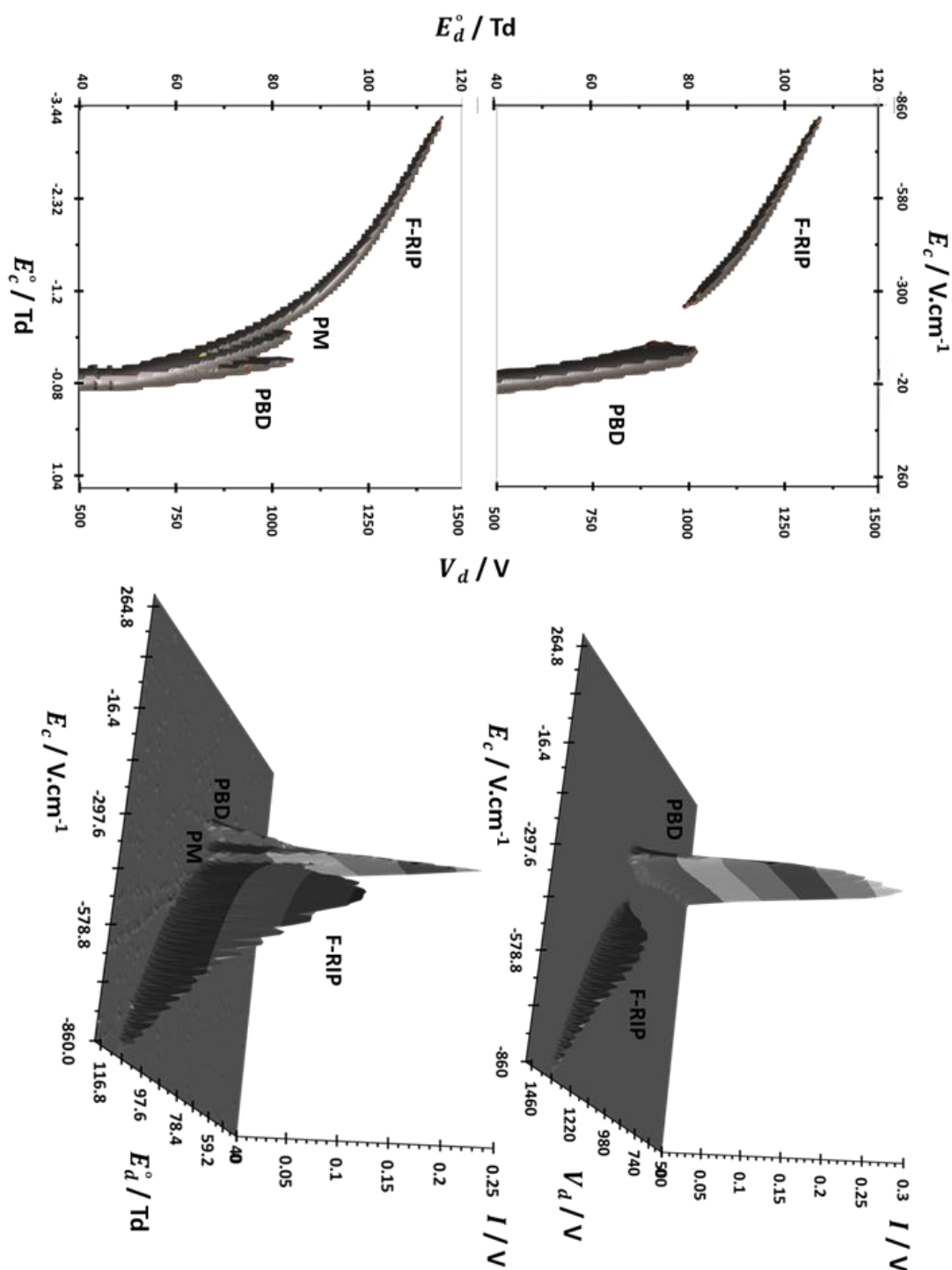


Figure 3. 13 Contour and surface plots of d-IMS responses of ethanol vapours, collected at 80 °C d-IMS ion filter temperature, showing formation of hydrated proton (H_3O^+) (F-RIP) at 1.9 $mg.m^{-3}$ (top) and 0.55 $mg.m^{-3}$ (bottom) as a product of fragmentation/ dissociation. PBD - proton bound dimer and PM - protonated monomer.

At a lower concentration of 0.055 mg.m^{-3} (Figure 3.13, bottom) the protonated monomer was formed but again diminished with increasing dispersion field strength and was completely suppressed for $E_d > 84 \text{ Td}$ or $1050 V_d \text{ V}$. This was accompanied by a rise in the hydrated proton abundance reaching a maximum at E_d of 94 Td or $1170 V_d \text{ V}$. Note: No other ion was observed (protonated alkene), suggesting a different fragmentation mechanism to the one described by Brown (Section 1.7.2) [144].

This, for the first time, directly revealed a pattern of fragmentation of the protonated ethanol, generating H_3O^+ and possibly a neutral C_2H_4 via the proposed mechanism shown in Equation 3.1.

3.4.4 *n*-Propanol

3.4.4.1 Concentration relationships and unexpected complexity.

The topographic plot of *n*-propanol d-IMS responses from 1950 mg.m^{-3} to 0.01 mg.m^{-3} collected at an ion filter temperature of $100 \text{ }^\circ\text{C}$ and 88 Td or $1100 V_d \text{ V}$, is shown in Figure 3.14. The main trends in the d-IMS *n*-propanol responses in respect to changing concentration can be categorised within four zones:

- Zone 1: Modification, highest concentration (1950 to 160 mg.m^{-3}), dominated by proton bound cluster $(PrOH)_nH^+$ ($n = 2$ to 3),
- Zone 2: dominated by proton bound dimer $(PrOH)_2H^+$ (160 to 25 mg.m^{-3}),
- Zone 3: proton bound dimer $(PrOH)_2H^+$ decomposition and formation of fragment (25 to 0.7 mg.m^{-3}),
- Zone 4: Production of low intensity fragment and reactant ion $(H_2O)_nH^+$.

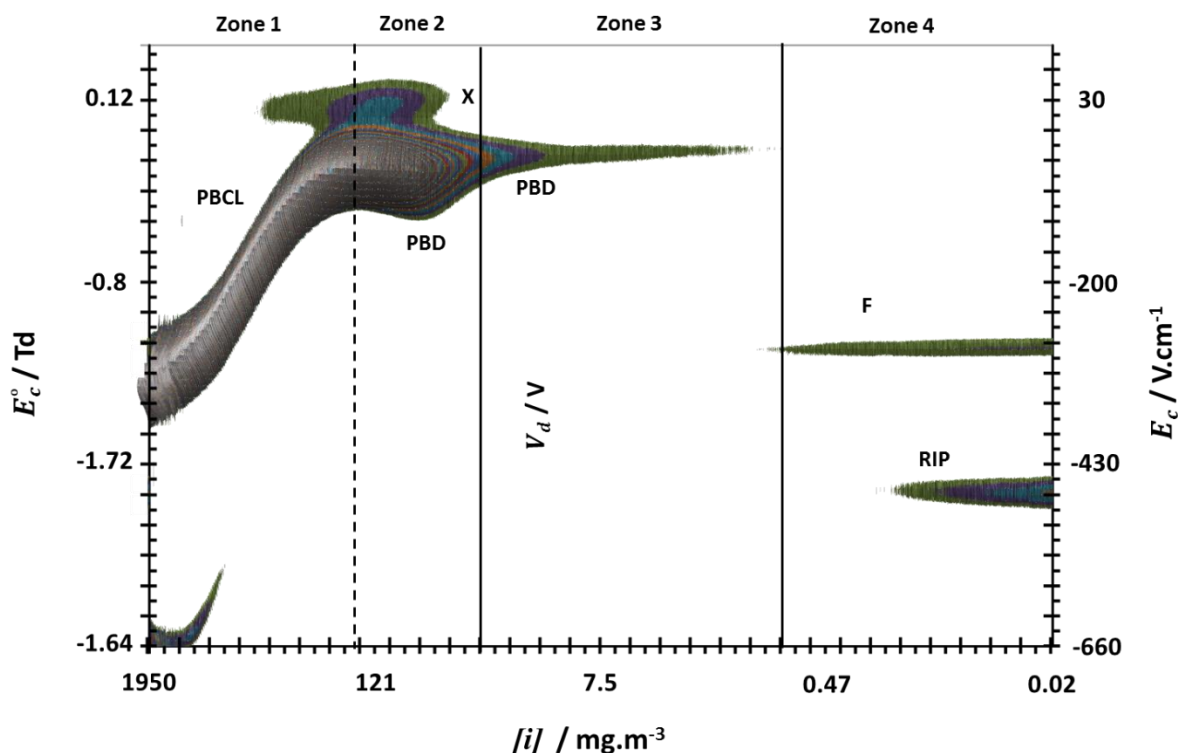


Figure 3. 14 Topographic plot of n-propanol d-IMS responses recorded during the exponential washout experiment, at ion filter temperature of 100°C and 88 Td (1100 V_d V), across concentrations of 1950 mg.m^{-3} to 0.01 mg.m^{-3} . Zones 1 to 4 shows different ions and dispersion behaviour, related to the concentration levels. Note: PBCL - proton bound cluster ($\text{PrOH})_n\text{H}^+$ where $n=2$ to 3; X - unidentified feature; PBD - Proton bound dimer; F - fragment; RIP - reactant ion peak. Black vertical dotted line shows calculated level for the first ion-neutral collision.

3.4.4.2 Zone 1

The changes in the dispersion behaviour of the proton bound cluster ion ($\text{PrOH})_n\text{H}^+$ ($n=2$ to 3), influenced by the collisions with neutrals from 1950 mg.m^{-3} down to approximately 130 mg.m^{-3} (zone 1) agreed with theoretical calculations (Section 2.5.4) on ion/neutral collisions. The calculated limit for first ion/neutral collision during the low field segment of the dispersion wave-form was 160 mg.m^{-3} and is indicated by dashed line in Figure 3.14.

3.4.4.3 Zone 2

Below 160 mg.m^{-3} , a well-defined signal was present at the compensation field of -0.25 Td or 61.8 V.cm^{-1} and this existed down to around 25 mg.m^{-3} , assigned as a proton bound dimer ($\text{PrOH})_2\text{H}^+$. Traces of another signal were also seen at the compensation field of 0.15 Td or 38.0 V.cm^{-1} (X), and it was unclear if the signal was associated with a

proton bound trimer or a fragment ion. Observations at lower concentration indicated more complicated behaviour.

3.4.4.4 Zone 3

The abundance of the proton bound dimer reduced rapidly within zone 2 resulting in only traces between 25 mg.m⁻³ and 0.7 mg.m⁻³. Unexpectedly, no other ion was being formed from the dimer decomposition, apart from a trace signal (F) at a compensation fields of -1.14 Td or -283.8 V.cm⁻¹. Theoretical calculations within the zone 3 indicate formation of both protonated monomer (PrOH)H⁺ and proton bound dimers (PrOH)₂H⁺, at ratios of 16 :1 and 412:1 for 25 mg.m⁻³ and 1 mg.m⁻³ respectively. The distance of the ion F from the dimer ion, seems to be too big to indicate formation of the monomer ion, instead a smaller, fragment ion, is suggested.

3.4.4.5 Zone 4

At concentrations between 0.03 mg.m⁻³ and 0.2 mg.m⁻³ two features were present. First, the hydrated proton of the RIP ($E_c/N = -1.87$ Td or $E_c = -468.V$ cm⁻¹) and a second signal (F) ($E_c/N = -1.14$ or $E_c = -283.8$ V.cm⁻¹).

3.4.4.6 Extracted spectra

Figure 3.15 presents extracted spectrum of d-IMS responses at 25 mg.m⁻³ and 0.1 mg.m⁻³ showing ions on the compensation field scale against their intensity I in V, as well as a closer look at the ions' background levels. In the spectrum a hydrated proton (RIP) was discernible at 0.1 mg.m⁻³, while calculations indicate that the ion would not be predicted to be produced until concentrations had reduced to 0.03 mg.m⁻³. The presence of this feature is indicative of fragmentation processes. Another feature, not seen in the experimental washout topographical plot, was a trace signal at -0.82 Td (or -205 V.cm⁻¹) (X2), which could be associated with traces of protonated monomer ions, not observed at higher concentrations. Feature X1 was most likely a siloxane contaminant.

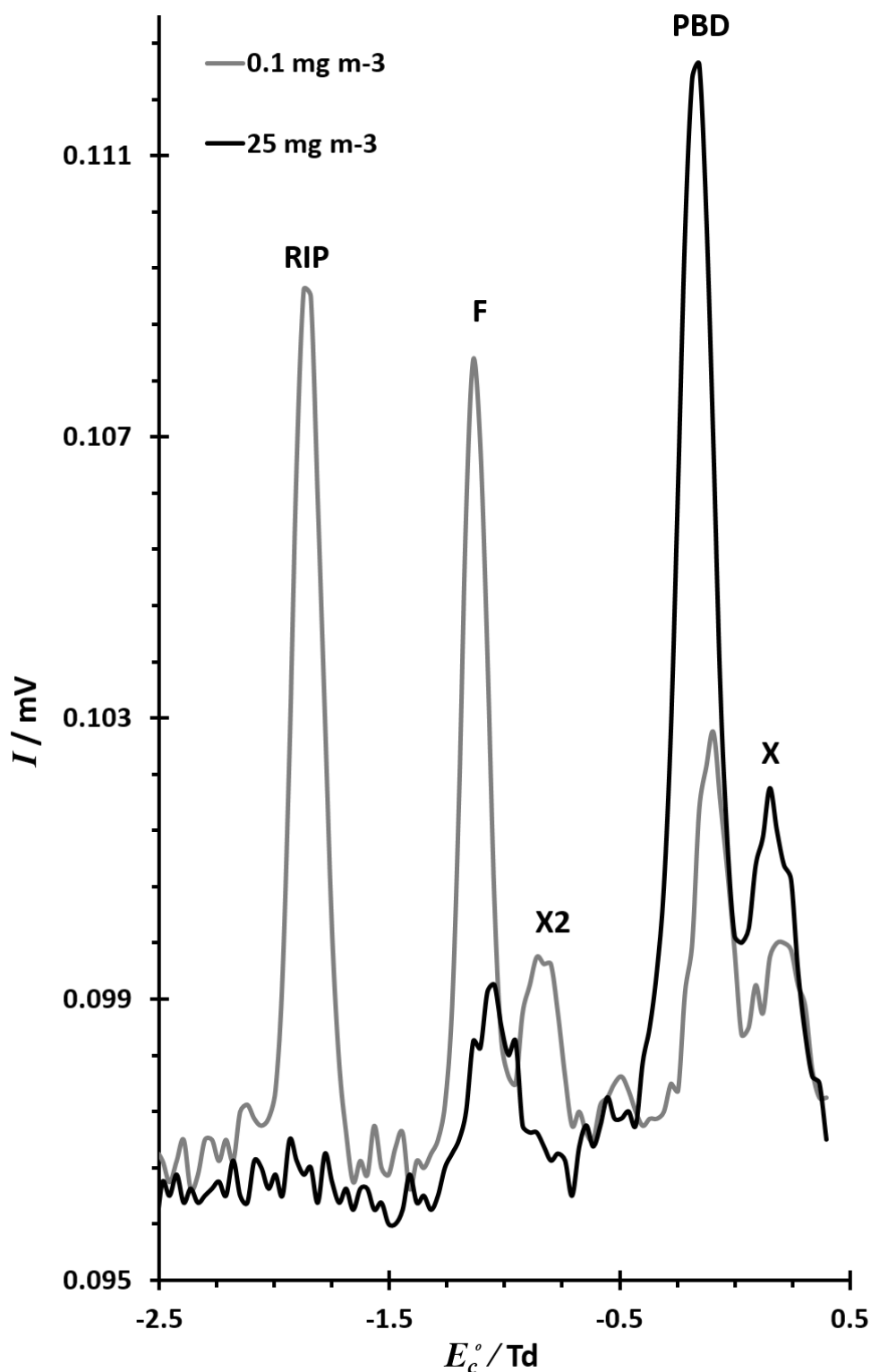


Figure 3. 15 D-IMS spectrum of extracted ions obtained for n-propanol from the exponential dilution experiment at 25 mg.m^{-3} and 0.1 mg.m^{-3} , ion filter temperature was 100°C with 88 Td ($1100 V_d$ V). Proton bound dimer (PBD), fragment (F) and reactant ion peak (RIP) are presented, with ions position on the compensation field E_c° scale of -0.25 Td, -1.14 Td and -1.87 Td (or -61.8 V.cm^{-1} , -283.8 V.cm^{-1} and -468.6 V.cm^{-1}), respectively. Unidentified ions X1 and X2 are also observed at 0.15 Td and -0.82 Td (or 35 V.cm^{-1} and -205 V.cm^{-1}).

To investigate the possible fragmentation of n-propanol in d-IMS, the following studies were performed:

- Preliminary exponential washout experiments at fixed dispersion fields (described in Section 3.4.4.7). These studies were supported with APCI-d-IMS-MS data as well (details in Section 3.4.4.8),
- Studies of the influence of dispersion field and ion filter temperature by capturing dispersion plots at fixed concentration (described in Section 3.4.4.9).

Note: Exponential washout summary of experiments and conditions is given in Table 3.4.

3.4.4.7 Preliminary investigation of temperature effect

Figure 3.16 presents a segment of a topographic plot of n-propanol exponential washout data collected at 60 °C and 72 Td or 900 V_d V. No fragmentation pattern was observed with typical dimer/monomer/RIP kinetics. Also the formation of the hydrated proton at around 0.03 mg m^{-3} agrees with theoretical calculations.

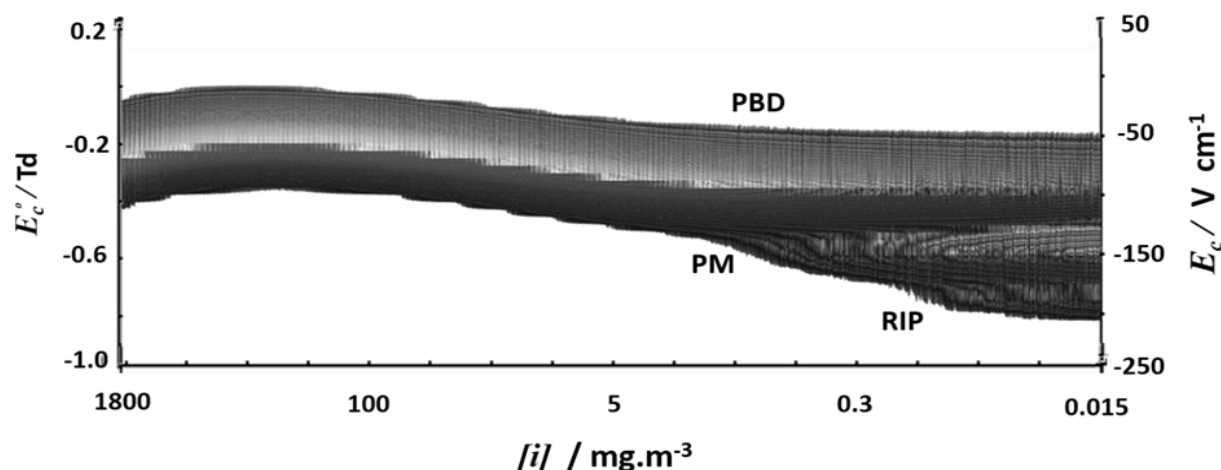


Figure 3. 16 Topographic plot of n-propanol d-IMS responses recorded during the exponential washout experiment at ion filter temperature of 60 °C and 72 Td (900 V_d V), across the concentration range of 1800 to 0.015 mg.m^{-3} . Note: PBCL - proton bound cluster $(PrOH)_nH^+$ where $n=2$ to 3; PBD - Proton bound dimer; PM - protonated monomer; RIP - reactant ion peak.

Increasing the temperature to 115 °C and 88 Td or 1100 V_d V (Figure 3.17) resulted in fragmentation process with two fragment/dissociation products observed: a well-defined signal F at the compensation field of -1.0 Td (254 V.cm^{-1}) and traces of a signal F1 at -0.67 Td (167 V.cm^{-1}).

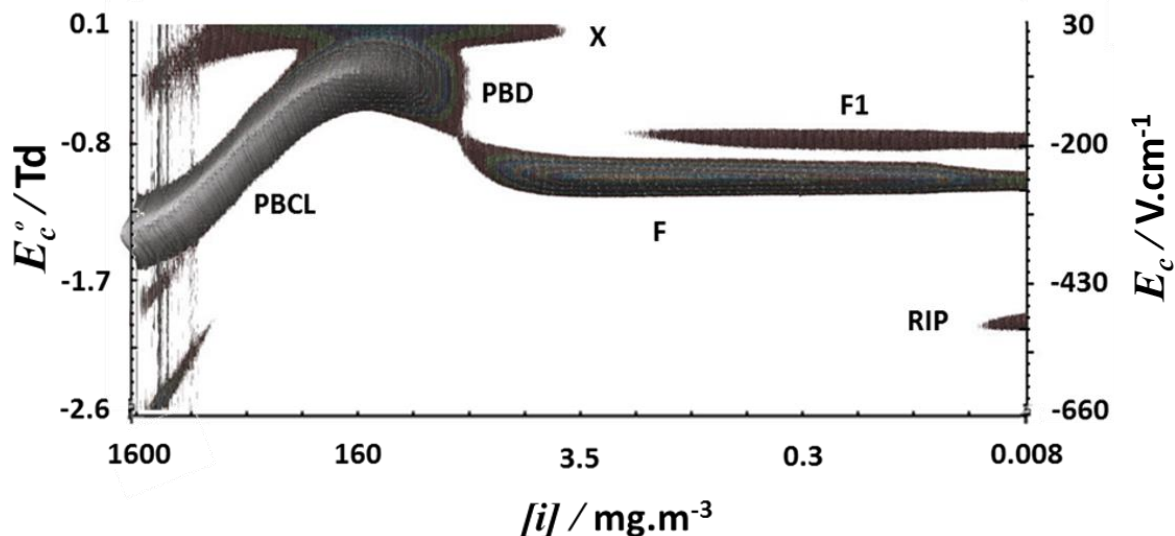


Figure 3. 17 Topographic plot of n-propanol d-IMS responses recorded during the exponential washout experiment at ion filter temperature of 115°C and 88 Td (1100 V_d V), across the concentration range of 1600 to 0.008 mg.m^{-3} . Note: PBCL - proton bound cluster $(PrOH)_nH^+$ where $n= 2$ to 3; PBD - Proton bound dimer; F and F1 - fragment ions; X - unknown contaminant RIP - reactant ion peak.

From the above results it is seen that the changes in electric field and temperature amplitude produces totally different responses for n-propanol in d-IMS and is a direct proof of the fragmentation/dissociation process induced via increases in ion energies.

3.4.4.8 APCI d-IMS-Mass Spectrometry of n-Propanol with electric field induced decomposition of ions

Ions formed in a ^{63}Ni ion source were heated with electric fields and mass-analysed. Figure 3.18 presents the data obtained from an n-propanol washout experiment (Sections 2.5.3 and 3.4.3) and shows how ion abundances changed as the voltage amplitude (electric field) was increased.

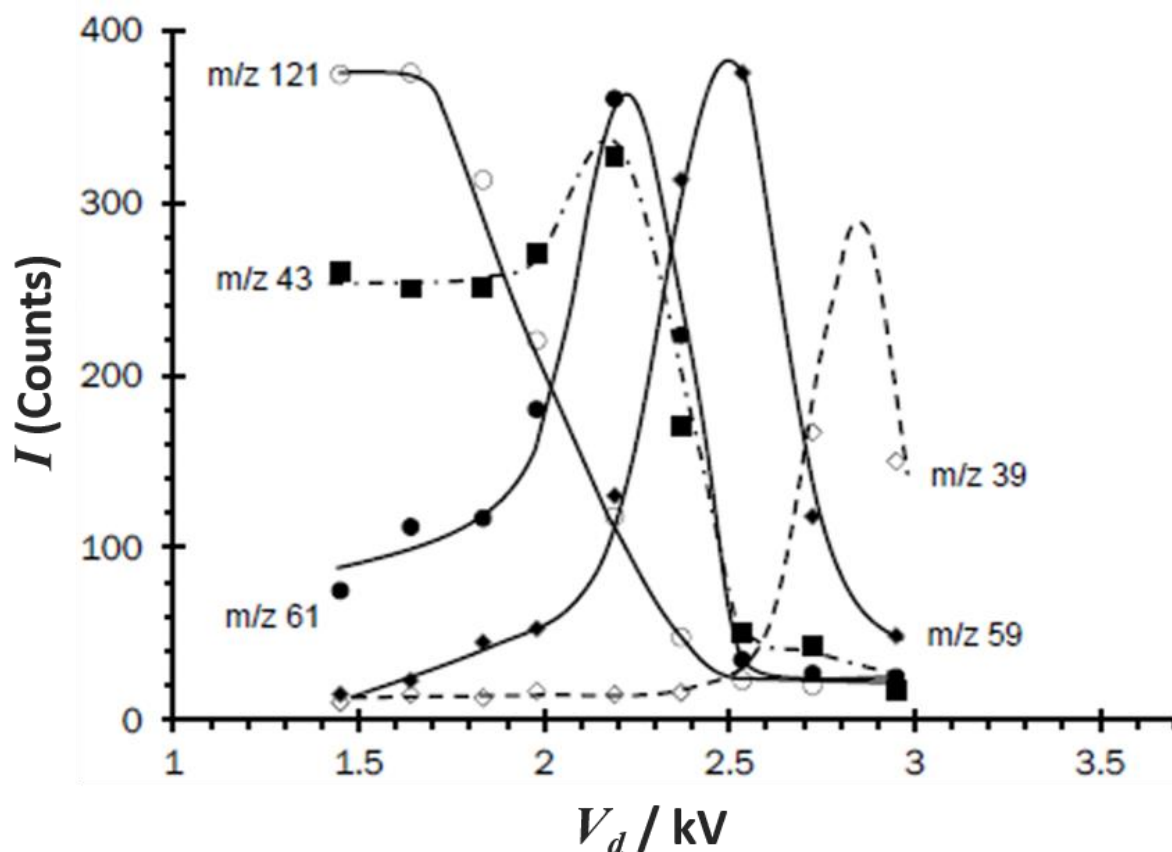


Figure 3. 18 The effect of dispersion field amplitude V_d on ion dissociation of n-propanol, showing the dissociation of a proton bound dimer PBD ($m/z = 121$) to yield a protonated monomer PM ($m/z = 61$) and fragment ion ($m/z = 43$). Increasing V_d resulted in further ion dissociation products at $m/z = 59$ and finally $m/z = 39$. Figure adapted from Ruszkiewicz et.al with permission of Royal Society of Chemistry [166].

At the lowest electric field strengths, below an applied dispersion voltage amplitude of 1.7 kV the proton bound dimer m/z 121 was the most prominent ion (375 counts) with two dissociation products at m/z 61 (75 counts) and m/z 43 (250 counts) also present. Increasing the dispersion voltage amplitude to 2.2 kV resulted in the depletion of the proton bound dimer with the abundance of the m/z 61 and m/z 43 reaching maximum intensities of ca 370 counts and 340 counts respectively. Another dissociation product, m/z 59, was created in parallel with the m/z 61 and m/z 43 entities, increasing in-line with increasing dispersion voltage. Above a dispersion voltage of 2.2 kV the m/z 59 dissociation product ion become the dominant species, reaching a maximum intensity at a dispersion voltage of 2.5 kV, as the abundance of m/z 61 and m/z 43 ions reduced to near zero. Finally, at a dispersion voltage above 2.5 kV the abundance of m/z 59 fragment ion reduced to near zero accompanied by the emergence of m/z 39

dissociation product ion reaching a maximum intensity estimated to fall in the range 180 counts to 300 counts at a dispersion voltage of 2.9 kV.

3.4.4.9 Dispersion field and ion-filter temperature interactions in d-IMS

Dispersion plots in Figure 3.19 for n-propanol from 70 to 130°C show that the protonated monomer ion $(PrOH)H^+$ was discernible only at 70°C, and then only at dispersion field (E_d/N) values between 60 Td (V_d of 750 V) to 75 Td (V_d of 940 V). A proton bound dimer ion $(PrOH)_2H^+$ was observed at (E_d/N) values from 40 Td (V_d 500 V) to 100 Td (1250 V) and as the ion filter temperature increased the intensity of the proton bound dimer appeared to be suppressed significantly at lower dispersion field strengths. Similar to the ethanol experiment was the unexpected, and previously unreported phenomenon, of the apparent regeneration of the reactant ion signal accompanying the suppression of the dimer ion signal; indicative of the production of hydrated protons. Figure 3.19, taken from n-propanol dispersion data at a filter temperature of 70°C shows the extracted maximum dispersion plot signal plotted against the blank data for H_3O^+ . As the dispersion field increased the intensity of the signal H_3O^+ increased from an almost zero level starting at 65 Td (860 V_d V) and reached a maximum at 84 Td (1050 V_d V), followed by a decline. In contrast the blank dispersion plot shows peak intensity decreasing smoothly with the increased field due to wall-losses associated with the reduction in the acceptance aperture that occurs with increasing field. (This is observed for all ions in planar embodiments of d-IMS.) Any rise in ion intensity with increasing dispersion field, as shown for n-propanol, originates from a chemical reaction and suggests formation of H_3O^+ .

In the dispersion plots (Figure 3.19) the suppression of the dimer was accompanied by an appearance of another ion at the compensation field (E_c/N) = -1.5 Td (E_c -473 V.cm⁻¹) and (E_d/N) of 117 Td (V_d 1490 V). The signal appears at increasingly lower compensation field values with increased temperature and can be associated with the fragmentation/dissociation patterns shown in Figure 4.18 (the d-IMS-MS experiment used to study electric field induced decomposition). The underlying processes that generated the observed responses may be described in similar terms to the chemistry of alcohol product ions observed with PTR-MS [144].

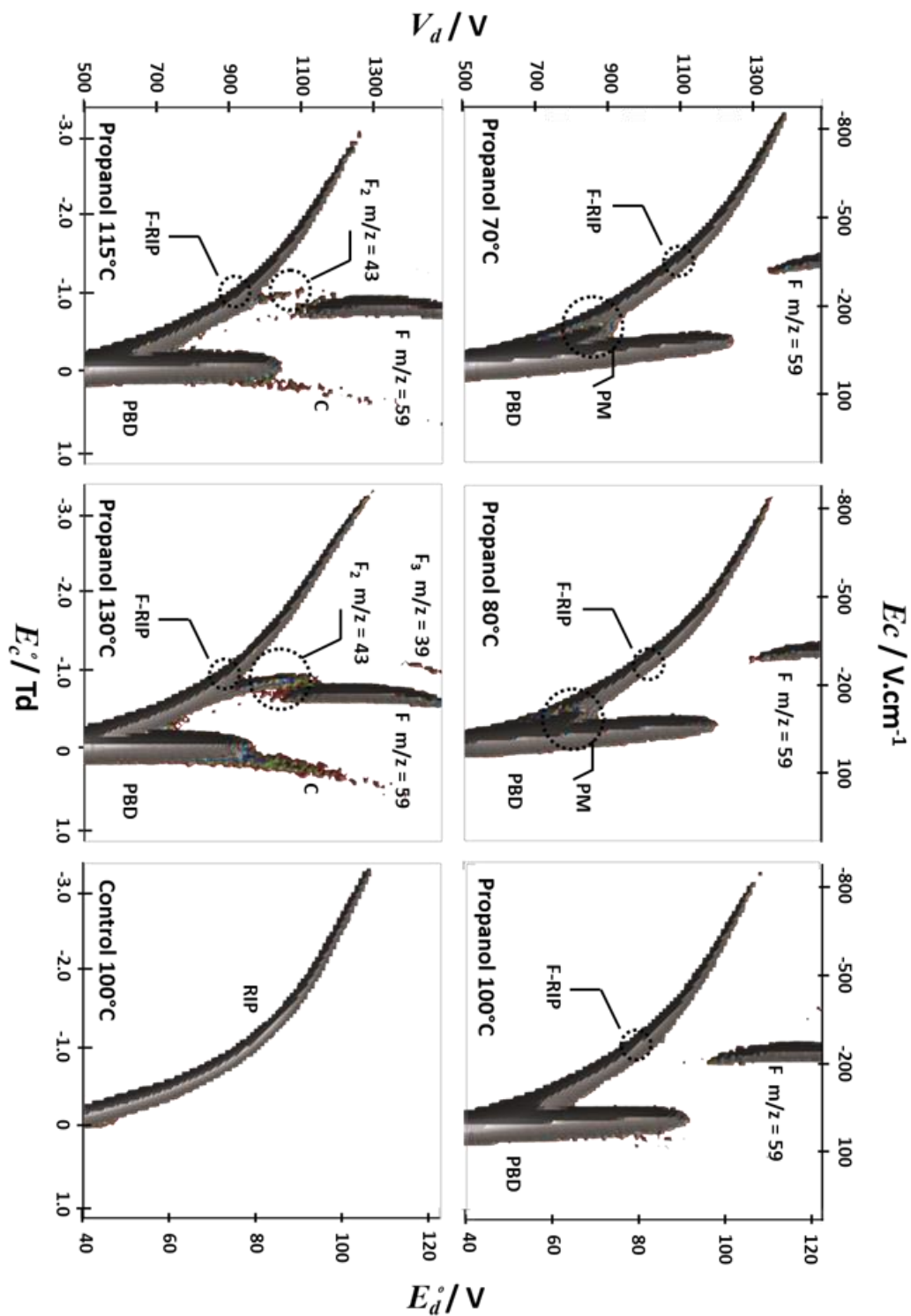


Figure 3. 19 Dispersion plots showing the combined effect of filter temperature and dispersion field ($E_c/V \text{ Td}$) on d-IMS responses to n-propanol at 0.02 mg.m^{-3} . The mass assignments are tentative. Note: PBM: proton bound monomer; PBD: proton bound dimer; and, C: trace contamination attributed to siloxanes, F and F2 : fragment ions and F-RIP: regenerated reactant ion peak.

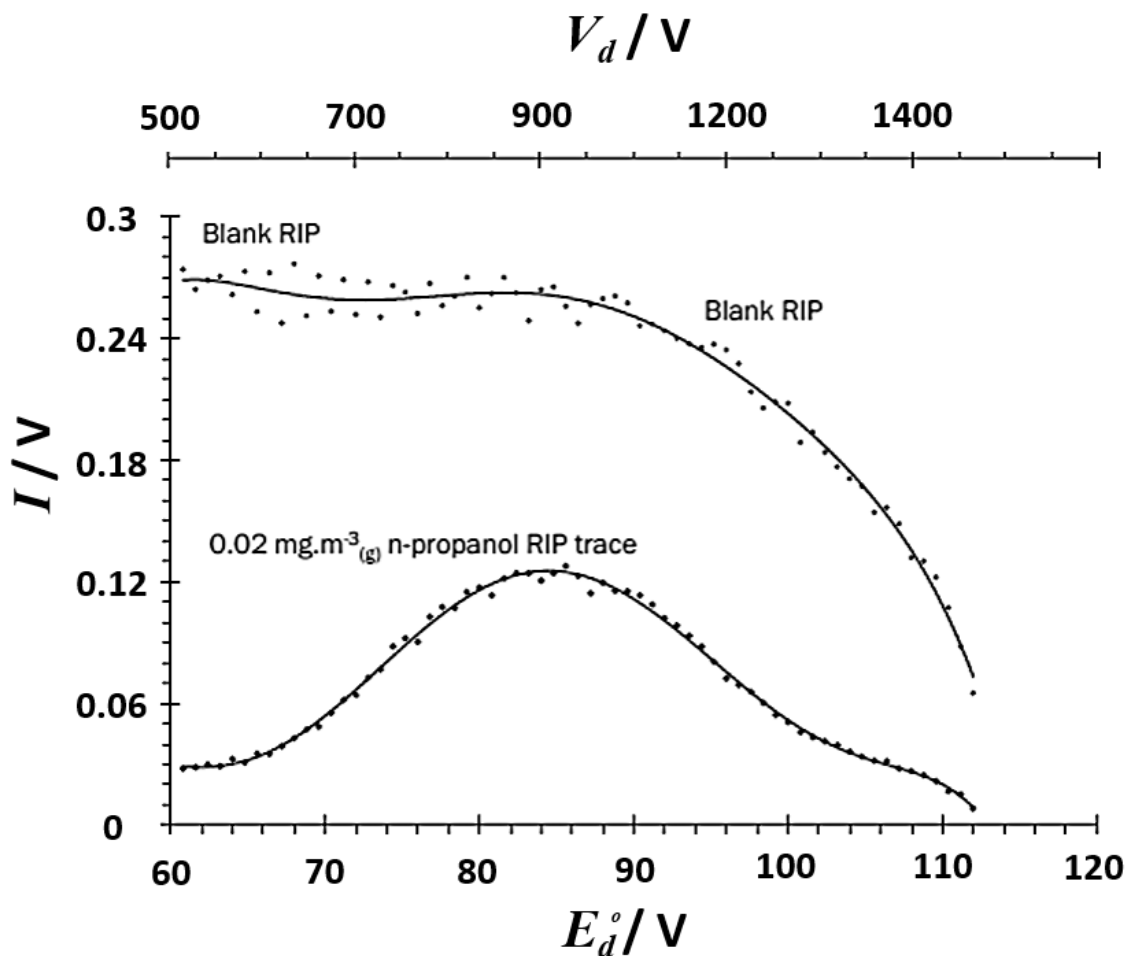
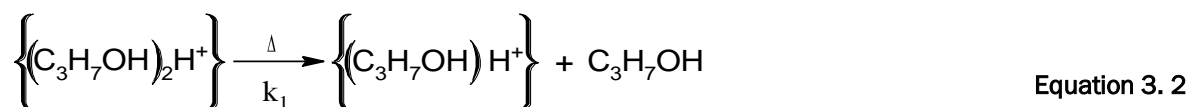


Figure 3.20 Evidence of formation of H_3O^+ with increasing dispersion field E_d/N . The top trace is a blank dispersion obtained in the absence of analyte and shows the effect of increasing field strength on the intensity of the H_3O^+ signal. The signal intensity decays with the reducing acceptance aperture of the d-IMS. The bottom trace shows the H_3O^+ signal intensity observed under the same dispersion fields in the presence of 0.02 mg.m^{-3} propanol. At the start of the dispersion field programme the H_3O^+ signal reflects the depletion of the reactant ion peak to form proton bound dimer and protonated monomer. Increasing dispersion field E_d/N resulted in a signal profile indicative of the regeneration of H_3O^+ in line with the dissociation and fragmentation processes postulated in Equations 3.3 and 3.4.

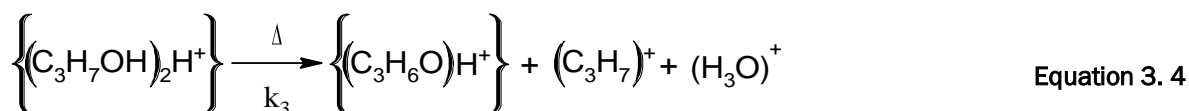
At low dispersion fields and ion filter temperature the predominant n-propanol species appears to be a proton bound dimer (m/z 121), increasing the energy of the ion cluster causes dissociation generating a product (m/z 61) most likely protonated monomer via reaction shown in Equation 3.2



The protonated monomer may undergo a dehydration reaction (Equation 3.3) resulting in a fragment ion (m/z 43), reported previously in PTR-MS studies at electric fields of 138 Td [144].



The creation of an m/z 59 species from n-propanol has not been reported, although it was observed at trace levels with 2-propanol. Proton bound dimers were also not reported within PTR-MS studies, and the difference in pressure may enable different fragmentation mechanisms. The creation of m/z 59 species along with the production of m/z 19 may also be explained if the dissociation of a proton bound dimer is invoked (Equation 3.4).



This hypothesis is supported by the close relationship between the decomposition of the protonated dimer and the formation of the m/z 59 ion. Extracted dispersion voltage values for the fragment formation and dimer decomposition against ion filter temperature is shown in Figure 3.21 that highlights how as the filter temperature was increased the dispersion field required for the formation of the fragment reduced. Note that the slopes are almost identical.

The m/z 39 fragment C_3H_3^+ was observed with PTRMS studies at electric fields of 138 Td [144], and is thought to result from the sequential loss of H_2 (Equation 3.5) and at this stage the tentative assignment for C_3H_3^+ is a cyclic entity [142,167,168].



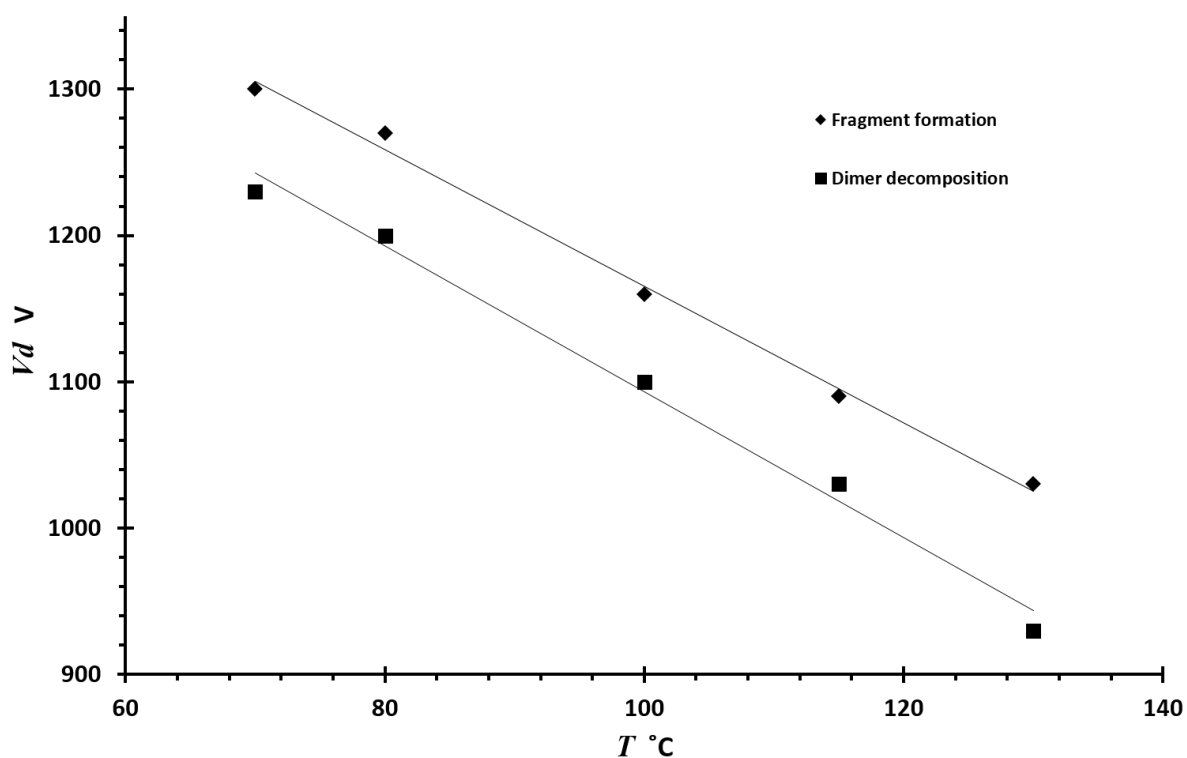


Figure 3.21 Dispersion voltage V_d values for the fragment formation ($m/z = 59$) and dimer decomposition against ion filter temperature.

The absence of a distinctive protonated monomer signal may be explained if the dissociation of the proton bound dimer was rate limiting, and followed by subsequent fast dissociation/fragmentation ($k_1 < k_2$). This has been observed with butyl acetates in a conventional IMS drift tube [134], and with esters in other d-IMS studies [84]. This behaviour has been attributed to the energy partition and the heat capacity of the larger proton bound dimer compared to the protonated monomer. The onset of ion decomposition is remarkably sensitive to ion mass and in the instance of ethanol, the difference in mass between protonated monomer and proton bound dimer is only 46 Da. Nonetheless, the protonated ethanol monomer at 70 °C was decomposed completely at $E_d/N = 78$ Td ($975 V_d$ V) while the proton bound dimer persisted until $E_d/N = 103$ Td ($1287 V_d$ V). The dispersion plots acquired at 115 °C and 130 °C (Figure 3.19), show two further dissociation/decomposition processes, albeit at lower yields. The feature observed at dispersion field of 110 Td ($1375 V_d$ V) at 130 °C was consistent with the formation of $C_3H_3^+$ (Equation 3.5). The feature branching from the hydrated proton reaction ion peak at dispersion field of 72 Td ($900 V_d$ V) and with a compensation field of -0.75 Td ($-118 V \cdot cm^{-1}$)

was perhaps consistent with the formation of $C_3H_7^+$ from the decomposition of a proton bound dimer (Equation 3.4). In PTR-MS studies at intermediate (115 Td) to high field strengths (138 Td) the fragment ion observed for 1-propanol was $C_3H_5^+$ [144]; the possible generation of such a fragment cannot be excluded.

3.4.5 *n*-Butanol

3.4.5.1 Concentration relationships

Figure 3.22 is a topographic plot of *n*-butanol d-IMS responses across the concentration range of 1920 mg.m⁻³ to 0.002 mg.m⁻³ collected at ion filter temperature of 100 °C and a dispersion field of 88 Td or 1100 V_d V. The main trends in the d-IMS *n*-butanol responses associated to concentration can be categorised within four zones:

- Zone 1: Modification, highest concentration (1920 mg.m⁻³ to 210 mg.m⁻³), dominated by proton bound cluster $(BuOH)_nH^+$ ($n= 2$ to 3),
- Zone 2: dominated by proton bound dimer $(BuOH)_2H^+$ (210 mg.m⁻³ to 120 mg.m⁻³),
- Zone 3: slow proton bound dimer $(BuOH)_2H^+$ decomposition and formation of fragment ion (120 mg.m⁻³ to 0.05 mg.m⁻³),
- Zone 4: Production of the reactant ion $(H_2O)_nH^+$ (0.05 mg.m⁻³ to 0.002 mg.m⁻³).

3.4.5.2 Zone 1

The changes in the dispersion behaviour of the proton bound cluster ion $\{(BuOH)_nH^+$ ($n= 2$ to 3) $\}$ was influenced by collisions with neutrals from 1950 mg.m⁻³ down to approximately 200 mg.m⁻³ and agrees with theoretical predictions (Section 1.8.4). The calculated limit for an ion/neutral collision during the low field segment of the dispersion waveform was 220 mg.m⁻³; indicated by a dashed line in Figure 3.22. Another signal (X) was observed at the compensation field close to 0.09 Td (or 23 V.cm⁻¹), which was not observed in the other alcohol tests. This signal was affected by neutral concentrations to a much smaller degree than the main cluster ion, suggestive that the signal was associated with a larger ion. This could be an *n*-butanol tetramer, which would be too large to be affected by collisions with neutrals in a significant way. An extracted spectrum of ions at 1000 mg.m⁻³ and 210 mg.m⁻³ is presented in Figure 3.23.

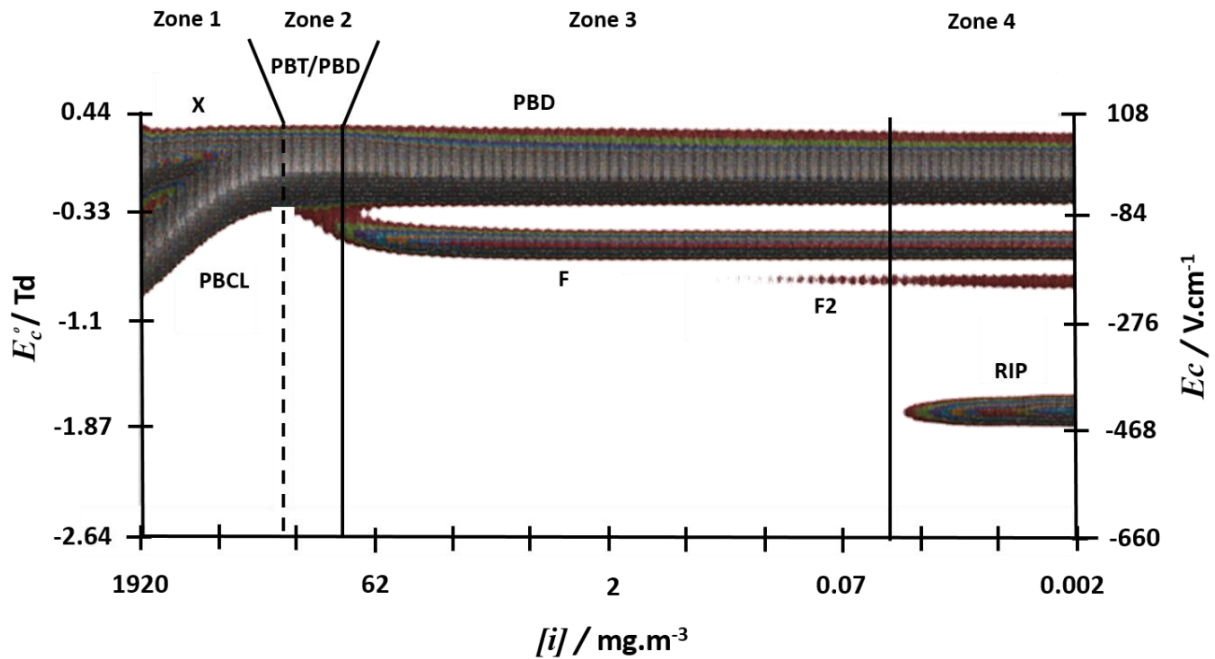


Figure 3. 22 Topographic plot of n-butanol d-IMS responses recorded during the exponential washout experiment at an ion filter temperature of $100^{\circ}C$ and a dispersion field of 88 Td ($1100 V_d V$), across the concentration range of $1920 mg \cdot m^{-3}$ to $0.002 mg \cdot m^{-3}$. Zones 1 to 4 show different ions and dispersion behaviour, related concentration. Note: PBCL - proton bound cluster $(BuOH)_n H^+$ where $n= 2$ to 3 ; X - unidentified feature; PBT -proton bound trimer; PBD - Proton bound dimer; F - fragment; RIP - reactant ion peak. Black vertical dashed line shows calculated level for the first ion-neutral collision.

3.4.5.3 Zone 2

Between $210 mg \cdot m^{-3}$ and $120 mg \cdot m^{-3}$, a single signal was observed at a compensation field of 0 Td or $0 V \cdot cm^{-1}$. Calculations show that at this concentration mostly proton bound dimer $(BuOH)_2 H^+$ is expected to be formed with small amounts of proton bound trimer $(BuOH)_3 H^+$; ratio of 7:93 and 3:98 at $200 mg \cdot m^{-3}$ and $100 mg \cdot m^{-3}$ respectively. An extracted spectrum of ions at $210 mg \cdot m^{-3}$ can be found in Figure 3.23.

3.4.5.4 Zone 3

Between $120 mg \cdot m^{-3}$ and $0.02 mg \cdot m^{-3}$ the spectrum was dominated by a proton bound dimer signal, with a peak width that decreased with reducing concentration (Figure 3.23, trace for $80 mg \cdot m^{-3}$). This was consistent with the proton bound trimer noted in Zone 2 still being present, although unresolved from the proton bound dimer ion. At $80 mg \cdot m^{-3}$ the proton bound trimer was no longer formed.

Within Zone 3, two new features emerged:

- one from 120 mg.m⁻³ and at a compensation field of -0.49 Td (-122 V.cm⁻¹);
- and the second feature at trace levels, from \approx 0.5 mg.m⁻³ and a compensation field of 0.74 Td (-184 V.cm⁻¹).

Those were most likely fragment ions, which will be described further in Sections 3.5.5.7 and 3.5.5.8. Figure 3.24 shows an extracted spectrum of the ions observed at 0.07 mg.m⁻³.

3.4.5.5 *Zone 4*

The reactant ion peak was discernible at concentration below \approx 0.05 m⁻³ at a compensation field of -1.66 Td (or 414.4 V.cm⁻¹). This was in accordance with this theoretical calculations (Section 1.8.2). Extracted spectra of n-butanol, with exact position of the ions on the compensation field scale and ions intensities are shown in Figure 3.24.

3.4.5.6 *Extracted spectra*

Figures 3.23 and 3.24 present extracted spectrum of d-IMS responses at five concentrations from 0.002 mg.m⁻³ to 1000 mg.m⁻³. Further studies on fragmentation processes with n-butanol investigated the effect of field and ion-filter temperature, by capturing dispersion plots at fixed low levels of concentrations as well as d-IMS-MS studies.

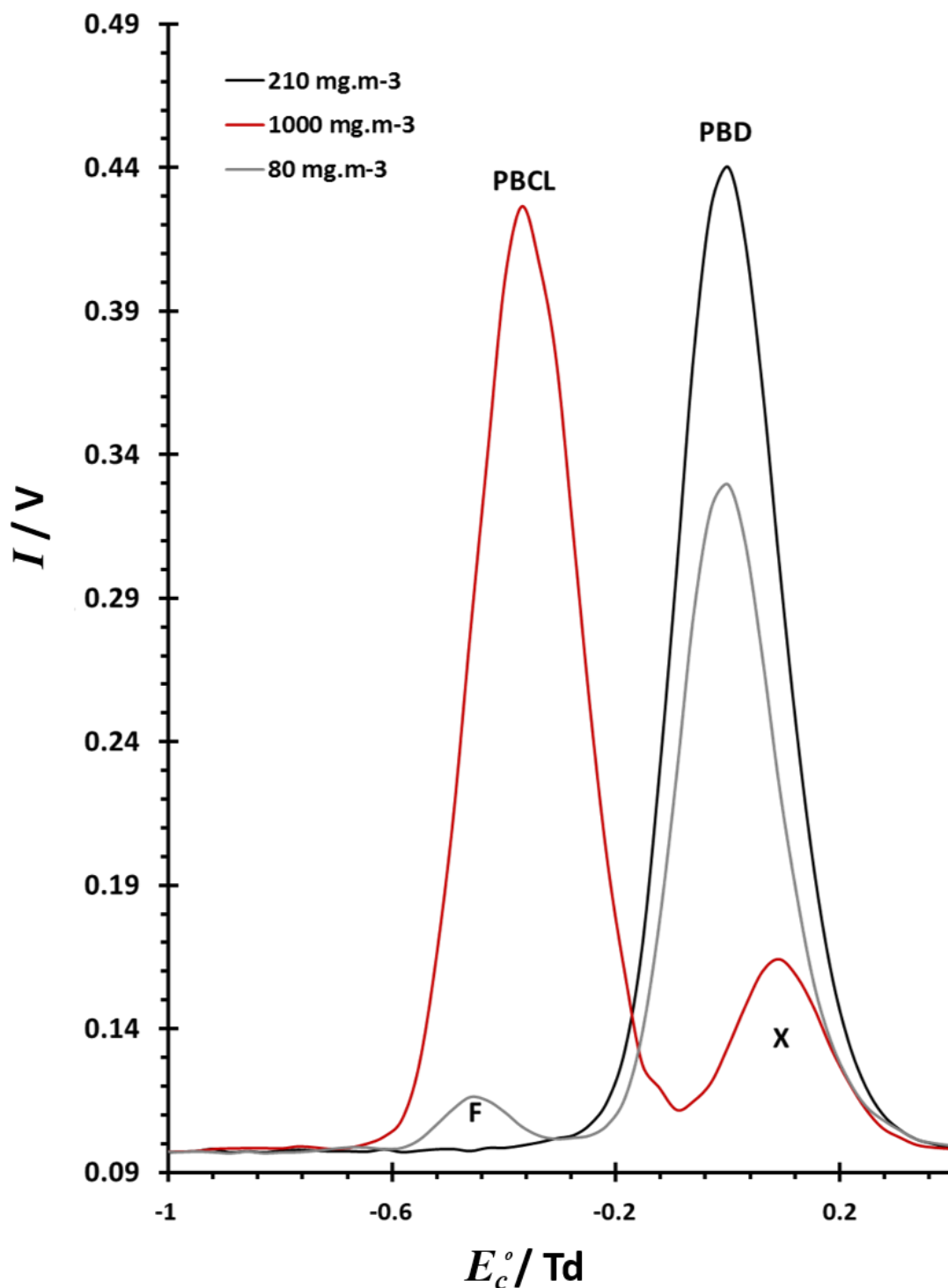


Figure 3. 23 D-IMS spectrum of extracted ions obtained for n-butanol from the exponential dilution experiment at concentrations of 1000 mg.m⁻³, 210 mg.m⁻³ and 80 mg.m⁻³ with an ion-filter temperature of 100 °C and a dispersion field of 88 Td (1100 V_d V). Proton bound cluster ions (PBCL), proton bound dimer (PBD), an unidentified peak (X), possibly a proton bound tetramer cluster ion and a fragment (F) are shown at - 0.37 Td, -0.03 Td, 0.1 Td and - 0.49 Td (-92 V.cm⁻¹, 0.2 V.cm⁻¹, 23.4 V.cm⁻¹ and - 122 V.cm⁻¹, respectively).

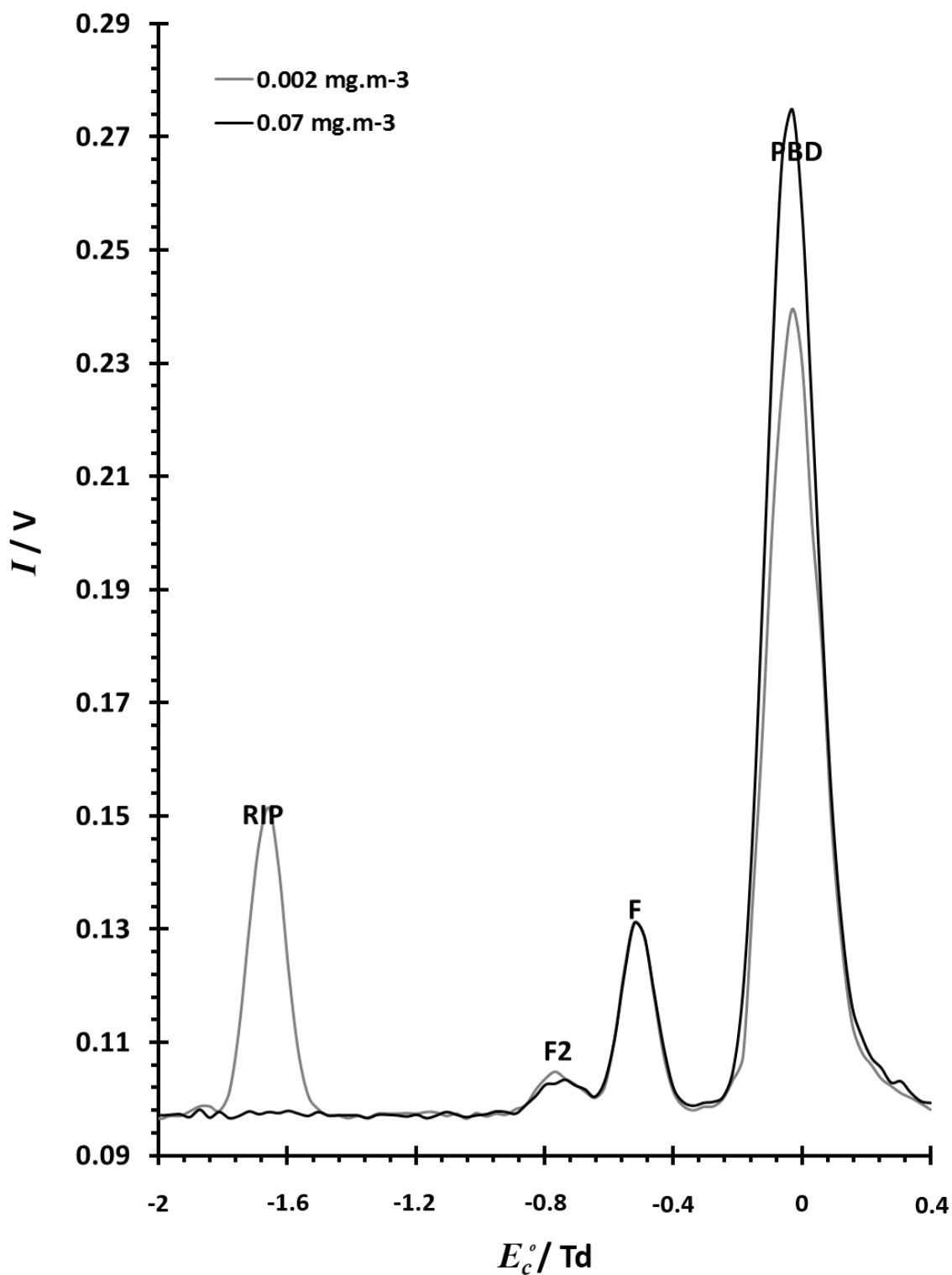


Figure 3. 24 D-IMS spectrum of extracted ions obtained for n-butanol from the exponential dilution experiment at concentrations of 0.07 mg.m⁻³ and 0.002 mg.m⁻³ obtained with an ion-filter temperature of 100°C and a dispersion field of 88 Td (1100 V_d V). Proton bound dimer (PBD), Fragments (F and F2) and reactant ion peak (RIP) are shown with ions position on the compensation field E_c^o scale of - 0.03 Td, -0.49 Td, 0.77 Td and -1.66 Td (or -7.4 V.cm⁻¹, -122.6 V.cm⁻¹, -191.8 V.cm⁻¹ and -414.4 V.cm⁻¹), respectively).

3.4.5.7 APCI Mass Spectrometry of n-Butanol with electric field induced decomposition of ions

The electric field induced fragmentation of n-butanol revealed similar behaviours to those observed for n-propanol but with greater complexity (Figure 3.25). At electric field strengths, below an applied voltage amplitude of 1.7 kV the proton bound dimer ($m/z = 149$) $(BuOH)_2H^+$ was the most abundant. Above this voltage amplitude the proton bound dimer was depleted rapidly with an approximate 10 % yield of a dissociation product ion ($m/z 57$) and an approximately 1% yield of the hydrated protonated monomer ($m/z 93$).

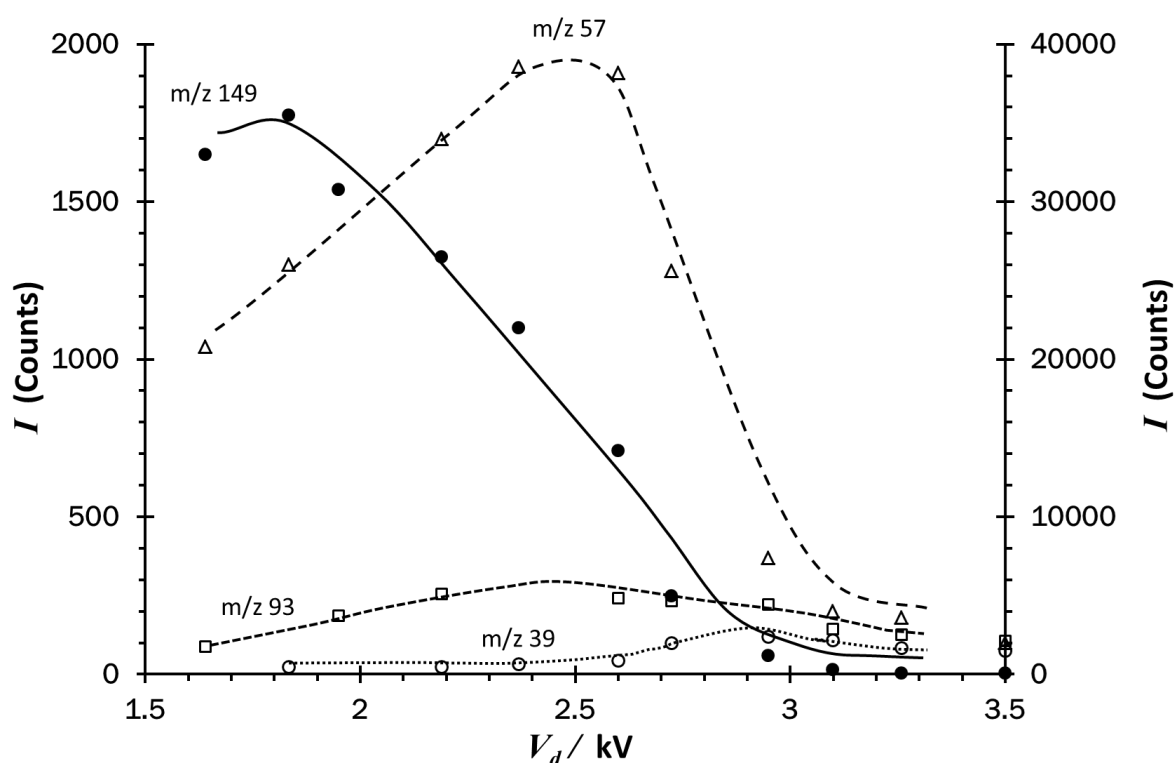


Figure 3. 25 The effect of field amplitude V_d on ion dissociation of n-butanol, showing the dissociation of a proton bound dimer ($m/z = 149$, secondary Y axis) to yield a hydrated protonated monomer ($m/z = 93$, primary Y axis) and fragment ion ($m/z = 57$, primary Y axis). Increasing V_d resulted in further ion dissociation producing ion at $m/z = 39$ (primary Y axis).

Increasing the dispersion voltage amplitude to 3 kV resulted in the formation of another dissociation product ion ($m/z = 39$). The relationship of the yield of the $m/z 93$ product ion (hydrated proton monomer $[(BuOH)H^+(H_2O)]$) to the dispersion voltage amplitude is not as well defined as the other species; perhaps indicating the possibility of two overlapping and unresolved profiles. The most abundant dissociation product ion

appears to be related to the formation of $m/z = 57$ species. However the formation of a $m/z = 39$ dissociation product ion, at low yields (0.3% of the proton bound dimer intensity), starting at a dispersion voltage amplitude of about 2.5 kV indicates a carbon-carbon bond cleavage accompanied by the formation of a smaller single carbon atom entity (possibly protonated formaldehyde) that was not observed in this experiment. The appearance of the $m/z = 39$ species coincides with the maximum yield of the $m/z = 93$ and $m/z = 57$ dissociation product ions.

3.4.5.8 *Dispersion field and ion-filter temperature interactions in d-IMS*

In Figure 3.26 the dispersion plots for n-butanol at a concentration of $0.001 \text{ mg}\cdot\text{m}^{-3}$ obtained at 40°C , 45°C , 50°C and 70°C show the fragmentation of protonated monomer with little or no proton bound dimer present. The formation of a dissociation/fragmentation product ion at 40°C and dispersion field of 90 Td ($1125 \text{ V}\cdot\text{cm}^{-1}$) was evident with the dispersion field decreasing to 59 Td ($875 \text{ V}\cdot\text{cm}^{-1}$) as the filter temperature was increased to 70°C . This observation was consistent with the formation of the $m/z = 57$ dissociation/fragmentation ion observed in the d-IMS-MS study (Section 3.4.5.7). The ion of $m/z = 39$ was not observed at this range of temperatures but was seen when a temperature of 100°C was applied (See Figure 3.2) at a dispersion field above 116 Td. As well as dissociation of the fragment ions the intensity of the reactant ion peak increased from a depleted state at low dispersion fields values to a maxima before diminishing with increasing field; similar to n-propanol. Reaction (Equation 3.5) postulates that (H_3O^+) may be generated during dissociation and this is evident in Figures 3.26 and 3.27.

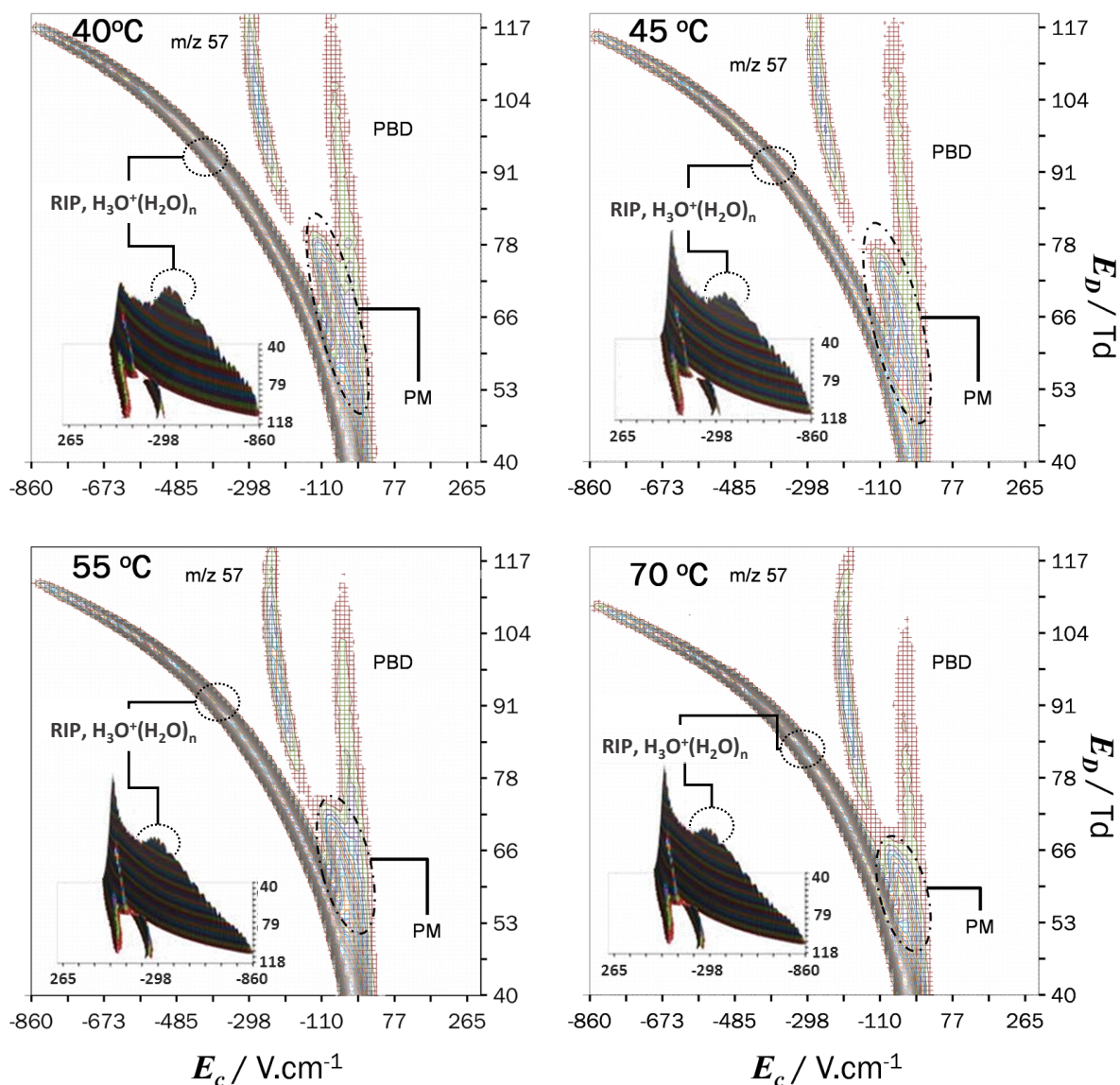
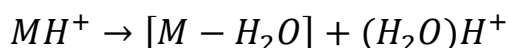


Figure 3.26 Four dispersion plots and contour maps showing the combined effect of ion filter temperature and dispersion field E_d° on d-IMS responses to n-butanol at 0.001 mg.m^{-3} . Inserts show responses rendered in 3-D highlighting the nature of the generation of hydrated protons from the dehydration reactions.

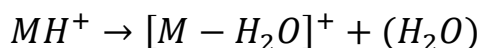
3.4.6 Summary of ion chemistry of alcohols

Alcohols from ethanol to n-butanol were observed to undergo fragmentation/dissociation reaction in d-IMS at temperatures above 70°C , via dehydration and dehydrogenation reactions. No fragmentation was observed in case of methanol.

Two mechanisms are proposed for fragmentation/dissociation of protonated monomer ions, see Equations 3.6 and 3.7. The proton may be attached to either alkene or water, or both, with a ratio depending on the effective temperature of the ion.



Equation 3. 6



Equation 3. 7

For ethanol at fields above 84 Td or 1050 V_d V product ions of protonated monomer and proton bound dimer are decomposed to only form hydrated proton. For n-propanol and n-butanol an increase in H_3O^+ ion intensity, followed by a decrease was observed between 60 Td and 110 Td dispersion field strengths. Figure 3.27 shows a normalised intensity of the H_3O^+ ion at 80 °C for ethanol (together with blank) and at 70 °C for n-propanol and n-butanol (together with blanks). Note that for n-butanol the rise is small due to low level (0.001 mg.m⁻³) of vapours and therefore high level of background H_3O^+ ions. Nevertheless the rise is observed.

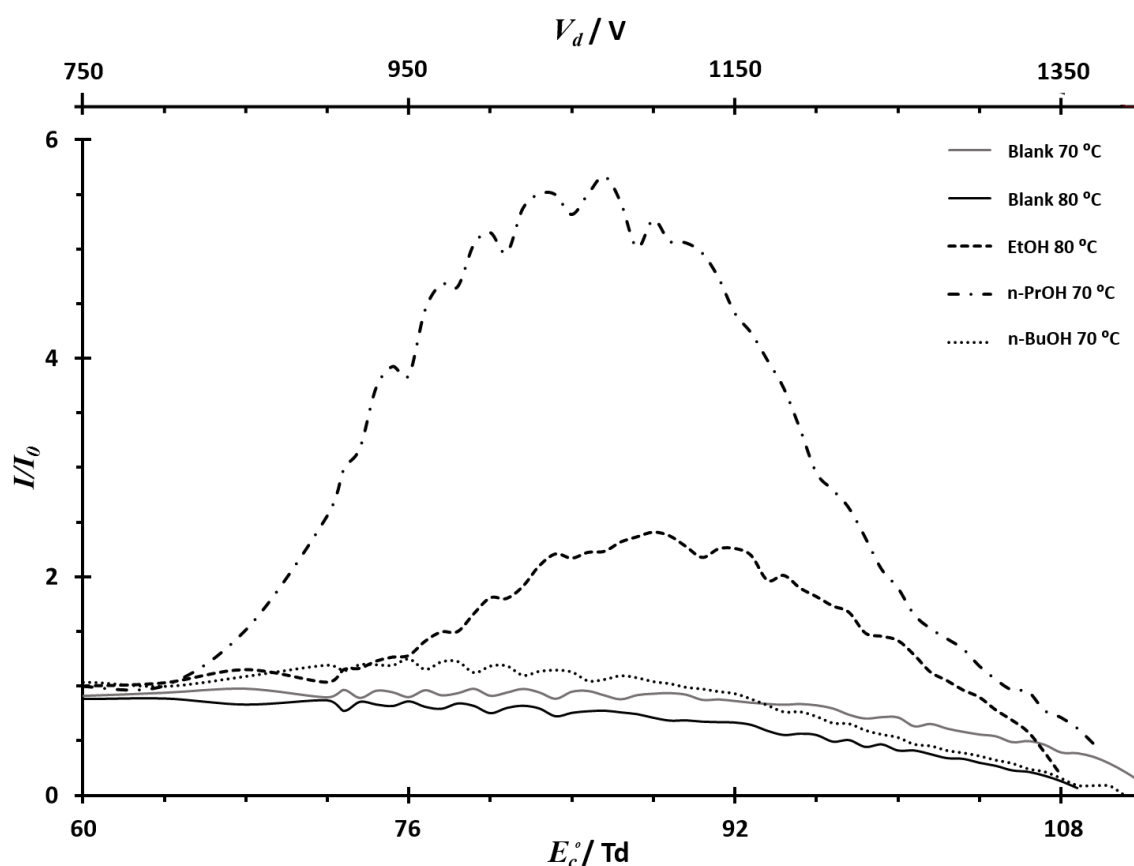
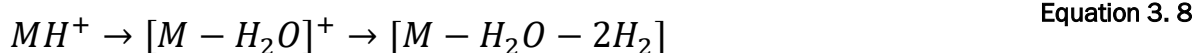


Figure 3. 27 Normalised Intensity (I/I_0) of H_3O^+ signal extracted from dispersion plots of ethanol and blank at 80 °C and n-propanol and n-butanol and blank at 70 °C, showing regeneration of the hydrated proton (H_3O^+).

For both, n-propanol and n-butanol, the ions associated with m/z of protonated alkenes (43 and 57, respectively) were also observed. For n-butanol the formation of this ion was directly associated with decomposition of the protonated monomer (which at 70 °C was completely decomposed at 68 Td or 850 V_d V). In these studies it became apparent that as the temperature was increased the dispersion field required for decomposition of the protonated monomer and proton bound dimer and in consequence for the formation of the fragment/dissociation product (Figure 3.28, ion m/z=57) decreased. For n-propanol the ion associated with a protonated alkene was only seen at lower dispersion fields and only at higher temperatures. The reason for this maybe that the ion trajectory on the compensation field scale was not resolved from the hydrated proton peak, which dominated the spectrum. Only at higher temperatures was it possible to distinguish these features from each other. Nevertheless, the ion associated with 43 m/z was not present at dispersion fields above 90 Td or 1120 V_d V.

Dehydrogenation pathways also seems apparent for both n-propanol and n-butanol, see Equation 3.8. The ion was only seen at high fields above 110 Td or 1370 V_d V and only at elevated temperatures, 130 °C for n-propanol and 100 °C for n-butanol.



Another fragmentation pathway was observed for n-propanol, where a fragment/dissociation product (m/z = 59) dominated the spectrum between 90 Td and 120 Td (1120 to 1500 V_d V), and was affected by ion-filter temperature. The formation of the ion was associated with the decomposition of the dimer ion also affected by a combination of dispersion field and ion-filter temperature (Equation 3.4).

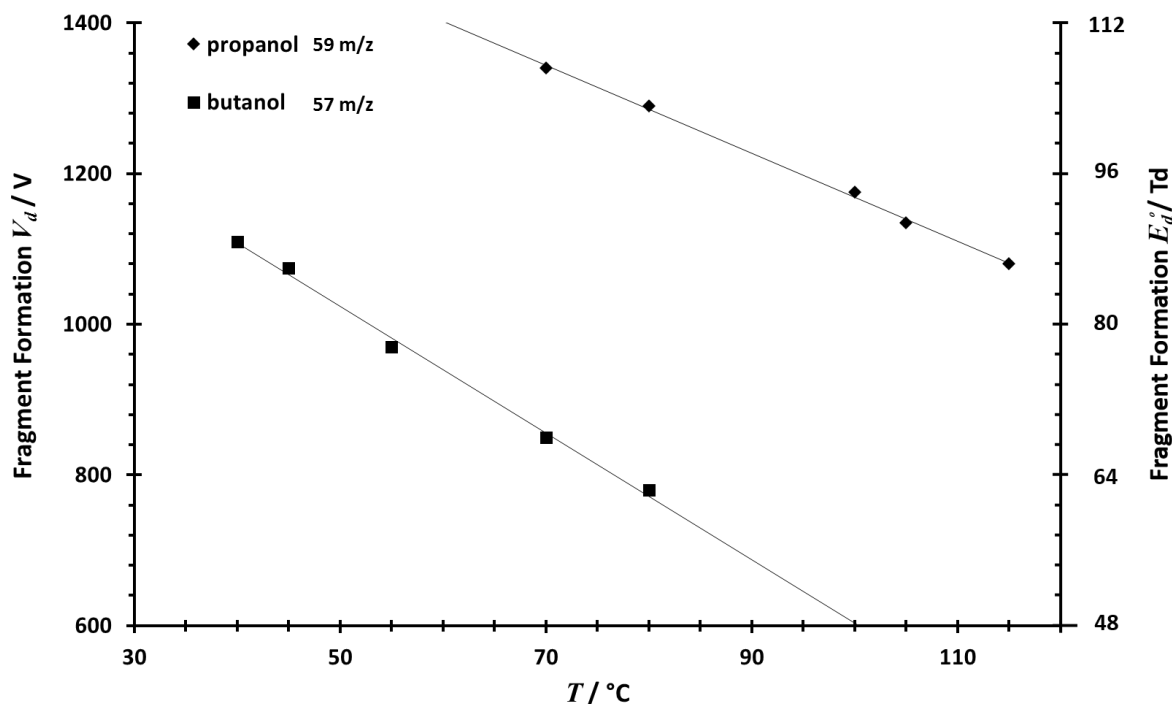


Figure 3.28 Relationship between the minimum dispersion field required to form fragment ions observed for n-propanol ($m/z = 59$) and n-butanol ($m/z = 57$) and the temperature of the d-IMS ion-filter.

The pathways shown in Equations 3.6 and 3.8 were reported for alcohols and are in agreement with studies by PTR-MS [144]. However, differences in kinetics and ratios are apparent. Formation of a hydrated proton, Equation 3.6, has only been reported previously for ethanol. Formation of an ion with $m/z = 59$ has been reported for 2-propanol but not for n-propanol, as in this study.

In general an ion-solvation equilibrium model does not predict ions detected in d-IMS for alcohols. The reason is that fragmentation/dissociation process occur at elevated effective temperatures for the ions. Further the model does not include the formation of mixed clusters (hydrated clusters) and this may explain some differences in ion abundances (predicted vs experimental) in case of methanol, where fragmentation was not observed. Nevertheless, the model was useful in identifying and characterising unexpected phenomena within the experiment.

3.5 Conclusions

The experiments in this study isolated dissociation/fragmentation product ions that have not been previously described.

Whenever a d-IMS measurement with alcohols is above 40°C and fields above 80 Td , dehydration reactions are possible and will be controlled by T_{eff} which is determined by the combination of the experimental parameters of ion-filter temperature and dispersion field (E_d/N). The onset of changes in the spectral patterns at characteristic temperatures and dispersion field values varies with carbon number for all alcohols except methanol, which undergoes no fragmentation. The selection of these experimental parameters determines in large measure the resultant characteristics of the observed spectra, and the subsequent possible analytical utility of comparison of spectra between d-IMS platforms and laboratories.

Over a relatively narrow range of temperature and vapour concentration, ion peaks undergo a slide in compensation voltage maxima values, and this cannot be attributed to alpha function modification. Rather, the ion is being transformed during residence in the d-IMS analyser. Applications for measuring alcohols with d-IMS should account for these behaviours. Future developments of d-IMS, should address these factors by designing the ionisation inlet to ensure ions pass into the d-IMS in filter in purified gases and unreacted sample or matrix neutrals are vented.

The model on ion-solvation equilibrium, is not useful in predicting distribution of ions for n-alcohols in d-IMS.

Chapter 4 Recovery and Detection of Alcohols and Toxic Substances from Human Saliva

4.1 Study Overview and Objectives

Analysis of alcohols for medical application is an on-going research interest [169]. In emergency medicine where toxicity screening is indicated the time to reliable detection can save lives, especially when symptoms may obscure the underlying problem, such as in cases of methanol poisoning when the patient appears to be intoxicated with ethanol. This study sought to develop an approach for separating, extracting and detecting toxic alcohols, diols and γ -hydroxybutyric acid from samples of human saliva using a polydimethylsilicone (PDMS) sampler and TD-GC-d-IMS system. There were four main research objectives for this study:

- optimisation of the GC-d-IMS responses for methanol, ethanol, ethanediol, 1,3-propanediol and γ -hydroxybutyric acid;
- calibration of GC-d-IMS responses to the analytes over toxicological concentrations;
- extraction of analytes from spiked saliva samples, using a PDMS oral sampler, for detection by TD-GC-d-IMS;
- and, evaluation of the results for efficacy for rapid screening of toxic substances

4.2 Experimental

4.2.1 Chemicals

Ethanol (EtOH), methanol (MeOH), ethylene glycol (EG), propylene glycol (PG), sodium chloride (purity of these compounds $\geq 99.8\%$) and butanoic acid, 4-hydroxy-, ammonium salt (GHB) in methanol ($1 \text{ mg}\cdot\text{cm}^{-3}$) were obtained from Sigma Aldrich, see Table 4.1. The carrier gas was obtained from BOC, UK, and purified by passing through two triple-bed gas purifiers mounted in series (Thames Restek). Nitrogen was generated on site (PEAK Scientific, UK, model nk-10L-HP) and purified by passing through a charcoal adsorbent-bed gas-purifier (Varian), a moisture filter (Varian), and a triple-bed gas purifier (Thames Restek), all mounted in series. Water ($>18\text{M}\Omega$) was generated on site.

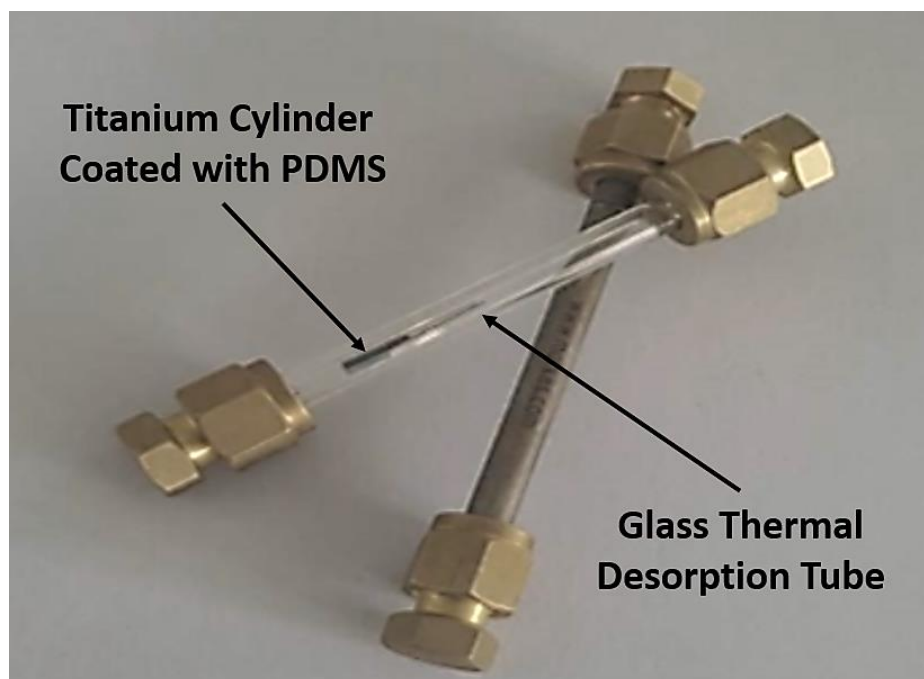
Table 4. 1 Summary of chemicals used in the experimental procedure, where *IE*: ionization energy, *PA*: proton affinity, *T_{Bp}*: boiling point.

Compound	<i>IE</i> / eV	<i>PA</i> / kJ.mol ⁻¹	<i>T_{Bp}</i> / °C	CAS	Formula
Methanol	10.84	754.3	64.7	67-56-1	CH ₃ OH
Ethanol	10.48	776	72.6	64-17-5	C ₂ H ₅ OH
Ethylene glycol	10.55	815	197.3	107-21-1	C ₂ H ₆ O ₂
Propylene glycol	10.80	876.2	182.2	57-55-6	C ₃ H ₈ O ₂
⁽¹⁾ GHB	n.f.	n.f.	295.6	591-81-1	{C ₄ H ₇ O ₃ }-{NH ₄ } ⁺

⁽¹⁾ Obtained as a methanolic solution of concentration 1 mg.cm⁻³ in Methanol.

4.2.2 PDMS sampler

A titanium cylinder (6 mm long, 2 mm o.d. C-SPTD5-6MM Markes International Ltd) coated on the internal and external surfaces with polydimethylsiloxane (internal wall thickness 1 µm and external wall thickness 0.5 mm) was used to recover VOCs from the saliva. This approach has been described previously for the in-vivo sampling of Saliva VOCs [170]. The saliva sampler was prepared by cleaning with Milton® sterilising liquid (Suffolk, UK) and then rinsing with deionised water before conditioning under vacuum at 190 °C for 15 hr. Once conditioned the PDMS rods were inserted into a cleaned and conditioned glass thermal desorption tube (Picture 4.1) and thermally desorbed for 10 min at 190 °C; the resultant GC-MS trace provided verification that the PDMS sampling media was free of contamination. On removal from the thermal desorption unit the thermal desorption tube containing the PDMS coated titanium cylinder was immediately capped, sealed and stored at 4 °C. Before use the saliva-samplers were thermally desorbed again under the conditions in Table 4.5 to remove any traces of possible VOC contamination that may have occurred during storage and to provide further verification that the sampler was free of contamination.



Picture 4. 1 PDMS d-IMS rod inserted into a glass thermal desorption tube.

4.2.3 Ethics, participant preparation and saliva sampling.

The study was conducted in accordance with the ethical principles of Good Clinical Practice and the Declaration of Helsinki. The local ethics committee (Ethical Advisory Committee, Loughborough University, Loughborough, LE11 2DT) approved the studies (References G10-P23 and G10-P24) The participants were healthy adult volunteers who gave written informed consent. Participants were recruited from Loughborough University staff, students and their social networks.

On the morning of their study visit participants were asked not to: brush their teeth; use any personal care products, or eat breakfast. Participants were also asked to only drink cold water, and refrain from flavoured or caffeinated drinks, or drinks containing fruit juice(s). All saliva samples were taken in an in-vivo sample station located in a small internal room, where privacy was ensured, at the Centre for Analytical Science at the Chemistry Department of Loughborough University. A chaperone, of the same gender as the participant, was present during sample collection and access was restricted to only those researchers and participants involved in the sampling process. After an introduction to the study the participants were familiarised with the passive drool approach that was used to obtain a sample of their saliva, before proceeding to provide approximately 15 cm³ of saliva. The participants sat with their head tilted forward to

cause saliva to pool at the front of their mouth and then drain from their lips into a glass collection vial. On completion of sampling, the vial was sealed promptly with a Teflon faced screw-top cap and immediately transferred to a laboratory where 1.8 cm³ of the saliva sample was pipetted into to a 2 cm³ chromatography vial, and sealed immediately with a screw cap fitted with a silicone septum. This aliquot of saliva was used within 3 hr of collection. Saliva residues were disposed by diluting with a disinfectant solution and rinsed down a sink with a copious flow of running water. No cells or DNA were retained or stored.

4.2.4 Methods

Three instrument configurations were used in this study. For optimisation purposes the exponential dilution approach was used (Section 2.5.2 and 2.6). Method development and calibration were undertaken using liquid injections to a GC-d-IMS, see Section 2.5.4. Characterisation of the recovery of the analytes from spiked saliva samples was undertaken using a thermal desorption unit interfaced to the GC-d-IMS, see Section 2.5.5.

4.2.4.1 Optimisation of d-IMS responses

Multi-linear regression modelling was used to optimise the: dispersion-field; temperature; number of compensation-field steps; and compensation-field step duration (DOE PRO XL Software for Microsoft Excel, SigmaZone). The experimental design was generated using a central composite design (CCD) [171] for four factors at four levels, resulting in 26 separate d-IMS experiments (Table 4.2). The data was collected with replicates at five different concentrations. The d-IMS parameters were optimised for maximum sensitivity while maintaining “satisfactory” resolution ($R \geq 1$) between the ion clusters generated within the ⁶³Ni ionisation source. Final conditions, used for the studies are shown in Table 4.3. The heating and cooling rates of the d-IMS filter were too slow to enable multiple ion filter temperatures to be selected within a single chromatographic run. Further, switching the number of steps and step duration in the d-IMS spectra during a chromatographic run was not possible. Consequently mid-range levels were used.

Table 4. 2 Four factorial design with levels selected for response d-IMS optimisation study.

Ref	V_d / V	$T / ^\circ\text{C}$	N	δ / ms	Ref	V_d / V	$T / ^\circ\text{C}$	N	δ / ms
1	800	80	50	10	14	1250	120	50	50
2	800	80	50	50	15	1250	120	100	10
3	800	80	100	10	16	1250	120	100	50
4	800	80	100	50	17	1000	100	75	30
5	800	120	50	10	18	1000	100	75	30
6	800	120	50	50	19	800	100	75	30
7	800	120	100	10	20	1250	100	75	30
8	800	120	100	50	21	1000	80	75	30
9	1250	80	50	10	22	1000	120	75	30
10	1250	80	50	50	23	1000	100	50	30
11	1250	80	100	10	24	1000	100	100	30
12	1250	80	100	50	25	1000	100	75	10
13	1250	120	50	10	26	1000	100	75	50

Table 4. 3 Operational parameters selected (predicted from multiple linear regression).

Compound	$E_d / T_d \text{ or } V_d / V$	$T / ^\circ\text{C}$	N	$\Delta t / \text{ms}$
Methanol	100 or 1250	100 (108)	110 (60)	10 (48)
Ethanol	72 or 900	100 (80)	110 (60)	10 (50)
Ethylene glycol	92 or 1150	100 (100)	110 (75)	10 (10)
Propylene glycol	92 or 1150	100 (120)	110 (75)	10 (30)
GHB	84 or 1050	100	110	10

4.2.4.2 Calibration of d-IMS responses

Calibration of the d-IMS responses under optimised conditions was undertaken using gas chromatography to introduce defined masses and concentrations of the analytes to the d-IMS. This was done through the manual injection of standard dichloromethane (DCM) solutions.

A schematic diagram of the set-up is shown in Section 2.5.4. Summary of the concentrations used in the study and their calculated on column masses are shown in Table 4.4. Full experimental parameters are given in Table 4.5

Table 4. 4 Summary of the concentration ranges selected for the calibration of the spiked saliva standards $[i]_{(\text{liq})}$ and their on column masses M_{col} used to characterise the recovery of the analytes from by TD-GC-d-IMS.

Compound	$[i]_{(\text{liq})} / \text{mg} \cdot \text{dm}^{-3}$	$M_{\text{col}} / \text{ng}$
Methanol	10 to 500	0.2 to 10
Ethanol	250 to 2000	5 to 40
Ethylene glycol	100 to 3400	2.5 to 85
Propylene glycol	100 to 3000	2.6 to 80
GHB	20 to 500	0.6 To 12.9

4.2.4.3 *Characterisation of spiked saliva samples*

Instrumental parameters used in the studies are summarised in Table 4.5 and a system description can be found in Section 2.5.5. A 100 mg.cm^{-3} aqueous stock solution of ethanol, methanol, ethylene glycol, and 1,3-propandiol was prepared and aliquots of the volumes required to generate the required concentrations were spiked and mixed into the saliva samples within three hours of the saliva being collected. To account for the lower concentration of the GHB standard, and to maintain a constant saliva background a different approach was adopted for the GHB characterisation experiments. This was due to the compound being supplied, as a salt solution in MeOH. Here 0.9 cm^3 of the saliva was used, and spiked with the required aliquot volume of the 1 mg.cm^{-3} GHB methanolic solution, before the volume was made up to 1.8 cm^3 with physiological saline ($\text{NaCl}_{(\text{aq})} 8.5 \text{ g.dm}^{-3}$). The ammonia present in the saliva and the GHB salt co-eluted with methanol and suppressed the formation of methanolic product ions (Ammonia has a higher proton affinity than methanol). This interference was eliminated by the addition of $150 \text{ }\mu\text{l}$ of 8 % HCL solution into the saliva samples before the sampling rod was placed into the vial. Figure 4.1 shows d-IMS responses from saliva before and after acidification of the sample containing 500 mg.dm^{-3} of methanol.

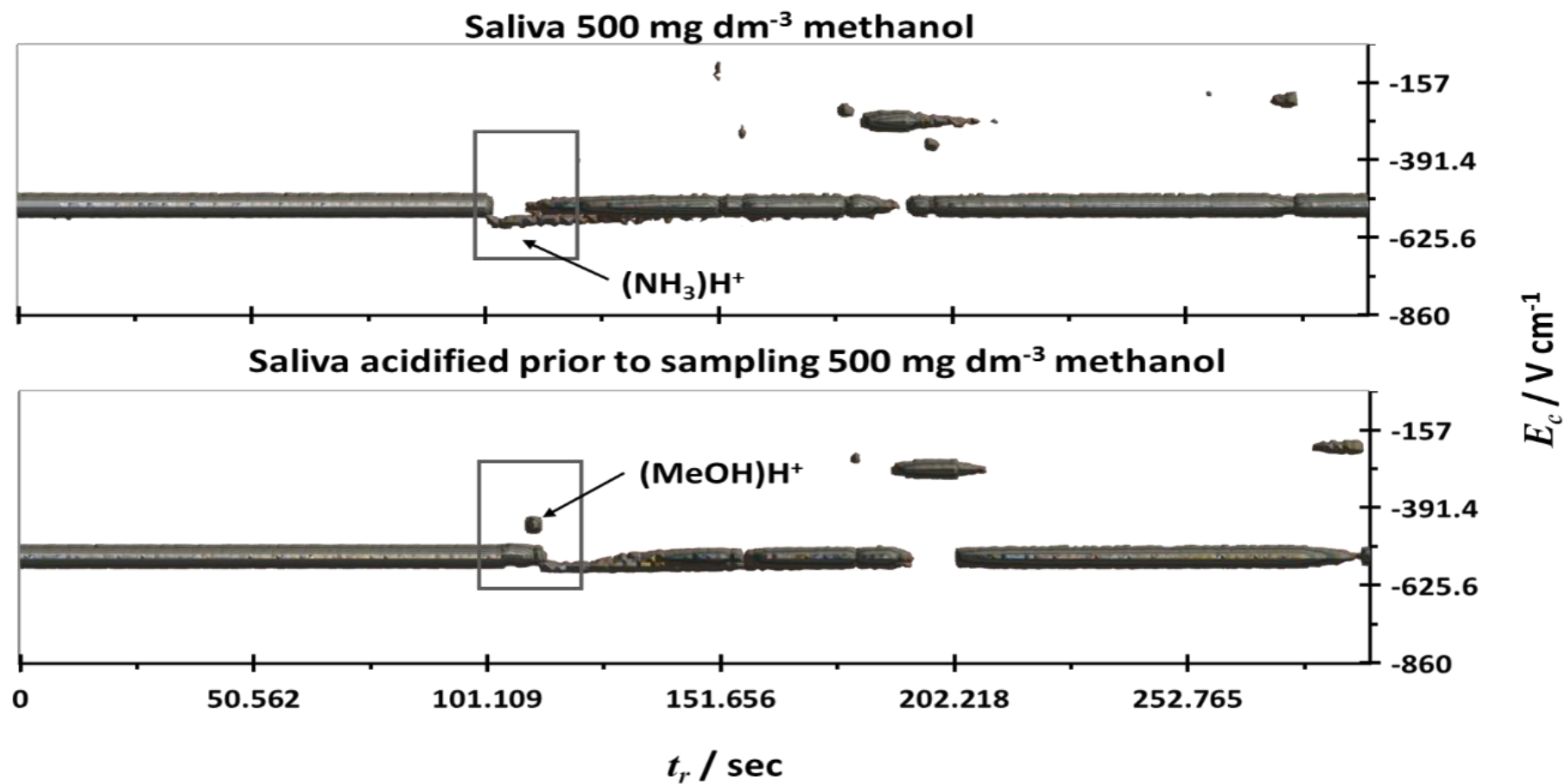
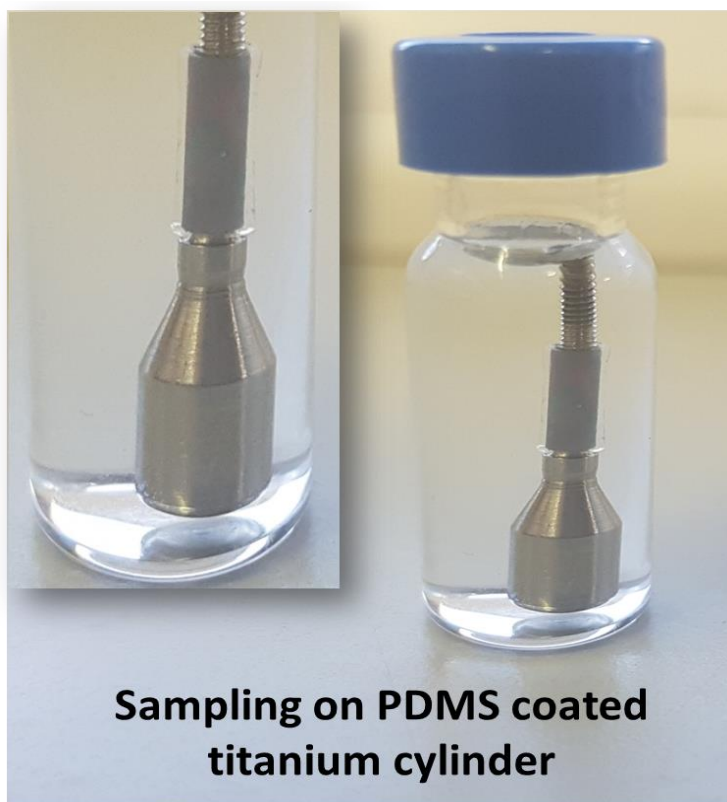


Figure 4. 1 D-IMS responses from 500 mg.dm⁻³ methanol in saliva (top) and acidified saliva (bottom).

As soon as the saliva standard had been prepared a PDMS coated titanium cartridge was removed from its sealed thermal desorption tube and placed into the vial, using the sampler holder (Picture 4.2). This enabled reproducible insertion and removal of the sampler, and prevented the accumulation of saliva inside of the titanium cartridge. As soon as the sampler had been placed into the vial the vial was sealed immediately. It was important that this procedure was undertaken in a fast and reproducible manner to minimise the effects of evaporative losses in the study.

The sealed vial was then placed into a heating-block, maintained at 37 °C, for 10 min. At the end of the extraction-time the vial was uncapped and the PDMS coated titanium tube was removed with stainless steel tweezers and excess fluid removed by gently wiping it with a lint-free wipe ('Kimcare' Kimberly-Clark Professional, UK). The PDMS coated titanium tube was then placed immediately into a glass thermal desorption tube and analysed. Cross-contamination checks were run by taking blank runs between every measurement. The reproducibility of the method was tested using an ethanol standard at 250 mg.dm⁻³ 5 times. The RSD for the method was estimated to be 8.3 %.



Picture 4. 2 Photograph of a PDMS coated titanium tube fitted to its holder in a sampling vial. Insert shows close up detail.

Table 4. 5 Instrument parameters used for d-IMS calibration and saliva analysis.

Parameter	GC-d-IMS	TD-GC-d-IMS	Units
Gas chromatograph conditions			
Carrier gas	He	He	
Injection temperature	200		°C
Injection volume	0.2		
Split flow	10.2	see below	cm ³ .min ⁻¹
Carrier gas flow	1.5	1.5	cm ³ .min ⁻¹
Carrier gas pressure	172	172	kPa
Phase	Trifluoropropylmethylpolysiloxane		
Column length	30	30	m
Column diameter	0.32	0.32	mm
Phase thickness	0.5	0.5	µm
Temperature start	30	30	°C
Hold-time start	1.5	1.5	min
Temperature ramp-1	6	6	°C. min ⁻¹
End temperature-1	60	60	°C
Hold-time-1	2	2	min
Temperature ramp-2	20	20	°C. min ⁻¹
Temperature final	180	180	°C
Hold time final	2	10	min
Differential mobility spectrometry			
Transport gas	N ₂	N ₂	
Dispersion field frequency	1.2	1.2	MHz
Dispersion field mark space ratio	1:3	1:3	
Humidity of the transport gas	22.5 to 26.3	22.5 to 26.3	mg.m ³
Transport gas flow rate	300	300	cm ³ .min ⁻¹
d-IMS ion filter temperature	100	100	°C
Compensation field scan range	-500 to 100 / -2.45 to 0.43	-500 to 100 / -2.45 to 0.43	V.cm ⁻¹ / Td
Compensation field scan increment	109.1	109.1	V.cm ⁻¹
Compensation field scan dwell-time	10	10	ms
Dispersion field/voltage start (MeOH)	100/1250	25/100	Td/ V
Dispersion field start hold time (MeOH)	0 to 125	0 to 125	S
Dispersion field/voltage step-1 (EtOH)	72/900	18/72	Td/ V
Dispersion field step-1 hold time (EtOH)	125 to 185	125 to 185	S
Dispersion field/voltage step-2 (EG, PG)	92/1150	23/92	Td / V
Dispersion field step-2 hold time (EG, PG)	185 to 600	185 to 600	min
Dispersion field/voltage start (GHB)	84/1050	21/84	Td / V
Thermal Desorption			
Tube purge duration		1	min
Tube purge flow		32	cm ³ .min ⁻¹
Tube purge temperature		35	°C
Primary desorption temperature		180	°C
Primary desorption Split		0	cm ³ .min ⁻¹
Primary desorption time		5	min
Cold trap low temperature		0	°C
Secondary desorption temperature		300	°C
Secondary desorption Split		12	cm ³ .min ⁻¹
Secondary desorption time		5	Min

4.2.5 Data analysis

The experimental data (r), was exported into a spreadsheet (Microsoft Excel) arranged by signal against compensation voltage V_c / V and retention time t_r / s (scans). 140 V_c steps were obtained for each scan. An extract of a small part of the raw data is shown in Figure 4.2, where signal I (orange) is shown against V_c (green) and t_r (violet).

	A	B	C	D	E	F	G	H	I
1									
2	V_c	-43	-42.41	-41.83	-41.24	-40.66	-40.07	-39.48	-38.9
3	ret time								
4	0	0.1098	0.1127	0.1118	0.1127	0.1119	0.1131	0.1116	0.1114
5	1.016	0.1124	0.1121	0.1102	0.1117	0.1121	0.1132	0.1128	0.1136
6	2.016	0.1109	0.1129	0.1127	0.1117	0.112	0.1128	0.1112	0.1109
7	3.031	0.1125	0.112	0.1121	0.1117	0.1139	0.1126	0.1114	0.1106
8	4.047	0.1125	0.111	0.1121	0.1136	0.112	0.1125	0.1135	0.1122
9	5.063	0.1128	0.1118	0.1093	0.1112	0.1128	0.1117	0.1124	0.112
10	6.063	0.1101	0.1133	0.1131	0.1124	0.1087	0.112	0.1096	0.1124

Figure 4.2 An extract of raw d-IMS data, obtained from the studies on alcohol responses using GC-d-IMS and TD-GC-d-IMS systems.

The surface plots of the d-IMS responses were produced by de-noising, zeroing and filtering the raw data. Further subtraction of the reactant ion peak (RIP) signal, enabled integration of the product ion signals against retention time and/or compensation voltage. Chromatograms were created from the processed data (R_n). Steps of the data processing are summarised in the flowchart below (Figure 4.3) alongside with some graphical representation of the processing steps.

It is important to note that data recording was started manually after injection or thermal desorption, causing slight differences in retention times between runs, so the data were aligned to eliminate this effect. Values of dispersion and compensation fields were additionally converted into values of reduced electric field in Td, within the narrative.

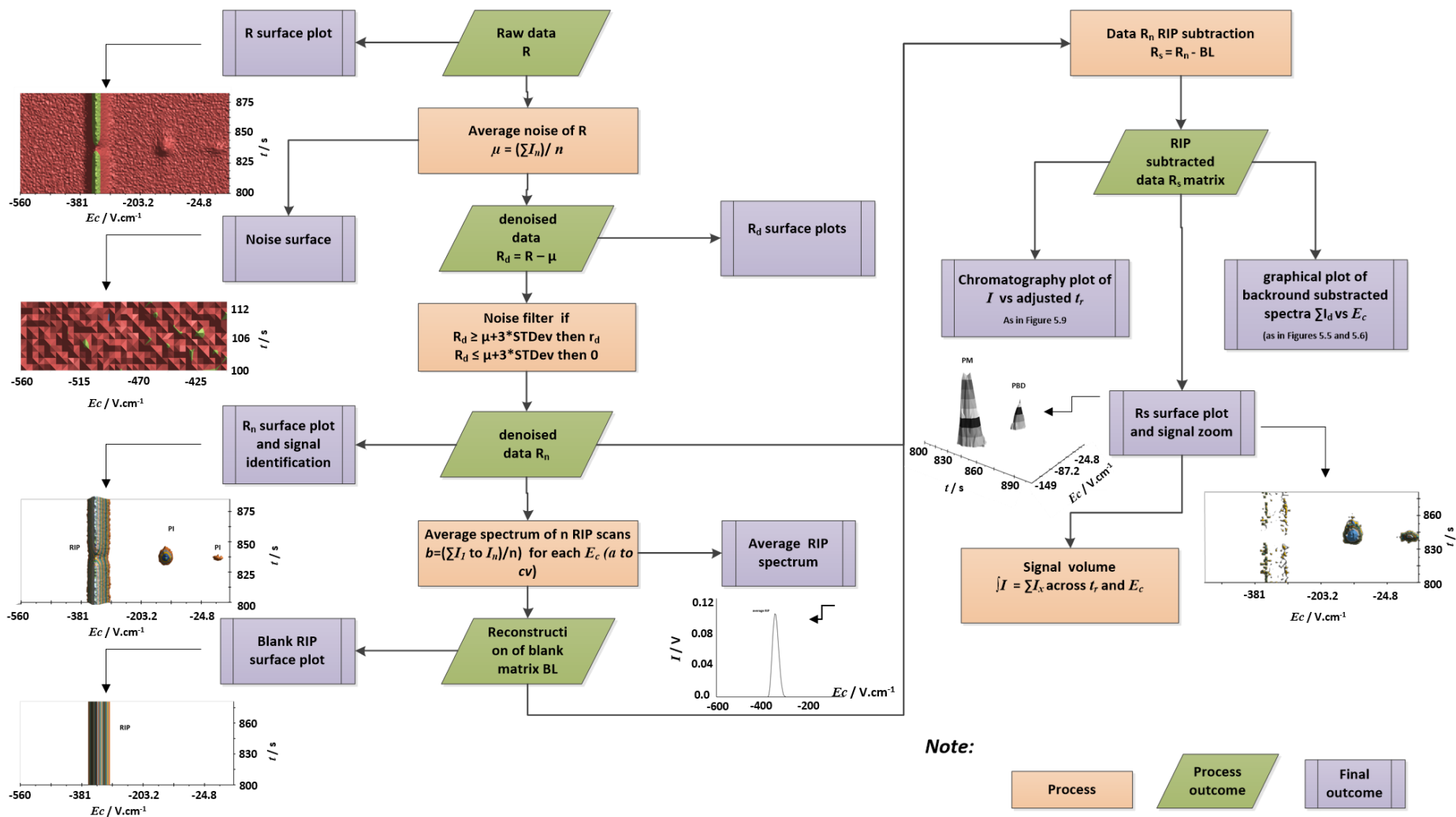


Figure 4.3 Flowchart presenting steps taken during data processing of the d-IMS data, obtained from the studies on alcohol responses using GC-d-IMS and TD-GC-d-IMS.

Further, calibration graphs were produced and linear regression analysis were performed using equations shown in Table 4.6.

Table 4. 6 Parameters obtained from linear regression analysis together with used Equations.

Symbol	Parameter	Formula
B_1	Slope	$B_1 = \frac{n\sum(xy) - \sum x\sum y}{n\sum x^2 - (\sum x)^2}$
B_0	y-intercept	$B_0 = \frac{\sum y - B_1\sum x}{n}$
$R^2_{(y/x)}$	Correlation coefficient	$R^2 = \left(\frac{n\sum(xy) - \sum x\sum y}{\sqrt{[n\sum x^2 - (\sum x)^2][n\sum y^2 - (\sum y)^2]}} \right)^2$
$S_{(y/x)}$	Standard error of predicted y	$S_{y/x} = \sqrt{\frac{1}{n-2} \left[\sum (y - \bar{y})^2 - \frac{[\sum (x - \bar{x})(y - \bar{y})]^2}{\sum (x - \bar{x})^2} \right]}$
Δy	Delta y for 95% confidence interval	$\Delta y = \frac{t * S_{(y/x)}}{n}$
\hat{y}	Predicted y	$\hat{y} = B_0 + B_1x$
$y_{95\%}$	Y with 95% confidence interval	$y_{95\%} = y \pm \Delta y$

4.3 Results

4.3.1 Signal identification and calibration of the d-IMS responses

Figure 4.4 shows contour plots of GC-d-IMS responses for methanol (A), ethanol (B), ethylene glycol (C), 1,3-propandiol (D) and GHB (E) at three levels of column-loading covering the ranges of analyte concentrations associated with the physiological thresholds of these compounds. The five dispersion-field levels used (Table 4.3) enabled analytical responses to be resolved.

Note: The final contour plot, shown in the Figure 4.4 was combined from two separate runs, where compounds A to D were run as a mixture and GHB was run separately; the compound was supplied as a solution in methanol, so could not be included with methanol as a mixture.

Figure 4.5 shows background subtracted differential mobility spectra obtained from the responses shown in Figure 4.4 for methanol (A), ethanol (B) and ethylene glycol (C), while Figure 4.6 compares the background subtracted spectra for 1,3-propanediol (D) and GHB (E). The dotted lines in these figures indicate the boundary of the reactant ion peak that was removed by the background subtraction in the data processing. The observed responses were complicated with shifts in compensation-field maxima with increasing concentration, and the generation of features embedded within the reactant ion peak that were only discernible after background subtraction. Such phenomena were indicative of the formation of fragment ions and, or, “auto-modification” of the alpha functions of the product ion.

With a dispersion-field of 100 Td ($1250 V_d V$) and a column-loading of 10.2 ng, methanol yielded a single peak attributed to a hydrated protonated monomer ion at a compensation-field of -1.78 Td ($-444 V.cm^{-1}$), that was partially obscured within the reactant ion peak (Figure 4.4 A and 4.5 A). Reducing the column-loading to 2.0 ng resulted in a compensation-field shift for the hydrated protonated monomer cluster ion to -1.77 Td ($-439.6 V.cm^{-1}$). At a lower limit of a 0.20 ng column-loading, only one peak was observed at -1.77 Td ($-439.6 V.cm^{-1}$). These observations are consistent with d-IMS responses obtained during exponential washout experiment (Section 3.4.2). The concentration of methanol vapours reaching d-IMS was estimated using column loading, flows and retention time for the peak elution, which at the maximum of the peak was estimated to be: $18 \mu g.m^{-3}$, $180 \mu g.m^{-3}$ and $918 \mu g.m^{-3}$ at 0.2 ng, 2 ng and 10.2 ng column loading, respectively.

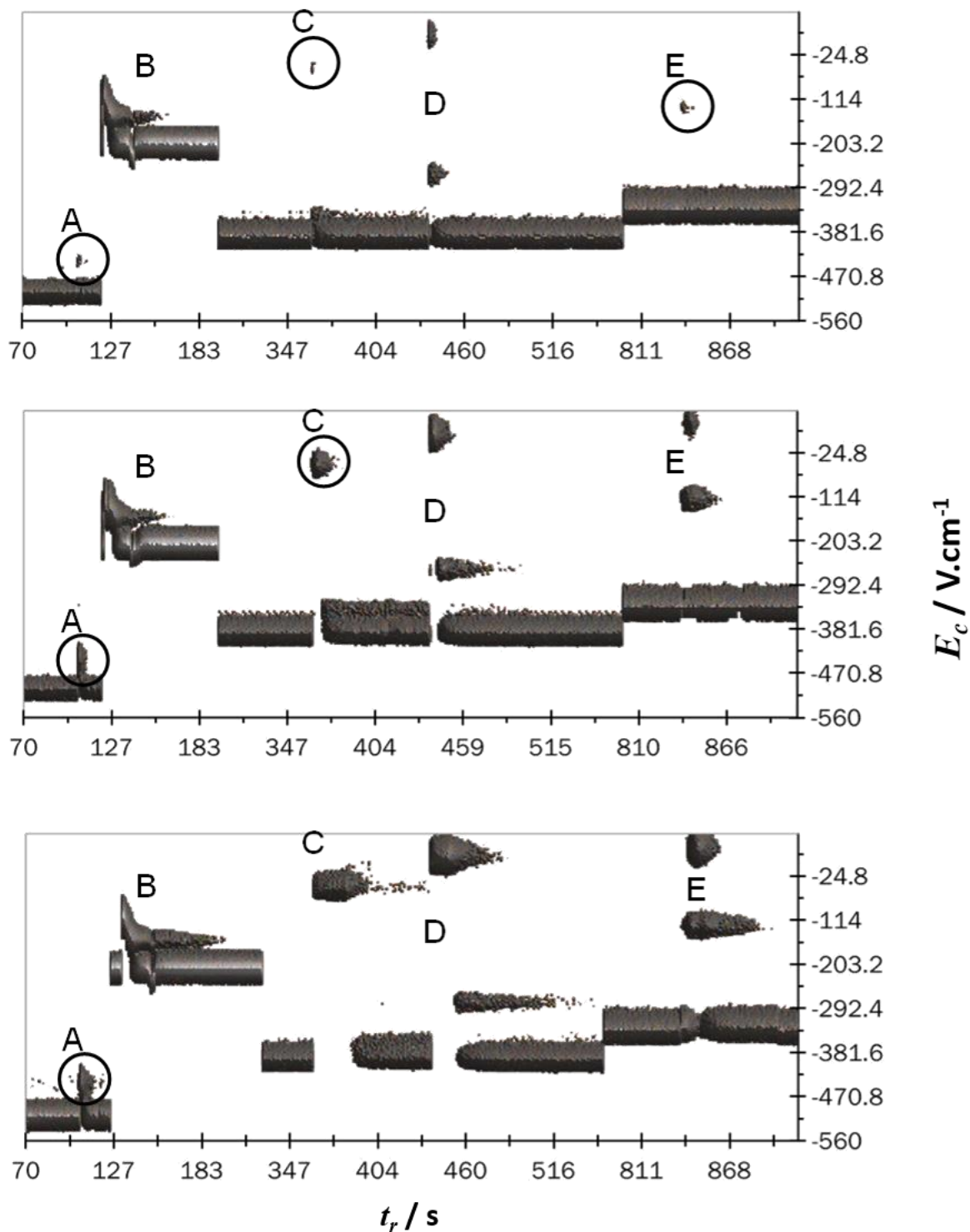


Figure 4. 4 GC-d-IMS response surfaces from methanol (A), ethanol (B), ethylene glycol (C), propylene glycol (D) and GHB (E) under optimized conditions at representative sample masses. Note the shifting position of the reactant ion peak as the dispersion field was switched. Top: responses produced from 200 pg , 5.1 ng, 2.9 ng, 2.7 ng and 510 pg of methanol, ethanol, ethylene glycol, propylene glycol and GHB respectively. Similarly the middle surface shows responses for 2.0 ng, 15.3 ng, 14.3 ng, 13.4 ng and 1.9 ng, while the bottom trace shows responses for 10.2 ng, 40.7 ng , 81 ng, 80.4 ng, 12.9 ng. Graph adapted from Ruszkiewicz et. al [169] with permission of Royal Society of Chemistry.

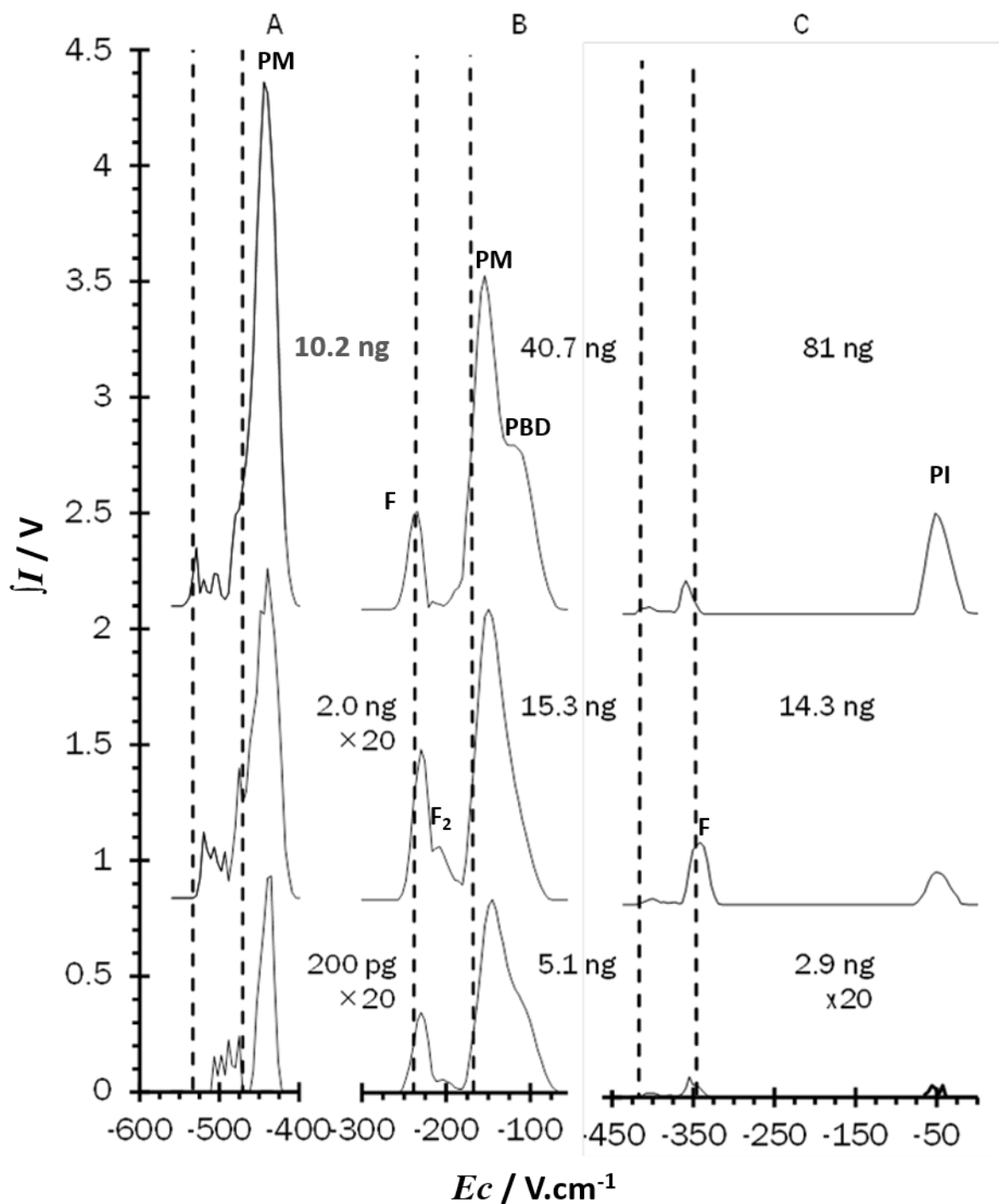


Figure 4.5 Background subtracted differential mobility spectra extracted from the GC-d-IMS response surface shown in Figure 4.4 for methanol (A), ethanol (B), and ethylene glycol under optimized conditions at representative sample masses. The dotted lines indicate the position of the reactant ion peak in the spectrum (hydrated proton clusters). Note: PM – protonated monomer, PBD – proton bound dimer, F and F₁ – fragment ions. Figure adapted from Ruszkiewicz et. al [166].

At a dispersion-field of 72 Td ($900 V_d$ V) ethanol (Figures 4.4 B and 4.5 B) yielded a complicated response with features consistent with the fragmentation described in Section 3.4.3. The responses of product ions were not fully resolved from the H_3O^+ ion which overlaid an unresolved protonated monomer and proton-bound dimer observed at E_c values of approximately -0.96 Td, -0.62 Td, -0.5 Td ($-235 V.cm^{-1}$, $-154.2 V.cm^{-1}$ and $-122.8 V.cm^{-1}$), respectively. Two other species under the RIP were also present. The higher intensity species may be attributed to regenerated hydrated proton H_3O^+ , described in Sections 3.4.3.7-8. The slight shift in the maximum of the regenerated H_3O^+ peak (of about $+10 V.cm^{-1}$) cannot be attributed to the modification of the dispersion behaviour via influencing the alpha parameter (threshold calculated to be $133 mg.m^{-3}$). It has been reported that at extremely low concentration levels (which in this case maybe the number of the fragment ions produced), can lead to erroneous assignment at the E_c scale. The estimated levels of concentrations of analyte in the d-IMS ion filter at the max of the chromatographic peak was calculated to be $183 \mu g.m^{-3}$, $550 \mu g.m^{-3}$ and $1465 \mu g.m^{-3}$ at 5.1 ng, 15.3 ng and 40.7 ng level of loading.

At a dispersion-field of 88 Td ($1100 V_d$ V), ethylene glycol (Figure 4.4 C and 4.5 C) produced a clearly resolved feature at 0.21 Td or $-51.6 V.cm^{-1}$, attributed to a proton bound dimer ion, along with two features obscured by the reactant ion peak. Knowing about the fragmentation of the alcohols in the d-IMS system it seems reasonable to propose fragmentation is likely to be present as well with this molecule. The weakest of these features, completely obscured by the reactant ion peak was observed at a compensation-field of -1.61 Td or $-403.8 V cm^{-1}$, across the range of column-loadings. The other feature, partially obscured by the reactant ion peak, was observed to shift from a compensation-field of -1.42 Td or $-359.2 V cm^{-1}$ with a column-loading of 81 ng, to -1.33 Td or $-337 V cm^{-1}$ with a column loading of 14.3 ng, which again cannot be explained by auto modification. The feature could be a product of the dehydration reaction, which under high effective temperature of the ion, can lead to hydrated proton [172]. However, at this stage there is insufficient mass spectral data to support this proposition. The lowest column loading applied generated a low intensity split product ion peak that straddled 1.33 Td or $-337.4 V cm^{-1}$. The estimated levels of maximum concentration of vapour levels reaching the d-IMS ion filter at the max of the ion peak was estimated to be 261, 515 and $1458 \mu g.m^{-3}$ at 2.9, 14.3 and 81 ng level of loading, respectively.

At the same dispersion-field (88 Td, 1100 V_d V) 1,3-propanediol yielded (Figure 4.4 D and 4.6 D) two features, both resolved from the reactant ion peak. The peak at a compensation-field of 0.07 Td or 15.4 $V.cm^{-1}$ was attributed to a proton bound dimer ion. The feature attributed to a protonated monomer was observed to shift to more negative compensation-fields with increasing column-loading. At 80 ng the peak maximum was at a compensation-field of -1.14 Td or -283.4 $V.cm^{-1}$, shifting to -1.05 Td or -261.2 $V.cm^{-1}$ when the column-loading was reduced to 2.7 ng. The estimated maximum concentration levels reaching d-IMS filter based on the peak elution time, were estimated to be: 243 $\mu g.m^{-3}$, 482 $\mu g.m^{-3}$ and 1440 $\mu g.m^{-3}$ at 2.7 ng, 13.4 ng and 80 ng level of loading, respectively.

GHB (Figure 4.5 E) also showed complex behaviour with a dispersion-field of 92 Td (1150 V_d V). In addition to well-resolved protonated monomer and proton bound dimer ions, fragment ions obscured within the RIP envelope were also evident, and the compensation-field maxima of these fragment ions shifted with increasing column-loading of GHB. The protonated monomer had a compensation field peak maximum at -0.53 Td or 131.8 $V.cm^{-1}$ and the proton bound dimer compensation-field maxima was observed at -0.3 Td or 33.2 $V.cm^{-1}$. No discernible trend in a shift in compensation-field maxima was observed with column loading for the protonated monomer ion, and the proton bound dimer was not formed at the lowest column loading of 510 pg. At a column loading of 12.9 ng two unresolved fragment ions were discernible within the RIP envelope. The most intense feature was at -310.2 $V.cm^{-1}$ or -1.24 Td with a shoulder at -296.8 $V.cm^{-1}$ or -1.19 Td. Reducing the column loading to 1.9 ng resulted in a single fragment ion with a compensation-field peak maximum at -301.2 $V.cm^{-1}$ or -1.3 Td and at a column loading of 510 pg the fragment ion was still observable with a compensation-field peak maximum of -288 $V.cm^{-1}$ or -1.24 Td. The estimated maximum concentration levels reaching d-IMS filter based on the peak elution time, were estimated to be: 46 $\mu g.m^{-3}$, 171 $\mu g.m^{-3}$ and 464 $\mu g.m^{-3}$ at 0.51 ng, 1.9 ng and 12.9 ng level of loading, respectively.

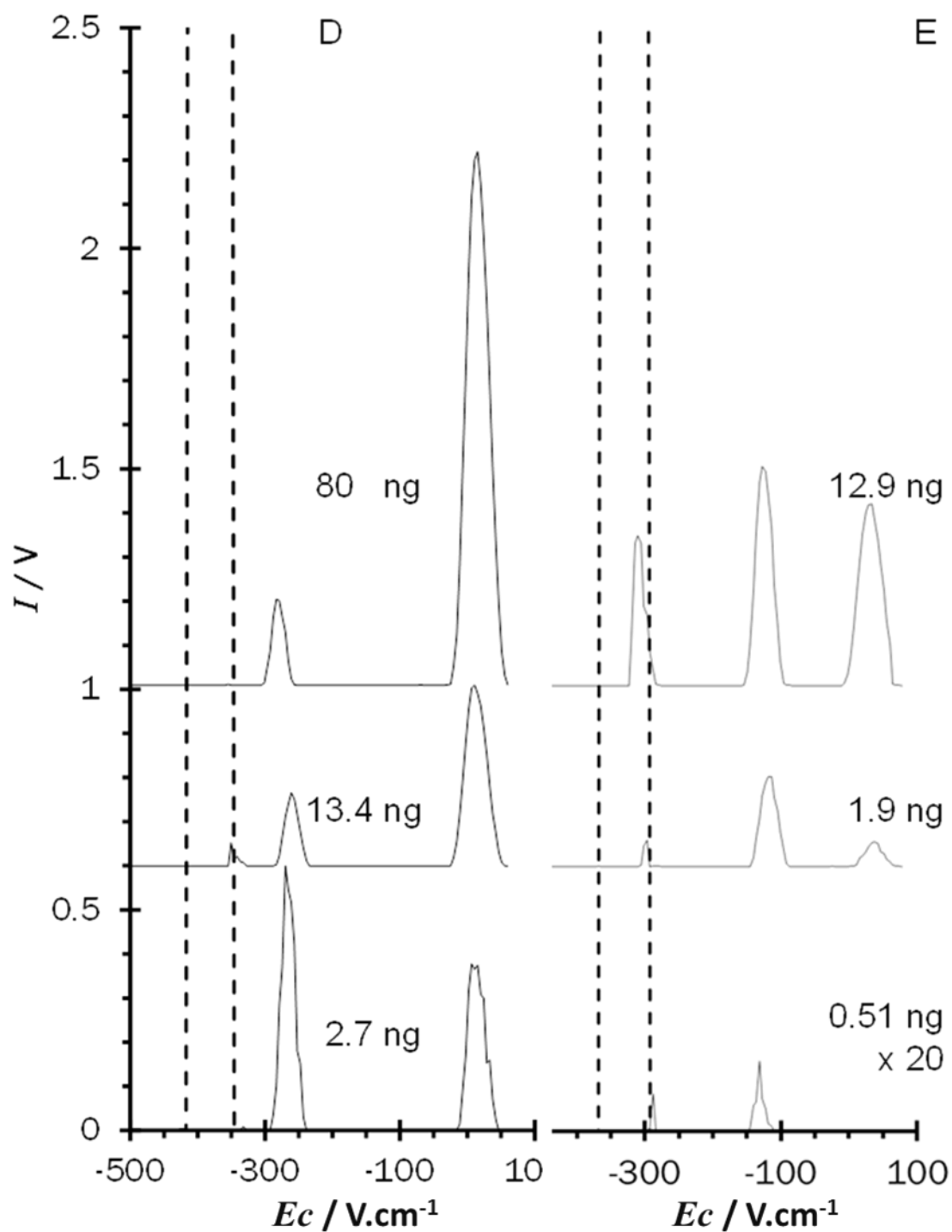


Figure 4.6 Background subtracted differential mobility spectra extracted from the GC-d-IMS response surface shown in Figure 4.4 for 1,3-propanediol (D) and GHB (E) under optimized conditions at representative sample masses. The dotted lines indicate the position of the reactant ion peak in the spectrum (hydrated proton clusters). Note: PM - protonated monomer, PBD - proton bound dimer, F - fragment. Figure adapted from Ruszkiewicz et. al [166] with permission of Royal Society of Chemistry.

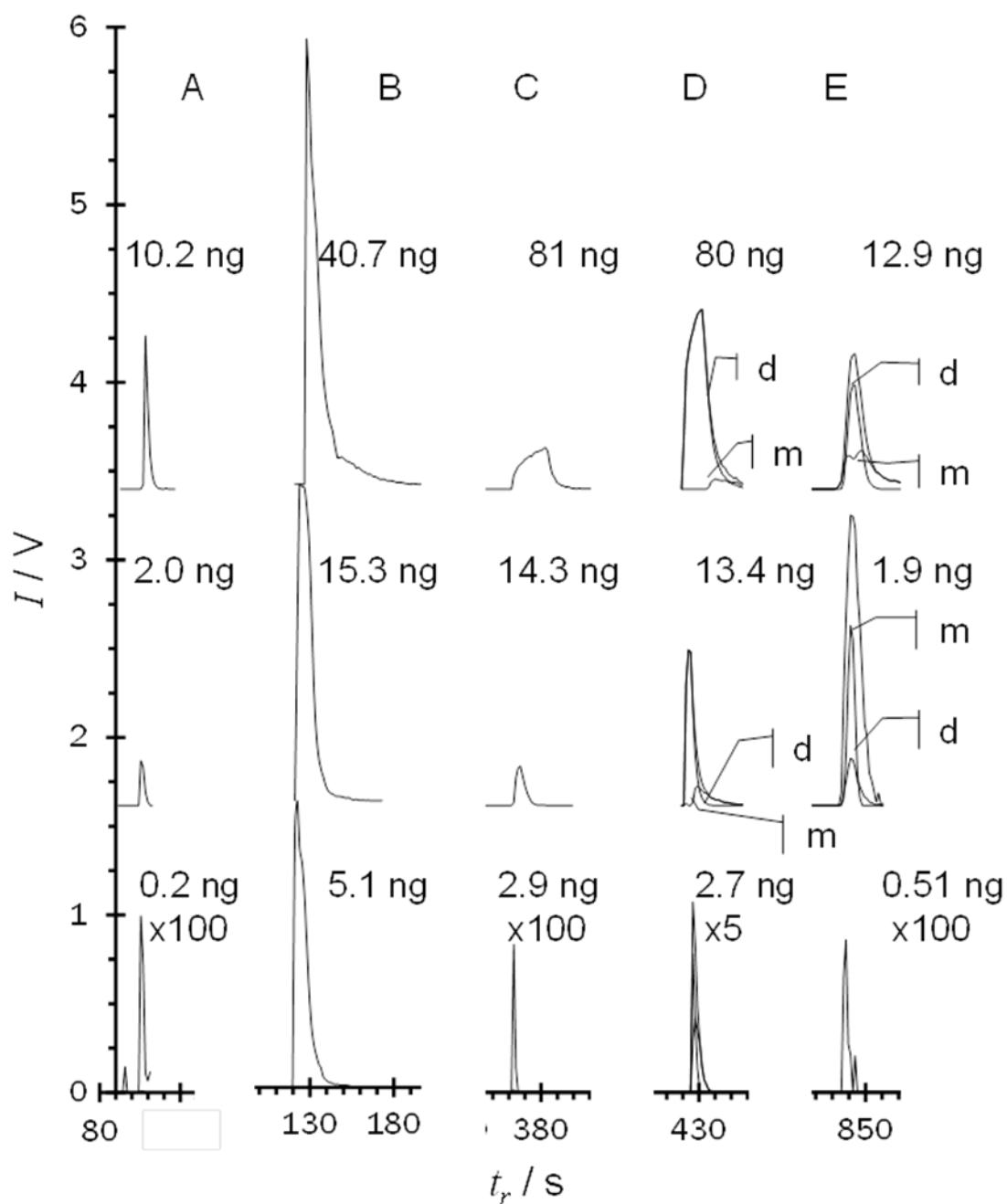


Figure 4.7 Selected differential mobility chromatography for methanol (A), ethanol (B), ethylene glycol (C), 1,3-propanediol (D) and GHB (E) under optimized conditions at representative sample masses. Protonated monomer (PM) and proton bound dimer (PBD) responses are shown for propylene glycol and GHB as well as the total ion responses, see Figure 4.6. The responses shown for methanol, ethanol and ethylene glycol are the total ion responses, see Figure 4.5.

Chromatograms generated from the response surfaces are shown in Figure 4.7. Calibration curves were produced from the integration of the proton bound dimer ion for

the two glycols and GHB. The ethanol calibration was based on the integration of the complicated feature containing unresolved protonated monomer and proton bound dimer ions while the methanol calibration peak volume was taken from the protonated monomer ion response. The integrated peak volume (I), Equation 4.1, was calibrated against the on-column mass of analyte to give linear calibrations over concentration ranges of toxicological relevance

$$I(\text{V.s}) = B_0(\text{V.s}) + B_1(\text{V.s.ng}^{-1}) \times m_i(\text{ng}) \quad \text{Equation 4. 1}$$

Table 4.7 summarises the results of the linear regression analysis, related to the linear portion of the calibration graph of the d-IMS ($[i]_{(liq)}$), used to characterise the recovery of the analytes from TD-GC-d-IMS, where the L_oD , slope (B_1) and intercept (B_0) were calculated. Limits of detection for methanol, ethylene glycol and GHB ranged between 0.42 ng and 0.63 ng on column loading. Propylene glycol's limit of detection was slightly higher at 1.42 ng and ethanol's was the highest at 4.62ng.

Table 4. 7 Summary of the linear regression analysis obtained from the calibration of the d-IMS ($[i]_{(liq)}$) within linear range region.

Compound	$[i]_{(liq)}/\text{mg.dm}^{-3}$	$B_0/\text{V.s}$	$B_1/\text{V.s.ng}^{-1}$	L_oD^*/ng	$R^{2\text{lin}}$
Methanol	10 to 250	-0.02	0.27	0.42	0.994
Ethanol	250 to 1000	-8.22	0.28	4.62	0.983
Ethylene glycol	100 to 500	-0.02	0.27	0.52	0.994
Propylene glycol	100 to 500	-0.48	0.30	1.42	0.997
GHB	20 to 500	-0.18	0.31	0.63	0.995

The calibration curves are shown in Figure 4.8, with a quadratic regression superimposed onto the linear calibration for all of the compounds apart from GHB; for which a linear fit was obtained across the entire concentration range. The dotted lines indicate the 95% confidence limit of the predicted y values over the linear region.

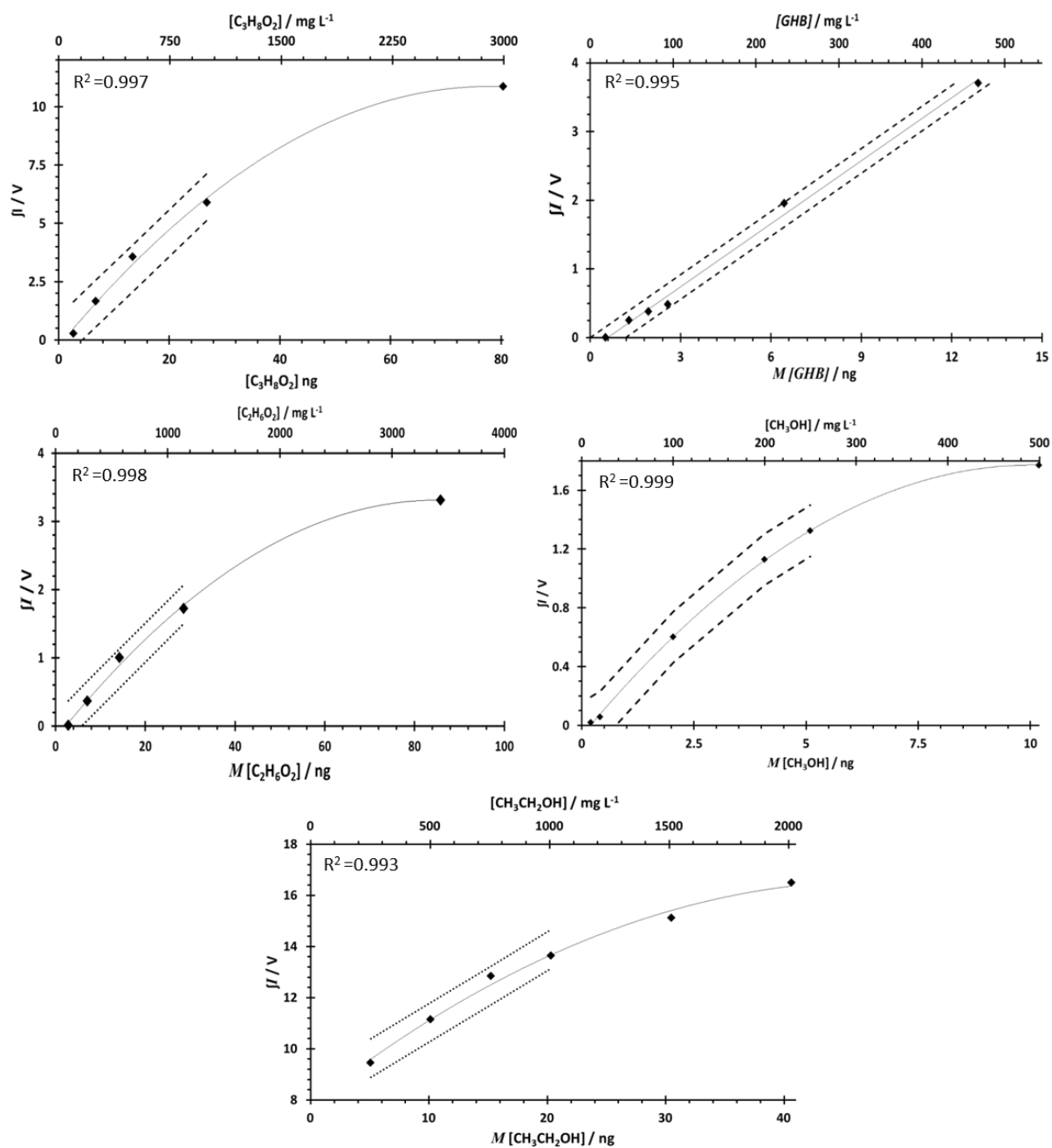


Figure 4. 8 Summary of calibration curves for methanol, ethanol, ethylene glycol, propylene glycol and GHB, within their toxicological level range of concentration. Calibration based on peaks of PM (Methanol), sum of PM and PBD (Ethanol) and PBD (two glycols and GHB).

4.3.2 Characterisation of spiked saliva samples

The responses obtained from saliva spiked with a range of concentrations of the analytes are summarised in Figure 4.9 and Figure 4.11. Figure 4.9 presents extracted chromatographic d-IMS responses at the concentration levels chosen for each analyte (A to E). Data was collected using instrumental parameters shown in Table 4.5 and

retention times were manually aligned during post processing, to correct for timing misalignment from the manual operation of the recording system used in recorded data.

The chromatography isolated substantial numbers of, and as yet uncounted, VOC present in human saliva samples. An example topographic plot of a GC-d-IMS response, generated from a blank saliva sample, is presented in Figure 4.10. Saliva VOC profiles were observed to be variable with intra-, and inter- subject differences observed.

Regardless of the large number of compounds recovered from saliva, it was possible to identify the analytes of interest reliably, based on their compensation field and retention times. Figure 4.11 shows d-IMS responses for MeOH (A), EtOH (B), propylene and ethylene glycol (C) and GHB (D) extracted from PDMS rods at their toxicological concentration thresholds. The intensities of the responses observed reflected the combined interactions of physical-chemical processes involved:

- the competitive adsorption/absorption behaviour of the analytes onto/into the PDMS sampler medium;
- the product ion dynamics noted above for the five compounds;
- and interactions with the saliva matrix.

Matrix interactions in drooled saliva are problematic in that microbiological activity and the stability of an analyte are related to the analyte's concentration, and will have a time dependent element. Those processes are described by adsorption and diffusion laws (such as in Langmuir model). Further the physical chemical properties of the saliva may also vary between samples.

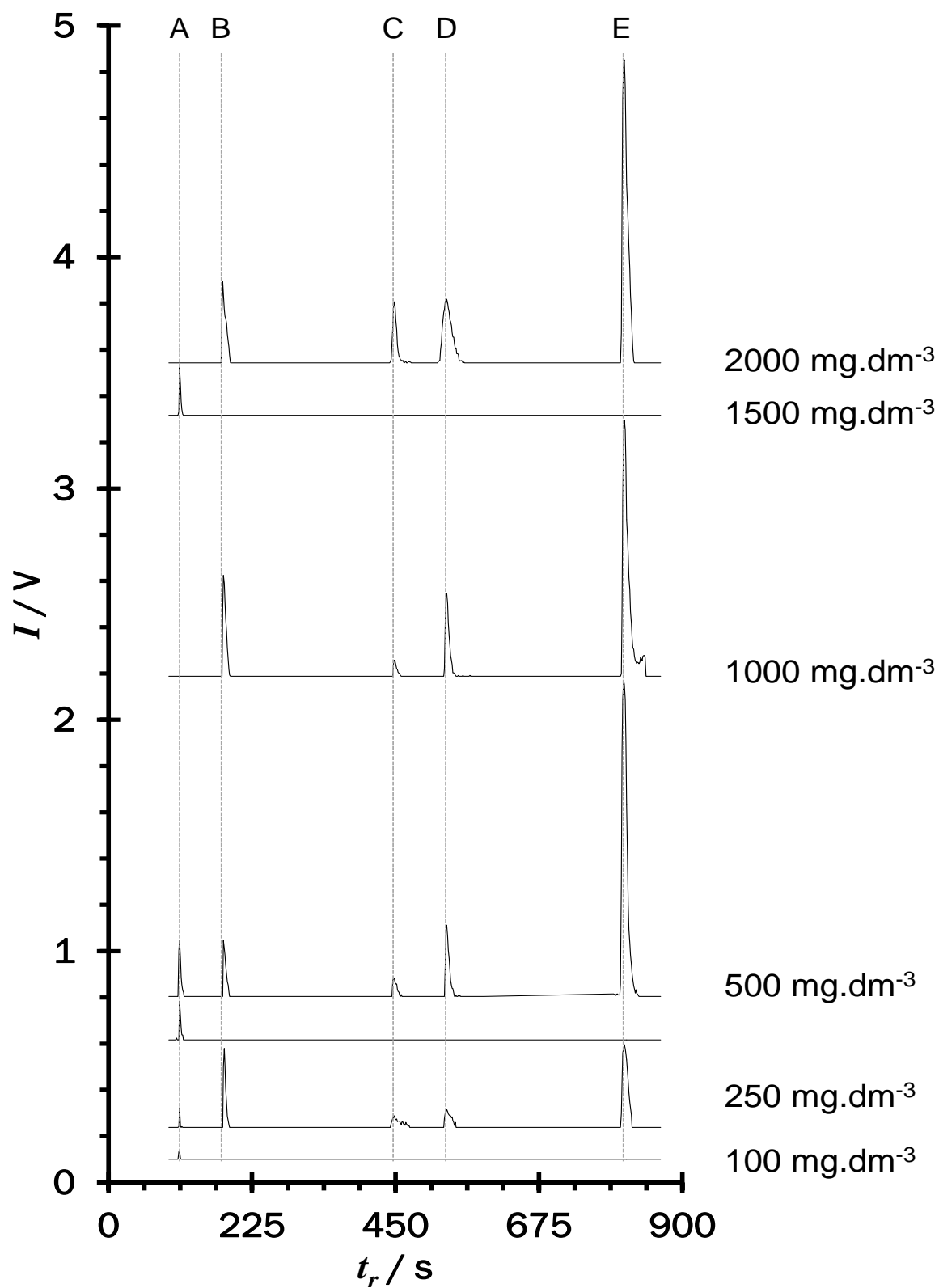


Figure 4. 9 Selective compensation field gas chromatographic traces obtained by thermal desorption gas chromatography differential mobility spectrometry for the five analytes at the concentration ranges studied. A - Methanol, B - Ethanol, C - Ethylene Glycol, D - Propylene Glycol, E- GHB.

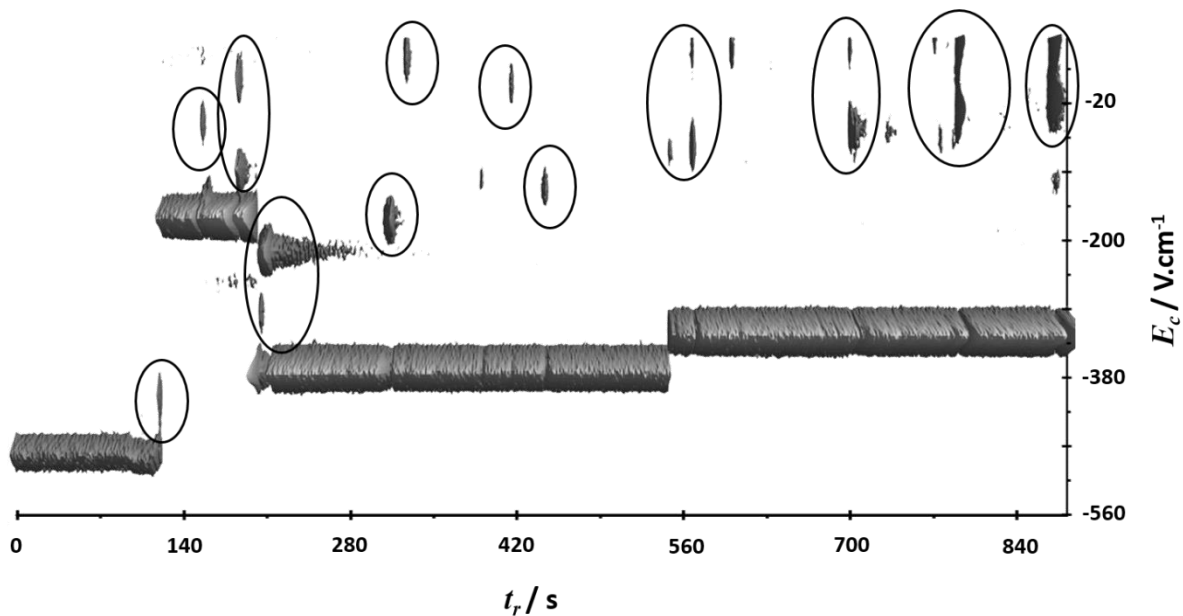


Figure 4. 10 Example of d-IMS responses obtained from blank saliva samples, recovered using PDMS cartridge. Each highlighted signal refers to unidentified compound presented in blank saliva samples.

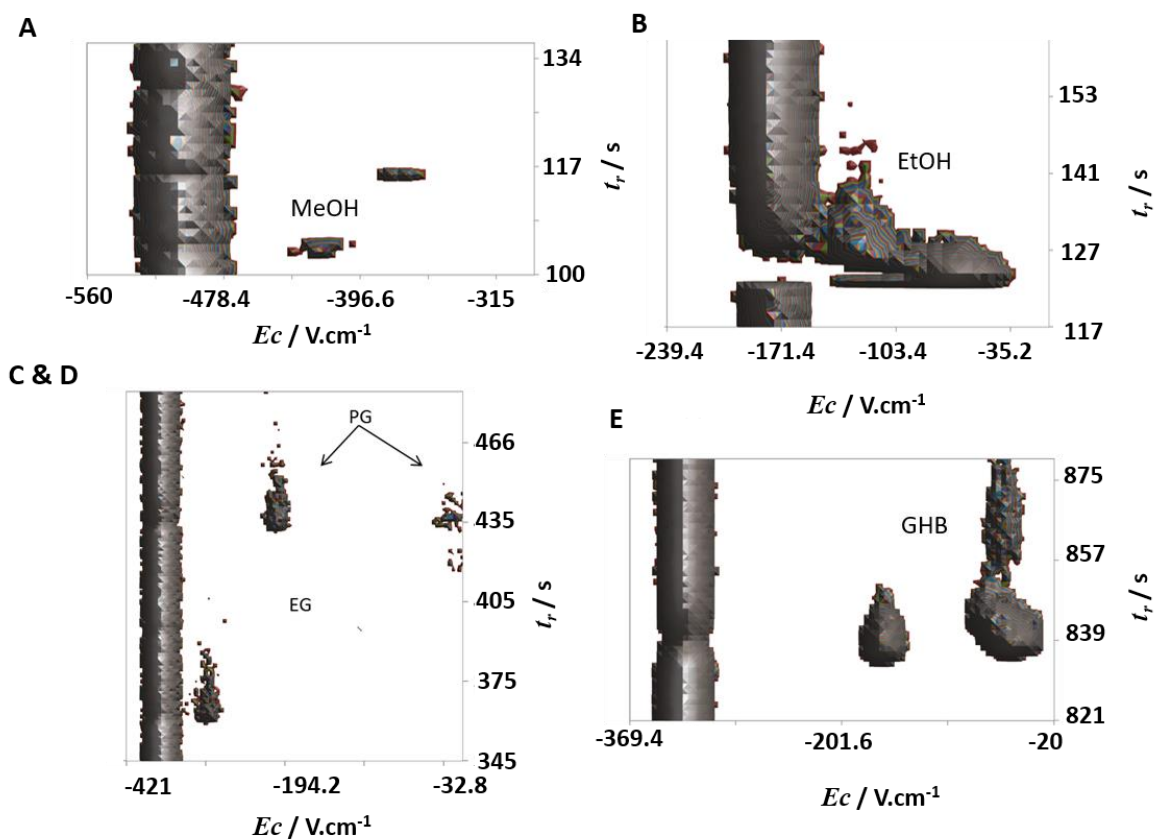


Figure 4. 11 Close up on TD-GC-d-IMS responses to MeOH (A), EtOH (B), propylene and ethylene glycol (C and D) and GHB (E). At their toxicological levels of 100 mg.dm^{-3} (A) and 250 mg.dm^{-3} (B, C, D and E) and calculated recovered on column masses of 350 pg (A), 29 ng (B), 1.87 ng (D) and 10 ng (E).

The complexity of the chromatogram made background subtraction problematic and subsequently it was not possible to investigate fragment ion artefacts with confidence. The on-column masses of methanol recovered were estimated to fall in the range 350 pg to 3 ng over the range of concentrations in saliva of 100 mg.dm⁻³ to 2 g.dm⁻³ and the concentration levels reaching d-IMS ion filter were estimated (using retention times) at the peak maximum to be 0.02 mg.m⁻³ and 0.27 mg.m⁻³ for the same concentrations in saliva. The potential of false evaluation of responses at high concentration levels (above alpha modification threshold) being mistaken with low concentration responses was evaluated. Figure 4.12 demonstrates (obtained from exponential washout experiment of methanol, Section 3.4.2), the response for methanol at 0.27 mg.m⁻³ and 250 mg.m⁻³ concentration level gives the same spectrum and peak intensity. The response at 0.27 mg.m⁻³ in the d-IMS, was produced from 3000 mg.dm⁻³ MeOH concentration in the saliva, which is already death risk threshold for the patient and treatment need to be rapid anyway. This aspect is important when optimising flows and dilutions to avoid such misinterpretation also the presence and intensity of the RIP is an important element in this context.

Recoveries of the highly polar ethylene glycol were lower with 7 ng obtained at high saliva loadings of 3000 mg.dm⁻³, contrasted with 1,3-propanediol recoveries of up to 22 ng at the same level. GHB was the most efficiently recovered from saliva with 10 ng recovered at 100 mg.dm⁻³ increasing to an estimated on-column mass of 34 ng at 400 mg.dm⁻³. Figure 4.13, summarise obtained responses for all of the compounds by plotting their I against concentrations present in the saliva. The three inserts are extracted signals for analytes of most concern with respect to toxicity: top, methanol at 100 mg.dm⁻³; middle, the monomer signal for ethylene glycol at 250 mg.dm⁻³; and bottom, the monomer and proton bound dimer signals for GHB at 250 mg.dm⁻³.

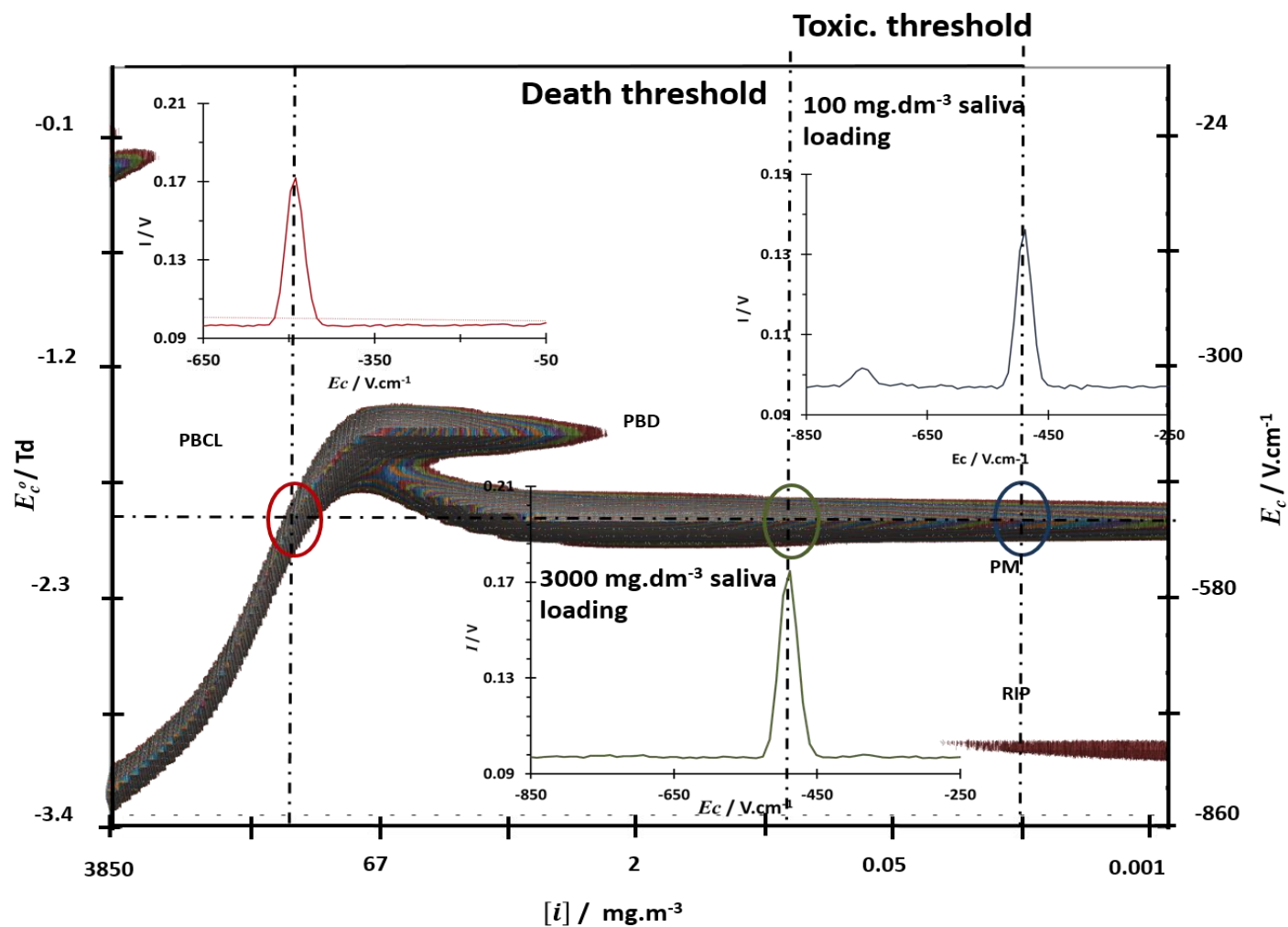


Figure 4. 12 MeOH exponential washout (Section 3.4.2) and estimated responses expected to be seen for MeOH at 0.27 and 0.02 mg.m⁻³, recovered from saliva concentrations of 3000 and 100 mg.dm⁻³, respectively. Mind possible misinterpretation which could be made between 0.27 mg.m⁻³ (risk of death level) and extremely high concentration of 250 mg.m⁻³.

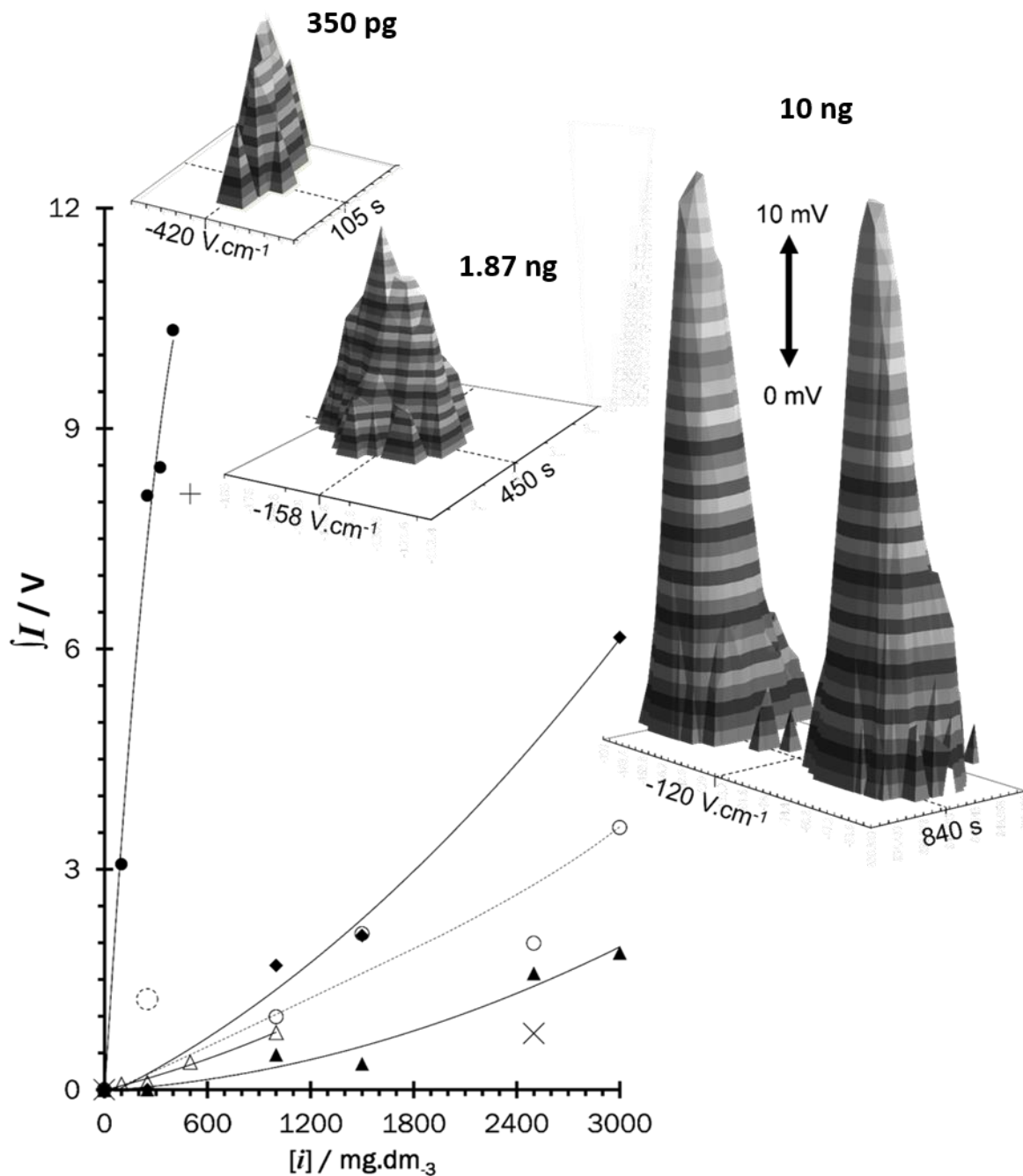


Figure 4.13 Integrated responses for a range of spiked saliva concentrations for methanol (open triangles), ethanol (open circles), ethylene glycol (solid triangles), 1,3-propanediol (solid diamonds) and GHB (solid circles). Three outliers are shown. Dotted circle, cross and plus symbols for outliers observed with ethanol, 1,3-propanediol and GHB respectively. Figure adapted from Ruszkiewicz et. al. [166] with permission of Royal Society of Chemistry.

A previous study with this sampler contrasted the responses obtained from drooled saliva samples against those obtained by sampling directly in the mouth, under the tongue next to the salivary glands. Sampling in the mouth was found to be more sensitive and more reproducible than adopting a passive drool approach. Further, obtaining a

passive drool sample requires significantly more patient / participant training and compliance than placing a small rod under their tongue and as such is likely to be a more practical approach to working with patients/participants who may have analytes at levels high enough to be a cause of concern for their safety and welfare [170]. Nevertheless the adoption of a passive drooled-saliva approach enabled a matrix that approximated the intended sampling conditions to be acquired safely and practicably. Finally, the loss of the more volatile methanol and ethanol to the saliva headspace and hence from the experiment also needs to be acknowledged as a methodological weakness.

4.4 Conclusions

This pilot study demonstrated the effective recovery, detection and semi-quantitative estimation of all the analytes of interest to this work. This represents a potentially useful methodological advance in the rapid assessment of alcohol toxicity. Embodied within a TD-GC-d-IMS or a TD-GC-IMS it provides a fieldable approach for a rapid screen and evaluation protocol for alcohols present at toxic levels from a single non-invasive sample. This has not been possible previously and has the potential for the development of point-of-care toxicity assessment in emergency room settings. The next stage for this approach would be studies on catabolites such as formaldehyde, formic, glycolic and oxalic acids, which could not only increase the confidence of the results but also determine the stage of the toxicological reaction in the human body.

The apparently simplicity of the analytes belies significant complexity in the ion chemistries associated with their detection using ambient ionisation or radioactive ionisation approaches. As shown in the previous chapter and in the literature on mass spectrometric studies with alcohols, fragment ions are formed associated with proton transfer ionisation approaches [141,144,173] and the presence of signals due to product ion fragmentation would not appear to be without precedent. The alcohol product ions, and their fragment ions, are highly mobile (K strongly dependent on electric field (E/N)) and therefore are associated closely with the water-based reactant ion signals, also highly mobile species. Increasing resolution between the reactant ion signal and analyte signals by increasing the dispersion field strength has the combined effect of reducing the analytical sensitivity by reducing the acceptance aperture of the ion filter while at the same time promoting fragmentation reactions [174 and 135]. The possible ion fragmentation of GHB has not been reported previously.

Compensation field maximum shifts were only observed in cases of possible fragment ions, obscured with the RIP peak. This cannot be attributable to the auto-modification of the transport gas by analyte neutrals due to the levels delivered into the d-IMS filter were in all cases below the modification threshold, calculated to be at 88 mg.m⁻³ and 133 mg.m⁻³ for MeOH and EtOH (Section 1.8.4) and 137 mg.m⁻³ (EG), 168 mg.m⁻³ (PG) and 229 (GHB) mg.m⁻³, assuming 50ppm rule (Section 1.8.4). Possible explanation maybe, the low levels of fragment ions, which may lead to errors identification at the E_c scale.

The study of fragmentation mechanisms, products and their ramifications for alcohol determination by differential mobility spectrometry along with the development of detection and signal processing algorithms to enable peak-shift from auto-modification of the differential mobility transport gas to be handled efficiently are logical next steps in the development of this area. Alongside the delivery of a clinical pilot study within an appropriate poisons unit to assess the efficacy of this approach in patients, benchmarked to current gold-standard toxicity screens.

Chapter 5 Alcohols Mixtures

Initial aim of this thesis was to explore the use of alcohols as modifiers in combinations with different dopants³. The intent was to create chemical codes made intentionally complicated for security labelling applications, which could only be resolved and detected by using a specific modifier/analyte combination (Section 1.6.3). The very first experiments revealed unexpected phenomena in the behaviour of the analysed mixture of alcohols, including apparent changes in the mobility of ions over a narrow range of concentrations and regeneration of reactant ions. These observations were not understood at the time what led to major changes in hypothesis and objectives of this thesis and resulted in fundamental and comprehensive study on the behaviour of alcohols in d-IMS (Chapter 3) and developed method for recovery and detection of alcohols from human saliva (Chapter 4). This Chapter describes the very first few experiment, which results led to changes in the objectives described above and demonstrates the observed anomalies in alcohols mixture ions behaviour.

5.1 Study Overview

In this Chapter an extensive experimental design is described, built to study gas phase interactions in analyte-modifier system as well as optimisation and validation of the specially constructed experimental set-up required to perform such studies. Finally demonstration of the results obtained from the first performed experiment between 2-butanol (analyte) and methanol (modifier) is included, which led to changes in the research objective.

5.2 Preliminary Experimental Design.

Experimental design was constructed in a form of a colour wheel design, to study intermolecular interactions within the mixtures of chosen analyte (A) and modifier (M), see Figure 5.2 The design, was built to study mixtures of three different analytes (or dopants) with four different modifiers, each indicated by different colour section. Each section of the wheel is built of 5 double rings zones (Zones 1 to 5). Internal ring, belongs to an analyte and is built of four intensity colour cells, corresponding to four studied

³ In case where only two compounds are present within the mixture (and one is a modifier), the dopant can also be refer to as analyte. The termin “analyte” will be used in this Chapter.

vapour concentration levels of the analyte, introduced via piezoelectric injections. External ring, belongs to a modifier and is built of gradually changing colour's intensity cells, corresponding to changing concentration from the exponential dilution washout. The concentration also gradually changes between the Zones. Note that the concentration levels (colour cells) of the analyte, are constant between the Zones 1 to 5 and only concentration of modifier is changing. The experiment start within the cell S at high concentration level of the modifier (dark colour cell) and finishes within cell F, when the concentration of the modifier is low (pale colour cell). The design gives a base for further development of the work, which together with the knowledge on the fragmentation can be used to produce complex responses within the chemical label and extend the knowledge on intramolecular interactions of gas mixtures.

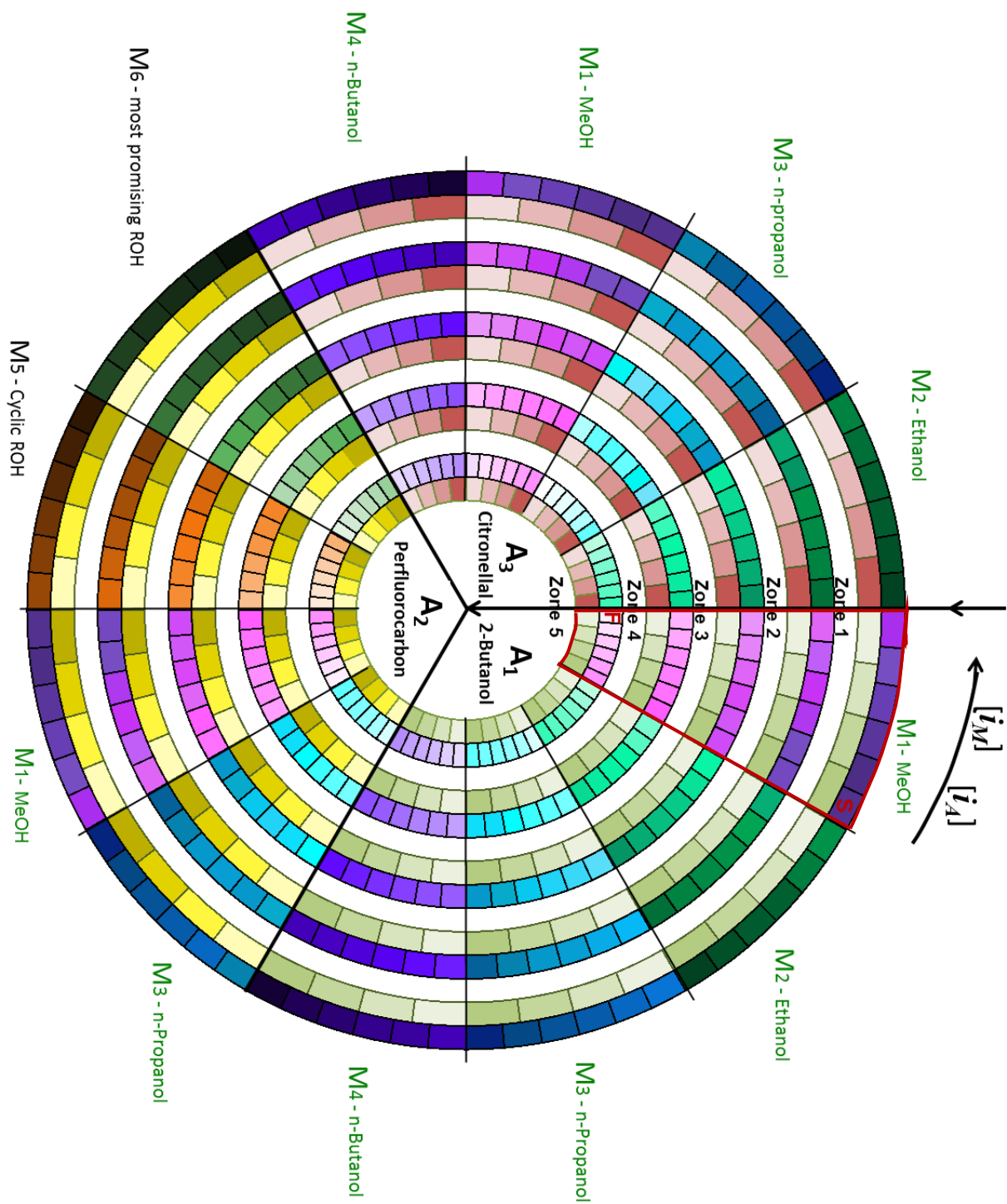


Figure 5. 1 Wheel design to perform extended study on combination of analyte (A) and modifier (M) intermolecular interactions.

5.3 Experimental

5.3.1 Chemicals

Methanol (MeOH) and 2-butanol (2-BuOH) were obtained from Sigma Aldrich, see Table 5.1. Nitrogen was generated on site (PEAK Scientific, UK, model nk-10L-HP) and purified by passing through a charcoal adsorbent-bed gas-purifier (Varian), a moisture filter (Varian), and a triple-bed gas purifier (Thames Restek), all mounted in series.

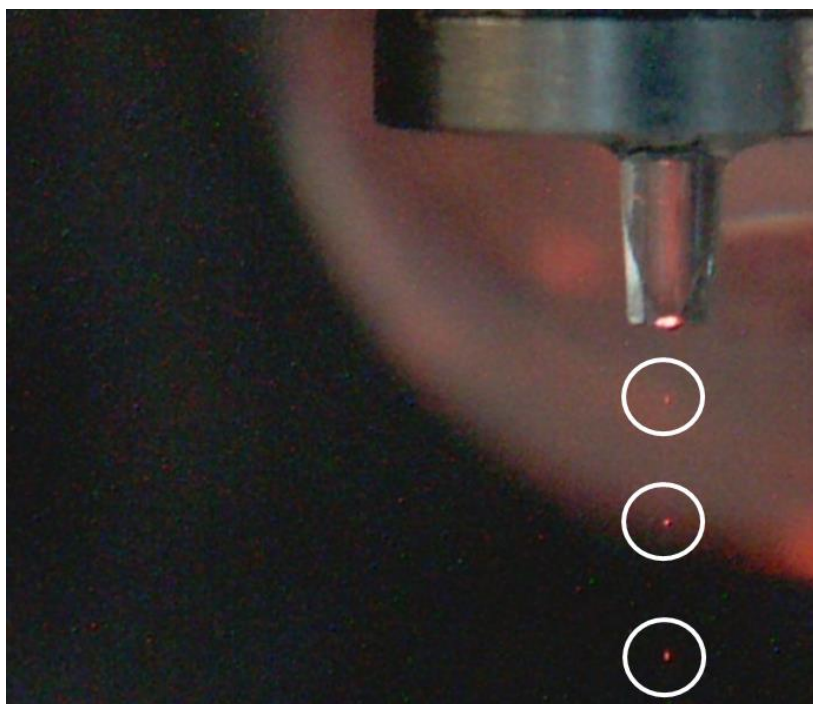
Table 5. 1 Properties of the alcohols: M - molecular mass, PA - proton affinity, Bp - boiling point, d - density, CAS number. Note: ^a ChemSpider and ^b NIST

Compound	$M^b / \text{g mol}^{-1}$	$PA^b / \text{kJ mol}^{-1}$	$Bp^b / ^\circ\text{C}$	$d^a / \text{g cm}^{-3}$	CAS
		1			
Methanol	32	754.3	64.7	0.79	67-56-1
2-Butanol	74.1	815	98	0.81	78-92-2

5.3.2 Methods

5.3.2.1 Optimisation of the bipolar waveform

To enable the stable and reproducible actuation of the organic liquids from piezoelectric injections, an appropriate waveform need to be applied to the crystal (Section 2.5.6.3). The nature of the waveform required to actuate a liquid varies due to differences in physical and chemical properties of the liquid (e.g. surface tension and viscosity). The experimental approach for the waveform optimisation was a four-factor, 2-centroid point central composite design (CCD), giving a total of 26 factorial combinations. The four factors in the design model were the dwell voltage V_d , dwell time t_d , echo voltage V_e and echo time t_e of the bipolar waveform. Those four parameters shown the most significant influence on droplet formation in previous studies [175]. The temperature in the reservoir was set to 21 °C and frequency of actuations ω to 100 Hz. additionally, the vacuum pressure was previously optimised in set of test to increase a liquid suspension at the PZX crystal orifice. Results obtained for optimisation of 2-butanol liquid is given in Table 5.2. Picture 5.1 shows optimised pico-litre volume droplets being jetted from piezoelectric injector.



Picture 5. 1 Jetting optimised pico-litre volume droplets of 2-BuOH, using piezoelectric injector.

Table 5. 2 Optimised parameters of the bipolar waveform for piezoelectric injections of 2-butanol.

	V_d / V	$t_d / \mu s$	V_e / V	$t_e / \mu s$
2-butanol	32.0	14.0	-1.0	1.5

5.3.2.2 *Digital control of piezoelectric actuator*

In previous work, a control of jetted liquid concentration was demonstrated via control of the flows in the interface [161]. In this study an experiment was performed to establish if concentration level of 2-butanol vapours can be controlled digitally via changing applied voltage within the interface. The experiment was carried out using Microfab PZX injector with 60 microns crystal orifice. 2-butanol was dispensed under the previously optimised waveform into pre-weighed 1 cm³ volume clear glass vial. The vial was placed in the bigger 20ml headspace vial containing about 2 cm³ of dry ice, to prevent vaporisation of liquid and capped with metal cap with about 4mm orifice in the septum. The injector head was placed within the orifice during jetting process. The liquid was then jetted at six different frequencies, in the range of 2 to 1000 Hz, for period of time of 60, 300, and 600 s (Table 5.3). The temperature of the orifice was monitored during the experiment and was between 20.5 and 22.0 °C. The experiment was done in quintuple and repeated on two separate days. A previously tested negative absolute backpressure was applied to the reservoir throughout the experimental procedure and was equal to -0.02

psi. The vials were capped immediately after jetting with plastic vial cap and weighed with an electronic balance, Ohaus Discovery, (Thetford, UK), model DV-215CD with 0.01 mg resolution. The average individual droplet mass was calculated using Equation 5.1.

Table 5.3 Jetting conditions during digital control studies on 2-butanol, where ω is the frequency in Hz, t_j is jetting time in s and T is temperature of the orifice in °C.

ω	t_j	T
1000	60	22.6
100	300	21.8
50	300	22.2
20	300	22.4
10	600	21.5
2	600	21.8

$$\bar{m} = \frac{\Delta m}{t_j} / \omega \quad \text{Equation 5.1}$$

Note: m : individual droplet mass in g ; $[\Delta m]$: mass of vial difference before and after actuation in g; t_j : time of actuation in s; ω : frequency of actuation in Hz.

The stability of droplet were calculated as the relative standard deviations in mean weight per droplet, from the quintuple data sets (Table 5.4) and in all cases the RSD was below 10%. The relative standard deviation in mean droplet mass between frequencies used was calculated to be 7.9%.

Table 5.4 Summary of the gravimetric data obtained from digital control experiment of 2-butanol, where ω is frequency in Hz, \bar{m} is mean weight of the droplet from quintuple replicate in ng

ω	\bar{m}	<i>RSD %</i>
1000	82.9	1.5
100	69.7	9.6
50	72.8	8.8
20	77.6	4.0
10	85.6	9.2
2	82.0	9.0

5.3.2.3 Studies on alcohol mixture

Two independent delivery systems were used in the study to introduce analyte (2-BuOH) and methanol (MeOH) into the d-IMS specially constructed to study d-IMS responses of the analyte/modifier system in relation to changing concentration level (Section 2.5.6). In the first instance an individual dispersion plots of 2-BuOH analyte at four different concentration levels (72, 144, 288 and 576 $\mu\text{g}\cdot\text{m}^{-3}$) were recorded and exponential washout of the methanol modifier at fixed dispersion field was performed. Next the final

mixture experiment was carried out in accordance to the experimental design (highlighted in red, Figure 5.1). Piezoelectric injections of 2-BuOH at four different concentration levels (given above) were performed at five different concentration zones of the methanol exponential washout using piezoelectric injector, and spectra at fixed dispersion field and dispersion plots were collected for each 2-BuOH concentration. This was repeated for each MeOH concentration zones (Zones 1 to 5). Conditions used in the experiment are given in Table 5.5.

Table 5.5 Experimental conditions used in 2-butanol/methanol studies.

Parameter	Value	Units
PZX mode conditions for 2-BuOH injections		
Carrier gas		N ₂
Back pressure	-0.16	Psi
Interface flow F_1	180	cm ³ .min ⁻¹
Interface exhaust flow F_2	24	cm ³ .min ⁻¹
Interface Split flow F_3	155	cm ³ .min ⁻¹
Interface suction flow F_4	1	cm ³ .min ⁻¹
Jet pump flow F_5	940	cm ³ .min ⁻¹
Jet pump Split flow F_7	620	cm ³ .min ⁻¹
Injection frequency	1, 2, 4 and 8	Hz
Heating block temperature	100	°C
Heating rope temperature	100	°C
Average droplet volumen \bar{m}	83	ng
Dwell voltage V_D	32	V
Dwell time T_D	14	µs
Echo voltage V_E	-1	V
Echo time T_E	1.5	µs
Exponential dilution mode conditions for methanol washout		
Transport gas		N ₂
Exponential dilution flow F_9 (MeOH)	10	cm ³ .min ⁻¹
Humidity of the transport gas	25 to 30	mg.m ⁻³
Injection volume (MeOH)	100	µl
Exponential flask temperature	120	°C
D-IMS conditions		
<u>Dispersion plots</u>		
Dispersion field (E_d/N) or dispersion voltage (V_d)	40 to 120 or 500 to 1500	Td or V
Compensation field (E_c/N) or (E_c) range	-3.44 to 1.2 or -860 to 300	Td or V
Number of E_c steps N_s	100	
E_c step dwell-time	10	ms
d-IMS transport gas flow (F_8)	320	cm ³ .min ⁻¹
d-IMS filter temperature	100	°C
<u>Fixed scans</u>		
Dispersion field (E_d/N) or dispersion voltage (V_d)	103 or 1300	Td / V
Compensation field (E_c/N) or (E_c) range	-3.44 to 1.2 or -860 to 300	Td / V
Number of E_c steps N_s	100	
E_c step dwell-time	100	ms
d-IMS transport gas flow (F_8)	320	cm ³ .min ⁻¹
d-IMS filter temperature	100	°C

5.3.2.4 Vapours concentrations

The concentrations of jetted liquid's vapours entering d-IMS filter, in the system shown in Figure 2.16 and Figure 2.17 (Section 2.5.6), can be calculated via Equations 5.2 and 5.3.

$$Q = (m \times \omega \times 60) \quad \text{Equation 5. 2}$$

Note: Q : mass flux of injected liquid in glass liner in $\mu\text{g} \cdot \text{m}^{-1}$ m : mass of liquid per actuation in μg ,
; $[\omega]$: frequency of actuation in Hz

$$i_{d-IMS} = Q \times \frac{F_4}{F_4 + F_3} \times \frac{F_8}{F_8 + F_7} \quad \text{Equation 5. 3}$$

Note: i_{d-IMS} : concentration of vapours of injected liquids within d-IMS transport gas flux in $\mu\text{g} \cdot \text{cm}^{-3}$; $[F_3, F_4, F_7, F_8]$ interface and system gas flows in $\text{cm}^3 \cdot \text{min}^{-1}$ (Figures 2.16 and 2.17, Section 2.5.6)

5.4 Results demonstration

Piezoelectric injections of 2-BuOH at four different concentration levels (72, 144, 288 and $576 \mu\text{g} \cdot \text{m}^{-3}$) were performed at five different concentration zones of the methanol exponential washout (Z1 to Z5) using piezoelectric injector, this is demonstrated in Figure 5.2. In the first instance a spectra at fixed dispersion field were collected, followed by collection of dispersion plots for each 2-butanol concentration level. This was repeated at each MeOH concentration zone.

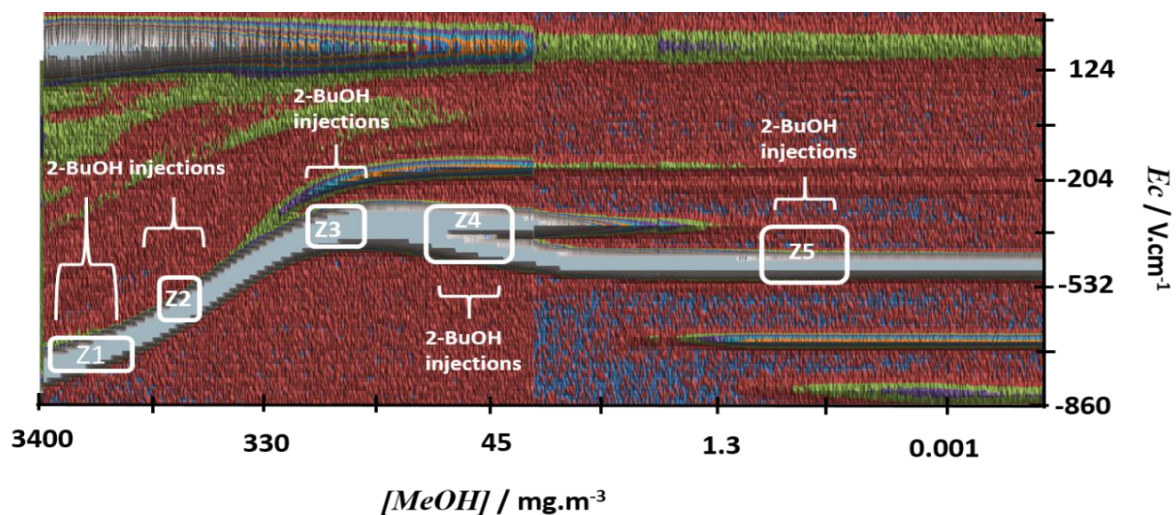


Figure 5. 2 Exponential washout of methanol at d-IMS dispersion field of 103 Td or $1300 V_d$ V and temperature of the d-IMS ion filter of 100°C . The squares from Z1 to Z5 demonstrate levels of methanol at which a 2-BuOH injections were performed during the mixed system. Note: the data was combined from two methanol washouts experiments due to recording error.

At the concentration level of MeOH, between 1800 and 80 mg.m⁻³, the methanol forms proton bound cluster ion $(MeOH)_nH^+$ (where n = 2 to 3), which dispersion behaviour is modified by collision with neutrals (Section 4.5.2.1). Injections of 2-Butanol at the highest concentration levels of methanol down to from 1800 to 1430 mg.m⁻³, showed complete suppression of the 2-BuOH signal. This has been reported for elevated levels of modifiers in d-IMS and FAIMS [176]. From 1420 mg.m⁻³ down to around 30 mg.m⁻³ much complexity in the ions behaviour was observed including:

- Suppression and regeneration of the methanol signal (Figure 5.3)
- Modification of the 2-Butanol responses (Figure 5.4)
- Distortion of spectra (Figure 5.4)
- Possible adduct formation (Figure 5.5)
- Fragmentation (Figure 5.5)
- Selective charge transfer (Figure 5.6)

At the concentration level of methanol below 5 mg.m⁻³ (Zone 5), no effect of methanol on the 2-butanol responses was observed.

Detailed interpretation of the experiment results is beyond the scope of this thesis. Great complexity observed in the alcohols experiment require more data and d-IMS-MS studies to be performed, to correctly interpret the chemistry of alcohols' mixtures. Nevertheless, the constructed system met the purpose of the study and can be used for future work. By following a colour wheel design a large data base of the d-IMS responses of different analyte/modifier can be produced and study on intermolecular interaction within d-IMS can be performed.

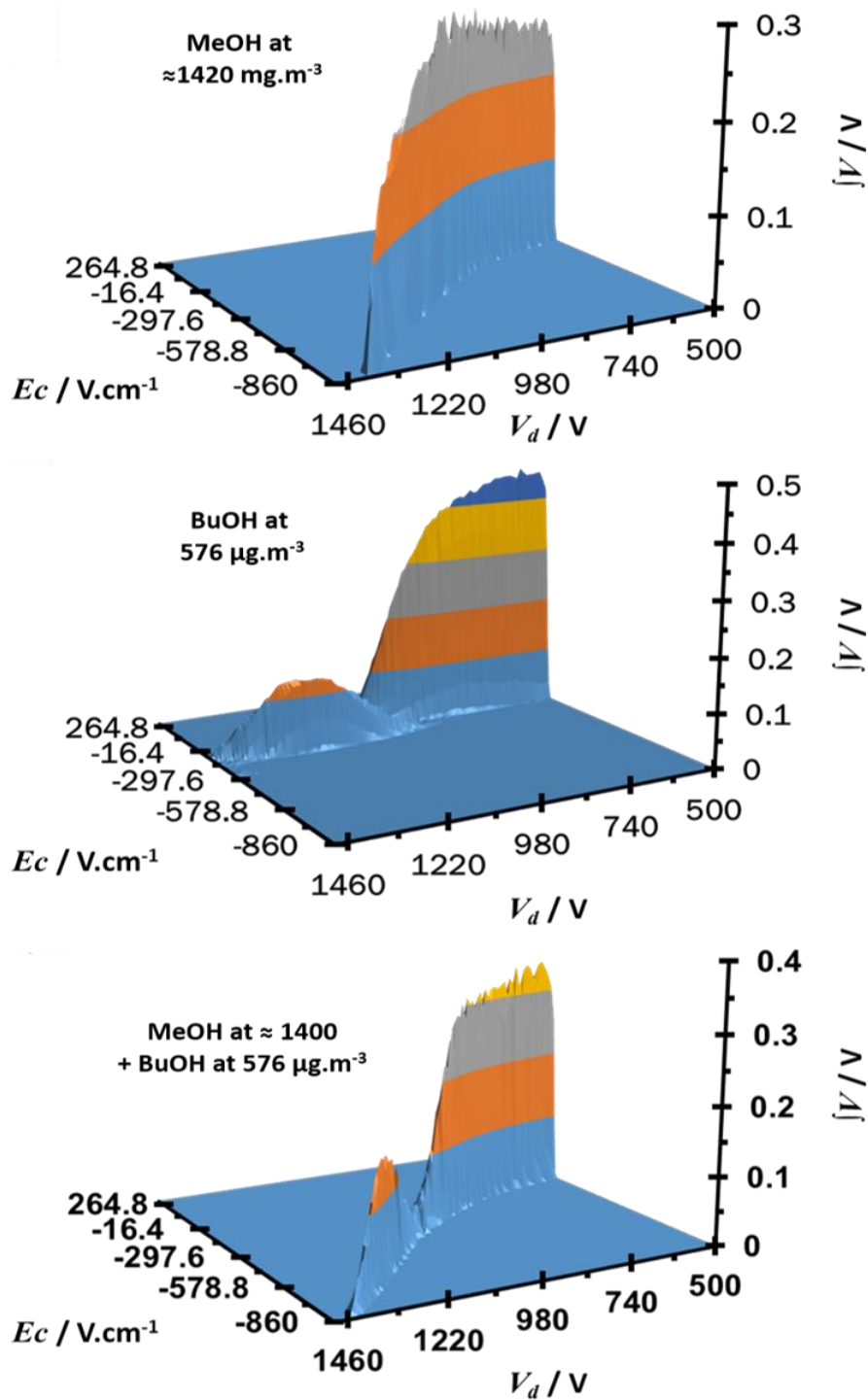


Figure 5.3 D-IMS dispersion plots of MeOH at $\approx 1420 \text{ mg.m}^{-3}$ concentration level (top) , 2-BuOH at $576 \text{ }\mu\text{g.m}^{-3}$ concentration level (middle) and MeOH/2-BuOH (Zone 1) mixed system at ≈ 1400 and $576 \text{ }\mu\text{g.m}^{-3}$ (bottom), showing changes in ion dynamics, with suppression of the MeOH signal followed by a rise in the mixed system.

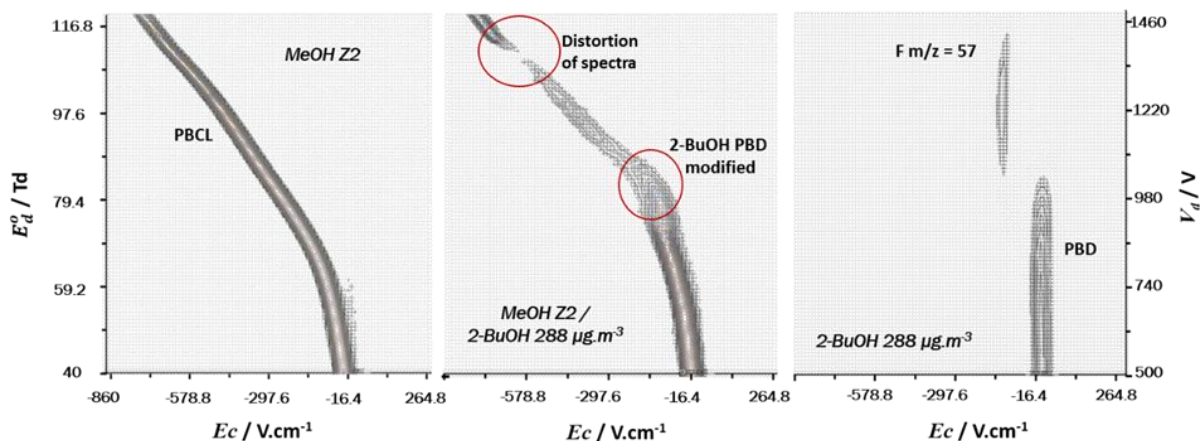


Figure 5. 4 D-IMS contour plots of MeOH at Zone 2 concentration level of $\approx 815 \text{ mg.m}^{-3}$ (left), 2-BuOH at the concentration level of $288 \text{ }\mu\text{g.m}^{-3}$ (right) and 2-BuOH/MeOH systems (Zone 2) at MeOH concentration between of 746 mg.m^{-3} and $576 \text{ }\mu\text{g.m}^{-3}$ of 2-BuOH level (middle) Dispersion plots captured at the d-IMS temperature of $100 \text{ }^\circ\text{C}$. Modification of PBD responses and distortion of spectra are observed. Note: PBCL - proton bound cluster ion, PBD - proton bound dimer, F - fragment.

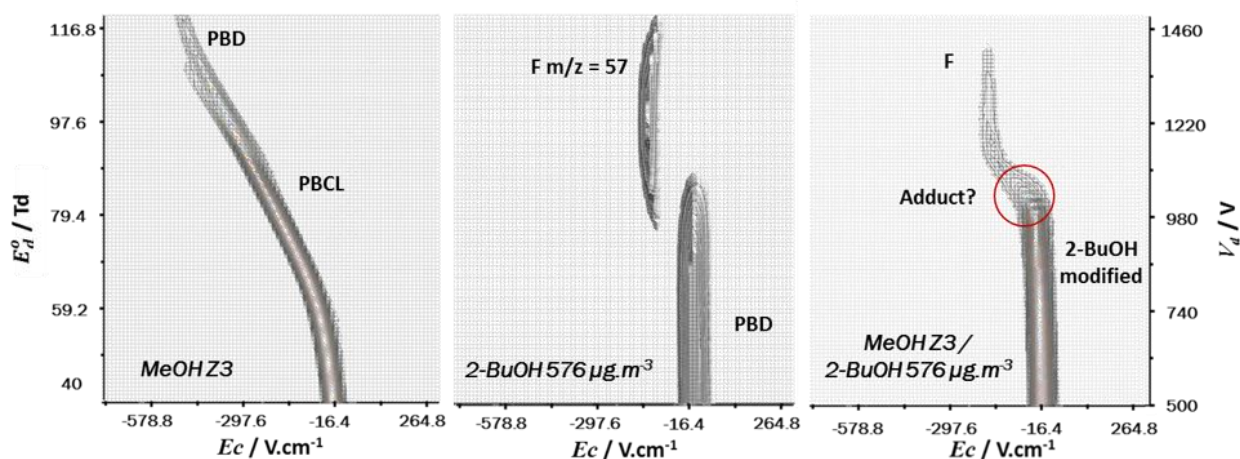


Figure 5. 5 Contour plots of d-IMS responses of MeOH at Zone 3 concentration level of $\approx 203 \text{ mg.m}^{-3}$ (left), 2-BuOH at $576 \text{ }\mu\text{g.m}^{-3}$ (middle) and 2-BuOH/MeOH systems (Zone 3) at MeOH concentration of 157 mg.m^{-3} and $576 \text{ }\mu\text{g.m}^{-3}$ of 2-BuOH level (right). Dispersion plots captured at the d-IMS temperature of $100 \text{ }^\circ\text{C}$. 2-BuOH fragment ion and possible adduct formation is observed. Note: PBCL - proton bound cluster ion, PBD - proton bound dimer, F - fragment.

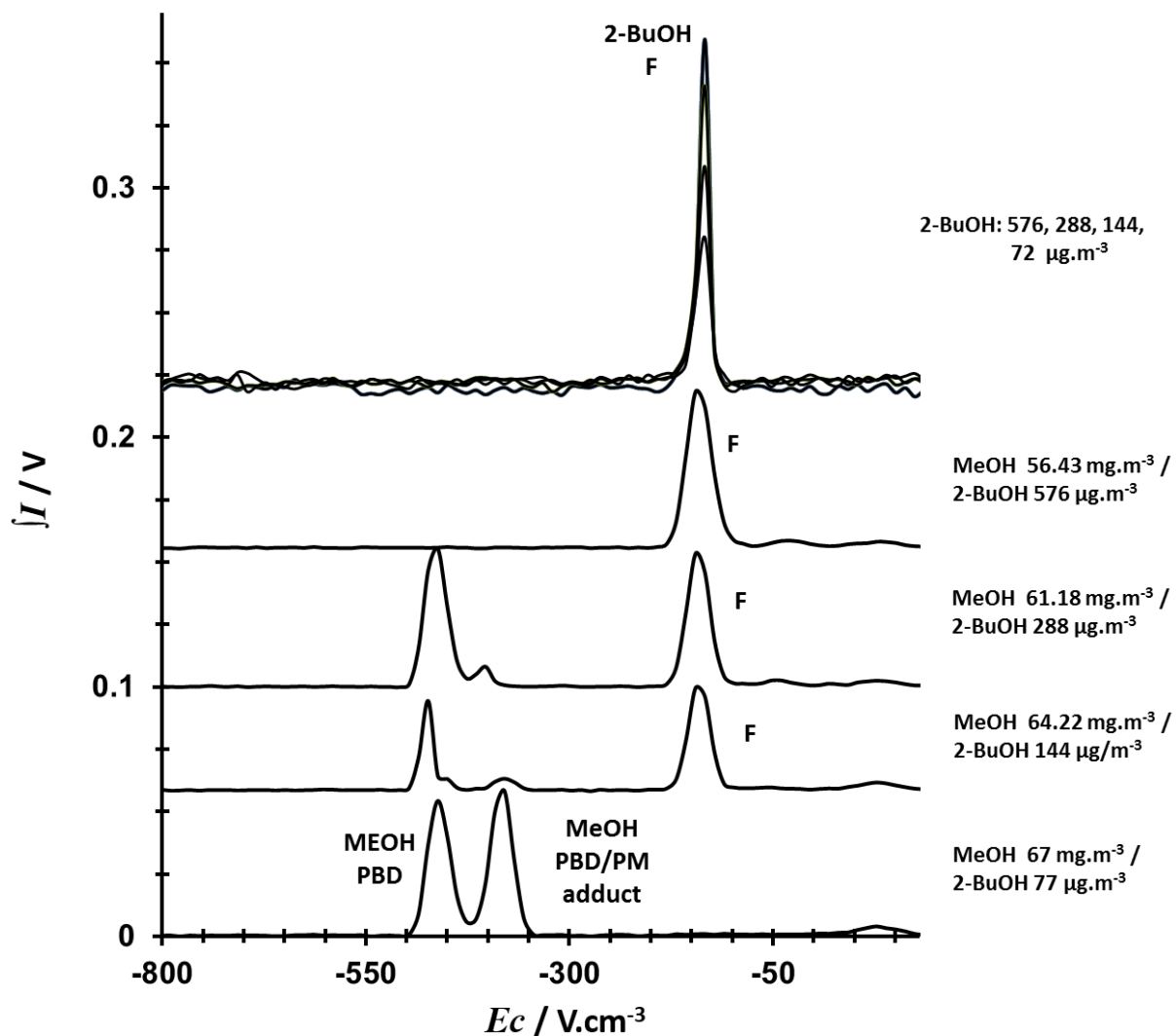


Figure 5.6 Extracted spectra of d-IMS responses for MeOH, 2-BuOH and MeOH/2-BuOH system collected at the d-IMS filter temperature of 100 °C and fixed dispersion field of 103 Td or 1300 V_d V. Selective ion transfer is seen between Methanol adduct and 2-BuOH fragment, when 2-BuOH was introduced at 144 and 288 $\mu\text{g.m}^{-3}$ concentration level within the Zone 4 of methanol washout. Note: PBD – proton bound dimer, PM – protonated monomer, F – fragment.

Chapter 6 Thesis Summary

6.1 Overview of the Research Findings and Review of the Studies

6.1.1 *Ion chemistry of alcohols*

This thesis describes the first systematic, exploratory studies on the ion chemistry of four common alcohols (methanol, ethanol, n-propanol and n-butanol) in differential ion mobility spectrometry (Chapter 3). The effect of analyte concentration and ion temperature, on ion formation has been investigated

The primary hypothesis on alcohol fragmentation in d-IMS has not been disproved. The data presented in Sections 3.4.2.6, 3.4.3.9, 3.4.4.9 and 3.4.5.8 demonstrate the effect of ion temperature, influenced by applied electric field and ion filter temperature upon d-IMS response, showing changes in ion chemistry under different conditions. The fragmentation of alcohols may occur in d-IMS at ion temperatures high enough to induce the process and this can be done by altering ion filter temperature and dispersion field. In this study the fragmentation was observed at an ion filter temperature as low as 40 °C with dispersion fields of 80 Td. The ion chemistries appear to be similar to those reported in PTRMS studies [144]. Proposed fragmentation patterns include dehydration, with regeneration of hydrated protons and the formation of alkenes as well as dehydrogenation at higher dispersion fields (above 116 Td). The proposal is supported by d-IMS-MS studies (Sections 3.4.4.8 and 3.4.5.7), that provide experimental identification of some fragment ions and evidence for the proposed fragmentation patterns. Further experiments with deuterated standards at higher mass accuracy will be a logical continuation from this preliminary study to better establish the reactions and mechanisms observed here. Another step would be to study common alkenes, which are the possible fragment/dissociation products of alcohol's dehydration reactions.

This study describes, for the first time, fragmentation and fragmentation patterns of alcohols in d-IMS.

At this stage it is unknown, whether the fragmentation/dissociation process is caused by excess of the internal energy gained from the reaction in the ionisation source or caused by the excess of energy from collisions with neutrals during transit through the d-IMS filter (CID). The second mechanism is most likely in case of n-propanol and n-butanol,

where our knowledge on proton transfer reaction cannot explain the experimental results.

The secondary hypothesis on the alpha function modification at elevated concentrations was also not disproved. The data on the effect of the analyte concentration upon d-IMS responses described in Sections 3.4.2.2, 3.4.3.2, 3.4.4.2 and 3.4.5.2 agreed with current models of ion-molecule clustering and were predicted using calculations shown in Section 1.8.4.

A new phenomena of adduct formation within the drift tube was an unexpected and interesting result. The continuous shift across a narrow concentration range from 80 mg.m⁻³ to 10 mg.m⁻³ observed in case of methanol, described in Section 3.4.2.5 is proposed to be associated with adduct cluster formation. This for the first time points to the possibility of the reaction being caused by the collisions with neutrals in the d-IMS ion-filter. This can happen if there are enough neutrals for a collision to take place that forms a proton bound dimer adduct. The concentration levels, at which the behaviour is observed are too low for phenomenon to be associated with collisions occurring in 600 ns time scale of the low field segment of the dispersion waveform. The proposed mechanism is that the collision happens during 2 ms transit of the ion through the ion-filter (which would give sufficient number of collisions). This again points to the conclusion that the d-IMS spectra maybe strongly complicated by collisions with neutrals.

A simple model on ion-molecule equilibrium failed to predict distribution of alcohols responses in d-IMS, however the model enabled identification of anomalies. A more rigorous approach, possibly based on density functional theory, that accounts for the combined effect of formation of hydrated clusters, energy of ion-dissociation and ion-neutral collision is needed. This computational chemistry was beyond the scope of this study but it is indicated as a necessary next step that moves from simple alcohols to more complicated structures.

These findings show that d-IMS responses can be much more complicated than those based on simple proton transfer reaction and ion-molecule equilibrium for cluster formation. These findings lead to the consideration of a new instrumentation design to remove neutrals from the ion stream, something that should be considered for the next generation instruments.

6.1.2 Recovery of toxic substances from human saliva

The second study in this thesis (Chapter 4) describes a pilot study for analysing toxic substances (methanol, ethanol, ethylene glycol, propylene glycol and gamma-hydroxybutyric acid) with TD-GC-d-IMS. D-IMS responses were optimised, and a GC method developed which allowed the simultaneous detection of the analytes. Calibration of the d-IMS instrument resulted in five calibration curves shown in Section 4.3.1 and Figure 4.8. Some fragmentation was also observed. The fragment/dissociation product ion signals were obscured with the reactant ion peak, and data processing approaches allowed these phenomena to be distinguished from the reactant ion. The compensation voltage at which those signals are present suggests a possible dehydration pattern for alcohols and diols, as described in Chapter 3 of this thesis. Small shifts were observed in position of those fragments depending on the concentration levels, which were not associated with the modification of the alpha parameter. Full exploration of the fragmentation behaviour of diols and GHB was beyond the scope of this study and further identification of the fragments would require studies using a d-IMS-MS approach. Nevertheless, and in spite of the fragmentation process reliable calibration were produced. An approach that uses a polydimethylsiloxane (PDMS) to recover the analytes from saliva appears to have potential for the detection of some poisons at their toxicological levels in saliva (Section 4.3.2, Figure 4.13) with semi quantitation of the recovered masses.

The next step in improving reliable detection of toxic substances in saliva would be to extend the methodology to the analysis of their metabolic products such as formaldehyde, formic and oxalic acid, which would not only bring another level of reliability of the detection but also estimation at what stage of the toxic metabolic reaction the patient is in.

This study represents a potentially useful methodological advance in the rapid assessment of alcohol toxicity.

6.1.3 2-Butanol/Methanol mixed system experiment

The work with butan-2-ol and methanol revealed the unexpected complexity such as fragmentation and regeneration of ions (Figures 5.3 to 5.6), that led to the hypothesis and objectives described in this document. The next stages of this research should look

at the ion chemistry of mixtures, perhaps starting with intermolecular processes before extending to larger entities where intramolecular processes between different functional groups may be governed by stereo-chemical factors that give rise to different fragmentation pathways. Part of the methodology to achieve this was developed as part of the preparatory work for this research.

6.1.4 Critical evaluation

Reflection on this study and the experimental approaches adopted identifies three aspects that could be improved.

- 1) Optimisation of the conditions. The choice of the dispersion field and temperature levels was found to be most important for detection and resolution of product ions. The design could possibly be extended to a larger and higher level design to allow all existing chemistries to be covered. This would enable the phenomena of the fragmentation to be fully exploited. The dispersion field values at which fragments are generated may be as useful as a designator as the compensation field values.
- 2) Introduction of the gamma-hydroxybutyric acid as ammonia salt in methanol, made single experiment of all analytes in the saliva impossible. The improvement could be made by using a solvent exchange method and removal of the methanol from the matrix solution, which would improve efficiency of the performed experiments
- 3) Analysis of the toxic substances metabolic products

6.2 Concluding Comments

The ion chemistry of four n-alcohols (from C₁ to C₄) in differential ion mobility spectrometer has been surveyed. Investigation of ion temperature and concentration has resulted in the discovery of fragmentation and adduct formation in d-MS, and confirmed the prediction of auto-modification. Overall this study presents data on the detection of alcohols, under a wide range of operational conditions. Such knowledge will be useful in the application of d-IMS to their monitoring, essential in closed spaces such as submarines or spacecraft or in medical applications. The application of these findings enabled a new and reliable non-invasive method for the fast recovery and detection of toxic substances such as methanol, ethanol, ethylene and propylene glycol and GHB,

from human saliva using TD-GC-d-IMS to be evaluated. The method has been shown to be sensitive enough to work at the toxicological concentrations for the analytes. It is being developed as part of a H2020 project (TOXI-triage 653409) for further clinical evaluation at the National Poisons Centre in Edinburgh and at the Norwegian National Unit for CBRNE Medicine at the Department of Acute Medicine of the Medical Division of Oslo University Hospital. The ambition is to provide fast toxicological screening to situations where such a measurement will save lives.

References

- 1 I.A. Buryakov, E.V. Krylov and E.G. Nazarov; International Journal of Mass Spectrometry (1993) **128**; p. 143
- 2 B.L. Carnahan and A.S. Tarassov, U.S. Patent no. 5420424 (1995)
- 3 M.R. Menlyadiev and G.A. Eiceman; Analytical Chemistry (2014) **86**; p. 2395
- 4 B.B. Schneider, T.R. Covey, S.L. Coy, E.V. Krylov and E.G. Nazarov; International Journal of Mass Spectrometry (2010) **298**; p. 45
- 5 A.A. Shvartsburg, R.D. Smith, A. Wilks, A. Koehl, D. Ruiz-Alonso and B. Boyle; Analytical Chemistry (2009) **81**; p. 6489
- 6 P. Hatsis and J. T. Kapron; Rapid Communication in Mass Spectrometry (2008) **22**; p. 735
- 7 B.M. Kolakowski and Z. Mester; The Analyst (2007) **132**; p. 842
- 8 A.A. Shvartsburg; Differential Ion Mobility Spectrometry. CRC Press. Taylor and Francis Group (2009)
- 9 E.J. Poziomek, G.A. Eiceman; Environ. Sci. Technol. (1992) 26; pp. 1313-1318
- 10 G.A. Eiceman, L. Garcia-Gonzalez, Y.F. Wang, B. Pittman, G.E. Burroughs; Talanta (1992) **39**, p. 459
- 11 H. Borsdorf and G.A. Eiceman; Applied Spectroscopy Reviews (2006) **41**; p. 323
- 12 E.V. Krylov, S.L. Coy, J. Vandermey, B.B. Schneider, T.R. Covey and E.G. Nazarov; Rev. Sci. Instrum. (2010) **81**; p. 024101
- 13 A.A. Shvartsburg and R.D. Smith; Journal of Am. Soc. Mass Spectrom. (2008) **19**; p. 1286
- 14 A.A. Shvartsburg, K. Tang, R.D. Smith; Journal of Am. Soc. Mass Spectrom. (2005) **16**; p. 1447
- 15 World Health Organisation; Global status report on alcohol and health 2014; URL: <http://www.who.int> ; accessed November 2015

-
- 16 Office for National Statistics; Alcohol-related deaths in the UK, 2014; URL: <http://www.ons.gov.uk/ons/index.html> ; accessed 23 August 2015
- 17 National Institute on Alcohol Abuse and Alcoholism, URL: <http://www.niaaa.nih.gov/alcohol-health/overview-alcohol-consumption/alcohol-facts-and-statistics>; accessed 23 August 2015
- 18 N. Brahmi, Y. Blel, N. Abidi, N. Kouraichi, H. Thabet, A. Hedhili and M. Amamou; *Clin. Toxicol. (Phila)*. (2007) **45**; p. 717
- 19 G.F. Williams, F.J. Hatch and M.C. Bradley; *Aust. Crit. Care* (1997) **10**; p. 113
- 20 The Wall Street Journal; After Poisonings, Czech Republic Bans Hard Liquor, URL: <http://www.wsj.com/articles/SB10000872396390443995604578000421386428846>; accessed 24 August 2015
- 21 J.L. Cascallana, V. Gordo and R. Montes; *Forensic Sci Int.* (2012) **220**; p. 1
- 22 E. Skrzydlewska, *Toxicol Mech Methods*. (2003) **13**; p. 277
- 23 C. Cursiefen and A. Bergua; *Br J Ophthalmol*. (2002) **86**; p. 1064
- 24 J.J. Liu, M.R. Daya, O. Carrasquillo and S.N. Kales; *Journal of Toxicol. Clin. Toxicol.* (1998) **36**; p. 175
- 25 P. Hantson and P. Mahieu; *Journal of Toxicol. Clin. Toxicol.* (2000) **38**; p. 297
- 26 ATSDR. Methanol toxicity. Agency for Toxic Substances and Disease Registry. *Am Fam Physician*. (1993) **47**; p. 163
- 27 T.P. Aufderheide, S.M. White, W.J. Brady and H.A. Stueven; *Ann. Emerg. Med.* (1993) **22**; p. 1916
- 28 C.V. Coulter, S.E. Farquhar, C.M. McSherry, G.K. Isbister and S.B. Duffull; *Clin Toxicol (Phila)* (2011) **49**; p. 900
- 29 J.M. Berg, J.L. Tymoczko and L. Stryer; *Biochemistry*. 5th edition (2002), New York: W H Freeman
- 30 M.J. Eckardt, S.E. File, G.L. Gessa, K.A. Grant, C. Guerri, P.L. Hoffman, H. Kalant, G.F. Koob, T.K. Li and B. Tabakoff; *Alcohol Clin Exp Res*. (1998) **22**; p. 998

-
- 31 B. Adinoff, G.H. Bone and M. Linnoila; *Med Toxicol Adverse Drug Exp.* (1988) **3**; p. 172
- 32 V. Zivković, B. Miletić, S. Nikolić and F. Juković; *Srp Arh Celok Lek.* (2010) **138**; p. 590
- 33 S. Stewart, D. Jones D and C. P. Day; *Trends Mol. Med.* (2001) **9**; p. 408
- 34 U. Rydberg and S. Skerfving; *Alcohol Intoxication and Withdrawal*; Plenum Press, New York (1997)
- 35 D.W. Crabb; *Keio. Journal of Med.* (1999) **48**; p. 184
- 36 National Statistics. *Statistics on Alcohol - England, 2015*; URL: www.hscic.gov.uk, accessed 23 August 2015
- 37 U.S Department of Health and Human Services NIAAA; *Alcohol and the brain neuroscience and neurobehavioral*; In: *Tenth Special Report to the US Congress on Alcohol and Health*; Rockville, MD. National Institute on Alcohol Abuse and Alcoholism (2000); p. 67
- 38 H. Marquardt, G. Siegfried, G. Schäfer, R.O. McClellan and F. Welsch; *Toxicology*; Academic Press (1999)
- 39 N-propanol alcohol; URL: <http://www.inchem.org>; accessed November 2015
- 40 J.K. Ilkin and G. Fortener; *Alcoholism Clin. Exp. Res.* (1985) **9**; p. 522
- 41 J.L. Unmack; *Health-Base Assessment and Recommendation for HEAC 2011*
- 42 M. Natowicz, J. Donahue, L. Gorman, M. Kane, J. McKissick, and L. Shaw; *Clin. Chemistry* (1985) **31**; p. 326
- 43 Isopropyl alcohol ; URL: <http://www.inchem.org>; accessed November 2015
- 44 R.J. Slaughter, R.W. Mason, D.M. Beasley, J.A. Vale, L.J. Schep; *Clin Toxicol* (2014) **52**; p. 470.
- 45 A. S. Church and M. D. Witting; *Journal of Emerg. Med.* (1997) **15**; p. 687
- 46 National Research Council (US) Committee on Toxicology; *Emergency and Continuous Exposure Limits for Selected Airborne Contaminants Volume 2*; Washington (DC): National Academies Press (US) (1984)

-
- 47 Occupational Safety and Health Administration; URL: https://www.osha.gov/pls/oshaweb/owadisp.show_document?p_table=STANDARDS&p_id=10286; accessed September 2015
- 48 E. Stremski and H. Hennes; *Pediatr Emerg Care* (2000) **4**; p. 238
- 49 BBC News; Prisoner drunk on swine flu gel; URL: <http://news.bbc.co.uk/1/hi/england/dorset/8272799.stm>; accessed September 2015
- 50 CBS News; Hand sanitizers linked to alcohol poisoning in kids, URL: <http://www.cbsnews.com/news/hand-sanitizers-linked-to-alcohol-poisoning-in-kids/>; accessed 29 September 2015
- 51 T. Limero, E. Reese, W. Wallace, P. Cheng and J. Trowbridge; *International Journal for Ion Mobility Spectrometry* (2012) **15**; p. 189
- 52 D.G. Barceloux, E.P. Krenzelok, K. Olson and W. Watson; *Journal of Toxicol. Clin. Toxicol.* (1999) **37**; p. 537
- 53 C.D. Peterson, A.J. Collins and J.M. Himes; *Eng. Journal of Med.* (1981) **304**; p. 21
- 54 C.L. Winek, D.P. Shingleton and S.P. Shanor; *Journal of Toxicol. Clin. Toxicol.* (1978) **13**; p. 297
- 55 J. Latus, M. Kimmel, M.D. Alscher and N. Braun; *Clin Kidney Journal* (2012) **5**; p. 120
- 56 J. A. Vale, B. Widdop and N. H. Bluett; *Postgraduate Medical Journal* (1976) **52**, p. 598
- 57 J. Brent; *Drugs* (2001) **61**; p. 978
- 58 C.L. Winek, W.W. Wahba, C.L. Winek Jr and T. Winek Balzer; *Forensic Science International* (2001) **122**; p. 107
- 59 G.A. Eiceman and Z. Karpas, *Ion Mobility Spectrometry*. Second edition CRC Press, Taylor and Francis Group (2005)
- 60 R.A. Miller, E.G. Nazarov and G. A. Eiceman, A. T. King; *Sensors and Actuators A* (2001) **91**; p. 301
- 61 O. Glasser; *Radiology* (1945) **45**; p. 425

-
- 62 E. Rutherford; The Velocity and Rate of Recombination of the Ions of Gases exposed to Röntgen Radiation; Philosophical Magazine, November 1897, p.422
- 63 J.J. Thomson; Conduction of Electricity through Gases. Cambridge University Press (1903) (revised 1906), London
- 64 P. Langevin; Annual Rev. of Chem. Phys. (1905) **5**; p. 245
- 65 A.M. Tyndall; The mobility of positive ions in gases. Cambridge Physical Tracts, Cambridge University Press (1938) London
- 66 R.T. Lattey; Proceedings of Royal Society of London (A) (1911) **84**; p. 173
- 67 J. E. Lovelock; Chemtech (1981) **11**; p. 531
- 68 E.W. McDaniel and E.A. Mason; The Mobility and Diffusion of Ions in Gases. John Wiley & Sons (1974) New York
- 69 F.W. Karasek; The Plasma Chromatograph.; Res. Dev. (1970) **21**; p. 34
- 70 M.J. Cohen and F.W. Karasek; Journal of Chromatogr. Sci. (1970) **8**; p. 330
- 71 H.E. Revercomb and E.A. Mason; Analytical Chemistry (1975) **47**; p. 970
- 72 T. Su, C.F. Elkie and M.T. Bowers; International Journal of Mass Spectrometry and Ion Processes (1978) **28**; p. 285
- 73 E.V. Krylov; International Journal for Ion Mobility Spectrometry (2012) **15**; p. 199
- 74 A.A. Shvartsburg,; F. Li, K.Tang and R. D. Smith; Analytical Chemistry (2006) **78**; p. 3706
- 75 E.V. Krylov, E.G. Nazarov and R.A. Miller; International Journal of Mass Spectrometry (2007) **266**; p. 76
- 76 E.V. Krylov, S.L. Coy, E.G. Nazarov; International Journal of Mass Spectrometry (2009) **279**; p. 119
- 77 N. Krylova, E.V. Krylov, G.A. Eiceman, J.A. Stone; Journal of Phys. Chem. A (2003) **107**; p. 3648
- 78 G.A. Eiceman, E.V. Krylov, B. Tadjikov, R.G. Ewing, E.G. Nazarov and R.A. Miller; The Analyst (2004) **129**; p. 297

-
- 79 R. Guevremont; Journal of Chromatography A (2004) **1058**; p. 3
- 80 R. Guevremont and R.W. Purves; Rev. Sci. Instrum. (1999) **70**; p. 1370
- 81 E.V. Krylov, E.G. Nazarov, R.A. Miller, B. Tagjikov and G.A. Eiceman; Journal of Phys. Chem. A (2002) **106**; p. 5437
- 82 E.G. Nazarov, S.L. Coy, E.V. Krylov, R.A. Miller and G.A. Eiceman; Analytical Chemistry (2006) **78**; p. 7697
- 83 D.P. Smith, K. Giles, R.H. Bateman, S.E. Radford and A.E. Ashcrofta; Journal of Am. Soc. Mass Spectrom. (2007) **18**; p. 2180
- 84 X. An, G.A. Eiceman, J.E. Rodriguez and J.A. Stone; International Journal of Mass Spectrometry (2011) **303**; p. 181
- 85 A.A. Shvartsburg, T. Bryskiewicz, R.W. Purves, K. Tang, R. Guevremont and R.D. Smith; Journal of Phys. Chem. B (2006) **110**; p. 21966
- 86 J. Marco, J.M. Orza, R. Notario, and J. L.M. Abboud, Journal of Am. Chem. Soc. (1994) **116**; p. 8841
- 87 C. B. Le Master, Prog. Nucl. Magn. Res. Spectrom. (1997) **31**; p. 119
- 88 M.T. Bowers, D.H. Aue, H.M. Webb, and R.T. McIver Jr; Journal of Am. Chem. Soc. (1971) **93**; p. 4314
- 89 E.P. Hunter and S.G. Lias; Journal of Phys. Chem. Ref. Data (1998) **27**; p. 413
- 90 S.G. Lias, J.F. Liebman and R.D. Levin, Journal of Phys. Chem. Ref. Data (1984) **13**; p. 695
- 91 A.M. Ellis and C.A. Mayhew; Proton Transfer Reaction Mass Spectrometry - Principles and Applications; Willey (2014)
- 92 D.I. Carroll, I. Dzidic, R.N. Stillwell, M.G. Horning and E.C. Horning; Analytical Chemistry (1974) **46**; p. 706
- 93 United States Environmental Protection Agency; URL: <http://www.epa.gov/radiation>; accessed December 2015
- 94 J.W. Leonhardt; J. Radioanal. Nucl. Chem. (1996) **206**; p. 333
- 95 V. Bocoş-Binţinţan, A.H. Brittain and C.L.P. Thomas; The Analyst (2002) **127**; p. 1211

-
- 96** G. Walendzik, J.I. Baumbach and D. Klockow; *Analytical and Bioanalytical Chemistry* (2005) **382**; p.1842
- 97** C.A. Hill and C.L.P. Thomas; *The Analyst* (2003) **128**; p.55
- 98** H.Y. Han, G.D. Huang, S.P. Jin, P.C. Zheng, G.H. Xu and J.Q. Li, H.M. Wang and Y.N. Chu; *Journal of Environmental Sciences – China* (2007) **19**; p.751
- 99** D. Witmer, J.F. Chen, B. Luckenbill and H.H. Hill; *Analytical Chemistry* (1994) **66**; p.2348
- 100** M.J. Waltman, P. Dwivedi, H.H. Hill, W.C. Blanchard and R.G. Ewing; *Talanta*. (2008) **77**; p. 249
- 101** J.A. Stockdale, L.G. Christophorou and G.S. Hurst; *Journal of Chem. Phys.* (1967) **47**; p. 3267
- 102** G.S. Hurst and T.E. Bortnes; *Capture of electrons in molecular oxygen.*; Health and Physics Division (1959)
- 103** A. Good, D.A. Durden and P. Kebarle; *Journal of Chem. Phys.* (1970) **52**; p. 212
- 104** R.G. Ewing, G.A. Eiceman and J.A. Stone; *International Journal of Mass Spectrometry* (1999) **193**; p. 57
- 105** E. Jazan and M. Tabrizchi; *Chemical Physics* (2009) **355**; p. 37
- 106** J. Puton, M. Nousiainen, M. Sillanpää; *Talanta* (2008) **76**; p. 978
- 107** P. Stefanowicz, K. Kapczynska, M. Jaremko and Z. Szewczuk; *Journal of Mass Spectrometry* (2009) **44**; p.1500
- 108** R. Guevremont and R. W. Purves; *Journal of Am. Soc. Mass Spectrom.* (2000) **11**; p. 1125
- 109** N. Krylova, E.V. Krylov and G.A. Eiceman; *Journal of Phys. Chem. A* (2003) **107**; p. 3648
- 110** G.A. Eiceman, E.G. Nazarov and J.A. Stone; *Analytica Chimica Acta* (2003) **493**; p. 185
- 111** G.A. Eiceman, E.V. Krylov, N.S. Krylova, E.G. Nazarov, R.A. Miller; *Analytical Chemistry* 2004 **76**; p. 4937

-
- 112** B.B. Schneider, T.R. Covey, S.L. Coy, E.V. Krylov and E.G. Nazarov; *Analytical Chemistry* (2010) **82**; p. 1867
- 113** D.S. Levin, P. Vouros, R.A. Miller, E.G. Nazarov and J.C. Morris; *Analytical Chemistry* (2006) **78**; p. 96
- 114** A. St-Jacques, J. Anichina, B.B. Schneider, T.R. Covey and D.K. Bohme; *Analytical Chemistry* (2010) **82**; p. 6163
- 115** W.B. Parson, B.B. Schneider, V. Kerttesz, J.J. Corr, T.R. Covey and G.J. Van Berkel; *Rapid Communication in Mass Spectrometry* (2011) **25**; p. 3382
- 116** T. Porta, E. Varesio, and G. Hopfgartner; *Analytical Chemistry* (2013) **85**; p. 11771
- 117** L.C. Rorrer III and R.A. Yost; *International Journal of Mass Spectrometry* (2015) **378**; p. 336
- 118** G.A. Eiceman, Y. Wang, L. Garcia-Gonzalez, C.S. Harden and D.B. Shoff; *Analytica Chimica Acta* (1995) **306**; p. 21
- 119** S.H. Kim, F.W. Karasek and S. Rokushika; *Analytical Chemistry* (1978) **50**; p. 152
- 120** NIST, National Institute of Standards and Technology; URL: <http://webbook.nist.gov/cgi/cbook.cgi?ID=C7664417&Mask=20>; accessed September 2015
- 121** T. Khayamian, M. Tabrizchi, M.T. Jafari; *Talanta* (2006) **69**; p. 795
- 122** R.R. Kunz, W.F. Dinatale and P. Becotte-Haigh; *International Journal of Mass Spectrometry* (2003) **226**; p. 379
- 123** Y. Sun and K.Y. Ong; *Detection Technologies for Chemical Warfare Agents and Toxic Vapors* (2004) CRC Press
- 124** T. Arthen-Engeland, S. Meyer-Plath, *Proceedings of the Ninth International; Chemical Weapons Demilitarization Conference, Luneburg, Germany* (2006)
- 125** Smith Detection LTD; URL: https://www.smithsdetection.com/index.php?option=com_k2&view=item&id=86:lcd-3-3&Itemid=1421&lang=en#.VqtlTvl4blU ; accessed September 2015
- 126** M. Jafari; *Talanta* (2006) **69**; p. 1054

-
- 127** G.A. Eiceman and J. Stone; *Analytical Chemistry* (2004) **74**; p. 392
- 128** G.E. Spangler, J.P. Carrico and D.N. Campbell; *Journal of Test. Eval.* (1985) **13**; p. 234
- 129** K. Daum, D. Atkinson, R. Erwing, W. Knighton and E. Grimsrud; *Talanta* (2001) **55**; p. 491
- 130** T. Bacon and K. Webber; *Acid and Halogen Gas Monitoring Utilizing Ion Mobility Spectroscopy (IMS).*; Technical Note, *Molecular Analytics* (2005)
- 131** P. Dwivedi, C. Wu and H.H. Hill; *Analytical Chemistry* (2006) **78**; p. 8200
- 132** J. Gross, *Efficiency of Electron Ionization*; *Mass Spectrometry: A Textbook*, Springer (2004) p. 196
- 133** E.A. Mason and T.W. Carr (Ed.), *Plasma Chromatography*, Plenum Press, New York (1984); p. 87
- 134** G.A. Eiceman, D.B. Shoff, C.S. Harden and A.P. Snyder; *International Journal of Mass Spectrometry and Ion Processes* (1988) **85**; p. 265
- 135** A.A. Schvartsburg, *Differential Ion Mobility Spectrometry*, CRC Press, Boca Raton, FA (2009)
- 136** S. Kandler, R.G. Lambertus, B.D. Dunietz, S.L. Coy, E.G. Nazarov, R.A. Miller and R.D. Sacks; *International Journal of Mass Spectrometry* (2007) **263**; p. 137
- 137** M. Maziejuk, J. Puton, M. Szyposzynska and Z. Witkiewicz; *Talanta* (2015) **144**; p. 1201
- 138** M.N. Danchevskaya and S.N. Torbin; *International Journal of Mass Spectrometry and Ion Processes* (1984) **56**; p. 251
- 139** R.D. Bowen, A.W. Colburn and P.J. Derrick; *Journal of Am. Chem. Soc.* (1991) **113**; p. 1132
- 140** J. Chul Choe; *Bull. Korean Chem. Soc.* (2006) **27**; p. 596
- 141** Z. Karpas, G.A. Eiceman, R.G. Ewing and C.S. Harden; *International Journal of Mass Spectrometry and Ion Processes* (1994) **133**; p. 47
- 142** G. Bouchoux, N. Choret and R. Flammang; *International Journal of Mass Spectrometry* (2000) **196**; p. 225

-
- 143** K. Buhr, S. van Ruth and C. Delahunty; International Journal of Mass Spectrometry (2002) **221**; p. 1
- 144** P. Brown, P. Watts, T.D. Mark and C.A. Mayhew; International Journal of Mass Spectrometry (2010) **294**; p. 103
- 145** L. Friedman, F.A. Long and M. Wolfsberg; Journal of Chem. Phys (1957) **27**; p. 613
- 146** S.T. Graul and R.R. Squires; International Journal of Mass Spectrometry and Ion Processes (1987) **81**; p. 183
- 147** C.L. Schalley and P.B. Armentrout; Modern Mass Spectrometry. Springer Science & Business Media (2003)
- 148** C. Warneke, J.A. De Gouw, W.C. Kuster, P.D. Goldan and R. Fall; Environ. Sci. Technol. (2003) **37**; p. 2494
- 149** R.S. Blake, K.P. Wyche, A.M. Ellis and P.S. Monks; International Journal of Mass Spectrometry (2006) **254**; p. 85
- 150** S. Inomata and H. Tanimoto; International Journal of Mass Spectrometry (2009) **285**; p. 95
- 151** P. Spanel, D. Smith, International Journal of Mass Spectrometry and Ion Processes, (1997) **167-168**; p. 375
- 152** The NIST Reference on Constants, Units, and Uncertainty. US National Institute of Standards and Technology; Accessed January 2016
- 153** M.W. Siegel; Atmospheric Pressure Ionization in T.W. Carr Plasma Chromatography Chapter 3; Plenum Press, New York (1984)
- 154** B. Eichelberger, T. Snow, and V. Bierbaum; Journal of the Am. Soc. for Mass Spectrom. (2003) **14**; p. 501
- 155** P. Kebarle; Journal of Am. Soc. Mass Spectrom. (1992) **3**; p. 1
- 156** E. Grimsrud and P. Kebarle; Journal of the Am. Chem. Soc. (1973) **5753**; p. 7939
- 157** Pick Scientific. Nitrogen Generator NG-10L-HP manual
- 158** D. Young, G A Eiceman, J Breach, A H Brittain and C.L.P Thomas; Analytica Chimica Acta (2002) **463**; p. 143

-
- 159** D. Young, C.L.P. Thomas J. Breech A.H. Brittain and G.A. Eiceman; *Analytica Chimica Acta* (1999) **381**; p. 69
- 160** V.H. Moll, V. Bocos-Bintintan and C.L.P. Thomas; GB patent no 2480803 (2011)
- 161** V.H. Moll, V. Bocoş-Binţinţan, J. Chappell, D. Hutt, A. Raţiu and C.L.P. Thomas; *International Journal for Ion Mobility Spectrometry* (2010) **13**; p. 149
- 162** L. Dillon, V. Stone, L. Croasdell, P. Fielden, N. Goddard and C.L.P. Thomas; *The Analyst* (2010) **135**; p. 306
- 163** T. Khayamian, M. Tabrizchi and N. Taj; *Analytical Chemistry* (2001) **370**; p. 1114
- 164** G. Nelson; *Gas Mixtures: Preparation and Control*. Lewis Publishers Inc. (1992)
- 165** J.M. Preston and L. Rajadhyax; *Analytical Chemistry* (1988) **34**; p. 31
- 166** D.M. Ruskiewicz, C.L.P. Thomas and G.A. Eiceman; *The Analyst* (2016) **141**; p. 4587
- 167** Gui-xia Liu, Ze-sheng Li, Yi-hong Ding, Qiang Fu, Xu-ri Huang, Chia-chung Sun, and Au-chin Tan; *Journal of Phys. Chem. A* (2002) **106**, p 10415
- 168** R. Mabrouki, Y. Ibrahim, X. Enli, M. Mautner and M.S. El-Shall; *Journal of Phys Chem. A* (2006) **110**, p. 7334
- 169** D.M. Ruskiewicz, L. Criado-Garcia , G.A. Eiceman and C.L.P. Thomas; *Journal of Breath Research* (2016) **10**; DOI 10.1088/1752-7155/10/1/017101
- 170** H.J. Martin; S. Riazanskaia and C.L.P. Thomas; *The Analyst* (2012) **137**; p. 3627
- 171** M. Ali Awan, I. Fleet and C.L.P. Thomas; *Analytica Chimica Acta* (2008) **611**; p. 226
- 172** W.B. Smith; *Tetrahedron* (2002) **58**; p. 2091
- 173** S.C. Smith, M.J. McEwan, K. Giles, D. Smith and N.G. Adams; *International Journal of Mass Spectrometry and Ion Processes* (2009) **96**; p. 77
- 174** G.A. Eiceman, Z. Karpas and H.H. Hill; *Ion Mobility Spectrometry*. Third edition; Publ. CRC Press, Taylor and Francis Group (2005)

-
- 175** J. Chappell, D.A. Hutt and P.P. Conway, Electronic system – Integration Technology Conference (2008) p. 1267
- 176** R. Smith (2014); An evaluation of miniaturised field asymmetric waveform ion mobility spectrometry hyphenated with time-of-flight mass spectrometry; Published PhD thesis. Loughborough University



Cite this: DOI: 10.1039/c6an00435k

Fragmentation, auto-modification and post ionisation proton bound dimer ion formation: the differential mobility spectrometry of low molecular weight alcohols†

D. M. Ruszkiewicz, C. L. P. Thomas* and G. A. Eiceman

Differential mobility spectrometry (DMS) is currently being used for environmental monitoring of space craft atmospheres and has been proposed for the rapid assessment of patients at accident and emergency receptions. Three studies investigated hitherto undescribed complexity in the DMS spectra of methanol, ethanol, propan-1-ol and butan-1-ol product ions formed from a ^{65}Ni ionisation source. 54 000 DMS spectra obtained over a concentration range of $0.01 \text{ mg m}^{-3}(\text{g})$ to $1.80 \text{ g m}^{-3}(\text{g})$ revealed the phenomenon of auto-modification of the product ions. This occurred when the neutral vapour concentration exceeded the level required to induce a neutral-ion collision during the low field portion of the dispersion field waveform. Further, post-ionisation cluster-ion formation or protonated monomer/proton bound dimer inter-conversion within the ion-filter was indicated by apparent shifts in the values of the protonated monomer compensation field maximum; indicative of post-ionisation conversion of the protonated monomer to a proton-bound dimer. APCI-DMS-quadrupole mass spectrometry studies enabled the ion dissociation products from dispersion-field heating to be monitored and product ion fragmentation relationships to be proposed. Methanol was not observed to dissociate, while propan-1-ol and butan-1-ol underwent dissociation reactions consistent with dehydration processes that led ultimately to the generation of what is tentatively assigned as a cyclo- C_3H_3^+ ion (m/z 39) and hydrated protons. Studies of the interaction of ion filter temperature with dispersion-field heating of product ions isolated dissociation/fragmentation product ions that have not been previously described in DMS. The implications of these combined findings with regard to data sharing and data interpretation were highlighted.

Received 22nd February 2016,

Accepted 19th May 2016

DOI: 10.1039/c6an00435k

www.rsc.org/analyst

Introduction

Alcohols' toxicity is a significant problem. Yearly deaths related to alcohols are reported as 15 500 in the UK and 88 000 in the USA¹ with ~2.5% due to acute poisoning.² The toxicological thresholds in blood have been reported as 200 mg dm^{-3} for methanol, 800 mg dm^{-3} for ethanol, and 400 mg dm^{-3} for isopropanol. High toxicity, with a risk-of-death, occurs at blood concentrations of approximately 890 mg dm^{-3} for methanol, 3500 mg dm^{-3} for ethanol and 1500 mg dm^{-3} for isopropanol.³

Methanol is associated with episodic poisoning outbreaks occurring worldwide^{4–6} from poorly purified or adulterated ethanol based products. It is the subsequent metabolism to

formic acid which is responsible for most of methanol's toxic effects in humans, including acidosis, blindness, damage to the central nervous system and death.^{4,7}

The estimated cost in the United Kingdom for the National Health Service from ethanol misuse is $\text{£}3.5 \times 10^9$ per year.⁸ Such a figure does not account for the wider societal effects associated with ethanol-dependency.^{9–11}

Accidental ingestion of isopropanol has been reported for children¹² and deliberate ingestion by adults, and young-adults in their teenage years, produces intoxication similar to ethanol.^{13,14} The toxicity of isopropanol is lower than methanol, similar to that of propan-1-ol and higher than that of the ethanol (due to the higher toxicity of the metabolic product acetone).¹⁵ Some concern has been expressed for the welfare of personnel in closed living quarters, such as spacecraft or submarines, from prolonged and continuous exposure to low concentrations.

Fuel-cell based sensors are commonly associated with the determination of the level of ethanol in breath for law enforce-

Centre for Analytical Science, Department of Chemistry, Loughborough University, UK. E-mail: C.L.P.Thomas@lboro.ac.uk

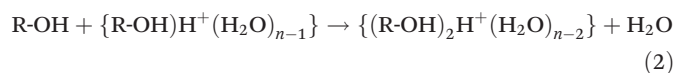
†Electronic supplementary information (ESI) available. See DOI: 10.1039/c6an00435k

ment. Other approaches have been described for the analysis of alcohols in air, breath, and include: gas chromatography (GC);^{16–18} mass spectrometry (MS);^{19–21} ion mobility spectrometry;²² and, differential ion mobility spectrometry (DMS).²³ Of particular interest to this study is the determination of alcohols by the Air Quality Monitor, a hyphenated and thoroughly integrated GC-DMS instrument, used on-board the International Space Station.²⁴

The formation of product ions within a DMS has been described elsewhere.²⁵ At ambient temperatures alcohols (R-OH) react through atmospheric pressure chemical ionisation (APCI) reactions with a hydrated proton reactant ions ($\text{H}^+(\text{H}_2\text{O})_n$) to form protonated monomers clustered with water through a displacement reaction, (1):

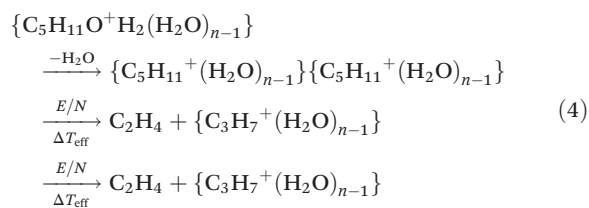
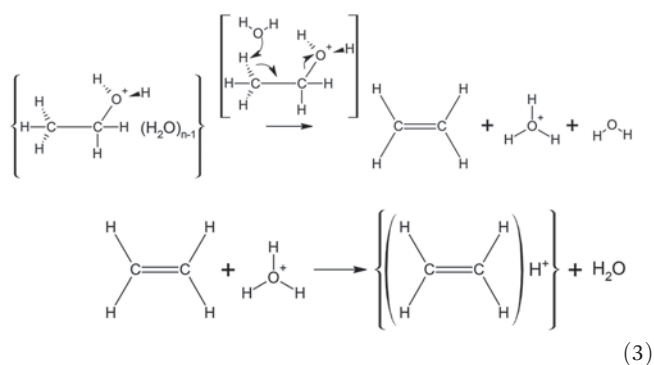


As concentrations of the alcohol (R-OH) increase, additional ion clusters, such as a proton-bound dimer, are formed per (2):



Increasing the alcohol concentration to ever higher levels can promote the formation of alcohol clusters (R-OH)_n including proton bound trimers ($n = 3$), tetramers ($n = 4$), and higher, reaching $n = 8$ in highly enriched atmospheres. Note though that n depends on temperature.²⁵

As ion energy, expressed as effective ion temperature (T_{eff}), is increased alcohol product ions decompose, and findings from proton transfer reaction mass spectrometry^{26,27} describe the dehydration of protonated monomers with increasing electric field (E/N) strength; T_{eff} was increased, see (3) and (4).



As energies are increased (T_{eff}), the protonated alkene can fragment further, (4). These reactions have been observed at

sub-ambient pressures with electric-fields of 100 Td; not unlike the field-strengths encountered with DMS.

In DMS, ions are passed by a transport gas through a channel formed from two parallel plates, the ion filter. A transverse alternating asymmetric electric field is applied across the filter and the resultant ion oscillations cause a net displacement in the ion's trajectory from the central-axis of the ion filter. This happens when ion mobility coefficients are field dependent, $K_{(E/N)}$, as shown in eqn (5):²⁵

$$K_{(E/N)} = K_{(0)}(1 + \alpha_{(E/N)}). \quad (5)$$

here $\alpha_{(E/N)}$ is a function with a polynomial fit of even powers which describes the change of the ion mobility coefficient (K) with electric field strength (E) normalized to the number density (N) as shown in eqn (6):

$$\alpha_{(E/N)} = \alpha_1^2_{(E/N)} + \alpha_2^4_{(E/N)} + \alpha_3^6_{(E/N)} + \dots \quad (6)$$

when the mobility coefficient ($K_{(E/N)}$) increases disproportionately with increased E/N or increased dispersion field (E_D), the alpha-function is termed positive and this behaviour may be attributed to several processes, the most significant of which is a cluster-decluster mechanism induced by the alternating asymmetric dispersion-field. A negative alpha-function may also be observed when the mobility coefficient decreases disproportionately with increasing dispersion-field as a result of ion heating through increased collision frequency and drag forces. The displaced ion trajectories may be restored to a stable path at the centre of the ion-filter and passed to a detector by applying a continuous weak dc electric field; termed the compensation-field.

Alpha-functions can be changed by modifying the transport gas with low molecular weight polar molecules (modifiers) at concentrations between 0.1% (v/v) to 3% (v/v). Modification of the transport gas with alcohols and other small polar molecules, including water, significantly changes the cluster-decluster phenomenon for positive alpha-function species and results in a displacement of the ion peak on the compensation-field scale. Such changes in compensation field can lead to improved separation of ion peaks.^{25,28}

The DMS spectral responses observed from the wide range of alcohol concentrations that may be encountered in direct breath monitoring for toxicity may be subject to combination of "auto-modification" of the transport gas by the alcohol analytes and post-ionisation dissociation of the protonated molecular ions. In parallel to this interest is the influence of GC-DMS instrument parameters on the resultant signals observed from samples taken on-board spacecraft. Consequently, the objective of the current study was to elucidate DMS responses to alcohols over a range of instrument parameters, with a particular interest in the influence of the dispersion-field (E/N) and transport gas temperature at ambient pressure.

Experimental

Instrumentation

A differential mobility spectrometer (model SVAC-V, Sionex, MA, USA) with a 5.0 MBq foil of ^{63}Ni ionisation source was operated with 1.18 MHz asymmetric waveform over a dispersion field (E_{D}) range 40 Td to 120 Td; the instrument setting was 10 kV cm^{-1} to 30 kV cm^{-1} . The compensation field could be scanned from -3 Td to 1 Td; -860 V cm^{-1} to $+300$ V cm^{-1} . The electrode-gap in the ion filter was 0.5 mm and the analyser region was 20 mm long. The instrument was operated using Sionex Expert software, Version 2.01. The transport-gas (300 cm^3 min^{-1} to 320 cm^3 min^{-1}) was purified nitrogen and water concentration was routinely monitored with a moisture monitor (Series 35 from Panametrics, UK) and maintained at 25 $\text{mg m}^{-3}(\text{g}) \pm 5$ $\text{mg m}^{-3}(\text{g})$ (34 ppm(v/v) ± 8 ppm (v/v)). The transport gas was mixed with the eluent from a heated 500 cm^3 round bottom exponential flask (7 cm^3 min^{-1} to 19 cm^3 min^{-1}), or a permeation source based test atmosphere generator.

A Shimadzu model 2020 mass spectrometer (Columbia, MD) was interfaced to a DMS constructed in-house using materials, dimensions, electronic control, and an ion source similar to the SVAC-V. The inlet for the DMS/MS instrument was comparable to the SVAC-V DMS. Note that in this experiment the dispersion field was used to induce ion heating and not separate the ions, and had a sinusoidal waveform. The DMS assembly included two ceramic plates with thickness of 1 mm, length of 30 mm, and width of 25 mm separated by a Teflon gasket (0.5 mm \times 30 mm \times 25 mm) with a 3 mm wide centre channel for gas and ion flow. These were held between two Teflon plates (4 mm \times 30 mm \times 25 mm) and secured under compression by two aluminium plates (5 mm \times 30 mm \times 25 mm) with six screws. At each end of this assembly were aluminium end caps ($20.5.5$ mm \times 5 mm \times 25 mm) attached to the aluminium plates with four screws. An $1/8$ " stainless steel union (Swagelok Corp., El Paso Valve and Fitting, El Paso, TX) was threaded into one cap, for inlet flow. A 111 MBq ^{63}Ni foil was fitted into the interior volume of this fitting. In the other cap, for connection to the mass spectrometer, a stainless $1/8$ " to $1/16$ " reducing union (Swagelok) was threaded and the capillary line from the mass spectrometer was held by compression in the $1/16$ " end of the union. This assembly was insulated using glass fibre insulating sheeting and the temperature was controlled by conduction from the transfer line, heated using resistive wire.

Chemicals and reagents

Methanol, ethanol, propan-1-ol, and butan-1-ol were obtained from Fisher Chemicals, Loughborough, UK; GC and HPLC purity $\geq 99.5\%$. The alcohols were purified further by purging with high-purity nitrogen and then analysed by GC-MS, the results of which indicated a purity $\geq 99.9\%$ with an additional peak identified as chloroform, which was used for cleaning the syringe, at an abundance of $<0.02\%$ of the respective alcohol peaks. Fig. S1† shows an example GC-MS of the purity

analysis, and the properties of each alcohol are given in ESI Table S1.†

Methods

Effect of vapour concentration. Alcohol test-atmospheres were delivered to the DMS at fixed dispersion-fields over six orders of magnitude concentration range by injecting 75 μl to 200 μl of a pure alcohol standard into a heated inlet, with a flow of between 6 cm^3 min^{-1} to 19 cm^3 min^{-1} of purified air passing into the exponential dilution flask.^{29–31} The exhaust from the exponential dilution flask was subsequently mixed into the transport gas of the DMS analyser; see above. A schematic of the experimental arrangement is shown in ESI Fig. S2.† Differential mobility spectra were continuously recorded by scanning the compensation field (*ca.* 1 Hz, see above) for between 12 h to 15 h, generating up to 54 000 spectra per experiment. The experimental conditions were selected to inhibit ion fragmentation while operating at the highest ion-filter temperature (T) possible (to reduce adsorption and hysteresis effects) and the lowest dispersion field (E_{D}) required to ensure resolution between the reactant and product ion species. The values chosen were: methanol $T = 60$ $^{\circ}\text{C}$ and $E_{\text{D}} = 117.6$ Td (29.4 kV cm^{-1}); ethanol, $T = 35$ $^{\circ}\text{C}$ and $E_{\text{D}} = 72$ Td (18 kV cm^{-1}) and, for propan-1-ol $T = 60$ $^{\circ}\text{C}$ and $E_{\text{D}} = 88$ Td (22 kV cm^{-1}). Other parameters for the operation of the DMS analyser are given in ESI Table S2.† The effective temperature of an ion (T_{eff}) was calculated for each dispersion-field investigated in the study by applying 1.5 $^{\circ}\text{C Td}^{-1}$ to the ion-filter temperature.³²

Mass analysis of ions. The identity of fragment ions produced by dispersion field heating was studied by a DMS/MS connected to dynamic test atmosphere generator where test-atmospheres were delivered to the DMS/MS from a 3 dm^3 exponential dilution flask at a flow rate of 1 dm^3 min^{-1} following the injection and mixing of 0.4 μl of a pure alcohol standard into the exponential dilution flask. The mass spectrometer was scanned continuously from m/z 20 to m/z 400 at 0.5 Hz over the analytes' concentration ranges of 0.02 $\text{mg m}^{-3}(\text{g})$ to 100 $\text{mg m}^{-3}(\text{g})$.

Studies of effective temperature of ions (T_{eff}). Studies of the influence of ion temperature, (T_{eff}) at a constant analyte concentration used permeation sources to generate test atmospheres. Pure alcohol standards were dispensed into 2.9 cm^3 chromatography vials and sealed with either a 0.5 mm or 0.1 mm thick PTFE membrane. The permeation sources were maintained at 40 $^{\circ}\text{C}$ for a period of five weeks and calibrated gravimetrically. A test atmosphere generator (TAG), using filtered compressed air as a diluent gas, was constructed to mix constant concentration test atmospheres into the DMS transport-gas, and replaced the exponential dilution flask in the inlet to the experiment. A schematic of the experimental arrangement is shown in ESI Fig. S2.† The concentrations of the analytes ranged from 25 $\mu\text{g m}^{-3}(\text{g})$ to 1 $\mu\text{g m}^{-3}(\text{g})$. Data were recorded in the form of dispersion plots with compensation-field scans (see above) run against a programmed increase in the dispersion field-strength; across the range 40 Td to 120 Td

(10 kV cm⁻¹ to 30 kV cm⁻¹), at ion-filter temperatures across the range 45 °C to 130 °C.

Further details of data acquisition, experimental parameters, and the permeation sources are given in the ESI Tables S2 and S3.†

Results and discussion

Concentration dependence of differential mobility spectra of alcohols

The objective of this experiment was to reveal auto-modification phenomena, and possible ion clustering artefacts in the DMS ion filter, see below. To do this the potential formation of ion fragments that would obscure the experimental observations needed to be prevented. This required balancing three experimental parameters: the ion temperature T_{eff} was to be kept below the threshold at which fragment ions would be generated; the ion-filter temperature was to be set at a temperature high enough to limit adsorption and hysteresis within the instruments that would confound the measurements; and, the

dispersion field was selected at the lowest value required to provide resolution between the reactant and product ions without causing enough ion heating to induce ion fragmentation. Differential mobility spectra for methanol, ethanol, and propan-1-ol at gas temperatures of 30 °C and 60 °C are shown in Fig. 1 as contour plots of ion intensity, compensation field strength (E_C/V cm⁻¹ and Td), and $\ln(\text{concentration})$ from 0.01 mg m^{-3(g)} to 1.80 g m^{-3(g)}. At low concentrations ion peaks for protonated monomer, proton-bound dimer and residual levels for the hydrated proton reactant ion peak (RIP) were discerned. The responses for all three compounds followed similar trends; exemplified by the ethanol responses; middle trace Fig. 1.

At concentrations below 0.2 mg m^{-3(g)} and at a temperature of 35 °C the ethanol responses show a residual RIP, a protonated monomer and a proton bound dimer at compensation fields (E_C) of -0.72 Td (-180 V cm⁻¹), -0.63 Td (158 V cm⁻¹) and -0.2 Td (50 V cm⁻¹) respectively. The peaks are not fully resolved. As the concentration increases to 0.4 mg m^{-3(g)} the RIP and protonated monomer are depleted and the proton bound dimer becomes the dominant ion species, consistent

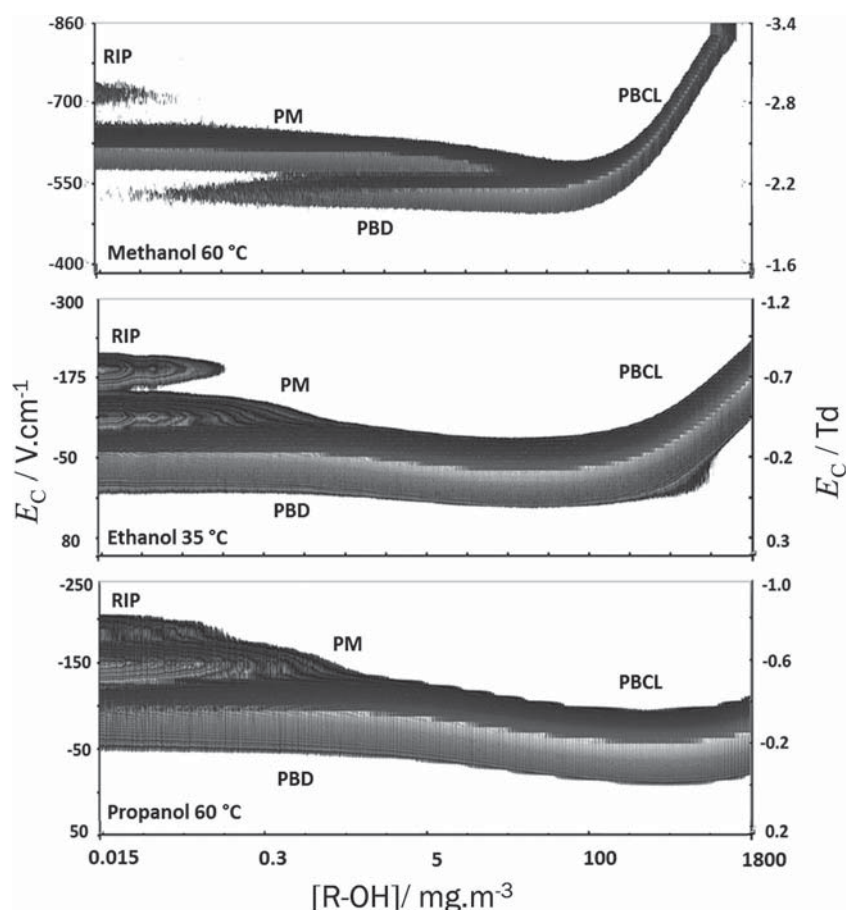


Fig. 1 Topographic plots of DMS signal intensity, compensation-field E_C and gas-phase concentration $[\text{R-OH}]$ from an exponential dilution flask for the first three n -alcohols (methanol – top, ethanol – middle and propanol – bottom) Data were collected over the concentration range from 15.0 $\mu\text{g m}^{-3(\text{g})}$ 1.80 $\text{g m}^{-3(\text{g})}$ at dispersion fields of 117.6 Td for methanol, and 72 Td for ethanol and 88 Td for propanol. (29.4 kV cm⁻¹ 18 kV cm⁻¹, and 22 kV cm⁻¹ respectively) and DMS ion-filter temperatures of 60 °C, 35 °C and 60 °C respectively for methanol, ethanol and propanol.

with (1) and (2). Calculations of distributions of ions at these concentrations are generally consistent with relative peak abundances seen in Fig. 1 (ESI Fig. S3† shows an example calculation). These patterns were observed for all alcohols with appropriate E_c values for field dependent mobility. Peak widths at half height were *ca.* 0.5 Td (126 V cm^{-1}).

Above concentrations of $0.2 \text{ mg m}^{-3}_{(g)}$, the E_c values of the protonated and proton bound dimer merged with a continuous shift in E_c for the proton bound dimer peak from -2.0 Td to $+0.32$ Td at a concentration of approximately $100 \text{ mg m}^{-3}_{(g)}$. Calculations of ion distributions show that at $50 \text{ mg m}^{-3}_{(g)}$ the fractional value for proton-bound trimer is 0.75 and trends toward a maximum at $200 \text{ mg m}^{-3}_{(g)}$ (the fractional value of proton-bound tetramer increases over 0.001 only at $400 \text{ mg m}^{-3}_{(g)}$). Since ions and unreacted sample vapour flow together through the ion filter, the shift in the peaks' compensation-field values over the range $0.01 \text{ mg m}^{-3}_{(g)}$ to $100 \text{ mg m}^{-3}_{(g)}$ may be attributed to the sequential formation of the proton bound dimer, from the protonated monomer, and then, as the concentration increases still further, the formation of proton bound trimer; denoted as a proton-bound cluster ion "PBCL" in Fig. 1.

At concentrations above $100 \text{ mg m}^{-3}_{(g)}$ the trend in the PBCL peak E_c shift reversed, so that at a concentration of 1800 mg m^{-3} the PBCL peak had an apparent E_c of -0.7 Td. Such modification of the alpha-function by high concentrations of ethanol has been described extensively in the DMS literature, and the phenomenon of an analyte modifying its DMS response may be termed auto-modification.

This interpretation of the observed responses implies that ion lifetimes exceed their residence time in the ion-filter and that ion temperatures are slightly higher than the gas temperature since the effective temperature of the ion (T_{eff}) is increased by absorbing field energy according to eqn (7):

$$\frac{3}{2}k_b T_{\text{eff}} = \frac{3}{2}k_b T + \frac{1}{2}\zeta M v_d^2 \quad (7)$$

where: k_b , Boltzmann constant; T , gas temperature; M , ion mass; and v_d , drift velocity of the ion swarm given by,

$$v_d^2 = K_0^2 N_0^2 \left(\frac{E}{N}\right)^2 \quad (8)$$

The term ζ is a correction for inefficient transfer of field energy to the ion for fragmentation. A correction from thermal to field supplemented T_{eff} is $1.5 \text{ }^\circ\text{C per Td}$ has been reported previously in two studies.^{31,33}

Spectra obtained with the DMS analyser at $100 \text{ }^\circ\text{C}$ (Fig. 2), a typical temperature for analytical applications with GC/DMS instrumentation, exhibited significant differences from those described in Fig. 1. A prominent difference was observed in the case of propan-1-ol, with ion peaks for protonated monomer and proton bound dimer being absent over the concentration range $0.02 \text{ mg m}^{-3}_{(g)}$ to *ca.* $3 \text{ mg m}^{-3}_{(g)}$ with a resolved RIP below concentrations of *ca.* $0.2 \text{ mg m}^{-3}_{(g)}$. Another significant difference was the appearance of

additional ion peak at an E_c of -1.10 Td, indicative of a smaller ion than the protonated monomer ion over a concentration range from 0.02 mg m^{-3} to 3 mg m^{-3} . Similar behaviour was also observed for ethanol, but not methanol, and these observations are indicative of fragmentation reactions.

Previous studies with proton transfer reaction mass spectrometry described the dehydration of protonated alcohols above electric-field strength of 92 Td, followed by dehydrogenation when the electric-field strength was increased above 138 Td.²⁷ The combined effect of temperature and electric-field was not described. Direct extrapolation of such mass spectrometric findings to DMS with a polarizable atmosphere with increased N was not considered trivial and consequently, studies of T and dispersion-field (E/N) interactions were undertaken and are described below.

APCI mass spectrometry of alcohols with electric field induced decomposition of ions

Ions formed in a ^{63}Ni ion source and heated with electric fields were mass-analysed and Fig. 3 describes the data obtained from propan-1-ol and butan-1-ol challenges showing how ion abundance changed as the electric-field amplitude was increased.

Propan-1-ol. At the lowest electric field strengths, below an applied voltage amplitude of 1.7 kV the proton bound dimer m/z 121 was most prominent (375 counts) with two dissociation products at m/z 61 (75 counts) and m/z 43 (250 counts) also present. Increasing the voltage amplitude to *ca.* 2.2 kV resulted in the depletion of the proton bound dimer with the abundance of the m/z 61 and m/z 43 reaching maximum intensities of *ca.* 370 counts and 340 counts respectively. Note however that another dissociation product, m/z 59, was created in parallel with the m/z 61 and m/z 43 entities, increasing in-line with increasing voltage amplitude. Above a voltage of 2.2 kV the m/z 59 dissociation product ion became the dominant species, reaching a maximum intensity at 2.5 kV, as the abundance of m/z 61 and m/z 43 ions reduced to near zero. Finally, at an applied voltage above 2.5 kV the abundance of m/z 59 fragment ion reduced to near zero accompanied by the emergence of m/z 39 dissociation product ion reaching a maximum intensity estimated to fall in the range 180 counts to 300 counts at an applied voltage of 2.9 kV.

Butan-1-ol. The electric field induced fragmentation of butan-1-ol revealed similar, albeit more complicated, behaviours to those observed for propan-1-ol. Below an applied voltage amplitude of 1.7 kV the proton bound dimer ($m/z = 149$) was most prominent. Above this value the proton bound dimer depleted rapidly with an approximate 10% yield of a dissociation product ion ($m/z = 57$) and an approximately 1% yield of hydrated protonated monomer ($m/z = 93$), Fig. 3. Increasing the voltage amplitude to 3 kV resulted in the formation of another dissociation product ion ($m/z = 39$). The relationship of the yield of the m/z 93 product ion (hydrated protonated monomer) to the voltage amplitude was not as well defined as the other species; perhaps indicating the possibility of two overlapping and unresolved profiles. The most abun-

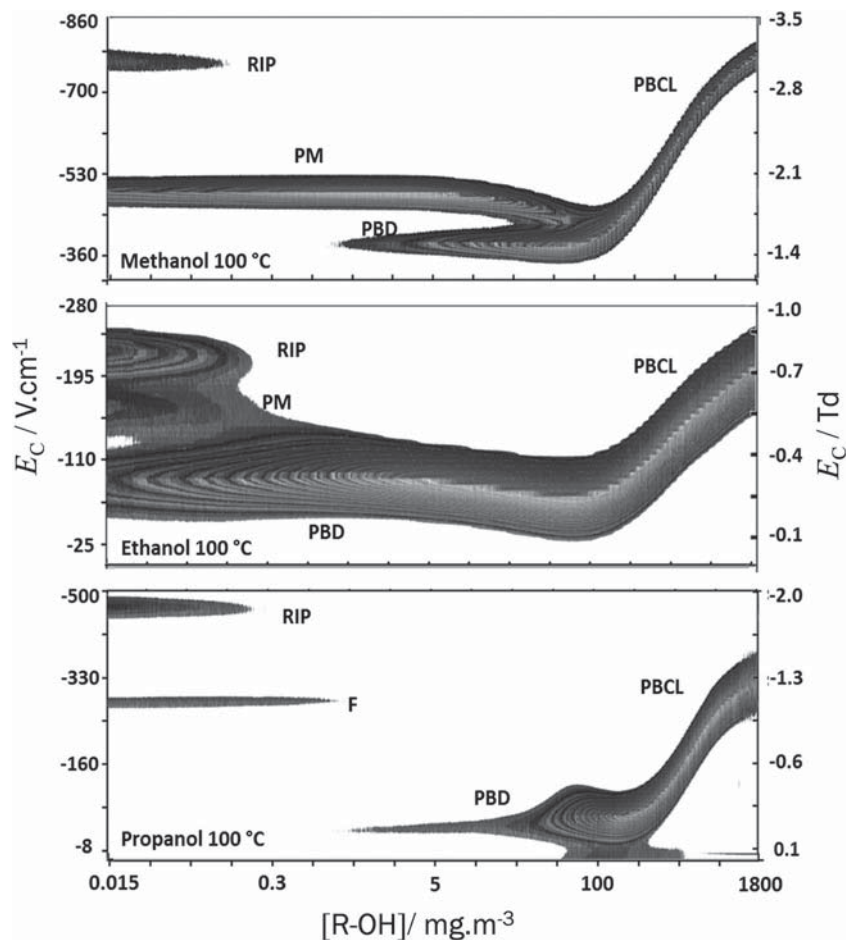


Fig. 2 Topographic plots of intensity, compensation field and vapour concentration from measurements by a DMS analyser equipped with exponential dilution flask for first three *n*-alcohols (methanol – top, ethanol – middle and propanol – bottom). Data were collected over the concentration range from $1.80 \text{ g m}^{-3}(\text{g})$ to $15.0 \text{ } \mu\text{g m}^{-3}(\text{g})$ at dispersion fields of 117.6 Td for methanol, and 72 Td for ethanol and 88 Td propanol (29.4 kV cm^{-1} 18 kV cm^{-1} and 22 kV cm^{-1} respectively), with the DMS ion-filter temperature maintained at $100 \text{ }^\circ\text{C}$.

dant dissociation product ion appeared to be related to the formation of $m/z = 57$ species. However the formation of a $m/z = 39$ dissociation product ion, at low yields (*ca.* 0.3% of the proton bound dimer intensity), starting at a dispersion voltage amplitude of about 2.5 kV indicates a carbon–carbon bond cleavage accompanied by the formation of a smaller single carbon atom entity (possibly protonated formaldehyde) that was not observed in this experiment. The appearance of the $m/z = 39$ species coincides with the maximum yield of the $m/z = 93$ and $m/z = 57$ dissociation product ions.

Influence of temperature and dispersion field

Dispersion plots for methanol, propan-1-ol, and butan-1-ol obtained at temperatures over the range $40 \text{ }^\circ\text{C}$ to $120 \text{ }^\circ\text{C}$ at constant concentrations are shown in Fig. 4–6.

Methanol. Methanol (Fig. 4) may be regarded as a reference experiment where the effect of increasing the cell-temperature on differential mobility may be discerned. The alpha-function for the protonated methanol monomer was little affected by cell-temperature, with the cluster ion $\text{CH}_3\text{OH}_2^+(\text{H}_2\text{O})_n$ being

principally a mono-hydrate. (Fractional values for $n = 2$ were calculated to be 0.14 at $80 \text{ }^\circ\text{C}$, 0.05 at $100 \text{ }^\circ\text{C}$, and 0.01 at $120 \text{ }^\circ\text{C}$). Nonetheless, changes in the alpha function for these ions were measurable and separation of the reactant ion and product ion peaks occurred at dispersion fields that decreased with increased temperature: 98 Td (24.5 kV cm^{-1}) at $80 \text{ }^\circ\text{C}$, 89 Td (22.25 kV cm^{-1}) at $100 \text{ }^\circ\text{C}$ and 78 Td (19.5 kV cm^{-1}) at $120 \text{ }^\circ\text{C}$. Increasing cell-temperature also boosts the T_{eff} of the product ion while changing the nature of the low-field cluster ion at higher dispersion fields. It is helpful to note that differential mobilities are determined by difference between the low-field, and high-field mobilities that product ions experience throughout the asymmetric waveform of the dispersion field. (Increasing cell temperature results in the mobilities of the low field ion clusters tending towards their high-field forms so reducing their differential mobility).

A minor presence of a feature attributed to an ammonium ion was observed in all methanol dispersion plots. The source of this impurity was not identified and it was not detected in the GC-MS purity assays. Note that no proton-bound methanol

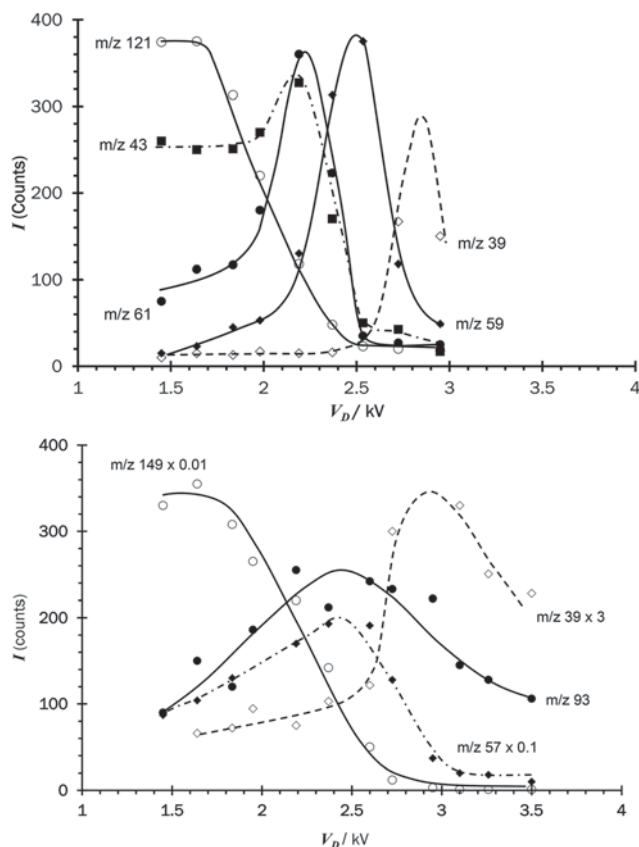


Fig. 3 Ion intensity I vs. applied ion heating voltage V_D , showing the effect of dispersion field amplitude (V_D) on ion dissociation at a DMS temperature of ca. 80 °C. Top: Ions associated with propanol showing the dissociation of a proton bound dimer ($m/z = 121$) to yield a protonated monomer ($m/z = 61$) and a dehydration fragment ion ($m/z = 43$). Increasing V_D resulted in further ion dissociation with the products at $m/z = 59$ and finally $m/z = 39$. Bottom: Ions associated with butanol (scaled to enable straightforward comparison). Here the proton bound dimer dissociates to a dehydration dissociation product ion ($m/z = 57$ at ca. 10% yield) and a hydrated protonated monomer ($m/z = 93$ at ca. 1% yield). Above $V_D = 2.5$ kV the $m/z = 39$ dissociation product was observed once more.²⁷

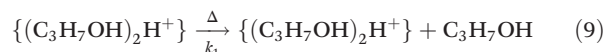
dimer or fragment ions were observed throughout this range of cell-temperatures and dispersion field strengths.

Propan-1-ol. Dispersion plots in Fig. 5 for propan-1-ol from 70 to 130 °C indicated complicated behaviours, with a feature possibly attributable to a protonated monomer discernible only at 70 °C and then only at E_D values between 60 Td (15 kV cm⁻¹) to 75 Td (18.75 kV cm⁻¹). A cluster ion was observed at E_D values from 40 Td (10 kV cm⁻¹) to 100 Td (25 kV cm⁻¹). This feature depleted rapidly with increasing E_D value and as the ion-filter temperature was increased the E_D value at which this feature ended appeared to reduce significantly. An unexpected and previously unreported phenomenon was the apparent regeneration of the RIP signal that accompanied disappearance of the cluster ion signal, indicating the creation of hydrated protons. Fig. 6, taken from propan-1-ol dispersion data at a cell-temperature of 70 °C shows the extracted ((H₃O)⁺(H₂O)_{*n*}) maximum dispersion plot signal. As E_D

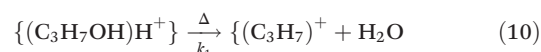
increased the intensity of the ((H₃O)⁺(H₂O)_{*n*}) signal increased from an almost zero level starting at 65 Td (17.25 kV cm⁻¹) and reaching a maximum at 84 Td (21 kV cm⁻¹), followed by a decline. In contrast the blank dispersion plot shows peak intensity decreasing smoothly with increasing E_D due to wall-losses associated with the reduction in the acceptance aperture that occurs with increasing E_D ; observed for all ions in planar embodiments of DMS. Any rise in ion intensity with increasing E_D , as shown for propan-1-ol, originates from a chemical reaction and suggests formation of (H⁺(H₂O)_{*n*}).

Accompanying the depletion of the cluster ion signal was an appearance of another ion $E_C = -1.5$ Td (-473 V cm⁻¹); $E_D = 117$ Td (29.25 kV cm⁻¹). The appearance of this ion at increasingly lower E_D values with increased temperature was consistent with the pattern of ion dissociation/fragmentation seen in the DMS-MS experiment used to study electric field induced decomposition, Fig. 3.

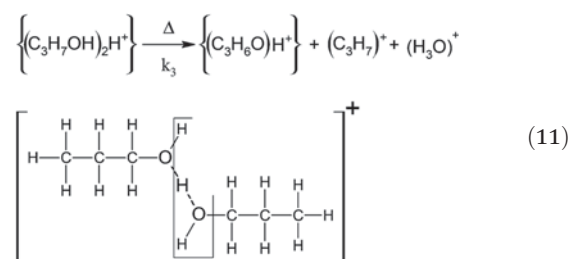
The instruments used in this study were not able to isolate and characterise fully the ion clusters observed; this will require the design and construction of a new DMS-MS instrument that isolates the product ions from neutral species before the ion filter. The underlying processes that generated the observed responses may be described in similar terms to the chemistry of alcohol product ions observed with PTRMS.²⁷ At low E_D and ion filter temperature the predominant propan-1-ol species appears to be a proton bound dimer ($m/z 121$), increasing the energy of the ion cluster causes dissociation generating a product ($m/z 61$) thought to be a protonated monomer (9).



The protonated monomer may undergo a dehydration reaction (10) resulting in a fragment ion ($m/z 43$), reported previously in PTRMS studies at electric fields of 138 Td.²⁷



The creation of an $m/z 59$ entity from propan-1-ol has not been reported, although it was observed at trace levels with propan-2-ol. Proton bound dimers were also not reported within PTRMS studies, and the difference in pressure and chemical speciation indicates that different fragmentation mechanisms may exist. The creation of $m/z 59$ species along with the production of $m/z 43$ and $m/z 19$ may be invoked through the dissociation of a proton bound dimer (11).



The $m/z 39$ fragment ($C_3H_3^+$) was observed with PTRMS studies at electric fields of 138 Td,²⁷ and is thought to result

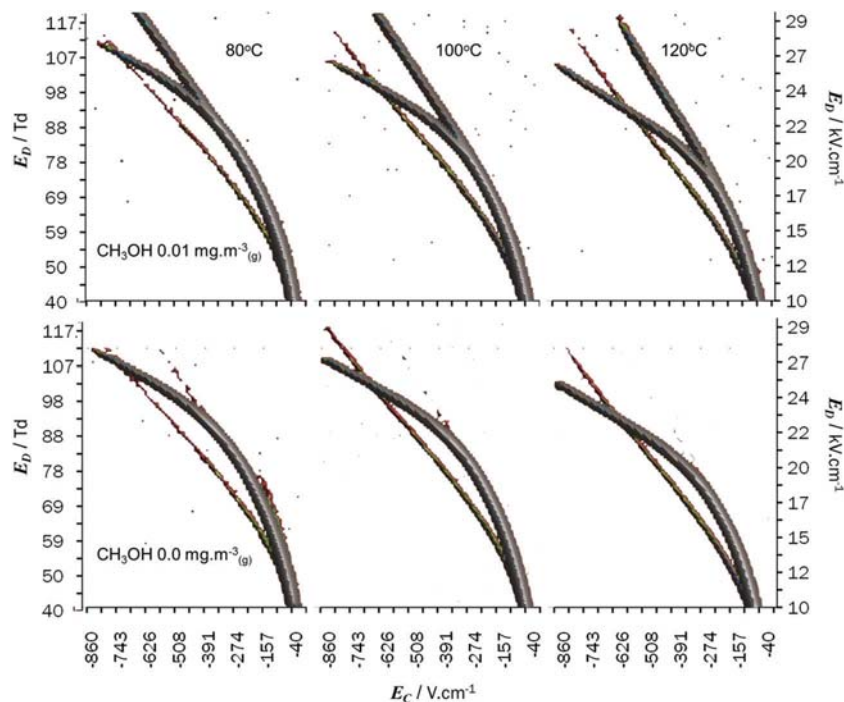
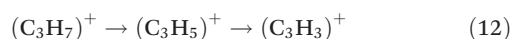


Fig. 4 Dispersion plot intensity contour maps showing the combined effect of cell-temperature and dispersion field (E_D) on compensation field (E_C). Top: Dispersion plots of methanol at $\approx 0.01 \text{ mg m}^{-3}(\text{g})$. Bottom: Blank dispersion plots. While the effect of temperature on the reactant ion hydrate proton clusters is evident, the methanol protonated monomer does not form dissociation ions and its dispersion behaviour is not affected significantly by increases in temperature over the range 80 °C to 120 °C.

from the sequential loss of H_2 (12) and at this stage the tentative assignment for C_3H_3^+ is a cyclic entity.^{34,35}



The absence of a distinctive protonated monomer signal may be explained if the dissociation of the proton bound dimer was rate limiting, and followed by subsequent fast dissociation/fragmentation ($k_1 < k_2$). This has been observed with butyl acetates in a conventional IMS drift tube,³⁶ and with esters in other DMS studies.³² This behaviour has been attributed to the energy partition and the heat capacity of the larger proton bound dimer compared to the protonated monomer. The onset of ion decomposition is remarkably sensitive to ion mass and in the instance of ethanol, the difference in mass between protonated monomer and proton bound dimer is only 46 Da. Nonetheless, the protonated ethanol monomer at 70 °C was decomposed completely at $E_D = 78 \text{ Td}$ (19.5 kV cm^{-1}) while the proton bound dimer persists until $E_D = 103 \text{ Td}$ (25.75 kV cm^{-1}).

The dispersion plots acquired at 115 °C and 130 °C (Fig. 5), show two further dissociation/decomposition processes, albeit at lower yields. The feature observed at $E_D = 110 \text{ Td}$ (27.5 kV cm^{-1}) at 130 °C is consistent with the formation of C_3H_3^+ (8). The feature branching from the hydrated proton reaction ion peak at $E_D = 72 \text{ Td}$ (18 kV cm^{-1}) and $E_D = -0.75 \text{ Td}$ (-118 V cm^{-1}) is perhaps consistent with the formation $(\text{C}_3\text{H}_7)^+$ from the decomposition of a proton bound dimer (7). In PTR-MS

studies at intermediate (115 Td) to high field strengths (138 Td) the fragment ion observed for propan-1-ol was C_3H_5^+ ;²⁷ the possible generation of such a fragment cannot be excluded in this study.

Butan-1-ol. In Fig. 6 the dispersion plots for butan-1-ol obtained at 40 °C, 45 °C, 50 °C and 70 °C show the fragmentation of protonated monomer with little or no proton bound dimer present. The formation of a dissociation/fragmentation product ion at 40 °C and $E_D = 90 \text{ Td}$ (22.5 kV cm^{-1}) is clearly evident with E_D decreasing to $E_D = 59 \text{ Td}$ (17.5 kV cm^{-1}) as the cell-temperature increases to 70 °C. This observation is consistent with the formation of the $m/z = 57$ dissociation/fragmentation ion observed in the mass spec study.

Dehydration of protonated monomers with the formation of hydrated protons

Reaction (7) postulates that $(\text{H}^+(\text{H}_2\text{O})_n)$ may be generated during dissociation and this was noted above and in Fig. 6; and was evident in the 3D plots of Fig. 5 and 7. This phenomenon was observed for propan-1-ol and butan-1-ol. Of further interest in the butan-1-ol response was the presence of two phases of $(\text{H}^+(\text{H}_2\text{O})_n)$ generation indicating the possibility of two sequential dehydration reactions.

Clustering in DMS drift tube

The apparent shift of the E_C maximum for the protonated monomer towards that for the proton bound dimer occurred over a relatively narrow range of experimental conditions of

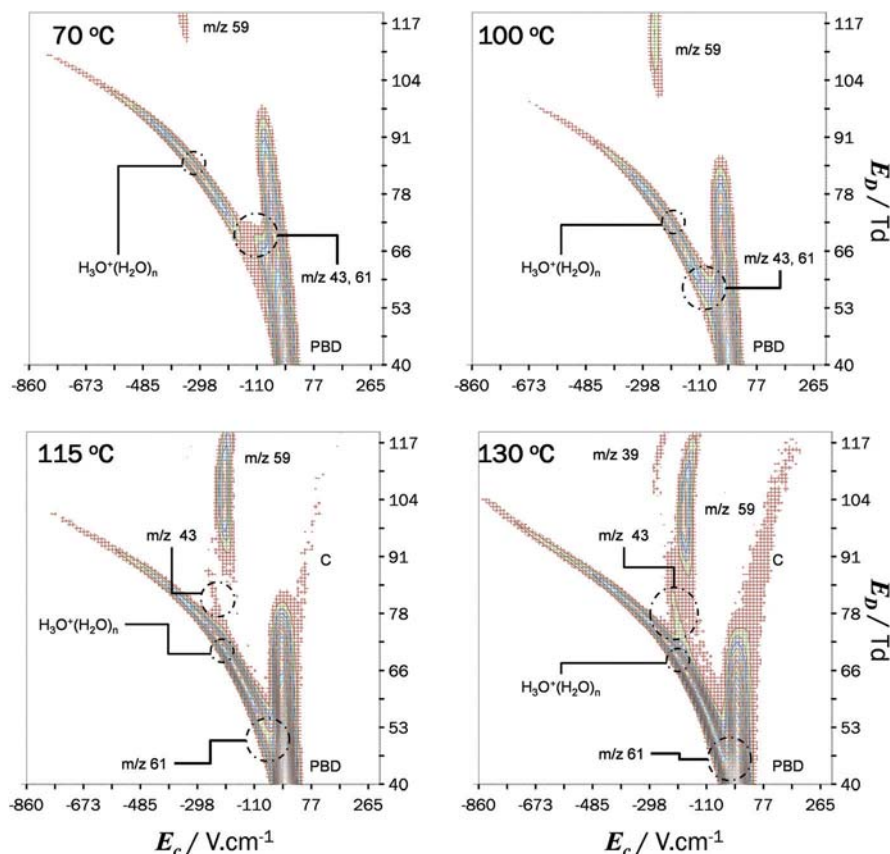


Fig. 5 Dispersion plot intensity contour maps showing the combined effect of cell-temperature and dispersion field (E_D) on compensation field (E_C) for *n*-propanol at $0.02 \text{ mg m}^{-3}(\text{g})$. The mass assignments are tentative and inferred from the DMS-MS data. Key: PBD: proton bound dimer, perhaps accompanied by mixed cluster ions; and, C: trace contamination attributed to siloxanes.

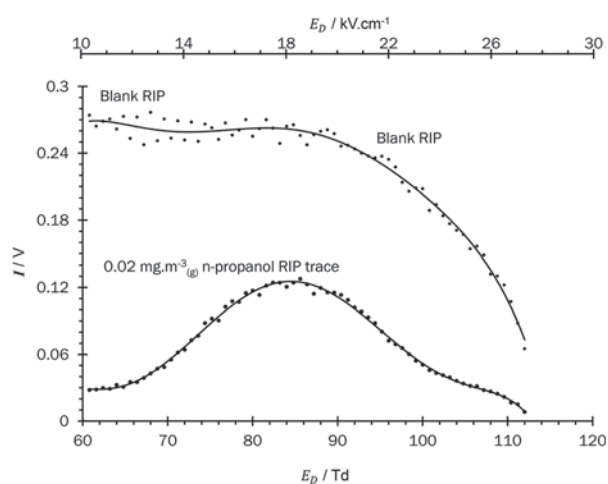


Fig. 6 Evidence of $(\text{H}^+(\text{H}_2\text{O})_n)$ formation with increasing E_D . The top trace shows the effect of increasing E_D on intensity of the $(\text{H}^+(\text{H}_2\text{O})_n)$ signal at an ion-filter temperature of $70 \text{ }^\circ\text{C}$. The signal intensity decays with the reducing acceptance aperture of the DMS. The bottom trace shows the $(\text{H}^+(\text{H}_2\text{O})_n)$ signal intensity observed under the same dispersion fields in the presence of $0.02 \text{ mg m}^{-3}(\text{g})$ propanol. At the start of the dispersion field programme the $(\text{H}^+(\text{H}_2\text{O})_n)$ signal reflects the depletion of the reactant ion peak to form PBD and PM. Increasing E_D resulted in a signal profile indicative of the regeneration of $(\text{H}^+(\text{H}_2\text{O})_n)$ in line with the dissociation and fragmentation processes postulated in eqn (9)–(11).

temperatures and vapour concentrations. This observation was unmistakable and repeatable and is apparent in Fig. 1 and 2. The number of ion-neutral collisions during the low-field segment of the waveform was well below 1, and the observed behaviour consequently cannot be described as a cluster-decluster mechanism with modification of the alpha-function. Modification of the alpha function was observed at higher vapour levels as seen in Fig. 1 and 2, where a cool ion can be solvated through 2 or more collisions.^{37–40} It is helpful to emphasise the convergence of the protonated monomer E_C maximum to the proton bound dimer compensation field maximum must be due to ion molecule collisions over time periods greater than 600 ns (the duration of the low field segment of the dispersion waveform), and be consistent with residence time of ions in the drift tube (1 to 2 ms). Two possible interpretations may be considered.

The ion may be envisaged as entering the drift tube as a protonated monomer (dotted line in Fig. S4†). A residence time of 2 ms in the DMS ion filter gives enough time for the ion to collide with a neutral alcohol molecule (ROH), creating a proton bound dimer with a different trajectory (dashed line in Fig. S4†). The result will be a shift in the ion's position on the E_C scale such that it falls between the monomer and

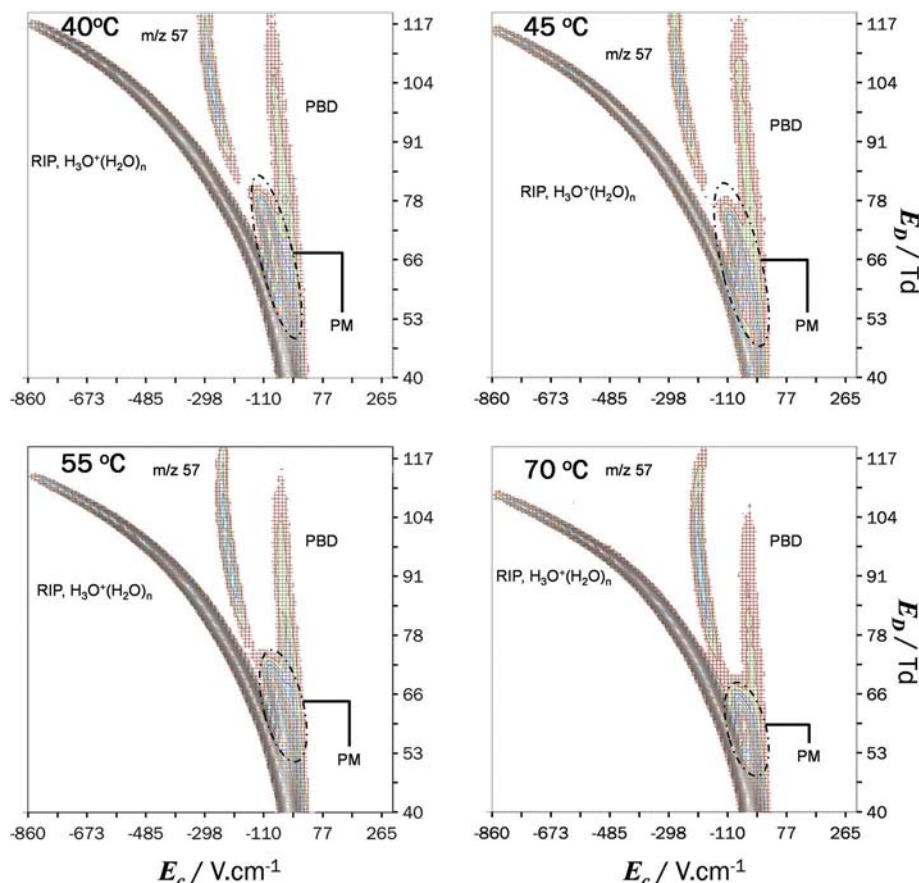


Fig. 7 Dispersion plot intensity contour maps showing the combined effect of cell-temperature and dispersion field (E_D) on compensation field (E_C) for *n*-butanol at $0.01 \text{ mg m}^{-3}(\text{g})$. Key: PBM: proton bound monomer; PBD: proton bound dimer.

proton bound dimer positions. This phenomenon is concentration dependent, the higher the concentration, the earlier the collision takes place, and the closer the modified trajectory will be to that of a proton bound dimer generated in the reaction region. The two distinct signals are seen to converge with the protonated monomer signal appearing to shift and merge with the proton bound dimer signal as the concentration increases. The ion entered the drift tube as a protonated monomer and was converted to proton bound dimer emerging at a CV which was a measure of where the conversion occurred in the ion-filter.

The alternative explanation invokes exchange between the protonated monomer and proton bound dimer during transit through the ion-filter. Collision numbers at this concentration and residence time are 20 to 50. While such interactions may be expected to cause band broadening it has been shown that exchange of neutral adducts on an ion core can be located over a range of drift times without band broadening or resolution of the two ion clusters providing the exchange is rapid in comparison to residence time in the drift tube.⁴¹

Increasing the cell-temperature inhibited this phenomenon which was eliminated at cell-temperatures above $130 \text{ }^\circ\text{C}$. While the two mechanisms cannot be unpacked from the experi-

ments here, these observations add an additional layer of complexity onto the fragmentation behaviour.

Conclusions

The experiments in this study isolated dissociation/fragmentation product ions that have not been previously described. The ion chemistries appear to be similar to those reported in PTRMS studies.²⁷ The formation of the fragment ion at m/z 39 from propan-1-ol and butan-1-ol raises the possibility of multi-step reactions and the possibility of further ion-neutral reactions. Follow-on experiments with deuterated standards at higher mass accuracy will be a logical continuation from this preliminary study to better establish the reactions and mechanisms observed here.

Whenever a DMS measurement with alcohols is above $80 \text{ }^\circ\text{C}$, dehydration reactions are possible and will be controlled by T_{eff} which is determined by the combination of the experimental parameters of cell-temperature and E_D . The onset of changes in the spectral patterns at characteristic T and E/N values varies with C-number for all alcohols except methanol, which undergoes no fragmentation. The selection

of these experimental parameters determines in large measure the resultant characteristics of the observed spectra, and the subsequent possible analytical utility of comparison of spectra between DMS platforms and laboratories.

Over a relatively narrow range of temperature and vapour concentration, ion peaks undergo a slide in E_C maxima values, and this cannot be attributed to alpha function modification. Rather, the ion is being transformed during residence in the DMS analyser. Applications for measuring alcohols should account for these behaviours.⁴² Future developments of DMS, should address these factors by designing the ionisation inlet to ensure ions pass into the DMS in filter in purified gases and unreacted sample or matrix neutrals are vented.

Acknowledgements

The authors wish to thank: the Engineering and Physical Science Research Council alongside John Hoggs Technical Solutions for the support of D. M. Ruszkiewicz through an Industrial Case Studentship Award; the researchers at NMSU for their help with the APCI MS studies, and Dr Matthew Turner at Loughborough University for his support of the laboratory experiments.

References

- National Institute on Alcohol Abuse and Alcoholism URL: <http://www.niaaa.nih.gov/alcohol-health/overview-alcohol-consumption/alcohol-facts-and-statistics>, visited 23 August 2015.
- Office for National Statistics; Defining alcohol-related deaths; discussion released 18 July 2006, URL: <http://www.ons.gov.uk/ons/index.html>, visited 24 August 2015.
- C. L. Winek, W. W. Wahba, W. W. Wienek Jr. and T. W. Balzer, *Forensic Sci. Int.*, 2001, **122**, 107–123.
- N. Brahmi, Y. Blel, N. Abidi, N. Kouraiichi, H. Thabet, A. Hedhili and M. Amamou, Methanol poisoning in Tunisia: report of 16 cases, *Clin. Toxicol.*, 2007, **45**(6), 717–720.
- G. F. Williams and F. J. Hatch, Bradley MCand case study of four patient, *Aust. Crit. Care*, 1997, **10**, 113–118.
- The Wall Street Journal; After Poisonings, Czech Republic Bans Hard Liquor, URL: <http://www.wsj.com/articles/SB10000872396390443995604578000421386428846>, visited 24 August 2015.
- EPA No CASR. (AEGLs) METHANOL report 2005 (67), URL: <http://www.epa.gov>, visited 13 July 2015.
- The NHS Information Centre; Statistics on Alcohol; England, 2013, p.53 URL: <http://www.hscic.gov.uk/catalogue/PUB10932/alc-eng-2013-rep.pdf>, visited 23 August 2015.
- U.S Department of Health and Human Services NIAAA, Alcohol and the brain neuroscience and neurobehavioral, in *Tenth Special Report to the US Congress on Alcohol and Health*, National Institute on Alcohol Abuse and Alcoholism, Rockville, MD, 2000, pp. 67–157.
- S. Stewart, D. Jones and C. P. Day, Alcoholic liver disease: new insights into mechanisms and preventative strategies, *Trends Mol. Med.*, 2001, **9**, 408–413.
- U. Rydberg and S. Skerfving, The toxicity of ethanol, in *The tentative risk evaluation, Alcohol Intoxication and Withdrawal*, Plenum Press, New York, 1977, 403–419.
- E. Stremiski and H. Hennes, *Pediatr Emerg Care*, 2000, **4**, 238–240.
- BBC News; Prisoner drunk on swine flu gel; URL <http://news.bbc.co.uk/1/hi/england/dorset/8272799.stm>, visited 29 September 2015.
- CBSNews; Hand sanitizers linked to alcohol poisoning in kids, URL: <http://www.cbsnews.com/news/hand-sanitizers-linked-to-alcohol-poisoning-in-kids/>, visited 29 September 2015.
- National library of medicine; Toxicology data network – isopropanol, URL: <http://toxnet.nlm.nih.gov/>, visited 13 July 2015.
- P. Pereira, E. Santos, T. Ferreira and J. Andrade, *Talanta*, 1999, **49**, 245–252.
- Y. Giang, S. Wang, C. Tsai, M. Lee and C. Ng, *Forensic Sci. J.*, 2007, **6**, 1–19.
- T. Macchia, R. Mancinelli, S. Gentili, E. Lugaresi, A. Raponi and F. Taggi, *J. Anal. Toxicol.*, 1995, **19**, 241–246.
- E. Gallego, X. Roca, J. Perales and X. Guardino, *J. Environ. Sci.*, 2008, **21**, 333–339.
- S. Ghimenti, S. Tabucchi, F. Bellagambi, T. Lomonaco, M. Onor, M. Trivella, R. Fuoco and F. Di Francesco, *J. Pharm. Biomed. Anal.*, 2015, **106**, 218–223.
- A. Jones, G. Mardh and E. Anggard, *Pharmacol., Biochem. Behav.*, 1983, **18**, 267–272.
- S. Sielemann, J. Baumbach, H. Schmidt and P. Pilzecker, *Anal. Chim. Acta*, 2001, **431**, 293–301.
- V. Bocos-Bintintan, V. Moll, R. Flanagan and P. Thomas, *Int. J. Ion Mobility Spectrom.*, 2010, **13**, 55–63.
- T. Limero, E. Reese, W. Wallace, P. Cheng and J. Trowbridge, *Int. J. Ion Mobility Spectrom.*, 2012, **15**, 189–198.
- G. Eiceman and Z. Karpas, *Ion Mobility Spectrometry*, Taylor and Francis Group, 2005.
- S. Inomata and H. Tanimoto, *Int. J. Mass Spectrom.*, 2009, **285**, 95–99.
- P. Brown, P. Watts, T. Märk and C. Mayhew, *Int. J. Mass Spectrom.*, 2010, **294**, 103–111.
- R. W. Purves, A. R. Ozog, S. J. Ambrose, S. Prasad, M. Belford and J. J. Dunyach, *J. Am. Soc. Mass Spectrom.*, 2014, **25**, 1274–1284.
- L. Dillon, V. Stone, L. Croasdell, P. Fielden, N. Goddard and P. Thomas, *Analyst*, 2010, **135**, 306–314.
- T. Khayamian, M. Tabrizchi and N. Taj, *Anal. Chem.*, 2001, **370**, 1114–1116.
- G. Nelson, *Gas Mixtures: Preparation and Control*, Lewis Publishers Inc., 1992.

- 32 X. An, G. Eiceman, J. Rodriguez and J. A. Stone, *Int. J. Mass Spectrom.*, 2011, **303**, 181–190.
- 33 X. An, G. Eiceman, R. Räsänen, J. Rodriguez and J. Stone, *J. Phys. Chem. A*, 2013, **117**, 6389–6401.
- 34 G.-xia Liu, Ze.-sheng Li, Yi.-hong Ding, Q. Fu, Xu.-ri Huang, C.-chung Sun and Au.-chin Tan, *J. Phys. Chem. A*, 2002, **106**, 10415–10422.
- 35 R. Mabrouki, Y. Ibrahim, X. Enli, M. Meot-Ner and M. S. El-Shall, *J. Phys. Chem. A*, 2006, **110**, 7334–7344.
- 36 G. A. Eiceman, D. B. Shoff, C. S. Harden and A. P. Snyder, *Int. J. Mass Spectrom. Ion Processes*, 1988, **85**, 265–275.
- 37 G. Eiceman, N. Krylova, E. Krylov and J. Stone, *Int. J. Ion Mobility Spectrom.*, 2003, **107**, 3648–3652.
- 38 G. Eiceman, E. Krylov, N. Krylova, E. Nazarov and R. Miller, *Anal. Chem.*, 2004, **76**, 4937–4944.
- 39 L. Rorrer and R. Yost, *Int. J. Mass Spectrom.*, 2011, **300**, 173–181.
- 40 B. Schneider, T. Covey and E. Nazarov, *Int. J. Ion Mobility Spectrom.*, 2013, **16**, 207–216.
- 41 J. Preston and L. Rajadhyax, *Anal. Chem.*, 1988, **34**, 31–34.
- 42 L. Criado-García, D. M. Ruskiewicz, G. A. Eiceman and C. L. P. Thomas, *J. Breath Res.*, 2016, **10**, 017101.



PAPER

A rapid and non-invasive method to determine toxic levels of alcohols and γ -hydroxybutyric acid in saliva samples by gas chromatography--differential mobility spectrometry

RECEIVED
21 September 2015REVISED
30 October 2015ACCEPTED FOR PUBLICATION
12 November 2015

PUBLISHED

L Criado-García^{1,3}, D M Ruszkiewicz^{2,3}, G A Eiceman² and C L P Thomas²¹ Department of Analytical Chemistry, Annex C-3 Building, Campus of Rabanales, Institute of Fine Chemistry and Nanochemistry, University of Cordoba, 14071 Córdoba, Spain² Centre for Analytical Science, Department of Chemistry, Loughborough University, Loughborough, LE11 3TU, UKE-mail: C.L.P.Thomas@lboro.ac.uk**Keywords:** methanol, ethanol, ethylene glycol, propylene glycol, γ -hydroxybutyric acid, saliva, thermal desorption gas chromatography differential mobility spectrometry

Abstract

A polydimethylsiloxane oral sampler was used to extract methanol, ethanol, ethylene glycol, 1,3-propanediol and γ -hydroxybutyric acid from samples of human saliva obtained using a passive drool approach. The extracted compounds were recovered by thermal desorption, isolated by gas chromatography and detected with differential mobility spectrometry, operating with a programmed dispersion field.

Complex signal behaviours were also observed that were consistent with hitherto unobserved fragmentation behaviours in differential mobility spectrometry. These yielded high-mobility fragments obscured within the envelope of the water-based reactant ion peak. Further, compensation field maxima shifts were also observed which were attributable to transport gas modification phenomena. Nevertheless, the responses obtained indicated that *in vivo* saliva sampling with thermal desorption gas chromatography may be used to provide a semi-quantitative diagnostic screen over the toxicity threshold concentration ranges of 100 mg dm^{-3} to 3 g dm^{-3} . A candidate method suitable for use in low resource settings for the non-invasive screening of patients intoxicated by alcohols and volatile sedatives has been demonstrated.

Introduction

Treatment of poisoning from the consumption of ethanol and the management of the intoxicated patient represents a significant burden on many health services. Further, poisoning from the consumption of other alcohols, notably methanol and ethylene glycol, occurs sporadically and from time to time outbreaks occur where food, drink or medicines are contaminated, resulting in significant mortality [1]. The essence of diagnosis is speed, and even in well-resourced healthcare settings the collection of blood samples for remote analysis may introduce delays that prevent effective treatment. In communities and regions without recourse to gold standard pathology services, or in cases where the number of patients runs into the hundreds, [2] clinical teams may be forced to

treat their patients symptomatically without recourse to reliable diagnosis. Other complications arise when intoxication from sedatives, such as γ -hydroxybutyric acid (GHB) taken intentionally or through malicious administration, is mistaken for ethanol abuse or, more seriously, is masked by ethanol consumption. Consequently it would appear there is a need, across all scales of health services, for faster point-of-care toxicity screening for methanol, ethanol, ethylene-glycol and 1,3-propanediol. It would also be helpful to be able to screen simultaneously for the presence of sedatives such as GHB and, more recently, γ -butyrolactone.

Ethylene glycol and 1,3-propanediol are highly soluble in aqueous media with Henry's law constants of $4 \times 10^6 \text{ mol kg}^{-1} \text{ bar}^{-1}$ and $910\,000 \text{ mol kg}^{-1} \text{ bar}^{-1}$ respectively, making headspace analysis (and, by implication, exhaled breath analysis) unlikely to be practicable; note that in comparison the Henry's Law constants for methanol and ethanol are $230 \text{ mol kg}^{-1} \text{ bar}^{-1}$ and $190 \text{ mol kg}^{-1} \text{ bar}^{-1}$, respectively.

³L Criado-García and D M Ruszkiewicz should be considered as joint first authors.

The utility of using saliva analysis for profiling methanol intoxication was proposed in 2009, [3] and subsequently an active membrane [4, 5] was used to recover and analyse methanol and ethanol from human saliva with determination by thermal desorption-gas chromatography-differential mobility spectrometry (TD-GC-DMS) across the concentration range 30 mg dm^{-3} to 500 mg dm^{-3} [6]. At that time, the possible utility of extending the approach to glycols was noted. In saliva fluids, drugs of abuse have been reported to be detectable for between 5 and 48 h in the ng cm^{-3} range [7] supporting the proposition of the development of saliva-based screens. Indeed, methanol and ethanol present in saliva samples have been previously determined by gas chromatography flame-ionization detection (GC-FID) with the proposition of extending the approach from confirmatory analyses to routine application in toxicology laboratories [8].

This research focussed on methanol, ethanol, ethylene glycol, 1,3-propanediol and GHB. Ethanol toxicity is dependent on individual tolerance and use, although levels greater than 3 g dm^{-3} to 4 g dm^{-3} may be fatal due to respiratory depression and blood ethanol concentrations between 500 mg dm^{-3} and 700 mg dm^{-3} may be considered to be the highest that may be tolerated without neurological effects [9]. Methanol, may cause metabolic acidosis, neurological injuries, and death when ingested. Blood-serum methanol levels greater than 200 mg dm^{-3} correlate with ocular injury, while the minimal lethal dose of methanol in adults is believed to be 340 mg kg^{-1} of body weight [10]. Ethylene glycol is moderately toxic and its toxic by-products first affect the central nervous system, then the heart, and finally the kidneys. Current recommendations are that treatment with Fomepizole is initiated immediately if blood-serum concentrations of methanol or ethylene glycol exceed 200 mg dm^{-3} . In contrast, ingestion of 1,3-propanediol is not as serious and large quantities are required to cause perceptible health damage in humans with blood-plasma concentrations over 4 g dm^{-3} associated with serious harm [11]. GHB has useful therapeutic uses such as treating narcolepsy, however, it is also a drug of abuse and is associated with assault. The therapeutic range is narrow and accidental overdosing is a common cause of injury with potentially fatal outcomes, normally associated with cardiorespiratory arrest [12].

The present work sought to extend the earlier TD-GC-DMS study to include a semi-quantitative diagnostic screen of alcohol toxicants and GHB based on a non-invasive saliva sampling methodology and establish whether direct extraction from saliva to a polydimethylsiloxane coupon [13] with recovery and analysis by TD-GC-DMS was feasible. The DMS platform was chosen as this technique has been demonstrated to be effective for the rapid, robust and sensitive detection and quantitation of alcohols in low-resource settings [14].

Experimental

Ethics, participant preparation and saliva sampling

It is helpful to note at the outset that the volunteers who participated in this research were not exposed to any chemical hazards. The study was conducted in accordance with the ethical principles of Good Clinical Practice and the Declaration of Helsinki. The local ethics committee (Ethical Advisory Committee, Loughborough University, Loughborough, LE11 2DT) approved the studies (References G10-P23 and G10-P24). Three healthy adult male non-smokers volunteered to participate in this study and gave written informed consent. The participants were recruited from Loughborough University staff, students and their social networks. Each participant provided two samples throughout the experimental campaign.

On the morning of their study visit, the participants were asked not to: brush their teeth, use any personal care products, or eat breakfast. Participants were also asked to only drink cold water, and to refrain from drinks that were flavoured, caffeinated, or contained fruit juice(s). All saliva samples were taken in an *in vivo* sample station located in a small internal room, where privacy was ensured, at the Centre for Analytical Science at the Chemistry Department of Loughborough University. A chaperone, of the same gender as the participant, was present during sample collection and access was restricted to only those researchers and participants involved in the sampling process. After an introduction to the study the participants were familiarised with the passive drool approach that was used to obtain a sample of their saliva [13], before proceeding to provide approximately 10 cm^3 of saliva. The participants sat with their head tilted forward to cause saliva to pool at the front of their mouth and then drain from their lips into a glass collection vial. On completion of sampling the vial was sealed promptly with a TeflonTM-faced screw-top cap. Immediately after sampling, the saliva was transferred to the laboratory where 1.8 cm^3 aliquots of the saliva sample was pipetted into 2 cm^3 chromatography vials, which were sealed immediately with a screw cap fitted with a silicone septum. These saliva aliquots were used immediately, within 3 h of collection and maintained at ambient temperature ($20 \text{ }^\circ\text{C} \pm 2 \text{ }^\circ\text{C}$) until disposal. Saliva residues were disposed of immediately after use by diluting with a disinfectant solution and rinsed down a sink with a copious flow of running water. No cells or DNA were retained or stored.

Chemicals

Ethanol, methanol, ethylene glycol, propylene glycol, sodium chloride (purity of these compounds was $\geq 99.8\%$) and butanoic acid, 4-hydroxy-, ammonium salt (GHB) in methanol (1 mg cm^{-3}) were obtained from Sigma: see table 1. The carrier gas was obtained from BOC, UK, and purified by passing it through two triple-bed gas purifiers mounted in series (Thames Restek). Nitrogen was generated on

Table 1. Summary of chemicals used in the experimental procedure.

Compound	IE/eV	PA/kJ mol ⁻¹	T _{Bp} /°C	CAS	Formula
Methanol	10.84	754.3	64.7	67-56-1	CH ₃ OH
Ethanol	10.48	776	72.6	64-17-5	C ₂ H ₅ OH
Ethylene glycol	10.55	815	197.3	107-21-1	C ₂ H ₆ O ₂
Propylene glycol	10.80	876.2	182.2	57-55-6	C ₃ H ₈ O ₂
GHB ^a	n.f.	n.f.	295.6	591-81-1	{C ₄ H ₇ O ₃ } ⁻ {NH ₄ } ⁺

^a Obtained as a methanolic solution of concentration 1 mg cm⁻³ in CH₃OH.

Note: IE: ionization energy, PA: proton affinity, T_{Bp}: boiling point, n.f: data not found.

site (PEAK Scientific, UK, model nk-10L-HP) and purified by passing it through a charcoal adsorbent-bed gas purifier (Varian), a moisture filter (Varian), and a triple-bed gas purifier (Thames Restek), all mounted in series. Water (>18 MΩ) was generated on site.

PDMS saliva sampler

A titanium cylinder (6 mm long, 2 mm OD C-SPTD5-6MM Markes International Ltd) coated on the internal and external surfaces with polydimethylsiloxane (internal wall thickness 1 μm and external wall thickness 0.5 mm) was used to recover volatile organic compounds (VOCs) from the saliva. This approach has been described previously for the *in vivo* sampling of saliva VOCs [13]. The saliva sampler was prepared by cleaning it with Milton[®] sterilising liquid (Suffolk, UK) and then rinsing with deionised water before conditioning under vacuum at 190 °C for 15 h. Once conditioned, the PDMS rods were inserted into a cleaned and conditioned glass thermal desorption tube and thermally desorbed for 10 min at 190 °C; the resultant GC-MS trace provided verification that the PDMS sampling media was free of contamination. On removal from the thermal desorption unit the thermal desorption tube containing the PDMS-coated titanium cylinder was immediately capped, sealed and stored at 4 °C. Before use, the saliva samplers were thermally desorbed again under the conditions in table 3 to remove any traces of possible VOC contamination that may have occurred during storage and to provide further verification that the sampler was free of contamination.

Instrumentation

Two instrument configurations were used in this study. Method development and calibration were undertaken using liquid injections into a GC-DMS. Characterisation of the recovery of the analytes from spiked saliva samples was undertaken using a thermal desorption unit interfaced to the GC-DMS (figure 1).

Multi-linear regression was used to optimise the differential mobility spectrometer operating parameters of: dispersion-field; temperature; number of compensation field steps; and compensation field step duration (DOE PRO XL Software for Microsoft Excel, SigmaZone). Data were generated from a central composite design (CCD) with each of the four factors at four levels with replicates at five different concentrations: see

table 2 [15]. The DMS parameters were optimised for maximum sensitivity while maintaining ‘satisfactory’ resolution between the ion clusters generated within the ⁶³Ni ionisation source see table 3, and figures 2–4.

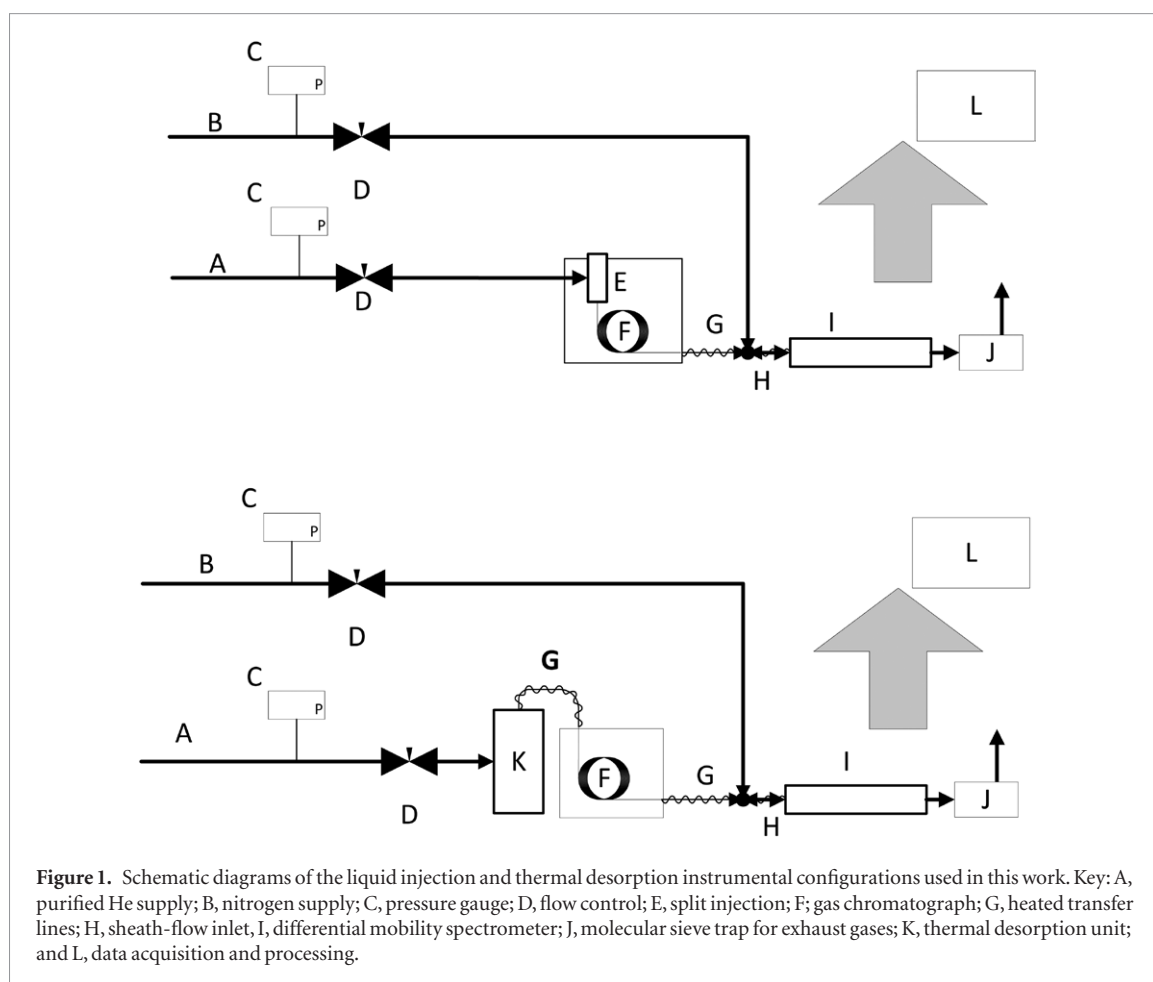
Calibration of the DMS under optimised conditions was undertaken using gas chromatography to introduce known on-column masses of the analytes injected in a solution of dichloromethane (figure 1 and table 3). A 30 m long wall-coated open-tubular capillary GC column with an internal diameter of 0.32 mm and a 0.5 μm thick trifluoropropylmethylpolysiloxane stationary phase (Rtx-200MS, Restek, UK) was interfaced to a DMS with a heated transfer line configured as a sheath flow interface [16] made from a 20 cm length of ¼" stainless steel tubing with the GC-column axially aligned within the tube. The transfer line was heat-traced with heating tape and maintained at 100 °C.

The DMS used in the study was a planar device (SDP-1 Sionex, MS USA) with a 0.5 mm gap between the two parallel electrodes and a 5.9 MBq ⁶³Ni ionisation source. The DMS was controlled through a virtual instrument (Sionex DMx Expert, Version 2.4.0) run on a Dell laptop (Inspiron, 4000). The data were saved to a Microsoft Excel spreadsheet file for post-run processing. The transport gas was purified nitrogen with water concentrations maintained in the range 22.5 to 26.3 mg m⁻³ (Panametrics Series 35 hygrometer)

A two-stage thermal desorption unit (Markes International Unity 2) was used to recover VOC extracts from saliva samples, with a cold trap for refocusing the recovered VOCs, packed with a mixed bed of Tenax TA and Carbograph 1TD. The 1.5 m long transfer line to the GC-column was a deactivated methyl-capped capillary column (Restek, UK) with an internal diameter of 0.23 mm ID maintained at 110 °C.

Characterisation of spiked saliva samples

The concentration ranges used in this study are summarised in table 4. A 100 mg cm⁻³ aqueous stock solution of ethanol, methanol, ethylene glycol, and 1,3-propanediol was prepared and aliquots of the volumes required to generate the required concentrations were spiked into the saliva samples within three hours of the saliva being collected. To account for the lower concentration of the GHB standard, and to maintain a constant saliva background in the GHB characterisation experiments, a different approach was adopted. Here 0.9 cm³ of the saliva was



used, and spiked with the required aliquot volume of the 1 mg cm^{-3} GHB methanolic solution, before the volume was made up to 1.8 cm^3 with physiological saline ($\text{NaCl}_{(\text{aq})} 8.5 \text{ g dm}^{-3}$). The ammonia present in the saliva and the GHB salt co-eluted with methanol and suppressed the formation of methanolic product ions (ammonia has a higher proton affinity than methanol). This interference was eliminated by the addition of $150 \mu\text{l}$ of 8 % HCL solution into the saliva samples before the sampling rod was placed into the vial.

Once the analytes had been added, the saliva standards were homogenised. Immediately after this had been done, a PDMS-coated titanium cartridge was removed from its sealed thermal desorption tube and placed into the vial, which was then sealed immediately. It was important that this procedure was undertaken in a fast and reproducible manner to minimise the effects of evaporative losses in the study. The sealed vial was then placed into a heating block, maintained at 37°C for 10 min. At the end of the extraction time, the vial was uncapped and the PDMS-coated titanium cartridge was removed with stainless steel tweezers and excess fluid removed by gently wiping it with a lint-free wipe ('Kimcare' Kimberly-Clark Professional, UK). The PDMS-coated titanium cartridge was then placed immediately into its glass thermal desorption tube and analysed. Cross-contamination checks were run by taking blank runs between every measurement.

Results and discussion

Evaluation of responses

Figure 2 shows the GC-DMS response surfaces from methanol (A), ethanol (B), ethylene glycol (C), 1,3-propanediol (D) and GHB (E) at three levels of column loading that span the ranges of analyte concentrations associated with the physiological thresholds of these compounds. The four dispersion-field levels used (table 3) enabled analytical responses to be resolved.

Figure 3 shows background subtracted differential mobility spectra obtained from the responses shown in figure 2 for methanol (A), ethanol (B) and ethylene glycol (C), while figure 4 compares the responses for 1,3-propanediol(D) and GHB (E). The dotted lines in these figures indicate the boundary of the reactant ion peak that was removed by the background subtraction in the data processing. The observed responses were complicated with shifts in compensation field maxima with increasing concentration, and the generation of features embedded within the reactant ion peak that were only discernible after background subtraction. Such phenomena were indicative of the formation of fragment ions, either by themselves or concurrently with 'auto-modification' of the alpha functions of the product ion.

With a dispersion field of 25 kV cm^{-1} and a column loading of 10.2 ng , methanol yielded two peaks,

Table 2. Top: DMS factor levels selected for response optimisation study, bottom operational parameters selected (predicted from multiple linear regression)

Ref.	$E_d/\text{kV.cm}^{-1}$	$T/^\circ\text{C}$	N	$\delta t/\text{ms}$	Ref.	$E_d/\text{kV.cm}^{-1}$	$T/^\circ\text{C}$	N	$\delta t/\text{ms}$
1	20	80	50	10	14	25	120	50	50
2	20	80	50	50	15	25	120	100	10
3	20	80	100	10	16	25	120	100	50
4	20	80	100	50	17	22.5	100	75	30
5	20	120	50	10	18	22.5	100	75	30
6	20	120	50	50	19	20	100	75	30
7	20	120	100	10	20	25	100	75	30
8	20	120	100	50	21	22.5	80	75	30
9	25	80	50	10	22	22.5	120	75	30
10	25	80	50	50	23	22.5	100	50	30
11	25	80	100	10	24	22.5	100	100	30
12	25	80	100	50	25	22.5	100	75	10
13	25	120	50	10	26	22.5	100	75	50

Compound	$E_d/\text{kV.cm}^{-1}$	$T/^\circ\text{C}$	N	$\delta t/\text{ms}$
Methanol	25	100 (108)	110 (60)	10 (48)
Ethanol	18	100 (80)	110 (60)	10 (50)
Ethylene glycol	23	100 (100)	110 (75)	10 (10)
Propylene glycol	23	100 (120)	110 (75)	10 (30)
GHB	21	100	110	10

Note: E_d is the dispersion field (some instruments use the term radiofrequency voltage); T is the gas temperature within the ion filter, sometimes referred to as ‘cell’ temperature; N is the number of steps in the differential mobility compensation field scan (defining the fidelity of the spectral features); and, δt is the dwell time for each step in the compensation field scan (defining the sensitivity of the response). The combination of N and δt defines the chromatographic performance of the system.

The heating and cooling rates of the DMS cell were too slow to enable multiple levels to be selected within a single chromatographic run. Further, switching the number of steps and step duration in the DMS spectra during a chromatographic run was not possible. Consequently, mid-range levels were used.

attributed to a hydrated protonated monomer cluster ion at a compensation field of -511 V cm^{-1} , which was obscured within the reactant ion peak, and a hydrated proton-bound dimer ion at -439.6 V cm^{-1} . Reducing the column loading to 2.0 ng resulted in a compensation field shift for the hydrated protonated monomer cluster ion to -502 V cm^{-1} accompanied by a hydrated proton-bound dimer response at between -444 V cm^{-1} and -439.6 V cm^{-1} . At a lower limit of a 0.20 ng column loading, only one peak was observed at -439.6 V cm^{-1} . These observations are consistent with an increase in the alpha-function [17] of a hydrated protonated methanol cluster ion with increasing methanol concentration [18] (modification of the transport gas) accompanied by the formation of a proton-bound dimer with increasing methanol concentration, albeit observed at the same compensation field as the unmodified hydrated protonated monomer cluster ion response observed at concentrations below the threshold at which proton-bound dimers form.

At a dispersion field of (18 kV cm^{-1}) ethanol also yielded a complicated response with features consistent with the generation of fragment ions overlaid with unresolved hydrated protonated monomer cluster ions, and hydrated proton-bound cluster ions, observed to fall at approximately -154.2 V cm^{-1} for the hydrated protonated monomer cluster-ion and -122.8 V cm^{-1}

for the proton-bound dimer cluster ion. Two features attributed to fragment ions were noted to be obscured within the reactant ion peak. One was at a compensation field of -238 V cm^{-1} at a column loading 40.7 ng and -230 V cm^{-1} at column loadings of 15.3 ng and 5.1 ng. The other was present at -216.6 V cm^{-1} at 40.7 ng, shifting to -207.6 V cm^{-1} at 15.3 ng and 5.1 ng.

At a dispersion field of 22 kV cm^{-1} ethylene glycol produced a clearly resolved feature at -51.6 V cm^{-1} , attributed to a proton-bound dimer cluster ion, along with two features obscured by the reactant ion peak. The weakest of these features, completely obscured by the reactant ion peak was observed at a compensation field of -403.8 V cm^{-1} across the range of column loading with no indication of auto-modification observed. However, the other feature, partially obscured by the reactant ion peak, was observed to shift from a compensation field of -359.2 V cm^{-1} , with a column loading of 81 ng, to -337 V cm^{-1} with a column loading of 14.3 ng. The lowest column loading applied generated a low-intensity split peak that straddled -337.4 V cm^{-1} . At the same dispersion field (22 kV cm^{-1}) 1,3-propanediol yielded two features, both resolved from the reactant ion peak. The peak at a compensation field of 15.4 V cm^{-1} was attributed to a proton-bound dimer ion cluster. The feature attributed to a hydrated monomer-ion cluster was observed to shift to more negative

Table 3. Instrument parameters.

Parameter	GC-DMS	TD-GC-DMS	Units
Gas chromatograph conditions			
Carrier gas	He	He	
Injection temperature	200		°C
Split flow	10.2	see below	cm ³ min ⁻¹
Carrier gas flow	1.5	1.5	cm ³ min ⁻¹
Carrier gas pressure	172	172	kPa
Phase	Trifluoropropylmethylpolysiloxane		
Column length	30	30	m
Column diameter	0.32	0.32	mm
Phase thickness	0.5	0.5	μm
Temperature start	30	30	°C
Hold-time start	1.5	1.5	min
Temperature ramp-1	6	6	°C min ⁻¹
End temperature-1	60	60	°C
Hold-time-1	2	2	min
Temperature ramp-2	20	20	°C min ⁻¹
Temperature final	180	180	°C
Hold time final	2	10	min
Differential mobility spectrometry			
Transport gas	N ₂	N ₂	
Dispersion field frequency	1.2	1.2	MHz
Dispersion field mark-space ratio	1:3	1:3	
[H ₂ O] in transport gas	22.5–26.3	22.5–26.3	mg m ⁻³
Transport gas flow rate	300	300	cm ³ min ⁻¹
DMS cell temperature	100	100	°C
Compensation field scan range	–500 to 100	–500 to 100	V cm ⁻¹
Compensation field scan increment	109.1	109.1	V cm ⁻¹
Compensation field scan dwell time	10	10	ms
Dispersion field start	25	25	kV cm ⁻¹
Dispersion field start hold time	0–125	0–125	s
Dispersion field step-1	18	18	kV cm ⁻¹
Dispersion field step-1 hold time	125–185	125–185	s
Dispersion field step-2	23	23	kV cm ⁻¹
Dispersion field step-2 hold time	185–600	185–600	min
Thermal desorption			
Tube purge duration		1	min
Tube purge flow		32	cm ³ min ⁻¹
Tube purge temperature		35	°C
Primary desorption temperature		180	°C
Primary desorption split		0	cm ³ min ⁻¹
Primary desorption time		5	min
Cold trap low temperature		0	°C
Secondary desorption temperature		300	°C
Secondary desorption split		12	cm ³ min ⁻¹
Secondary desorption time		5	min

compensation fields with increasing column loading. At 80 ng the peak maximum was at a compensation field of -283.4 V cm^{-1} , shifting to -261.2 V cm^{-1} when the column loading was reduced to 2.7 ng.

GHB also showed complex behaviour with a dispersion field of 23 kV cm^{-1} . In addition to well-resolved hydrated protonated monomer cluster ions and proton-bound dimer cluster ions, fragment ions obscured

within the RIP envelope were also evident, and the compensation field maxima of these fragment ions shifted with increasing column loading of GHB. Hydrated protonated monomer cluster ions had a compensation field peak maximum at -131.8 V cm^{-1} and the proton-bound dimer compensation field maxima was observed at 33.2 V cm^{-1} . No discernible trend in a shift in compensation field maxima was observed with column

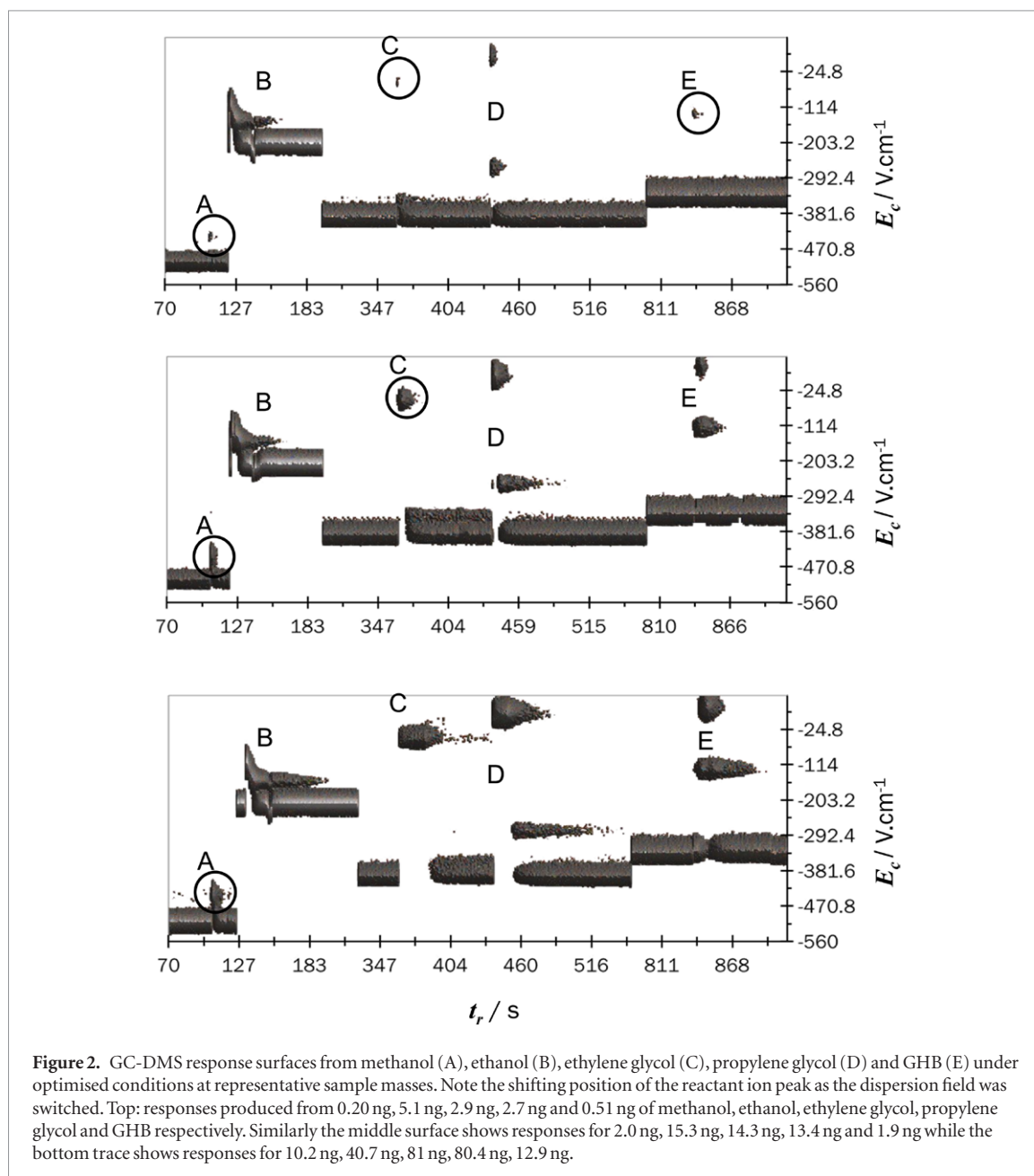
Table 4. Summary of the concentration ranges selected for the calibration of the DMS ($[i]_{(liq)}$) and the subsequent aliquot volumes ($V_{(s)}$) and the concentrations of the spiked saliva standards $[i]_{(s)}$ used to characterise the recovery of the analytes by TD-GC-IMS.

Compound	$[i]_{(liq)}/\text{mg dm}^{-3}$	$B_0/V \text{ s}$	$B_1/V \text{ s ng}^{-1}$	LoD ^a /ng	R^2
Methanol	10–250	−0.02	0.27	0.42	0.994
Ethanol	250–1000	−8.22	0.28	4.62	0.983
Ethylene glycol	100–500	−0.02	0.27	0.52	0.994
Propylene glycol	100–500	−0.48	0.30	1.42	0.997
GHB	20–500	−0.18	0.31	0.63	0.995

^a Estimated from linear regression.

Note: These ranges relate to the linear portion of the calibration range where the integrated peak volume (I) was given by:

$$I(V \text{ s}) = B_0(V \text{ s}) + B_1(V \text{ s ng}^{-1}).$$



loading for the hydrated protonated monomer cluster ion, and the proton-bound dimer was not formed at the lowest column loading of 0.51 ng. At a column loading of 12.9 ng two unresolved fragment ions were discernible within the RIP envelope. The most intense feature was at 310.2 V cm^{-1} with a shoulder

at -296.8 V cm^{-1} . Reducing the column loading to 1.9 ng resulted in a single fragment ion with a compensation field peak maximum at -301.2 V cm^{-1} and at a column loading of 0.51 ng the fragment ion was still observable with a compensation field peak maximum of -288 V cm^{-1} .

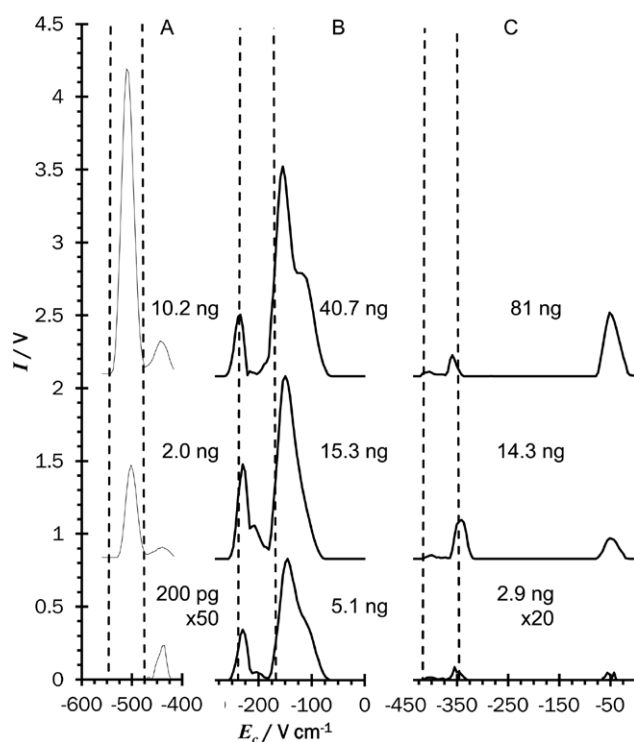


Figure 3. Background subtracted differential mobility spectra extracted from the GC-DMS response surface shown in figure 2 for methanol (A), ethanol (B), and ethylene glycol (C) under optimised conditions at representative sample masses. The dotted lines indicate the position of the reactant ion peak in the spectrum (hydrated proton clusters).

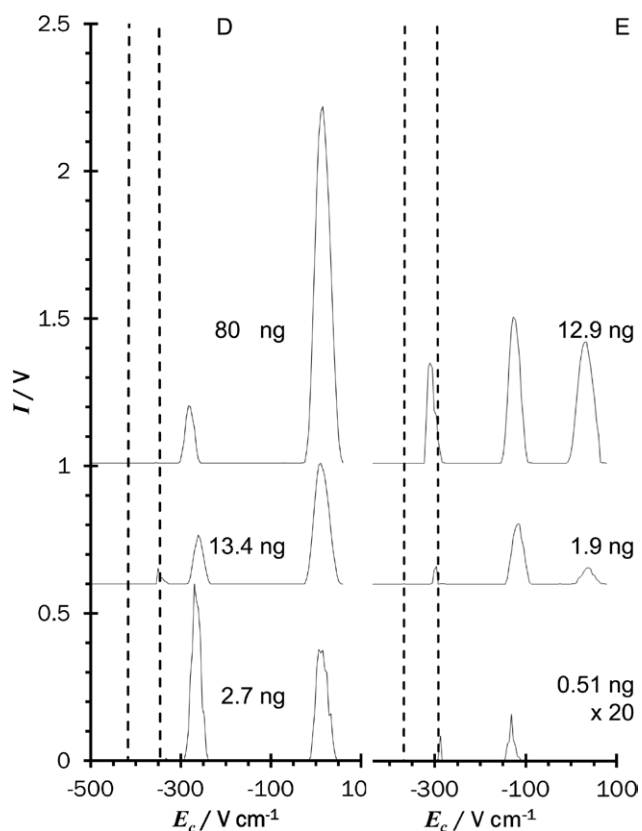


Figure 4. Background subtracted differential mobility spectra extracted from the GC-DMS response surface shown in figure 2 for 1,3-propanediol (D) and GHB (E) under optimised conditions at representative sample masses. The dotted lines indicate the position of the reactant ion peak in the spectrum (hydrated proton clusters).

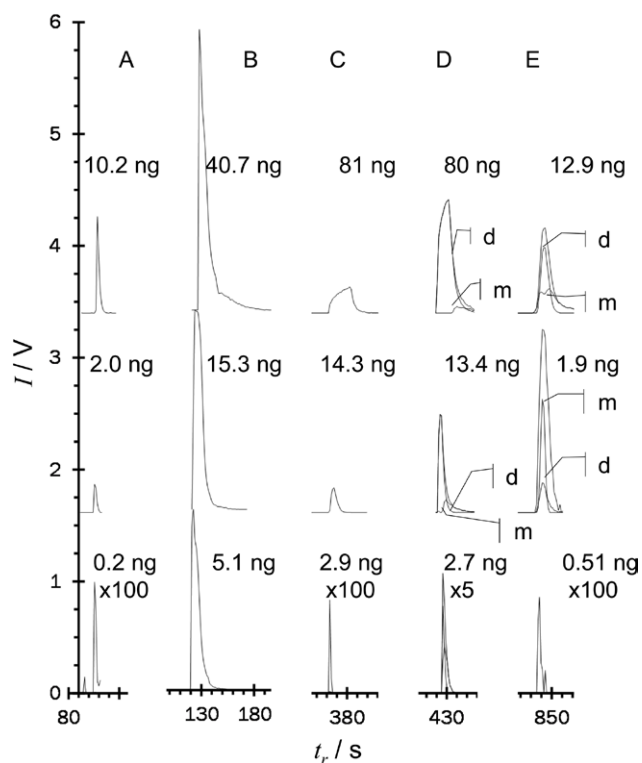


Figure 5. Selected differential mobility chromatography for methanol (A), ethanol (B), ethylene glycol (C), 1,3-propanediol (D) and GHB (E) under optimised conditions at representative sample masses. Protonated monomer (m) and proton-bound dimer (d) responses are shown for propylene glycol and GHB as well as the total ion responses, see figures and 4. The responses shown for methanol, ethanol and ethylene glycol are the total ion responses, see figure 3.

AQ1

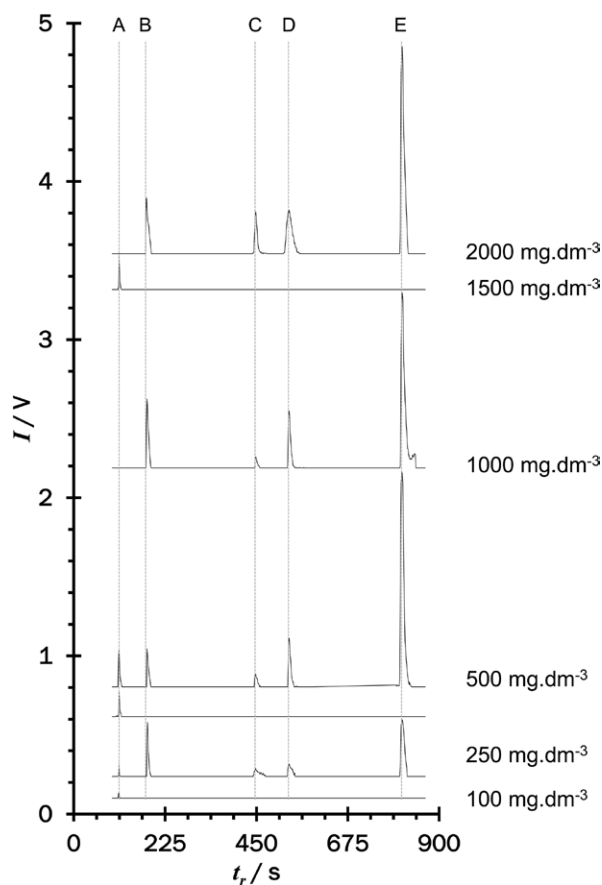


Figure 6. Selective compensation field gas chromatographic traces obtained by thermal desorption gas chromatography differential mobility spectrometry of saliva samples spiked with the five analytes at the concentration ranges studied. See table 3 for the instrumentation parameters. Note that the chromatography has been aligned during post-processing.

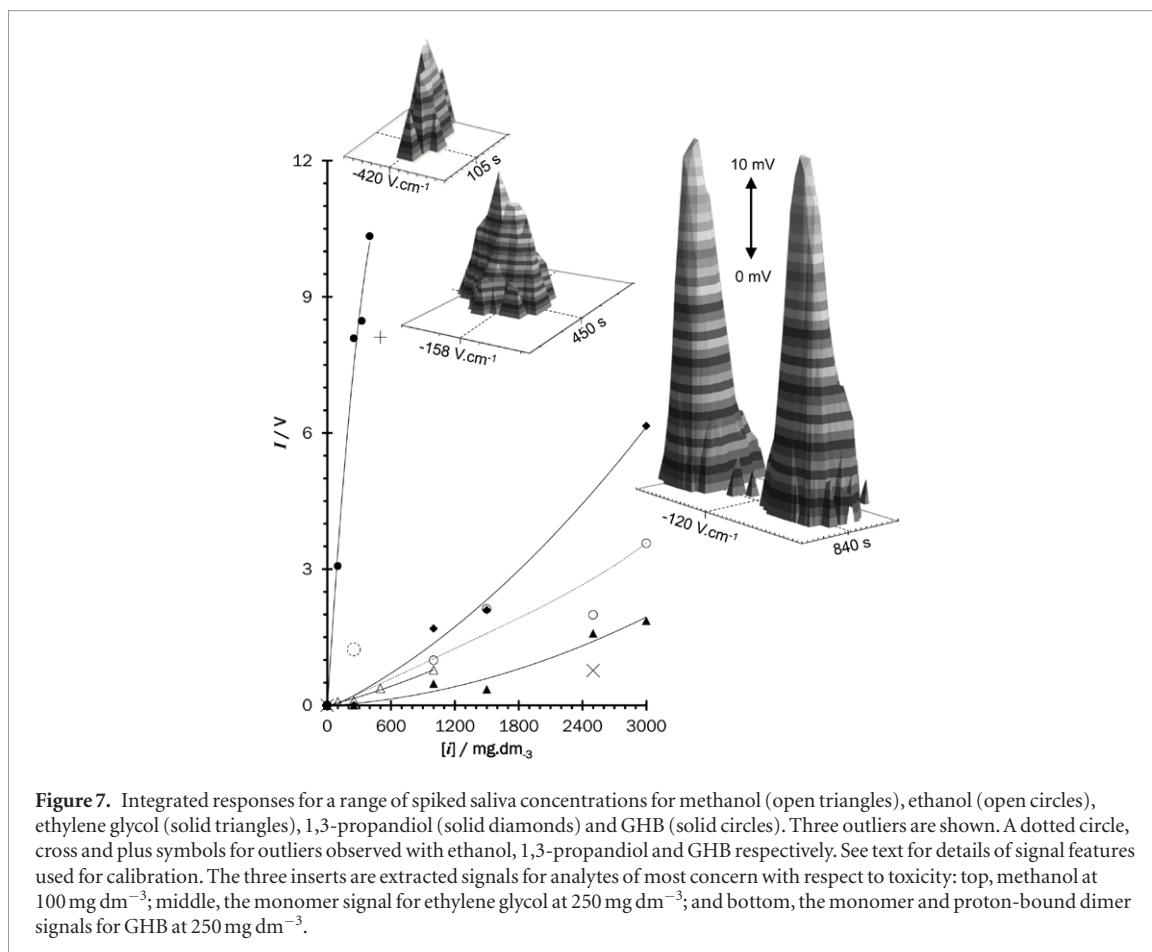


Figure 7. Integrated responses for a range of spiked saliva concentrations for methanol (open triangles), ethanol (open circles), ethylene glycol (solid triangles), 1,3-propanediol (solid diamonds) and GHB (solid circles). Three outliers are shown. A dotted circle, cross and plus symbols for outliers observed with ethanol, 1,3-propanediol and GHB respectively. See text for details of signal features used for calibration. The three inserts are extracted signals for analytes of most concern with respect to toxicity: top, methanol at 100 mg dm^{-3} ; middle, the monomer signal for ethylene glycol at 250 mg dm^{-3} ; and bottom, the monomer and proton-bound dimer signals for GHB at 250 mg dm^{-3} .

Despite the complexity of the responses it was possible to generate well resolved and analytically useful chromatographic peaks (see figure 5). The chromatograms for ethylene glycol, 1,3-propanediol and GHB were generated by integration of the differential mobility spectra across the proton-bound dimer ion features and the hydrated protonated monomer responses, and these are shown as discrete traces in figure 5 overlaid with the summed chromatographic response. For ethanol and methanol the chromatograms were generated by integration of the complicated features that contained hydrated protonated monomers and proton-bound dimer ions. Figure 5 shows the intensities of the peaks reflecting the differences in the ionisation efficiencies as well as the column loadings of the five compounds. Of particular note was the behaviour of ethylene glycol, with a peak shape that indicated a saturated response with significantly lower sensitivity compared to the other four compounds.

Calibration

Calibration of the differential mobility spectrometer was based on the peak volumes for the proton-bound dimer ion responses for the two glycols and GHB. The ethanol calibration was based on the integration of the complicated feature containing unresolved hydrated protonated monomers ion clusters and proton-bound dimer ions while the methanol calibration peak volume was taken from the proton-bound dimer ion response, and, at low concentrations, from the hydrated

protonated monomer cluster ion with the same value for the compensation field maximum. Table 4 summarises the calibration parameters data.

Saliva analysis

The responses obtained from saliva spiked with a range of concentrations of the analytes are summarised in figures 6 and 7. The chromatography contained substantial numbers of recovered compounds from the saliva sample, but nevertheless it was possible to identify the analytes reliably based on their compensation field and retention times.

The intensities of the responses observed reflected the combined interactions of: the adsorption/absorption behaviour of the analytes onto/into the PDMS sampler medium; the product ion dynamics noted above of the five compounds; and interactions with the saliva matrix. Matrix interactions in drooled saliva are problematic in that microbiological activity and stability of the analytes are likely to be related to the analytes' concentration and will have a time-dependent element. Further, the physical chemical properties of the saliva may also vary between samples. The previous study with this sampler contrasted the responses obtained from drooled saliva samples against those obtained by sampling directly in the mouth, under the tongue next to the salivary glands. Sampling in the mouth was found to be more sensitive and more reproducible than adopting a passive drool approach. Further, obtaining a passive drool sample requires significantly more

AQ2

participant training and compliance than simply placing a small rod under their tongue and, as such, is not likely to be a more practical approach to working with patients who may have analytes at levels high enough to be a cause of concern about their safety and welfare [13]. Nevertheless, the adoption of a passive drooled-saliva approach enabled an approximate matrix that allowed the intended sampling conditions to be acquired safely and practicably. Finally, the loss of the more volatile methanol and ethanol to the saliva headspace and, hence, from the experiment also needs to be acknowledged as a methodological weakness.

The fragmentation behaviour observed during the method development stage with liquid injections was not observed in the saliva studies. The presence of other closely eluting components within the chromatogram made background subtraction problematic and subsequently it was not possible to investigate fragment ion artefacts with confidence. The on-column masses of methanol recovered were estimated to fall in the range 0.35 ng to 3 ng over the range 100 mg dm⁻³ to 2 g dm⁻³, and similarly for ethanol the on-column masses were estimated to fall in the range 29 ng to 42 ng. Recoveries for ethylene glycol were lower with up to 7 ng obtained at high saliva loadings of 3 g dm⁻³ in contrast to 1,3-propanediol recoveries of up to 22 ng at the same level. GHB allowed the most efficient recovery from saliva with 10 ng recovered at 100 mg dm⁻³ increasing to an estimated on-column mass of 34 ng at 400 mg dm⁻³.

Conclusion

This pilot study demonstrates the effective recovery, detection and semi-quantitative estimation of all the analytes of interest to this work. This represents a potentially useful methodological advance in the rapid assessment of alcohol toxicity and, embodied within a TD-GC-DMS or a TD-GC-IMS, it provides a workable approach for a rapid screen and evaluation protocol for alcohols present at toxic levels from a single non-invasive sample. This has not been possible previously and has the potential for the development of point-of-care toxicity assessment in emergency room settings. Indeed, this study, in concert with others, is developing the concept of extending volatile biomarker measurement from the breath to a range of excretory routes. There are instances when breath sampling might be problematic (the propensity for an inebriated patient to vomit, for instance) and, as such, skin and saliva offer alternative routes for studying and exploiting the tissue/blood/breath/skin/saliva excretion mechanics for non-invasive diagnostics [19].

The apparent simplicity of the analytes belies significant complexity in the ion chemistries associated with their detection using ambient ionisation or radioactive ionisation approaches. Earlier mass spectrometric studies with alcohols have identified the formation of fragment ions associated with proton transfer ionisation approaches [20–22]. The presence of signals due

to product ion fragmentation would not appear to be without precedent. The alcohol product ions, and their fragment ions, are highly mobile and therefore are associated closely with the water-based reactant ion signals. Increasing resolution between reactant ion signals and analyte signals by increasing the dispersion field strength has the combined effect of reducing the analytical sensitivity by reducing the analytical area of the ion filter while, at the same time, promoting fragmentation reactions [23, 24]. The possible ion fragmentation of GHB has not been reported previously.

Compensation field maximum shifts attributable to the auto-modification of the transport gas by analyte neutrals was also observed and this is an area that will require further investigation to characterise it completely.

The study of fragmentation mechanisms, products and their ramifications for alcohol determination by differential mobility spectrometry along with the development of detection and signal-processing algorithms to enable peak-shift from auto-modification of the differential mobility transport gas to be handled efficiently are logical next steps in the development of this area. In parallel to such a study will be the refinement of the methodology to reduce the chromatographic run time to less than 300 s, and the continued development of the sampling approach to reduce the sampling time so that a total analytical run time of 600 s might be achieved. This would enable the delivery of a clinical pilot study within an appropriate poisons unit to assess the efficacy of this approach in patients, benchmarked to current gold standard toxicity screens.

Acknowledgment

The authors wish to thank the Spanish Ministry of Education, Culture and Sport for the pre-doctoral grant (AP 2009-3528) for the support of L Criado-García and the Engineering and Physical Science Research Council alongside John Hoggs Technical Solutions for the support of D M Ruszkiewicz through an Industrial Case Studentship Award. The authors also acknowledge and thank the volunteers who participated in this research.

References

- [1] Zhang G, Crews K, Wiseman H, Bates N, Hovda K E, Archer J R H and Dargan P I 2012 Application to include Fomepizole on the WHO model list of essential medicines URL: www.who.int/selection_medicines/committees/expert/19/applications/Fomepizole_4_2_AC_Ad.pdf, visited 21 September 2015
- [2] BBC News 2015 India alcohol poisoning: Mumbai death toll tops 100, URL: www.bbc.co.uk/news/world-asia-india-33224514, visited 21 September 2015
- [3] Heberlein A, Lenz B, Degner D, Hornhuber J, Hillemacher T and Bleich S 2009 Methanol levels in saliva—a non-invasive parameter that may be useful in detection of alcohol intoxication *Alcohol Alcohol.* **45** 126–7
- [4] Rezgui N D, Kanu A B, Waters K E, Grant B M B, Reader A J and Thomas C L P 2005 Separation and preconcentration phenomena in internally heated poly(dimethylsilicone)

AQ3

AQ4

AQ5

- capillaries: preliminary modelling and demonstration studies *Analyst* **130** 755–62
- [5] Kanu A B and Thomas C L P 2006 The presumptive detection of benzene in water in the presence of phenol with an active membrane-UV ionisation differential mobility spectrometer *Analyst* **131** 990–9
- [6] Bocos-Bintintan V, Moll V H, Flanagan R J and Thomas C L P 2010 Rapid determination of alcohols in human saliva by gas chromatography differential mobility spectrometry following selective membrane extraction *Int. J. Ion Mobil. Spectrom.* **13** 55–63
- [7] Verstraete A 2004 Detection times of drugs of abuse in blood, urine and oral fluid *Ther. Drug. Monit.* **26** 200–5
- [8] Mergen G, Kayaalti Z, Dural E, Aliyev V, Kaya S, Yalcin S, Karakus A and Soylemezoglu T 2011 Simultaneous headspace-GC-FID analysis for methanol and ethanol in blood saliva and urine: validation of method and comparison of specimens *LC GC Europe* **24** 292–7
- [9] Jones A W 1993 Pharmacokinetics of ethanol in saliva: comparison with blood and breath alcohol profiles, subjective feelings of intoxication, and diminished performance *Clin. Chem.* **39** 1837–44
- [10] Finkelstein Y and Vardi J 2002 Progressive parkinsonism in a young experimental physicist following long-term exposure to methanol *Neurotoxicology* **23** 521–5
- [11] Flanagan R J, Braithwaite R A, Brown S S, Widdop B and de Wolff F A 1995 *The International Programme on Chemical Safety: Basic Analytical Toxicology* (Geneva: World Health Organisation)
- [12] Zvosec D L, Smith S W, Porrata T, Strobl A Q and Dyer J E 2011 Case series of 226 γ -hydroxybutyrate-associated deaths: lethal toxicity and trauma *Am. J. Emerg. Med.* **29** 319–32
- [13] Martin H J, Riazanskaia S and Thomas C L P 2012 Sampling and characterisation of volatile organic compound profiles in human saliva using a polydimethylsiloxane coupon placed within the oral cavity *Analyst* **137** 3627–34
- [14] Limero T, Reese E, Wallace W T, Cheng P and Trowbridge J 2012 Results from the air quality monitor (gas chromatograph-differential mobility spectrometer) experiment on board the international space station *Int. J. Ion Mobil. Spectrom.* **15** 189–98
- [15] Ali Awan M, Fleet I and Thomas C L P 2008 Optimising cell temperature and dispersion field strength for the screening for putrescine and cadaverine with thermal desorption gas chromatography differential mobility spectrometry *Anal. Chim. Acta* **611** 226–32
- [16] Young D, Thomas C L P, Breech J, Brittain A H and Eiceman G A 1999 Extending the concentration and linear dynamic range of ion mobility spectrometry with a sheath flow inlet *Anal. Chim. Acta* **381** 69–83
- [17] Eiceman G A, Krylov E V, Tadjikov Ewing R G, Nazarov E G, and Miller RA 2004 Differential mobility spectrometry of chlorocarbons with a micro-fabricated drift tube *Analyst* **129** 297–304
- [18] Schneider B B, Nazarov E G and Cove T R 2012 Peak capacity in differential mobility spectrometry: effects of transport gas and gas modifiers *Int. J. Ion Mobil. Spectrom.* **15** 141–50
- [19] Amann A and Smith D (ed) 2013 *Volatile Biomarkers: Non-Invasive Diagnosis in Physiology and Medicine* (Boston: Elsevier)
- [20] Friedman L, Long F A and Wolfsberg M 1957 Study of mass spectra of lower aliphatic alcohols *J. Phys. Chem.* **27** 613–22
- [21] Smith S C, McEwan M J, Giles K, Smith D and Adams N G 1990 Unimolecular decomposition of a polyatomic ion a variable temperature selected ion flow drift tube: experiment and theoretical interpretation *Int. J. Mass Spectrom. Ion Process.* **96** 77–96
- [22] Karpas Z, Eiceman G A, Ewing R G and Harden C S 1994 Collision induced dissociation studies of protonated alcohol and alcohol-water clusters by atmospheric pressure ionization tandem mass spectrometry. Part 2. Ethanol, propanol and butanol *Int. J. Mass Spectrom. Ion Process.* **133** 47–58
- [23] Eiceman G A, Karpas Z and Hill H H 2013 *Ion Mobility Spectrometry* 3rd edn (Boca Raton: CRC Press)
- [24] Shvartsburg A 2008 *Differential Ion Mobility Spectrometry* (Boca Raton: CRC Press)